APPLICATIONS OF ELEMENTAL ANALYSIS FOR ARCHAEOMETRIC STUDIES: ANALYTICAL AND STATISTICAL METHODS FOR UNDERSTANDING GEOCHEMICAL TRENDS IN CERAMICS, OCHRE AND OBSIDIAN

A Dissertation
presented to
the Faculty of the Graduate School
University of Missouri-Columbia

In Partial Fulfillment
of the Requirements for the Degree

Doctor of Philosophy

---

by
RACHEL SARAH POPELKA-FILCOFF

Dr. J. David Robertson, Dissertation Supervisor

December 2006

The undersigned, appointed by the Dean of the Graduate School, have examined the dissertation entitled:

APPLICATIONS OF ELEMENTAL ANALYSIS FOR ARCHAEOMETRIC STUDIES:
ANALYTICAL AND STATISTICAL METHODS FOR UNDERSTANDING
GEOCHEMICAL TRENDS IN CERAMICS, OCHRE AND OBSIDIAN

Presented by Rachel Sarah Popelka-Filcoff

A candidate for the degree of Doctor of Chemistry

And hereby certify that in their opinion it is worthy of acceptance.

_____
Professor J. David Robertson

_____
Professor Michael D. Glascock

_____
Professor Silvia Jurisson

_____
Professor Michael Greenlief

_____
Professor Paul Duval

_____
Professor Marcus Rautman

I would like to thank my husband, David Filcoff, for reminding me of the humor in situations, especially the trials of graduate school, and not to take myself too seriously. He has been curious and supportive about my graduate research from the first day we met- and enough so to go to Peru on our research trip. He has also been wonderful computer support, but also very helpful in editing papers, photography of artifacts and design for my meeting posters. I would also like to thank my parents, Dr. Gerald and Leslie Popelka, for their support and being excellent mentors and role models as ethical scientists. Many thanks go to them as well for enduring many science fair projects and late-night last-minute changes to poster displays when I was younger. Thank you to my sister, Risa Popelka, who is now enjoying the challenges of graduate school. Thank you also to my extended family who have listened to my challenges and understood when I was working on my research.

ACKNOWLEDGMENTS

Many thanks to the members of my committee, especially Dr. J. David Robertson and Dr. Michael Glascock, who have both supported me and advised me throughout graduate school, including the National Science Foundation Fellowship, the Nuclear Chemistry Summer School program and the National Institute of Standards and Technology post-doctoral position. Dr. Robertson is an advocate for archaeometry in the world of analytical chemistry and a supporter of interdisciplinary studies. He instructed me in quality radioanalytical chemistry research and teaching. Dr. Glascock has been an advisor to me as early as high school, when I started this journey with a science fair project on 1904 World's Fair ceramics. He advised me then, and throughout graduate school, and taught me the way to do excellent archaeometry research. I thank them both for encouraging me to bridge my archaeology training with a Ph.D. in chemistry.

Many thanks also to the other members of my committee: Dr. Silvia Jurisson, for her thorough introduction to the basics of radiochemistry in her course; Dr. Michael Greenlief, for introducing me to the myriad aspects of mass spectrometry in his analytical chemistry course, Dr. Paul Duval, for his assistance in understanding geochemistry and inorganic chemistry, as well as his archaeological interests, and Dr. Marcus Rautman, for reminding everyone of the important archaeological questions at hand and providing an archaeological perspective.

My gratitude is also extended to the University of Missouri Chemistry department professors, students and staff for all of the ways that they have assisted me.

As archaeometry research is an interdisciplinary effort, this project could not been completed without the advice, assistance and support of the following individuals in no particular order: for general research: MURR Archaeometry Laboratory Staff, including the senior staff, the students and visiting scholars; for the Caborn-Welborn study: Dr. Jason Shergur, Dr. David Pollack; for the ochre studies: Dr. Carol Diaz-Granados, Dr. Christophe Descantes, Dr. James Wettstaed, Dr. Cheryl Seeger, Dr. Gretchen Moore, Dr. Cynthia Price, Dr. Kolleen Bean, Dr. Kevin Shelton, Dr. Nathan Craig, Dr. Mark Aldenderfer, Elizabeth Miksa, Henry Wallace, Rachel Green, Dr. Jonathan Erlandson, Matthew Boulanger; for the PXRF study: Robert J. Speakman, Dr. Nathan Craig, Dr. Mark Aldenderfer, and Dr. Gary Ehrhardt. In addition, I would like to thank many of the staff and students at the University of Missouri Research Reactor Center (MURR) for their assistance and patience and guidance.

These projects would not be possible without the funding from the University of Missouri-Columbia Department of Chemistry, the National Science Foundation grant that supports the MURR Archaeometry Laboratory (NSF-0504015) and a National Science Foundation Graduate Fellowship.

TABLE OF CONTENTS

LIST OF ILLUSTRATIONS

LIST OF TABLES

REE- rare earth elements

INAA- instrumental neutron activation analysis
XRF- X-ray fluorescence spectrometry
WD-XRF – wavelength dispersive X-ray fluorescence spectrometry
ED-XRF- energy dispersive X-ray fluorescence spectrometry
PXRF-portable X-ray fluorescence spectrometry
PIXE- particle induced X-ray emission
SEM- scanning electron microscopy
SEM-EDX- scanning electron microscopy and energy dispersive X-ray analysis
LA-ICP-MS laser ablation inductively coupled plasma mass spectrometry
ICP-MS inductively coupled plasma mass spectrometry
XPS-X-ray photoelectron spectroscopy
AES-Auger electron spectroscopy
SIMS-secondary ion mass spectrometry
RBS-Rutherford backscattering spectroscopy
IR- infrared spectroscopy
CRM- certified reference material
SRM- standard reference material
XRD – X-ray diffraction

LOD – limits of detection
LOQ- limits of quantification

SD- standard deviation
RSD- relative standard deviation
PCA- principal component analysis
PC- principal components
CDA- canonical discriminant analysis
FWHM- full width half maximum

APPLICATIONS OF ELEMENTAL ANALYSIS FOR ARCHAEOMETRIC STUDIES: ANALYTICAL AND STATISTICAL METHODS FOR UNDERSTANDING GEOCHEMICAL TRENDS IN CERAMICS, OCHRE AND OBSIDIAN

Rachel S. Popelka-Filcoff

J. David Robertson, Dissertation Supervisor

ABSTRACT

Three areas are covered in this dissertation: elemental analysis of Caborn-Welborn ceramics, elemental analysis and geochemical characterization of ochres, and construction and implementation of a portable XRF instrument for artifact analysis.

The first study is analysis of ceramics from Caborn-Welborn (Ohio Valley) archaeological sites, using both instrumental neutron activation analysis (INAA) and particle-induced X-ray emission (PIXE). By using principal components analysis and posterior discriminant analysis, it was possible to compositionally distinguish lower Ohio Valley ceramics in both extra-regional and local analyses.

The second study analyzes iron oxides (ochre) from several sources using instrumental trace analysis techniques, including INAA, and X-ray fluorescence spectrometry (XRF). Multivariate statistics of the data point to trends in the inter- and intra-source variability of ochre. Elemental results from Missouri, California, Oregon, Texas, Arizona, and Peru have been investigated. These trends in geochemistry lead to a better understanding of ancient ochre procurement.

The third study covers the set-up, design and system geometry calculations, testing, and calibration of a portable XRF system. The system was transported to and used successfully in southern Peru in August 2005 to characterize obsidian artifacts.

INTRODUCTION

This dissertation focuses on the application of elemental analysis to investigate archaeological questions and seeks to contribute to the understanding of fundamental geochemical relationships between source materials and artifacts. Subsequent multivariate statistics and data interpretation assist in understanding archaeological questions such as artifact procurement and artifact exchange. As such, this dissertation is a reflection of the field of archaeometry, which employs a number of analytical techniques as diverse as elemental analysis, DNA analysis, zoological and faunal analysis, and radiochemical dating to solve complex archaeological problems. [1-4] This work is also an inter-disciplinary effort that draws upon the fields of analytical chemistry, radiochemistry, geoscience, and statistics, as well as archaeology, anthropology, and ethnography. This dissertation's foundation is in archaeological chemistry, a fundamental area of archaeometry. While the definitions of the field of archaeometry may shift depending on the various schools of thought,[3, 5, 6] this dissertation fits the general definition of archaeometry, as it provides interpretations for chemical data gathered in response to archaeological questions. In particular, this dissertation focuses on the application of analytical chemistry and archaeological interpretation of inorganic artifacts including ceramics, obsidian, and ochre.

DISSERTATION CHAPTERS

Chapter 1

The opening chapter describes techniques used throughout the dissertation, including the fundamentals of the analytical methods, quantitative measurements, and specific facilities used to perform the experiments. A discussion explains the thought process used to choose

the appropriate method for a given archaeometric application. Studies of archaeological materials frequently involve more complex considerations than other types of analytical samples. This chapter also includes information on the advantages and disadvantages for each of the analytical methods employed in this dissertation including accuracy, precision, and limits of detection.

Chapter 2

Chapter 2 describes the concepts behind the provenance postulate, which is a fundamental requirement for many types of archaeometric studies. The multivariate statistical procedures used for interpretation of the elemental results, including cluster analysis, principal component analysis (PCA), and canonical discriminant analysis (CDA) are presented. A detailed discussion of the data transforms and statistics specifically used for the ochre study are also presented in this chapter.

Chapter 3

Chapter 3 describes the analytical procedures and data interpretation steps used for data from INAA (instrumental neutron activation analysis) and PIXE (particle induced X-ray emission) analysis for a collection of Caborn-Welborn ceramics from the Ohio River valley. By using principal components analysis and posterior discriminant analysis, it was possible to make a compositional distinction between lower Ohio Valley ceramics and ceramic samples collected on archaeological sites located in the southeastern part of the United States. Similar statistical analyses were employed to examine the elemental compositions of Caborn-Welborn ceramics and their distribution within the Caborn-Welborn region. Ceramic

specimens classified as Caborn-Welborn as well as central Mississippi Valley and Oneota-like sherds recovered from Caborn-Welborn sites appear to have been made locally using similar clays. However, the clays used to produce daub on house walls were found to differ from those used in ceramic vessels.

Chapter Four

Chapter 4 describes the multi-elemental analysis of ochre samples from several locations around the world. This chapter describes the geochemistry of the raw ochre material, and provides information about ancient and modern sources of ochre. A discussion covers existing literature on the ancient uses of ochre, modern ochre analysis, and provenance studies using methods other than elemental analysis. Further review describes previous elemental studies and interpretation. Ochre data from both INAA and XRF is presented and interpreted for sources in Missouri, Peru, Arizona, and Australia in terms of the provenance postulate. A meta-analysis of ochre studies from North America is also presented. Multivariate methods were used to interpret the results from both a chemical and archaeological perspective.

Missouri

This study examines the variation in the major, minor, and trace element patterns of ochre from iron oxide sources in southeastern Missouri in order to better understand the differences occurring within and between the sources. Samples were analyzed by INAA and XRF. The data were interpreted by Pearson's linear correlation and multivariate analysis. The data indicate geochemical trends in ochre that satisfy the provenance postulate.

Peru

Ochre and other associated artifacts are very common on the Terminal Archaic-Early Formative archaeological site of Jiskairumoko, southern Peru. At the site, ochre was found in several contexts on tools, palettes, burials, and in soil deposits within the structures, suggesting both symbolic and functional purposes for ochre use. Variations in color and context imply different uses for ochre. Instrumental neutron activation analysis was used to characterize the ochre samples found at Jiskairumoko. Multivariate analysis of the elemental data by principal components analysis suggests trends in the compositional data related to differences between ochre found at the site.

Arizona

In order to examine the possibility of identifying ochre from given locations, the original geochemical sources must be carefully sampled and characterized. This work describes the meticulous sampling and INAA of ochre from sources in the Tucson Basin in Arizona and the subsequent multivariate analysis of the data. This study has several goals, including characterizing variance in ochre geochemistry, identifying the most important elements for characterization of ochre, and establishing a database for future comparisons. Trends observed within the data lead to conclusions regarding elemental variability in ochre and possible ochre procurement and exchange.

North America

While the archeological contexts and some cultural meanings are well known, information about the geochemistry and provenance of ochre is poorly documented. This

work presents analytical data from INAA indicating geochemical trends within the sources of archaeological ochre. Ochre materials were sampled meticulously from geological sources and artifacts in order to comprehensively describe the elemental variations and associations within ochre sources. Interpretation of the multivariate data helped to identify trends within and between ochre obtained from several locations in the U.S. Understanding the geochemical trends may lead to an improved understanding of ochre procurement and technological uses of ochre by prehistoric humans.

Chapter 5

Chapter 5 describes the design, calibration, and utilization of a portable X-ray fluorescence instrument (PXRF). This chapter discusses the selection of the components and experiments to optimize the experimental setup as well as the precision and accuracy of the instrumentation when applied to archaeological projects. The results from a case study on obsidian from Peru are presented.

CHAPTER 1: ANALYTICAL METHODOLOGY

Source material and artifacts made of ochre, ceramic and obsidian artifacts were investigated in the course of this research. Several analytical techniques were used including instrumental neutron activation analysis (INAA), particle-induced X-ray emission (PIXE), X-ray fluorescence spectrometry (XRF) and portable X-ray fluorescence spectrometry (PXRF). Experimental design and choice of technique will be discussed for archaeological samples in general. Archaeological applications, advantages and disadvantages of experimental methods, precision, accuracy, and limits of detection will be discussed for each technique.

ANALYTICAL CHOICES FOR ARCHAEOMETRIC APPLICATIONS

Each of the aforementioned methods has been used extensively for other analytical problems, and the individual techniques have advantages and disadvantages for given archaeometric applications that must be understood before undertaking an analysis. Several aspects of analysis for archaeometric studies need to be taken into account. These include: sensitivity, accuracy, precision, effect on the sample (i.e., destructive or detrimental), bulk versus surface analysis, laboratory vs. *in situ* and appropriateness for the type of sample.[7, 8] Janssens et al. cited the six most important characteristics of a method for analyzing artifacts or artwork as the following: versatile, non-destructive, fast, universal, sensitive, and multi-elemental.[9]

For any analytical study, there should be a balance between the information acquired from the data, the cost, the time required to complete the analysis, the labor required, as well as the accuracy and precision required, all while achieving good quality control of the data.[7]

Sample preparation and the amount of analyte available are factors to consider for any analytical study. For archaeometric work, archaeologists and museum curators may be reluctant to provide a sample from an artifact. In this case, a non-destructive analysis method is preferred. Small amounts of sample can be used for destructive methods such as INAA, by removing a sample from an inconspicuous location on the artifact. The sample amount for INAA can be on the order of milligrams, whereas other techniques, such as XRF, may require grams of material.

Although more important for portable instrumentation when access to a location or sample may be limited, the time required to perform any analysis may also be an important consideration. Since a large number of samples are often required to answer most archaeological questions, the shorter the analytical time the better. Often, sample preparation time is a major part of the entire time required for sample analysis. However, this has to be balanced against the amount of information to be obtained.

Most of the methods used in this dissertation have multi-element detection limits in the parts per million range. For many elements, like the rare earth elements, the parts per million or tens of parts per million are the range of interest, as these are characteristic of the original source. Major components (elements in the percent range) are indicators of the original geochemistry of the material. However, nearly all of the analytical techniques can analyze in the percent concentration range, allowing determination of the major components of the material (although different calibrations may have to be used). Examples of this are determination of silicon in obsidian and ceramics and iron in ochre. Many of the techniques used in this dissertation have a wide dynamic range allowing determination of most elements in the sample matrix.

The precision and accuracy of the data from the method are important from both the analytical and archaeological standpoints. Precision of the methodology addresses the reliability of the measurements and ultimately contributes to the discriminative power of the results. Accuracy of the data is required for achieving the correct interpretation of the data and for comparison between studies performed at different times and at different laboratories. Bishop et al. discuss the importance of accuracy, sensitivity, and precision specifically for archaeometric studies.[10] The use of standards establishes method accuracy and quality control samples assist in monitoring the accuracy and precision of the analytical techniques.

The sampled area of the artifact being investigated is also an important part of any study. For analysis of ceramic pastes, bulk analysis of the entire material is appropriate. For museum specimens or artifacts of cultural significance, destructive sampling may not be possible. In these cases, sampling from an inconspicuous location on the artifact or non-destructive sampling is preferred. For analysis of pigments or other materials applied as a thin layer to an artifact, a surface analytical method would be appropriate. In the early days of archaeometric analysis, destructive bulk analysis was common, but recent advances in portable instrumentation have led to more options for surface analysis and *in situ* studies. With the advent of portable instrumentation, *in situ* analysis can be accomplished for both bulk and surface analyses.

X-ray fluorescence (XRF) and PIXE as well as other spectroscopic methods such as infrared spectroscopy and Raman spectroscopy have been recently adapted to portable instrumentation. Technological advances have allowed these methods to contribute in both fieldwork and museum settings. In addition, recent projects have been developed centering on the application of these portable techniques to not only accomplish the archaeometric

study but also to characterize and define the uses and limitations of the instrumentation in the field. Developments in the portable analytical methodology have led to subsequent innovations in the technology used to support the methods. In the case of portable XRF, such advances include compact X-ray tubes. For both portable PIXE and PXRF, Peltier-cooled silicon detectors allow transport of the instrument, something difficult with liquid-nitrogen cooled detectors. Data acquisition and software and control for most modern portable instruments are based on portable and palm top computers, making the entire instrument more field-adaptable as well as compatible with desktop computers in the laboratory. Although portable technology has the advantage of size, small weight and often battery-powered operation, sometimes the analytical information from such an instrument can be more limited than laboratory-based technologies.

Users of analytical techniques need to fully understand the archaeological questions and fundamental theory behind an archaeometric study. Also, human-made artifacts present a set of confounding factors that are more complex than typical geological or geochemical studies. Table 1.1 provides a summary of the advantages of each technique used in this dissertation, and Table 1.2 lists some of the disadvantages of each of these techniques.

Table 1.1: Advantages of each method discussed in this dissertation

INAA	PIXE	XRF	PXRF
Small sample size High precision (~5%)[11]	Non-destructive Can be converted to portable instrument	Non-destructive Can be converted to portable instrument	Non-destructive Portable
High accuracy (~1%)[11]	Near-surface analysis (5 μm depth)	Surface analysis (10-40 μm depth)	Surface analysis (10-40 μm depth)
Simple sample preparation	Concentrations calculated by mathematical models or matrix-matched standards	Concentrations calculated by mathematical models or matrix-matched standards	Concentrations calculated by mathematical models or matrix-matched standards
Minimal matrix effects		More available, less expensive	More available, less expensive
Multi-elemental Sensitivity to sub-ppm levels	Multi-elemental Sensitivity to ppm-lower detection limits than XRF[8]	Multi-elemental Sensitivity to ppm	Multi-elemental Sensitivity to ppm, higher LOD (limits of detection) than conventional XRF
Independent of sample chemical state	Independent of sample chemical state	Independent of sample chemical state	Independent of sample chemical state
Multiple parameters to optimize technique	Automated sample analysis	Automated sample analysis	

Table 1.2: Disadvantages for each method discussed in this dissertation

INAA	PIXE	XRF	PXRF
High cost		May require large sample	Elements to be measured Z> Na
Long analysis time	Higher limits of detection than INAA	Sometimes needs sample preparation into briquettes or fused glass-destructive	Higher limits of detection than INAA
Destructive to artifact (although inconspicuous drilling can be used)	Requires access to particle accelerator	Elements to be measured Z> Na	Fewer elements are measured than by INAA or XRF
Cannot be adapted to portable instrumentation		Higher limits of detection than INAA	Higher limits of detection than INAA and XRF
Requires access to reactor or other neutron source			

Instrumental Neutron Activation Analysis (INAA)

INAA analyzes materials through the interaction of neutrons with the sample matrix and subsequent measurement of characteristic delayed gamma rays. In the general analytical practice of INAA, the sample is irradiated with neutrons in a reactor or other neutron source. Capture of the neutron by the nucleus results in the formation of a compound nucleus. The compound nucleus is unstable and decays by the emission of prompt gamma rays, sometimes leading to a radioactive nucleus. This radioactive nucleus can decay in a variety of ways and is often accompanied by gamma-ray emission. Gamma-ray energies and half-lives are characteristic of the radioactive nucleus created by nuclear reactions between the target nucleus and neutrons. The reactions need to be known to identify the element of interest. The gamma-ray energy is specific to the isotope of interest, and the intensity of the gamma-

ray peak (number of counts in an integrated peak) is proportional to the concentration of the element in the sample. Figure 1.1 illustrates the nuclear reactions taking place in INAA.

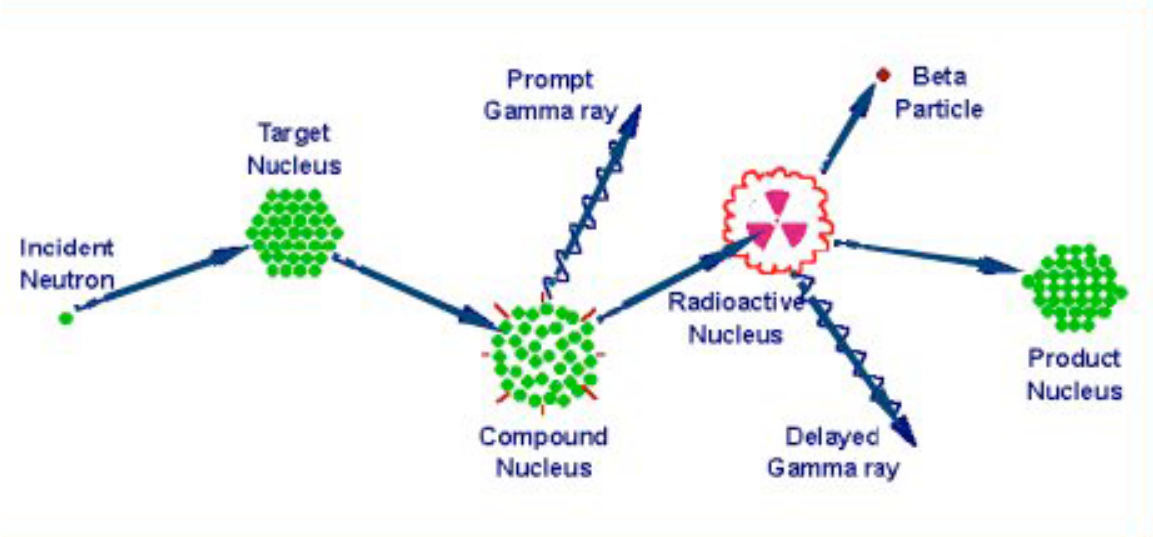

Figure 1.1: Interactions in instrumental neutron activation analysis.
Reprinted with permission from Michael D. Glascock

In the majority of cases, INAA relies on high probabilities for (n,γ) reactions with thermal neutrons. This is the probability (or cross section) that an incoming thermal neutron is captured by the sample nucleus and does not result in competing nuclear reactions with fast neutrons such as (n,α), (n,p), (n,2n) reactions, elastic and inelastic scattering. In most cases, thermal neutrons with a kinetic energy of ~0.025 eV have the highest cross-section (σ) for (n,γ) reactions. Sufficient thermal neutron flux is available most commonly in reactors, but is also available with other irradiation facilities.[11]

Figure 1.2 is an example gamma-ray spectrum from an ochre sample discussed later in this dissertation. This spectrum shows the major peaks of interest identified from measurement of the medium half-life elements. The gamma-ray energy is on the abscissa and

the intensity (counts) is on the ordinate. A description of the procedures used at MURR for ochre is presented in Chapter 4.

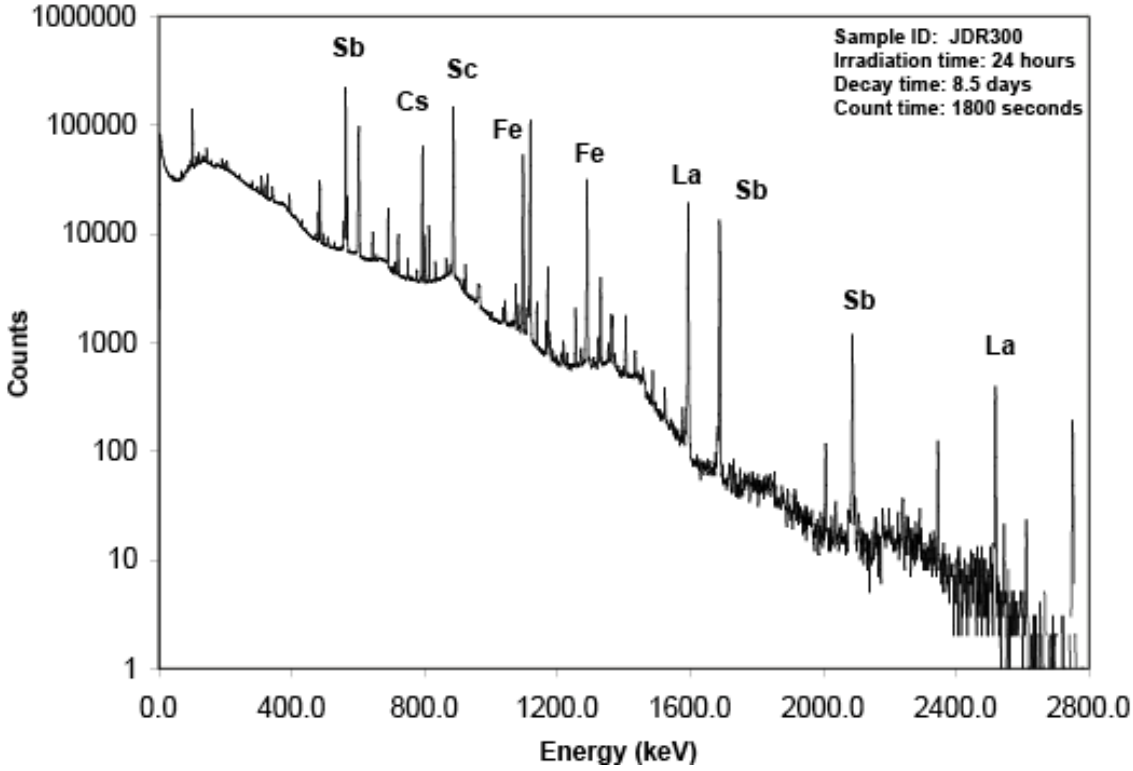

Figure 1.2: Example INAA spectrum for the medium count of an ochre sample. Peaks of interest are labeled above the peak.

At MURR, both short and long irradiations occur in the graphite reflector of the reactor. Short irradiations occur consecutively using pneumatic-tube facilities, and for long irradiations, samples are bundled together and irradiated simultaneously. In either case, after an appropriate amount of time (decay), high-purity gamma-ray detectors (HPGe, 25% relative efficiency) are used to measure the emitted gamma rays coming from the sample. The Genie software from Canberra is used to identify and integrate the counts under the peaks. Concentrations are determined by the comparator method in which unknowns are compared to standards of known concentration. INAA has excellent sensitivity (in most

cases ppm and in some cases ppt) for most elements, and typically over 30 elements can be measured in a "geological" sample at MURR. Table 1.3 lists the elements measured routinely in ceramic and ochre by INAA. More elements are routinely measured by INAA for ceramics, but in this dissertation, PIXE provided the supplemental elements.

Table 1.3: Elements measured in ochre and ceramic by INAA

Ochre	Al, As, Ba, Ca, Ce, Co, Cr, Cs, Dy, Eu, Fe, Hf, K, La, Lu, Mn, Na, Nd, Ni, Rb, Sb, Sc, Sm, Sr, Ta, Tb, Th, Ti, U, V, Yb, Zn, Zr
Ceramic	Ba, Ce, Co, Cr, Cs, Eu, Fe, Hf, K, La, Lu, Na, Rb, Sb, Sc, Sm, Ta, Tb, Th, Yb, Zn

Advantages and Archaeometric Applications

INAA has several advantages for archaeometric studies, including its excellent precision, accuracy, and sensitivity for 30-35 elements. Moreover, because the sample is transparent to the probe (neutrons), and because the sample is transparent to the signal (γ-rays) matrix effects for INAA are minimal.

Since the 1950's, several reactor-based laboratories have used instrumental neutron activation analysis to perform multi-elemental analysis of artifacts from around the world. In the United States, these include the University of Missouri-Columbia Research Reactor (MURR), National Institutes of Standards and Technology (NIST) and the Smithsonian Institution, Brookhaven National Laboratory, and the University of California-Berkeley. The multi-elemental capability of INAA measurements allows for studies of artifact sourcing, ancient exchange routes and ancient technologies. Over the years, tens of thousands of artifacts have been analyzed including ceramics[12, 13], obsidian, pigments, metals, bone and others.[14]

For this dissertation, INAA was used for ceramics and ochre. INAA has an established reputation as an excellent method for ceramics, making it a logical choice for the Caborn-Welborn study. As discussed in Chapter 3, a comparison data set by Steponaitis was also analyzed by INAA. All of the ochre samples in this dissertation were also analyzed by INAA. In this case, INAA is a good method for introductory work on a less-understood material such as ochre. INAA was able to provide precise and accurate elemental data for over 30 elements, and to identify the important elements for discrimination of ochre. For a summary of the INAA procedures at MURR used in this dissertation, see Glascock.[13] Data from the Caborn-Welborn study are presented in Appendix I. The data from the ochre studies are presented in Appendices II-V.

Quantitative INAA Analysis

From a practical standpoint, many INAA facilities worldwide calculate concentrations using the comparator method:

$$\frac{R_{std}}{R_{sam}} = \frac{M_{std}(e^{-\lambda t_d})_{std}}{M_{sam}(e^{-\lambda t_d})_{sam}} \qquad \text{Equation 1.1}$$

where R is the measured gamma counting rate (counts/second), M is mass of the element, t_d is the decay time for sample and standard, and λ is the decay constant for the isotope of interest. Practically, this method is simpler than the parametric INAA, where other factors such as neutron flux, elemental cross section, isotope abundance, gamma abundance and other factors must be well known. The general equation for production of activity from thermal neutrons in the sample is:

$$A = n\phi\sigma(1 - e^{-\lambda t_i})(e^{-\lambda t_d}) \qquad \text{Equation 1.2}$$

where A is activity, n is number of target atoms of the isotope of interest in the sample, ϕ is the thermal neutron flux, and σ is the thermal cross section in barns, λ is the decay constant, t_i is the irradiation time, and t_d is the decay time. This expression takes into account both the production and decay during irradiation as well as the post-irradiation decay. In reality, it is difficult to measure all of the variables with low uncertainty using the absolute INAA methods and therefore the comparator method is routinely employed.

As comparator INAA is practiced in the archaeometry community, CRMs (certified reference materials) either from NIST or other organizations that certify standard reference materials are used as primary standards. Aliquots of the CRM are analyzed under the same conditions (irradiation position, irradiation time, decay time, and counting time) as the samples. The mass of the element in the sample is calculated based on a comparison of the count rates obtained from the sample with those obtained from a CRM with a certified elemental concentration. In a typical INAA experiment, one or two SRMs (standard reference materials) are used as the comparator standard and one or two other SRMs are used as quality controls.

Since INAA has such low limits of detection, care must be taken throughout the experiment to minimize contamination of samples. Contamination can occur during sample handling, sample pulverization, or perhaps cross-contamination between samples. Steps are taken throughout to minimize these sources of contamination, such as the use of specific

tools for drilling and pulverizing the samples, as well as the use of high-purity vials for sample irradiation.

Irradiation by neutrons provides an ideal case for many samples. Most samples are transparent to neutrons, allowing an irradiation of the entire sample. The neutron flux is generally isotropic.[15] Although INAA is considered a simultaneous method, practically speaking, samples are irradiated and allowed to decay and counted depending on the length of the half-life of the isotope of interest. Only certain isotopes fit the criterion for INAA. These isotopes include those that are gamma-ray emitters with high probability of neutron interaction (high cross-section), in the thermal neutron region, and a half-life in the appropriate range of measurement.

Precision and Accuracy

Table 1.4 presents data for the quality control (NIST SRM 278 Obsidian Rock) standard where NIST SRM 1633a (Fly Ash) was used as the primary standard. These data span from 2000 to 2006, and were used as the quality controls in INAA for both the Caborn-Welborn ceramics and ochre projects discussed in later chapters. Certified values for NIST SRM 278 are provided in Glascock 2004.[16] If certified or accepted values are not available, literature values were used instead and these are indicated by italic font. All values are in ppm, except Fe, which is in weight percent.

Table 1.4: Elements measured by INAA in long counts for NIST SRM 278 from 2000-2006

	As	La	Lu	Nd	Sm	U	Yb	Ce	Co	Cr	Cs	Eu	Fe (%)	Hf	Rb	Sb	Sc	Sr	Ta	Tb	Th	Zn
NIST 278 MURR (n=28)																						
AVG	4.30	30.19	0.65	26.91	5.98	4.85	4.65	63.31	1.47	6.60	5.20	0.78	1.41	8.33	126.82	1.54	5.04	57.49	1.30	0.97	12.00	50.75
STDEV	1.04	0.46	0.03	4.00	0.15	0.43	0.20	1.66	0.03	1.21	0.08	0.02	0.03	0.13	3.88	0.30	0.09	10.94	0.03	0.05	0.19	3.45
RSD (%)	24.28	1.52	4.00	14.87	2.55	8.84	4.35	2.62	2.00	18.28	1.45	2.41	2.18	1.61	3.06	19.75	1.78	19.04	2.36	5.20	1.54	6.80
NIST																						
AVG	*4.7*	*32*	*0.77*	*30*	*5.9*	4.58	4.6	60	*1.8*	*6.6*	*5.2*	*0.78*	1.43	*8.5*	127.5	*1.79*	*4.8*	63.5	*1.29*	*1.06*	12.4	53
STDEV	*0.17*	*4*	*0.12*	*3*	*5*	0.04	0.6	6	*0.4*	*0.9*	*0.2*	*0.3*	0.01	*0.4*	0.3	*0.21*	*0.8*	0.1	*0.08*	*0.14*	0.3	5
Z	-0.37	-0.86	-0.31	-1.17	0.04	0.40	0.05	1.20	-0.50	0.00	0.01	0.00	-0.08	-0.24	-0.33	-0.34	0.25	-1.81	0.02	-0.21	-0.57	-0.77

Figure 1.3 plots z-score vs. elements determined in mid and long analyses except for Ni and Zr. Ni and Zr are elements typically difficult to analyze by INAA due to poor sensitivity in both the unknowns and standards because of low isotopic abundance, low gamma-ray abundance and low cross-sections for the isotopes of interest.

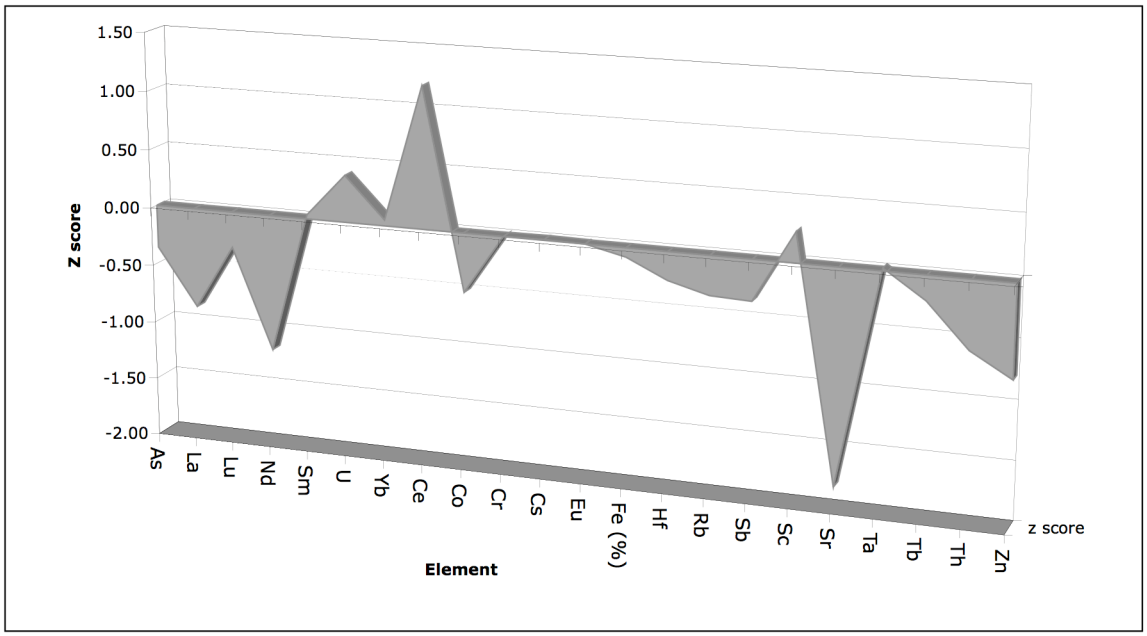

Figure 1.3: Accuracy of INAA based on quality control SRM 278, by z-score vs. element.

Figure 1.3 indicates that most elements measured by INAA fall between ± 2 standard deviations (97 percentile) for the z-score. Thus, the values agree closely with the certified and accepted values for the NIST standard. As seen in Table 1.4, most elements have a relative standard deviation below 10% except for As, Cr, Nd, Sb and Sr indicating a quite precise technique for this standard.

Table 1.5: Elements measured by INAA in long counts for Ohio Red Clay from 2000-2006

		As	La	Lu	Nd	Sm	U	Yb	Ce	Co	Cr	Cs	Eu	Fe (%)	Hf	Ni	Rb	Sb	Sc	Sr	Ta	Tb	Th	Zn	Zr
Ohio Red																									
n=13	AVG	14.83	49.83	0.59	45.37	8.95	2.98	4.36	112.56	22.61	90.34	10.15	1.74	5.04	7.38	62.97	180.23	1.09	18.35	31.65	1.49	1.22	14.96	96.59	199.31
	STDEV	0.83	0.66	0.03	3.33	0.36	0.64	0.11	4.12	0.41	1.94	0.19	0.05	1.21	0.17	22.74	5.12	0.05	0.35	39.21	0.03	0.08	0.32	9.05	29.27
	RSD (%)	5.59	1.32	4.48	7.33	4.03	21.64	2.60	3.66	1.81	2.15	1.88	2.70	24.09	2.30	36.11	2.84	4.33	1.92	123.86	1.74	6.85	2.13	9.36	14.69
MURR	AVG	14.8	50.1	0.588	46.1	9.17	3.24	4.32	112.3	22.7	90.2	10.1	1.723	5.048	7.34	76	180.8	1.1	18.3	58.3	1.49	1.24	14.9	92.8	179
	STDEV	1.10	1.00	0.021	5.8	0.4	0.4	0.21	2.7	0.5	1.9	0.2	0.045	0.152	0.2	17.6	5.3	0.07	0.5	19	0.05	0.2	0.3	11	23.1
	Z	0.02	-0.21	0.01	-0.24	-0.26	-0.26	0.08	0.10	-0.10	0.07	0.07	0.04	-0.34	0.07	-2.05	-0.18	-0.03	0.05	0.00	-0.04	0.08	0.85	2.81	-3.49

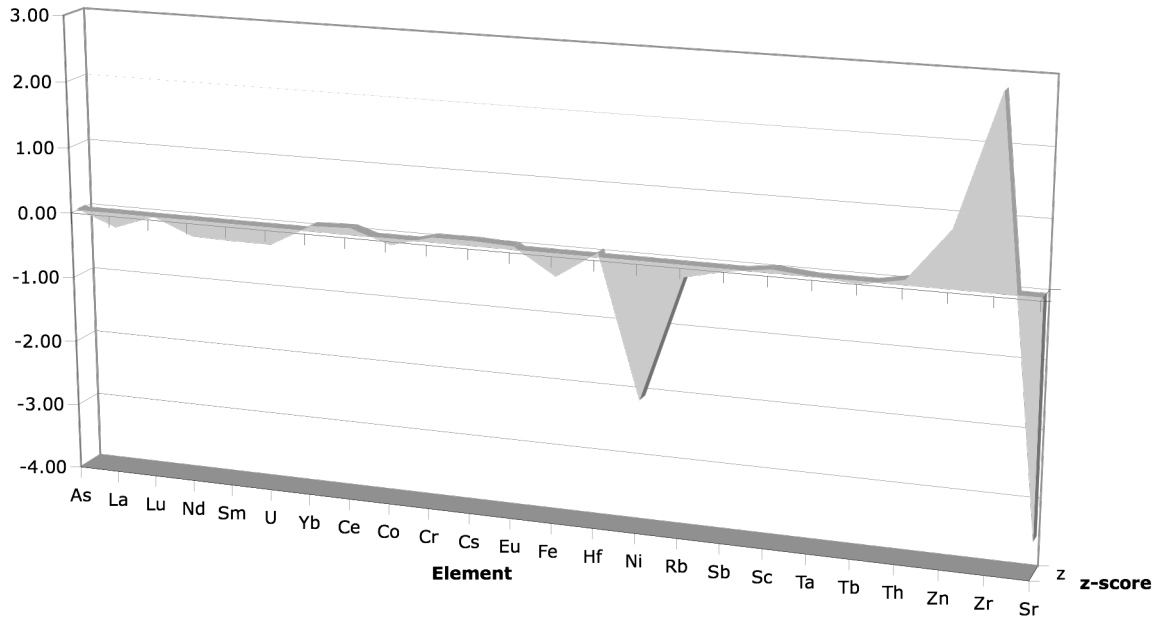

Figure 1.4: Accuracy of INAA based on quality control Ohio Red Clay, by Z score vs. element

A similar analysis was performed for Ohio Red Clay, another quality control standard routinely used at MURR for INAA analysis. Figure 1.4 demonstrates excellent accuracy for Ohio Red Clay, with most values of z close to 0. The outlier elements are Ni, Sr and Zr, which are not measured well by INAA. Relative standard deviations for values across Table 1.5 are also below 10% for most elements except for U, Fe, Sr, Zr and Ni. Again, Sr, Zr and Ni are generally problematic for INAA.

Limits of detection were estimated for elements in a high iron matrix such as ochre. These are estimates only and were found by examining the limit of detection for each element from the software output, and are presented in Table 1.6:

Table 1.6: Estimated LOD for elements in high Fe matrix by INAA

Element	Estimated Limits of Detection (ppm)
Al	2000
As	2
Ba	100
Ca	500
Ce	2
Co	0.1
Cr	2
Cs	0.3
Dy	0.2
Eu	0.02
Fe	500
Hf	0.2
K	2000
La	0.1
Lu	0.04
Mn	5
Na	20
Nd	5
Ni	150
Rb	10
Sb	0.1
Sc	0.02
Sm	0.02
Sr	100
Ta	0.1
Tb	0.2
Th	0.2
Ti	700
U	1
V	2
Yb	0.1
Zn	5
Zr	50

As can be seen in the results of Table 1.6, INAA has excellent sensitivity (low limits of detection, many in sub-ppm range) for many elements, especially for rare earth elements and others that are known to be important in source determination. As demonstrated by the data presented, INAA is a highly sensitive, precise, and accurate method for archaeometric studies of many materials ranging from obsidian to ceramic to ochre.

Particle Induced X-ray Emission (PIXE)

In general, PIXE is stimulated X-ray emission through interactions of high-velocity charged particles with atoms in the sample. The general description of PIXE is "particle-induced X-ray emission" although this is often synonymous with "proton-induced X-ray emission" (a specific type of PIXE). Charged particles typically used in PIXE include both protons and α-particles, which can be produced in particle accelerators such as Van de Graff instruments, as well as a radioactive source for the α-particles. Similar to XRF (as discussed later in this chapter), the inner shell electrons are ejected, followed by de-excitation of the ion. Then, outer electrons cascade into the inner shells to fill the electron vacancies, resulting in X-ray emission from the sample.[17]

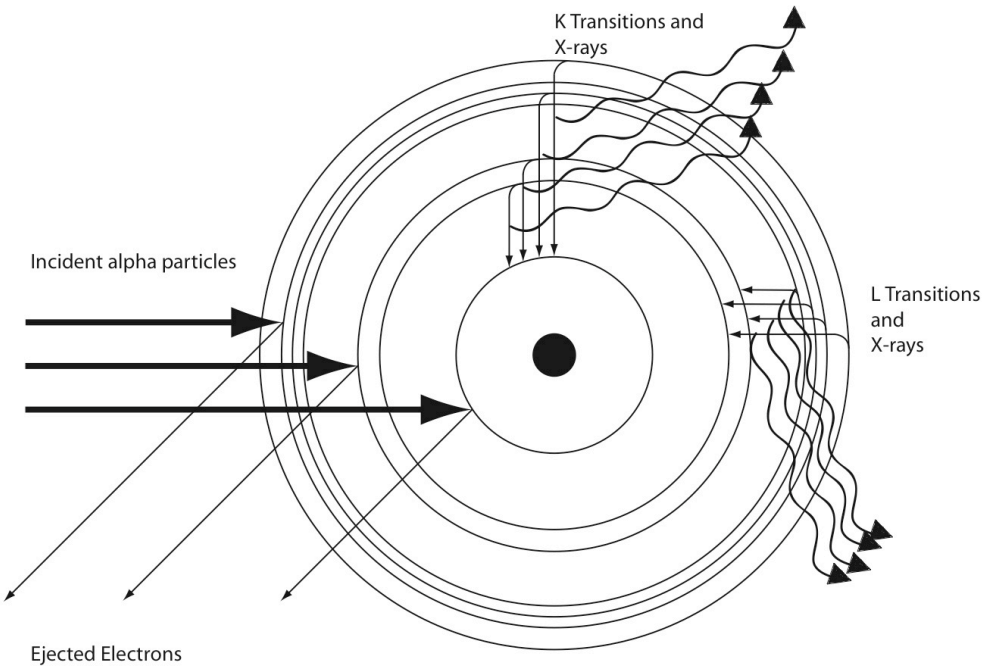

Figure 1.5: A schematic of the particle interactions and electronic transitions in PIXE

The energy of the X-ray emission is characteristic of the element, and the intensity of the emission is proportional to the concentration of the element in the sample.

PIXE has been utilized for the past two decades for elemental analysis, with several facilities set up worldwide, including the University of Guelph in Canada, (where the GUPIX software was developed), the University of Kentucky, and the Louvre Museum in France. Figure 1.6 shows the instrumental set up at Elemental Analysis Corporation, where the PIXE analyses for this dissertation were performed. For general information on PIXE and its applications, see Johansson et al.[17, 18]

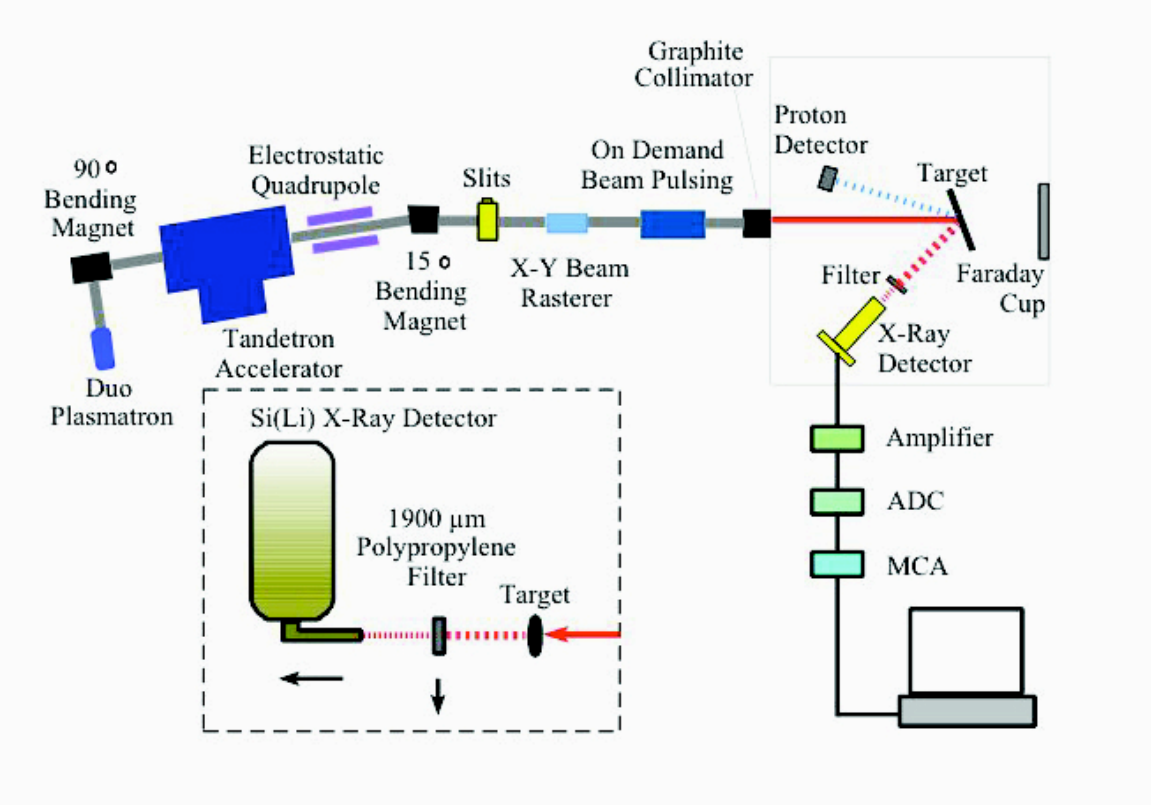

Figure 1.6: Experimental setup of PIXE.
Courtesy of Elemental Analysis Corporation, Lexington, Kentucky

For the Caborn-Welborn study, the following elements were measured by PIXE: Al, Ca, Cu, Ga, K, Mg, Mn, Ni, P, Si, and Ti.

Advantages and Archaeometric Applications

PIXE (particle induced X-ray emission) has several advantages for archaeometric analysis, most notably its capability for near-surface analyses. PIXE is also an important method for non-destructive applications to artifacts in both laboratory and portable instrumentation.[17, 19-21] Combination INAA and PIXE studies are useful as PIXE can measure certain elements, (notably Si, P, Cu and Pb) that INAA cannot.

PIXE has advantages over other X-ray techniques due to the use of high-energy particles. Among these are a higher rate of data collection for most elements due to lower bremsstrahlung scatter and improved sensitivity for the elements with lower atomic numbers as compared to XRF due to lower background.[8, 18] There is an improved signal-to-noise ratio for PIXE compared to photon-induced XRF due to the absence of intense Compton and Rayleigh scattering due to the much smaller amount of bremsstrahlung radiation. As PIXE employs a monoenergetic excitation source and the physics of the excitation process is well understood, a single system calibration can be applied across a wide range of sample matrices to generate accurate results.

Other advantages of PIXE include its capacity to provide rapid, multi-elemental analysis. In many cases, measurement of X-ray spectra and calculation of concentrations can be completed in a matter of minutes. The method also is very sensitive (1-10 ppm)[22] in the region of $11<Z<32$ and $75<Z<85$, ideal for the transition metals of interest in part of this dissertation. [17] In addition, PIXE is non-destructive to all "geological" artifacts and it can be adapted for use in a portable field device. PIXE is a near-surface analytical method (analyzes the first 1-10 μm of a sample), which makes it ideal for analysis of thin layers of pigments or other surface treatments on artifacts. Care must be taken in the application of PIXE to cloth and paper artifacts and paintings as irradiation often results in discoloration of the artifact or work of art.

A PIXE-based field device for elemental analysis is optimal for chemical analysis in non-standard lab situations by the use of radioactive sources and Peltier-cooled detectors.[19-21,23] In addition, the portable PIXE instrumentation is essential for measurements on artifacts that cannot be transported to a PIXE facility due to their size or fragility or other restrictions

on travel. PIXE has also been demonstrated for spot analysis by focusing the beam down to micron dimensions. Furthermore, PIXE analysis does not require that the samples be placed in a vacuum chamber as the particle beam can be extracted from the vacuum of the accelerator prior to irradiation of the sample. This makes the technique useful for analyzing artifacts or art that otherwise could not be placed under vacuum.

PIXE has many applications for archaeometric research for provenance and technical studies. These include ceramics, metals, glass, pigments, artwork, and others.[17, 18, 20, 24-35] In this dissertation, PIXE was used primarily for the Caborn-Welborn ceramic project. At the time of analysis, values for the short half-life elements for INAA were not available due to logistical constraints, and these were supplied by PIXE. In addition, PIXE provided values for elements such as P, Cu, and others not routinely measured by INAA. These data are discussed in Chapter 3 and presented in Appendix I.

Quantitative PIXE Analysis

Because the physics of PIXE is well understood, software such as GUPIX[36] can simplify and model spectra by considering the X-ray peaks as functions. The software also can model samples of varying thickness and calculate matrix effects. The software performs a semi-parametric analysis of the spectra, by comparing a model spectrum to a measured spectrum. The program then performs several iterations using the least-squares method to mathematically fit the spectrum and ultimately return calculated peak areas. For each element, the program returns the number of counts in each principal peak. For elements not detected,

the program provides a limit of detection calculation ($3 \cdot \sqrt{B}$), where B is the integrated background (non-peak) counts centered at the peak centroid and equal to one full width half-maximum (FWHM).[36] The GUPIX software uses an established database of K- and L- lines for X-ray emission, peak identification and concentration calculations. These data have been gathered from several sources, and include information on charged-particle stopping powers, X-ray attenuation coefficients, ionization cross-sections, X-ray emission rates and others.[36] Concentrations are calculated based on the X-ray yield, number of impinging particles, and system calibration H-factor. The H-factor takes into account the solid angle of the X-ray detector and the calibration of the charge measurement device into a constant. The H-factor is determined experimentally by using trace element standards of similar composition.

In the GUPIX program, the X-ray intensity or yield Y(Z,M) for element Z in matrix M is written as:

$$Y(Z,M) = Ylt(Z,M) \times C(Z) \times Q \times T \times \varepsilon \times W \times H(Z) \qquad \text{Equation 1.3}$$

where Ylt(Z,M) is the theoretical intensity or yield per charge unit per concentration per steradian for element Z in matrix M; C(Z) is the actual concentration of element Z in M; W is the detector solid angle; Q is the integrated alpha charge; ε is the intrinsic detector efficiency; T is the transmission through any filters; and H(Z) is the system calibration factor.

Ideally, a single H-factor will be obtained for a particular system set-up. An acceptable alternative from the calibration work is an H-factor curve that varies as a function

of atomic number of the element of interest. Pile-up and escape peaks are also taken into account by the software.

Precision and Accuracy

In general, PIXE is a relatively precise and accurate method. Table 1.7 provides a comparison between PIXE values from Element Analysis Corporation and NIST certified values for SRM-1633a Fly Ash.

Table 1.7: Comparison of PIXE values to NIST values for NIST SRM 1633a. Literature values are noted in italics.

	PIXE (n=4)			NIST	
	AVERAGE	**STDEV**	**RSD (%)**	**NIST 1633a**	**Error**
Na	2300	339	15	1700	100
Mg	5610	479	9	4550	10
Al	154630	2362	2	143100	10000
Si	228980	4224	2	228000	8000
P	1388	99	7	*1830*	*150*
S	2950	75	3	*2700*	*100*
K	17800	651	4	18800	600
Ca	10600	369	3	11000	100
Ti	9083	281	3	8230	390
Cr	220	25	11	196	6
Mn	161	21	13	179	8
Fe	82655	825	1	94000	1000
Ni	103	11	11	127	4
Cu	125	11	9	118	3
Zn	246	15	6	220	10
As	192	18	10	145	15
Sr	912	69	8	830	30

Figure 1.7 provides data from n=4 PIXE measurements of the NIST 1633a Flyash standard. It should be noted that these results are obtained from a single H-value calibration of the PIXE instrument at EAC used for both geological and biological sample analysis.[37]

Values are presented in ppm. All values are certified by NIST except for P and S for which literature values are used.[16]

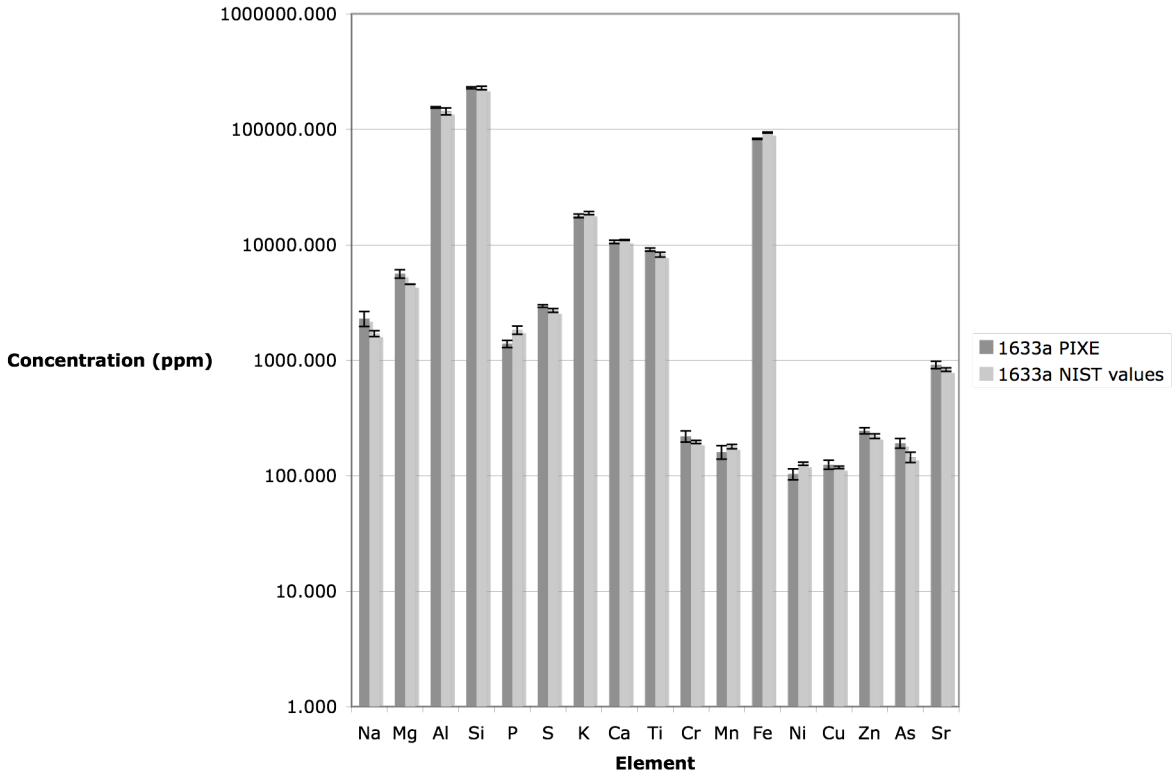

Figure 1.7: Comparison of PIXE and NIST and literature values for NIST1633a Coal Flyash. All values are certified by NIST except for P and S, which are literature values.

Most elements are close to the certified or accepted value provided by NIST. It can be observed that the PIXE values for 1633a are accurate when compared to certified/accepted values, although not as accurate as INAA. PIXE precision for this particular method and instrumentation is quite good as seen in the replicability of measurements (n=4) and low RSD values. The majority of elements are under 10% RSD and all are under 15% RSD for NIST 1633a. Data were not presented as Z scores due to greater differences in precision between

the PIXE and NIST values.

The limits of detection for this method are presented in the literature for coal and flyash.[22] Although the matrix is different than the ceramics investigated in this study, the LOD magnitudes should be similar. PIXE routinely has LOD on the order of 1 ppm for $20<Z<40$, and on the order of 10-100 ppm for $Z<20$ and $40<Z<70$, using K-emission lines up to $Z=50$. Limits of detection again drop to 1-10 ppm levels for high Z elements (rare earth elements) where the L-lines are used instead of K-lines.[22] Sensitivity in these regions is optimal for analyzing elements important for archaeometric work.

X-ray Fluorescence Spectrometry (XRF)

The XRF technique uses an X-ray source (either an X-ray tube or radioactive source) to stimulate electronic transitions. These transitions include the ejection of inner shell electrons, followed by cascading outer electrons into the inner shells to fill the electron vacancies, resulting in secondary X-ray emission from the sample. The process of X-ray fluorescence competes with Auger electron emission, with the probability of Auger occurring more frequently for the low Z elements. Another competitive process is the scattering of incident X-rays, which occurs as coherent or elastic scattering with no loss in photon energy (Rayleigh) or incoherent or inelastic scattering with loss of photon energy (Compton).[38]

The energy of the secondary X-ray emission is characteristic of the element in the sample, and the concentration of the element in the sample is proportional to the intensity of the secondary X-ray emission. In most archaeometric applications, the K and L and M transitions are used, with the K-lines representing transitions to the innermost shell, and L-

lines to the next innermost shell. A common X-ray tube has a maximum energy of 30 keV; therefore, for elements such as Ba whose K-lines are higher than 30 keV, the L-lines are used instead. The L-lines are used if the K-lines cannot be resolved from each other. In general, the K-lines are used for the lower Z elements, and the L-lines for higher Z elements such as Ba, Pb and others depending on the energy of the X-ray emission and the scale of acquisition of the data.[18] Figure 1.8 illustrates the X-ray interactions and transitions in XRF.

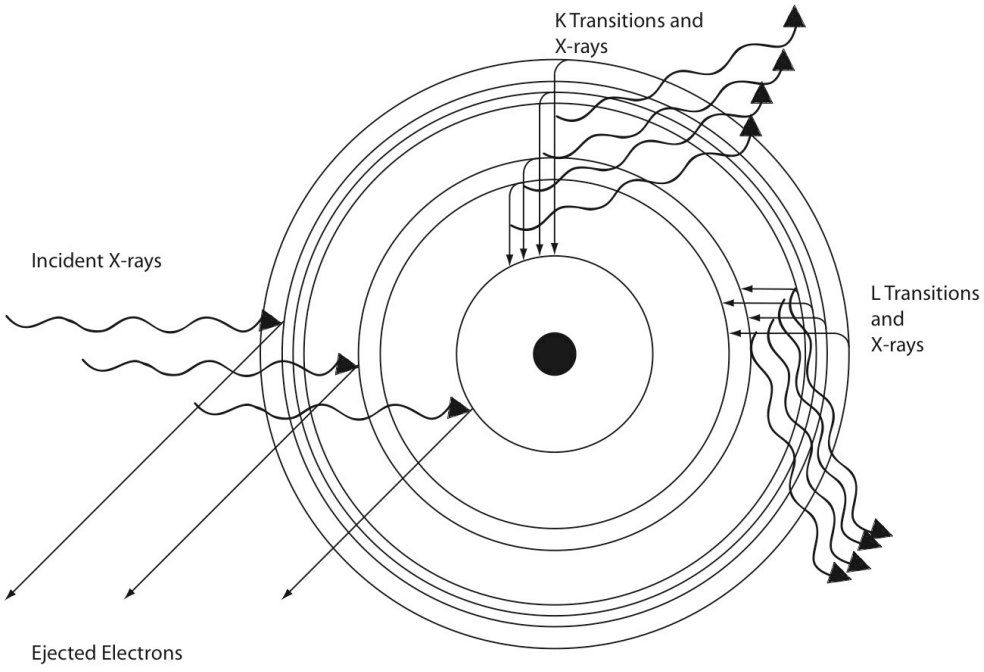

Figure: 1.8: A schematic of X-ray interactions and transitions in XRF

The system used in this dissertation was the Spectro X-Lab 2000, which is an energy-dispersive XRF spectrometer. The spectrometer also uses secondary targets to enhance data collection in certain regions of the spectrum. [39] Figure 1.9 shows a spectrum for an ochre sample studied in this work.

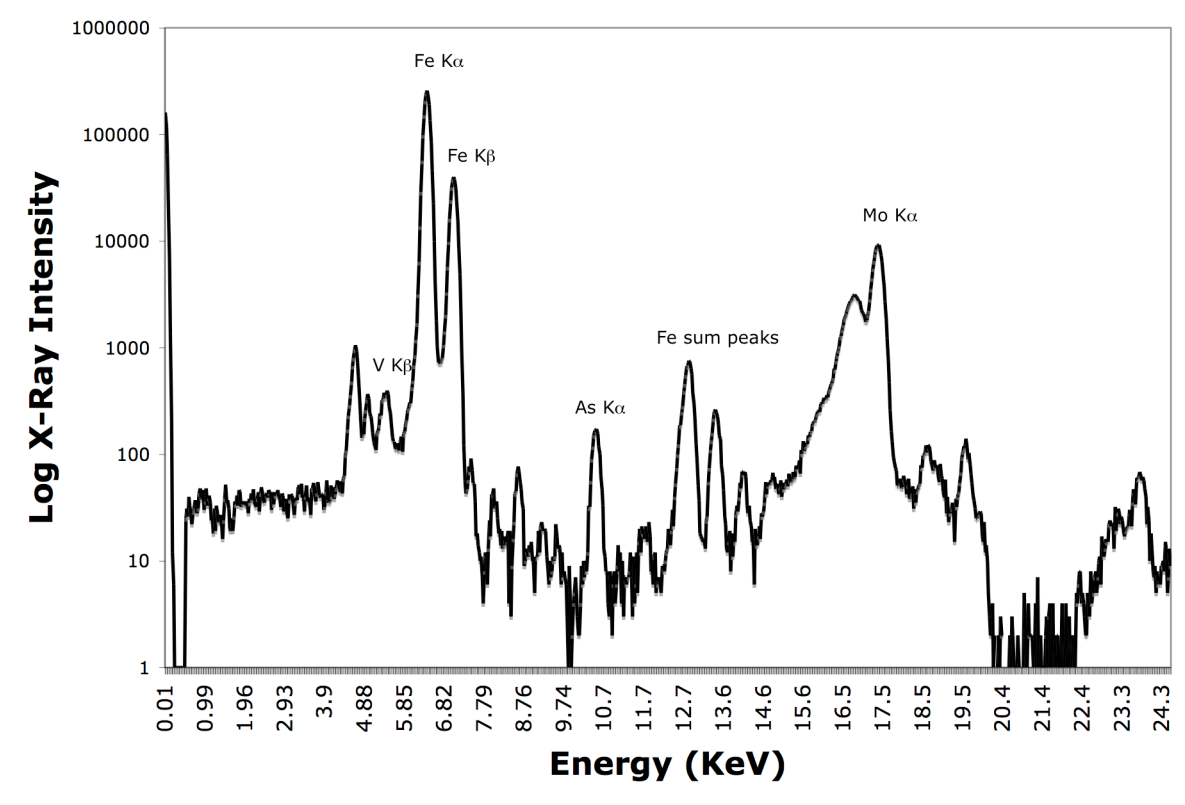

Figure 1.9: Example X-ray spectrum of an ochre sample with some peaks labeled (Missouri ochre #112, data from Compton/Secondary target of Spectro X-Lab 2000 XRF spectrometer)

The following elements were measured by XRF in this dissertation: Al, Si, P, S, K, Ca, Ti, V, Cr, Mn, Fe, Ni, Cu , Zn, Ga, As, Sr , Y, Zr , Ba, and Pb.

Advantages and Archaeometric Applications

XRF techniques have several advantages for archaeometric analysis: good accuracy and precision; fast and relatively inexpensive qualitative and quantitative analysis; extensive elemental coverage of elements of interest for archaeometry; models for geochemical analysis; and the capability of bulk or surface (10-40 μm depth) analysis.[38] Although less sensitive than INAA, XRF provides data in the ppm to tens of ppm for most trace elements up to percent levels for matrix elements. For XRF instruments, the analysis is often automated. For this study, 20 pressed pellets could be pre-loaded onto an automatic sample changing tray and analyzed sequentially in a matter of hours. In addition, XRF is a less expensive and more accessible technique than INAA. In general for lab-based instrumentation, the lightest element measured is sodium, but measurements can be made with good sensitivity across the periodic table.[7, 8] In a plot of sensitivity vs. atomic number, a bell-shaped curve is found, with the highest sensitivity for the elements in the middle portion of the periodic table.[38]

Since traditional XRF sample preparation requires 3-5 grams of material, these types of analyses can generally only be performed on samples for which significant portions may be destroyed during preparation for analysis. Typically the sample is powdered and either pressed into a briquette or fused into glass for analysis. The briquettes or glass pellets are resilient and can be analyzed multiple times without damage to the sample. Despite the larger sample, this method has several advantages for archaeometric studies as discussed above.

XRF methodology has been applied to a wide variety of archaeometric applications. The most common are ceramics, obsidian, and metals, but other applications include

paintings and other multi-layered artifacts. The literature describes a number of applications of XRF to studies of archaeological questions.[40-43] In this study, XRF was used in the initial studies of ochre. As the ochre study was an introductory work, XRF was used to identify other elements not measured by INAA (Si, Ca, P, Ni, Cu, Pb) to determine if these elements are important for differentiating between ochre sources. The results are discussed in Chapter 4 and the data are presented in Appendix II.

Quantitative XRF Analysis

In most cases, XRF analysis is assumed to be a bulk analysis by virtue of the homogenous sample preparation and exposure to X-rays. Another assumption for this study is that the sample submitted is homogenous throughout and is representative of the original artifact being analyzed. A general equation relating the concentration to the intensity of the X-ray emission is the following:

$$C = K \cdot I \cdot M \cdot S \qquad \text{Equation 1.4}$$

where C is the calculated concentration based on the remaining four factors. K is a constant when all analytical conditions and instrumentation are fixed. It is calculated for a particular instrumentation set up over a range of calibration standards.[44] I is the net peak intensity above background and M takes into account inter-element effects of primary and secondary absorption plus any possible enhancement and third element effects. This variable depends on the effectiveness of the method for correcting for these effects.[44] S is the specimen heterogeneity, which describes the penetration depth of the measured X-rays relative to the average particle size of specimen.[44, 45]

In XRF analysis, generally two methods are commonly used for quantitative analysis. These are the fundamental parameter (FP) and empirical methods. Most XRF systems use one exclusively or a combination of the two methods.

Empirical methods are based in a simple model of determining the response of the instrument to standards of known concentration and determining a function that fits the data. This response function is then employed for the unknown samples. Ideally, the function is linear in form, but in reality, to fit the data properly a polynomial function is necessary. Possible inconsistencies also occur when the standards are in a different physical form or not matrix matched to the samples. In general, thin film standards can be used, and assuming minimal thickness, the thickness, density, and matrix terms can be eliminated.[44] Spectrum deconvolution is based on measurements of pure elemental standards. From these standards, factors are calculated to describe the effects of these elements on other regions of spectrum. This method is used to correct interferences.[46]

The fundamental parameters method effectively models and quantifies elements based on mathematical modeling of the X-ray interactions within the sample. This approach is possible because of the physics of X-ray generation and interaction are well understood, and essentially unchanging from day-to-day and run-to-run. In addition, the fundamental constants for individual elements have also been experimentally determined. These include the mass absorption coefficients and fluorescence yields.[44] The X-ray sources are very consistent, as are the detection systems. Thus, data quantification can be achieved easily once the fundamental parameters of the system are understood and modeled properly. It has been demonstrated that the fundamental parameters method (FP) produces nearly equivalent results to those of the empirical method. However, there are some disadvantages to the FP

method. Accuracy for the fundamental constants can be as poor as ± 5%. In addition, other effects like window absorption, anode self-absorption, and multiple scattering are not taken into account, and separate experiments are required to model the spectrum.[44]

There are two types of interference problems with XRF: spectral interferences and matrix effects from surrounding elements in the sample. An example of a matrix effect occurs when attempting to quantify an element present in a surrounding matrix of other elements that may absorb or stimulate more fluorescence, thus distorting the quantitative results of the original element. Fortunately, the spectral interferences are usually consistent and well understood and relatively easy to correct.[47] For a summary of quantitative XRF analysis see Jenkins et al.[44] and for recent applications of XRF see Beckhoff et al.[48]

Precision and Accuracy

Precision is determined by the error in multiple measurements of a particular peak on certified standards. Reported levels of precision in the literature are on the order of 0.25-0.50%, assuming optimum measurement conditions, including resolution of peaks and minimal matrix effects.[8] Limits of detection are determined by the background.

Table 1.8 presents quality control data taken on NIST 690, NIST 2689 and Ohio Red Clay used in the XRF analyses of the ochre in this project. The Spectro X-Lab 2000 instrument uses a combination of empirical and FP methods for quantification.

Table 1.8: XRF results (mean ± s.d.) for NIST standards SRM 690 Iron Ore, SRM 2689 Fly Ash and Ohio Red Clay

Element	XRF (n=5)	NIST 690 Certified Value	RSD (%)	XRF (n=3)	NIST 2689 Certified Value	RSD (%)	XRF (n=4)	Ohio Red Clay Certified Value*	RSD (%)
Al [%]				12.18±0.08	12.94±0.21	0.7	10.9±0.4	8.89±0.15	4.1
Si [%]				22.87±0.27	24.06±0.08	1.2	28.89±0.850		2.9
P [%]				0.156±0.003	0.1±0.01	2.0	0.039±0.001		3.6
K [%]				2.66±0.06	2.2±0.03	2.1	4.13±0.07	3.31±0.03	1.8
Ca [%]				2.29±0.05	2.18±0.06	2.2	0.135±0.004	0.38±0.04	3.1
Ti [%]				0.91±0.02	0.75±0.01	2.3	0.72±0.03	0.57±0.02	3.8
V [µg/g]				377±13		3.5	259±11	198±3	4.1
Cr [µg/g]				217±5	[170]	2.3	94±11	89.2±1.8	11.7
Mn [%]				0.029±0.002	[0.0300]	5.2	0.027±0.001	0.025±0	2.5
Fe [%]	65.01±0.02	66.85	1.4	8.6±0.03	9.32±0.06	0.3	5.14±0.20	5.19±0.08	3.9
Cu [µg/g]				138±2		1.6	19±2.		10.5
Zn [µg/g]				239±4	[240]	1.5	95±4	97±6	3.8
As [µg/g]				142±2	[200]	1.6	14±1	13±4	3.7
Rb [µg/g]				148±1.		0.7	179±1	176±3	0.8
Y [µg/g]				79±1		1.5	41±1		2.3
Zr [µg/g]				290±3		1.1	269±8	166±10	2.9
Ba [µg/g]				832±6	[800]	0.7	654±6	614±26	1.0
Pb [µg/g]				76.0±0.3	[52]	0.5	16±2		12.3

Values in brackets indicate are recommended but not certified by NIST
*M. D. Glascock, Characterization of archaeological ceramics at MURR by neutron activation analysis and multivariate statistics. In Chemical Characterization of Ceramic Pastes in Archaeology, H. Neff, Ed. Prehistory Press: Madison, WI, 1992; pp 11.

Pressed pellets of NIST SRM 2689 Coal Fly Ash and NIST SRM 690 Iron Ore and Ohio Red Clay were used as quality control samples for the XRF analysis. SRM 690 has a very high Fe concentration and is low in other elements. In fact, very few other elements besides Fe are certified by NIST for this standard. Therefore, SRM 690 was used to validate the Fe values in high Fe samples (>50% Fe), as calibration of the XRF is normally not

adjusted for very high concentrations of Fe. Since Ohio Red Clay and SRM 2689 are low Fe, they were used to confirm all other elements in the analysis as well as samples with lower iron values. Table 1.8 lists the results of the XRF analysis of the standard reference materials. For the most part, values produced by XRF were within 2 sigma of the NIST or certified values, on at least three replicate analyses. In most cases, the relative standard deviation (RSD) is under 5% demonstrating good precision for the technique.

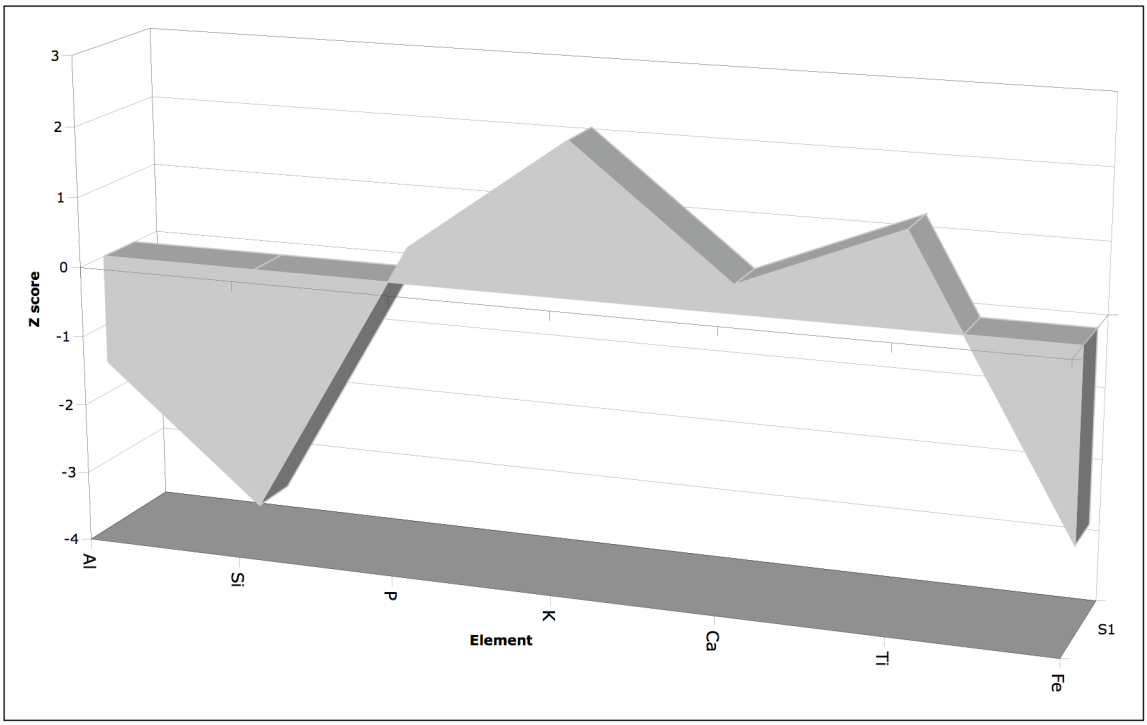

Figure 1.10: Accuracy of XRF based on quality control
SRM 2689 (Fly Ash), by Z score vs. element.

Figure 1.9 indicates that most elements reported for XRF fall between ± 2 deviations (97% percentile) for the z score, indicating that the values agree closely with the certified and accepted values of the NIST standard SRM 2689 only. Values for these elements are

presented in percent (%). Values for trace elements are not certified by NIST. In addition, the standard deviations for trace elements are not reported for this standard, therefore z scores cannot be calculated. The non-certified values are provided in Table 1.8.

Figure 1.11 displays a comparison of the XRF values for Ohio Red to the established values from MURR determined by INAA.

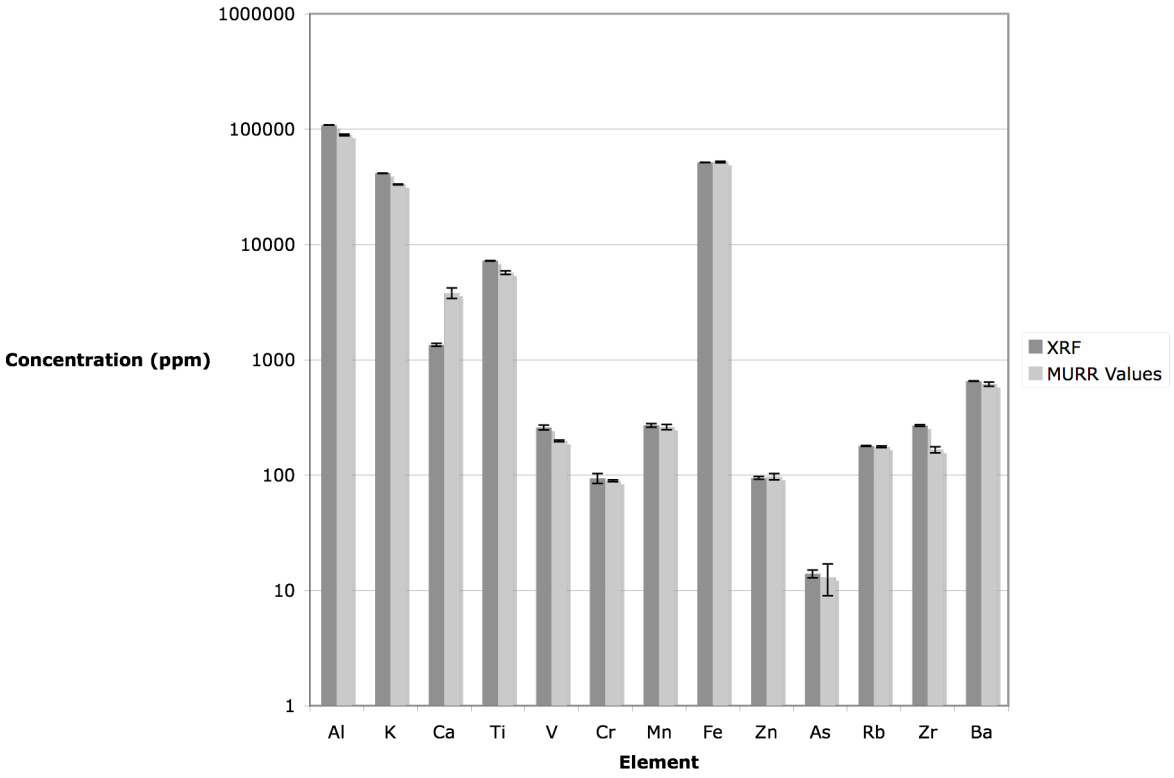

Figure 1.11: Comparison of XRF values of Ohio Red to established values by INAA at MURR

It can be observed from the above figure that XRF is fairly accurate, although for most elements the XRF values are slightly higher than the INAA values. Compared to the INAA values of Ohio Red discussed earlier, XRF values are not as accurate.

Table 1.9 reports the projected limits of detection for XRF, generated by the software as part of the Spectro X-Lab 2000 instrument. These were calculated using a blank pressed pellet comprised of the binder material used to prepare the samples for XRF. This binder blank sample was analyzed under the same conditions as the samples.

Table 1.9: Projected Limits of Detection for XRF

Element	Estimated Limit of Detection (ppm)
Na	63.0
Mg	6.4
Al	47.6
Si	30.0
P	30.0
S	20.0
K	2.1
Ca	0.5
Ti	2.0
V	0.1
Cr	0.3
Mn	0.2
Fe	4.6
Co	0.4
Ni	0.3
Cu	3.5
Zn	1.1
As	0.1
Rb	0.2
Sr	0.2
Y	0.4
Zr	0.4
Mo	0.5
Sn	0.5
Sb	0.5
Cs	3.1
Ba	3.6
La	5.6
Ce	11.6
Hf	0.3
Pb	0.6
Bi	0.3
Th	0.4
U	0.7

It can be seen from the results of Table 1.9 that XRF can be considered a sensitive method for most elements, with good limits of detection (ppm) in the elements of interest (transition metals and rare earth elements). XRF can also be used to determine major elemental

composition of artifacts (K, Na, Si, Ca, etc.). Like PIXE, the detection limits for lower Z elements are not as good (10-100 ppm), but these elements (Al, Si, Na, etc.) are usually present at the percent level in the matrix for archaeological materials such as ceramics and ochre. All in all, XRF provides a fast, accessible and less expensive method. It also has adequate precision and accuracy for most archaeological materials.

Portable X-ray Fluorescence Analysis (PXRF)

Portable X-ray fluorescence (or PXRF) is a variation on XRF. Recent technology has allowed the XRF method to be adapted for field studies and any application where XRF can be taken to the site for analysis. Technical advances such as miniaturized X-ray tubes and Peltier-cooled detectors have allowed smaller XRF setups that can be easily transported to archaeological sites and museums for analysis. Several models are available on the market ranging from hand-held devices to models that can be transported in a padded case. A more detailed description of the components, methods, precision, accuracy and limits of detection for PXRF will be covered in Chapter 5. A general overview of PXRF can be found in Piorek et al.[49] and Bichelmeier et al.[50]

Advantages and Archaeometric Applications

PXRF differs from standard XRF in several ways. For one, the samples are generally analyzed *in situ* or with very little sample preparation. In the case of paintings or large artifacts, the instrument is usually brought to the artifact. Samples such as smaller pieces of metal, obsidian or other material can be brought to the instrument, but they still undergo minimal sample preparation. Obsidian is simply washed with water to remove any possible

remaining dirt from the surface. Metals may have surfaces cleaned or burnished to remove the external corrosion layer. PXRF is most commonly performed in atmosphere, unlike lab-based XRF, which is performed under vacuum. This makes analysis simpler but also raises the limits of detection from ppm levels to tens to hundreds of ppm levels for most elements. Also, some lower Z elements are impossible to measure by PXRF. PXRF rarely uses secondary filters in coincidence with the X-ray source. In conventional XRF, these filters can provide an improved analysis for certain regions of the X-ray spectrum. For PXRF, a single unfiltered source will still be able to achieve quantitative results, but will likely experience higher background scatter in certain regions of the spectrum and perhaps not be able to resolve certain peaks. However, for most applications this is not an issue and the secondary filters are not used in favor of space and size considerations.

PXRF can be considered a surface method (measuring the top 10-40 microns of the sample), although in many cases it is assumed to be measuring bulk composition. As a result, the data are often affected by surface roughness and distortion. An ideal XRF analysis surface is flat and smooth, to minimize any scattering effects due to surface irregularities. Several studies have investigated these effects on the ability of the method and methods to obtain quantitative results despite complex surfaces on artifacts.[51]

The primary artifact investigated in this dissertation is obsidian from Peru. As discussed in Chapter 5, obsidian is a best-case scenario for understanding sourcing of artifacts and for testing a new analytical protocol, as the artifacts are homogenous, the sources are well characterized, and the source signature is easily identified compared to other types of artifacts. Data from the Peru obsidian studied by PXRF is presented in Appendix VI.

Quantitative PXRF analysis

Data quantification and analysis for PXRF is a development from traditional XRF techniques. PXRF systems and software use either empirical or FP quantitative analysis, or a combination of the two, as in lab-based XRF instrumentation. As discussed in Chapter 5, the Amptek instrumentation and software uses a FP quantification protocol only.

Precision and Accuracy

Because there is no certified standard for solid obsidian, the accuracy of the PXRF method was verified using established INAA values for the Chivay, Peru obsidian source. Precision of the method was determined by multiple measurements of several obsidian standards used in the artifact analysis. Further information on the precision, accuracy, and limits of detection for PXRF will be discussed in Chapter 5.

Summary

In summary, each of the four methods described and used in this dissertation (INAA, PIXE, XRF, and PXRF) have distinct advantages for the archaeological materials investigated (ceramics, ochre, and obsidian). For elemental studies of the materials, data on the characteristic elements important to each material is important for answering questions concerning sourcing and ancient exchange. Determining the most effective method for any type of archaeometric study is an important component of study design. Table 1.10 outlines the analytical methods used for each material in this dissertation, and it can be seen that a combination of methods is often essential to reveal trends in elemental geochemistry.

Table 1.10: Compilation of methods and archaeological materials investigated

Method/Material	INAA	XRF	PIXE	PXRF
Ceramic	X		X	
Ochre	X	X		
Obsidian	X	X		X

INAA offers high precision, accuracy and sensitivity for multi-elemental analyses, especially of the characteristic elements that are important in archaeometric studies. Despite its higher cost and limited availability, INAA provides data with the highest sensitivity for most of the elements of interest, which include the rare earth elements among others.

XRF also provides a multi-elemental approach to artifact analysis. It also has good precision and accuracy, and has sensitivity on the order of ppm for the transition metals. XRF is not as effective for rare earth elements; however it provides information for elements such as Si, Cu, P and Pb not routinely possible by INAA. XRF is more accessible and less expensive than INAA, and it can also provide a quicker turnaround for data.

Similar to XRF, PIXE is also a multi-elemental technique that has similar precision and accuracy. In contrast to laboratory-based XRF, PIXE has a much lower bremsstrahlung background, allowing better sensitivity. PIXE is useful especially for the transition metals and other higher atomic number elements ($11<Z<32$ and $75<Z<85$) as well as low Z elements compared to XRF. PIXE also differs from XRF in that it is a near-surface analysis method. PIXE measures the first few μm of the sample as compared to a depth of 10-50μm for XRF. However, PIXE generally needs specialized facilities and is not as accessible as XRF.

PXRF, a variation on XRF for fieldwork, offers a different set of capabilities. It is based in the instrumentation and software of lab-based XRF, and is becoming more accessible to researchers in all fields. A PXRF instrument can be transported to the archaeological site or museum rather than exporting fragile or important artifacts. Due to the nature of the instrumentation (less powerful X-ray tubes, no secondary filters, analyses performed in atmosphere), the precision, accuracy, and limits of detection are inferior to lab-based XRF. Limits of detection in tens to hundreds of ppm are more common for the elements of interest (i.e. transition metals, Sr, Ba, Pb, and others). Despite these limitations, for this study PXRF was successfully taken to Peru and demonstrated to be effective in chemically characterizing obsidian as described in Chapter 5.

CHAPTER 2: PROVENANCE POSTULATE AND MULTIVARIATE STATISTICS

The concept of the provenance postulate is fundamental to the research presented in this dissertation. This postulate, combined with advances in multivariate statistics, has permitted innovative directions in archaeometric studies. Multivariate statistics provide a way to interpret the variability in large data sets containing hundreds of samples and dozens of elemental variables. Multivariate analysis played a major role in this dissertation. A section discussing the specific statistical methods used for ochre analysis is also presented.

PROVENANCE POSTULATE

An essential concept for many types of archaeometric studies is the concept of the provenance postulate. Although this idea has been suggested several times throughout the literature, the first formal definition was presented by in 1977 by Wiegand et al. [52, 53] In order to fit the definition of the postulate, the data have to meet the following conditions: the compositional differences between sources must be greater than the compositional differences within each of the given sources. These compositional differences are expressed in the elemental signature of the sources.[54] There are additional assumptions about the data, which must be considered in order to fit the provenance postulate model. Wilson and Pollard[53] summarize these six assumptions as follows: (1) the chemical "fingerprint" from a source is represented in the artifact with no changes (or that the changes can be predicted and modeled, as in ceramics); (2) the source existed in ancient times, and is related to geographic identity rather than archaeological identity; (3) the differences in the "fingerprints" can be measured with adequate precision to differentiate between the sources; (4) that the mixing of

pure raw source materials either does not exist or the possibilities for mixing are understood; (5) that the diagenetic process (alteration of material over time) does not affect the "fingerprint" of the sample or that the diagenetic processes are understood; and (6) the interpretation of the data from an archaeometric project can be modeled by human socio-economic or other anthropological behaviors.[53] In addition, all relevant sources must be characterized in order to assign an artifact with confidence. Ideally, these parts of the provenance postulate are fulfilled by the research design and resulting data and analysis.

Archaeologically, provenance studies have been used to reconstruct ancient exchange routes, to interpret ancient social interactions, and to understand ancient economies. Two different approaches for provenance studies have been described by Glascock and Neff.[55] One approach is to characterize known sources, and understand the variability or differences between sources. In this case, "source" refers to the raw material source only.[56] Then, artifacts are analyzed and attributed to these characterized sources according to the best agreement between the compositional profiles of the artifacts and the sources. There is always a possibility for unknown sources or sub-sources to exist, and these commonly appear in the data analysis as outlier points on bivariate plots. These points then suggest the need for further identification and characterization of sources.

In the second approach, unknown artifacts are sampled and analyzed as a group. Multivariate statistics and pattern recognition are used to cluster the samples into meaningful groups. These statistics help to reduce massive amounts of data and identify the patterns within the data. Finally, archaeological conclusions can be drawn from the attributions of the artifacts to a particular group or origin.[55]

Provenance studies are more successful for some materials than others. Materials chemically unchanged or unmodified from the source such as obsidian, are the best-case scenario for sourcing studies. Characteristic trace elements in obsidian are integrated into the glass matrix, and the elemental patterns do not change over time. In addition, the volcanic glass is homogenous, obsidian sources are chemically unique and are created in specific volcanic regions. As a result, the artifacts can be directly traced to their sources. An exception is chert, which is also unchanging over time, but difficult to source.

Ceramics, however, present a much different case. They are composed of one or more clays and other materials (i.e., temper) mixed by humans and fired. Therefore, the trace element signatures of the artifacts are different from the clays and other raw materials used, and the particular recipe used to make the clay fabric. Fired ceramics are susceptible to diagenetic changes from the environment, possibly altering the trace element signature from the original source. Nevertheless, patterns relating to a particular workshop or area of regional pottery production can be identified and reasonable comparisons can be made between ceramics and clay sources.

Ochre presents yet a different set of challenges for provenance studies. Ochre sources have not been elementally characterized as extensively as ceramics and obsidian. Sources are widespread and not limited to a geographic region. Diagenetic changes can influence ochre materials over time. There is a high likelihood that ancient people mixed ochre with other pigments and binders, which further change the elemental signature. In addition, ochre-based pigments are often used as thin layers on artifacts and sample recovery can be difficult. However, in these initial studies, larger masses of ochre were used for sampling.

These issues and others will be discussed for the three materials presented above and the opportunities and challenges of examining the provenance postulate with each material.

Sampling and Statistical Methods

As part of any study, the artifact sampling and study design are important components even before considering aspects of multivariate statistical analysis. For characterization of artifacts, multiple sampling (ideally in the hundreds of samples) from several archaeological sites may be necessary to understand complex anthropological questions. Usually, a more accurate picture of variability can be developed as more and more samples are analyzed.

Multi-elemental analytical techniques, such as those used in this study, are important for determining as many elements as possible and lead to a more complete understanding of the sample. Certain elements may be useful for discriminating sources and artifact groups, but they may not be effective for others. In addition, some elements may be useful in one region or project but not others. Some authors[57] maintain that a select set of elements be used in statistical analysis, and that using all elements provided may actually confound the results. However, for introductory studies where the patterns are not known, it is essential to determine as many elements as possible.[56] The results of a study for a certain type of artifact or geographical region may provide an idea of the elements significant for discriminating between groups. After completing several exploratory studies, a smaller subset of distinguishing elements may be found to identify patterns for an artifact or region.

The ultimate goal of the multivariate statistical analysis is to understand the variance across the data set and to determine group or source associations based on pattern recognition. For most archaeological data sets, the amount of available information is quite

large. Statistical methods are used to identify complex patterns and trends within the data, although some patterns in the data may be obvious with minimal statistical treatment. Ideally, chemically similar samples will cluster into groups in both elemental plots and "hyperspace" (discussed later), representing affiliations based on original geochemistry. The results of the multivariate analysis can be interpreted for conclusions about artifact composition and exchange. Three statistical methods will be discussed in this chapter for the initial and iterative analysis of data sets. These include cluster analysis, principal component analysis (PCA) and canonical discriminant analysis (CDA). All of the multivariate statistical methods discussed in this chapter must be used with caution. While multivariate analysis can be used to uncover the data structure, in some ways it also imposes a structure on the data.[58]

Data transformation

An advantage of the analytical techniques used in these studies is that the methods are quite precise and accurate and, therefore, the data can be modeled using standard statistical methodology. For a given data set, the concentrations of elements may range over several orders of magnitude, from parts per billion (ppb) for trace elements to weight percent (%) for the matrix elements. It is difficult to make comparisons between measured variables containing large values with measured variables containing very small values without the possibility of favoring the larger values. However, by employing a $\log_{10}$ transform, any possible "weighting effect" of particular elements due to high concentrations is moderated, and all values are essentially on the same order of magnitude. For nearly all statistical analyses, data are transformed into the $\log_{10}$ values or standardized before being used in any statistical routines. In addition, $\log_{10}$ transform reduces the effects due to possible non-

normal distribution of the elements.[13] After the transform, the data are assumed to be log-normalized.[59]

In the MURR Archaeometry Lab procedures, when an element is not detected, a value of 0 is reported. Since it is not possible to take a $\log_{10}$ transform of the value 0, other substitutions are made. In the GAUSS routines,[13, 60, 61] (originally written by Hector Neff) , a small number near zero is substituted. This substituted value is calculated by the minimization of the Mahalanobis distance (discussed later) from the sample to the group centroid based on all other elements, such that the substituted value does not change the effective Mahalanobis distance for the sample from the centroid of its assumed group. For an introductory analysis the substitution is based on the whole data set as the group calculation, although substitutions can also be made based on subgroups of the data as determined in later data analysis. The substitution of these non-zero values allows the use of the element in the statistical analysis. For those element(s) where a majority of the samples have zero values, the elements are eliminated from the analysis.

Multivariate Statistical Analyses

From any given analysis, a large amount of elemental data usually is produced. In a typical INAA experiment, over 30 elements can be analyzed, multiplied by the number of samples, which often can reach into the hundreds. XRF and PIXE analyses may produce a similar number of element variables. Multivariate statistics provide a way to both model the data and understand the data structure through pattern recognition.[62]

For artifact types such as ceramics and obsidian, elemental analysis has been used to understand the fundamental geochemistry of the raw materials as well as the finished

artifact.[13, 61] Elemental analysis leads to the establishment of chemical patterns or "fingerprints" that are characteristic of a particular group. Analysis of both sources and artifacts can be used to locate ancient sources, understand ancient technologies and map ancient exchange.[13, 55, 61] These methods have been applied in chemical composition studies, typological studies and inter-assemblage comparisons.[63] Multivariate statistical methods are essential for not only distilling trends from a large data set, but also for discerning complex relationships between elements that co-vary in a data set, structure in a data set, and test hypotheses.[58, 64] Co-variance of elements in of the original materials (such as the rare earth elements) is common for geological samples, which comprise the majority of archaeological samples investigated.[13] Variation of elements in a data set may also be related to both natural and cultural influences, so these need to considered when interpreting archaeometric data.[58] For example, observed dilution of the samples in a data set may erroneously provide data that suggests a different grouping. An example of dilution is the addition of temper to a ceramic.[58, 61, 65]

Multivariate analysis techniques use the multidimensional model, where a point on a plot represents each sample in multidimensional space. The dimensions are the elemental variables measured. Within the multidimensional space (i.e. "hyperspace"), points of related samples form groups depending on sample composition.[64] The centroid of each group can be mathematically determined.

Sample variance can be described by the following equation:[52]

$$\sigma_m^2 = \sigma_n^2 + \sigma_a^2 + \sigma_p^2 \qquad \text{Equation 2.1}$$

where σ_m^2 is the total variance, which is a sum of the variance from the group composition σ_n^2, analytical errors σ_a^2 and sample preparation σ_p^2. Therefore, the total variance is the standard deviation of σ_m (measured mean) squared.[13, 64] This expression quantifies the variance of concentrations around the element mean. Sample covariance can also be calculated, and it is defined as the shared variance between two elements and their joint mean:

$$c_{xy} = \frac{\sum_{i=1}^{n}(x_i - \bar{x})(y_i - \bar{y})}{n-1} \qquad \text{Equation 2.2}$$

where x and y denote the two elements that co-vary, x_i and y_i are the concentrations of elements x and y in sample i, $\bar{x}$ and $\bar{y}$ denotes the mean concentrations for elements and n is number of samples tested.[13, 59, 64] The variance of x is defined as:

$$\sigma_x^2 = \frac{\sum_{i}(x - \bar{x})^2}{n-1} \qquad \text{Equation 2.3}$$

and the variance of y is defined in a similar manner. Equation 2.4 describes the correlation between x and y:[59]

$$r = \frac{c_{xy}}{\sigma_x \sigma_y} \qquad \text{Equation 2.4}$$

Equation 2.4 is the Pearson's correlation (r) which is discussed later in this section. Values for *r* range from -1 to +1, with +1 indicating perfect correlation and -1 representing a perfect inverse relationship. The units of covariance are the same units of *x* and *y* being tested, whereas correlation is dimensionless. Correlation is more sensitive to the "shape" of the distribution rather than the magnitude.[66]

Both sample covariance (Equation 2.2) and the sample correlation coefficient (Equation 2.4) are used in calculation of the covariance/correlation matrices used in multivariate statistical analysis discussed in this chapter. The results of Equations 2.1 and 2.2 are used to construct the variance/co-variance matrix used in PCA. Each element is assigned to a row and a column in a matrix, with the covariance values reported at the intersection of the elemental values. When the same elements intersect, variance values are used, as the covariance for the element against itself is equal to the variance.[13, 64]

Euclidean distance is also used in several of the routines to calculate the "straight-line" distances between samples. Equation 2.5 is the function for calculating Euclidean distance between two points x and y in n-dimensional space (hyperspace).

$$d(x,y) = \sqrt{\sum_{i=1}^{n} (x_i - y_i)^2} \qquad \text{Equation 2.5}$$

Since multivariate routines are computationally tedious, most are written into software packages that can be used easily on most personal computers. Some are commercially available such as SPSS, and others, like the GAUSS software at MURR are written for particular applications.[13, 60, 61] Although the statistical software facilitates the

computation of the procedures, the results must be interpreted carefully such that incorrect assumptions about sample or group associations do not result.

Cluster Analysis

Cluster analysis is frequently employed as an initial method to discern possible patterning or clustering in the elemental data. The term cluster analysis covers many methods used for classification of samples into meaningful groups. Clustering routines can be used in a variety of ways depending on the data and the structure of the clustering program. Some examples are Clustan, SPSS, and the cluster routine in the GAUSS software created and maintained at MURR.[13, 61] Although several clustering approaches are available, each routine strives to classify the samples into chemically-related groups. These categories are designed such that members of a group are alike within the group and different from other groups in the data set and are usually based on Euclidean distance.[67] Whether or not these groups are meaningful to the archaeological question is left up to the user for interpretation.[56] Cluster routines can also be used for hypothesis generation and testing of data sets.[66]

Hierarchical cluster analysis forms clusters of related samples.[58] Similar samples are grouped together, then the groups are linked together by similarity, and then grouping the remaining samples until all samples are related to each other through a dendrogram. This "tree-like" structure allows a one-dimensional visualization of how the samples are related to each other and to other clusters. Typical methods for grouping samples include calculating the dissimilarity between objects by the squared Euclidean distance among others.

$$d_{jk}^2 = \frac{1}{n}\sum_{i=1}^{n}[C_{ij} - C_{ik}]^2 \qquad \text{Equation 2.6}$$

Squared Euclidean distance is defined above, where the distance squared between samples *j* and *k* is calculated from the concentrations (*C*) of *j* and *k*. The value *n* represents the number of elements used in the analysis and behaves as a scaling factor.[13, 64]

A clustering algorithm, or linkage, can be calculated by several methods, with the most common methods being single linkage, complete linkage, average linkage cluster analysis and Ward's method.[59] Single linkage combines samples by finding the two most similar samples in the data matrix. Complete linkage forms groups by combining a sample into a group where the sample is similar with all members of the group at some pre-determined level. Average linkage is a combination of single and complete linkage, where samples are placed due to their similarity to members of the group as well as similarity to other samples in the matrix. Ward's method linkage finds the solution for the minimum variance in clusters.[66] It should be noted that each of the mentioned cluster analysis methods and others may produce different results. This is due to the fact that the classification routines highlight certain aspects of guidelines for group formation, and the same data set may have different results from different routines.[66] In addition, cluster analysis is a method that simultaneously uncovers and enforces data structure.[66]

For the case of uncorrelated data, cluster analysis provides a means to initially categorize samples. Although cluster analysis is a good beginning for data analysis, it is not regarded as a final method for group identification. One aspect that cluster analysis does not consider is the correlation and co-variance of elements. Correlation between elements are

observed frequently among the rare earth elements and other element groups in geological samples. Therefore cluster analysis does not provide a perfect solution for grouping of artifacts and only presents a starting point in data analysis.

Results of cluster analysis are generally plotted as a dendrogram, with linkage distance on the abscissa and the samples on the ordinate. Branches link the samples together to visually show group associations. For this dissertation, cluster analysis was performed in both GAUSS and Clustan[68] (Clustan Graphics, Edinburgh, Scotland) to initially investigate possible grouping within the data sets. Results from the cluster analysis were used as a starting point for data analysis but were not accepted as the final clustering results. Instead, results from PCA and CDA were used for final data interpretation.

Principal Component Analysis

Principal components analysis (PCA) has three main functions: 1) to remove correlation between variables in the data set, 2) to transform data into a new set of axes that preserves the Euclidian distance between samples and where data variance can be observed, and 3) to reduce the number of variables necessary to describe most of the variance in the data.[13, 64, 69, 70] A requirement for the data set is that the number of samples be equal to or greater than the number of variables. The use of PCA assumes that the data has some structure and that this structure can be modeled. It also presumes that the reduction of dimensions can lead to data interpretation without significant loss of information. In addition, the use of PCA in this study has a fundamental assumption that group separation has a chemical origin. If elements are correlated (e.g. rare earth elements), transformation into PC space allows a way to differentiate the elements and visually identify any groups.

The reduction of variables (elements) in PC space is important as a few principal components can be used to explain the same data in a few dimensions which is easier to conceptualize than 30 or more elemental variables measured in this study.[59] Displaying the samples in principal component (PC) space helps to identify patterns or groups within the data.

A way to describe PCA is as an uncorrelated linear combination of variables, where the coefficients are calculated to give the greatest distance between points on an axis.[64] Principal components are essentially linear transforms of the variables that maximize the geometric distance between samples. The first PC describes the maximum variance, the second PC describes the remaining variance after removing the first PC and is orthogonal to the first PC, and so on throughout the number of PCs in the data set. The first PC describes the maximum variance, the next PC (2), describes the maximum of the remaining variation.[58] There will be the same number of PCs as variables. The equations describing the transformation are:

$$P_1 = a_{11}X + a_{21}Y + a_{31}Z + \ldots + a_{i1}Q \qquad \text{Equation 2.7}$$

$$P_2 = a_{12}X + a_{22}Y + a_{32}Z + \ldots + a_{j2}Q$$

where the coefficients a_{ij} are used as the linear transform to arrive at the PC values in PC space, and X,Y,Z represent the elements (variables). The coefficients can then be applied to any sample, and then the sample can be plotted as a point in a graph of PC2 vs PC1.[59] Another advantage of PCA is that the analysis maintains the original variation in the data set.[54]

PCA can be used to describe the variance along two principal components and thus facilitate the search for patterns in the data. However, one pair of PCs may not adequately describe the whole data set, and multiple PCs may need to be used. In the GAUSS program, a results file is produced listing the percentage of the variance contributed by a component and the sum total of variance subsumed by successive components. The first PC reported describes the most variance, the second PC describes most of the remaining variance, and so on successively throughout the remaining PCs. Also reported in a results file are the eigenvalues associated with each element. Eigenvalues are the coefficients that transform the elemental concentration into a score on the eigenvector.[61]

Two types of analysis for PCA have been developed. R-mode factor analysis focuses on interrelationships between variables, and Q mode is based on interrelationships between objects.[58] By using simultaneous RQ factor analysis with variance-covariance matrix, analysis allows presentation of the results of both the data points (samples) and element vectors on the same bi-plot.[61] Simultaneous R- and Q-mode analysis was used for all of the PCA analyses presented in this study using the GAUSS software and is common in many recent archaeometric analyses.

In a R-Q mode plot, he vectors are projected onto the 2-dimensional plot and are a reflection of the coefficients in the PC equations. Each vector is related to the square root of the associated eigenvector.[61, 63, 64] Two vectors that are orthogonal to each other in PC space represent the greatest variance between sample. These types of plots are ideal for identifying the elements that are responsible for the most variance in the data set as well as how the individual samples differ on these elements. An examination of the first few PCs often

explains the majority of the variance, allowing identification of patterns in the data set corresponding to groups of data.

Bivariate elemental plots are used to identify and refine groups within the data set suggested from the PC analysis. Confidence ellipses are drawn around the groups to show the probability surfaces (in two dimensions) for group membership. The ellipses are drawn at a constant Mahalanobis distance from the group centroid.[64] The shape and distribution of the Mahalanobis distance are defined by the density of data points and their direction away from the centroid. Typically, the ellipses are drawn at the 90 or 95% confidence level. For this study, PCA was used to determine the data structure and possible groupings within the data.

Additional tests are featured in the GAUSS software for determination of group fit. These post-classification analyses are based on Mahalanobis distance probability calculations. Results of these post-classification tests can assist with group assignments and determination of outlier samples.

Mahalanobis distance calculations take into account correlation between variables and the group association. Mahalanobis distances are used to calculate probability of membership of a sample to a group.[71] The equation for Mahalanobis distance is:

$$D_{kA}^2 = \sum_{i=1}^{n} \sum_{j=1}^{n} [C_{ik} - A_i] \cdot I_{ij} \cdot [C_{jk} - A_j] \qquad \text{Equation 2.8}$$

where the distance between sample k and the centroid of the group A is calculated using the mean concentrations of elements i and j in the group (A_i and A_j), and I_{ij} is the ijth elements

inverse for the variance-covariance matrix.[64] For a Mahalanobis distance calculation, the number of samples used must exceed the number of variables by at least one.[71]

Canonical Discriminant Analysis (CDA)

Canonical discriminant analysis is a multivariate method different than principal component analysis with a different set of assumptions. Instead of determining structure or groups within a data set, the data are assumed to belong to one or more mutually exclusive groups where the data structure has already been determined.[72] In addition, the data are assumed to exist in equal covariance matrices and have a multivariate normal distribution.[72]

CDA determines the factors that distinguish between known groups, assuming that the group characteristics are different from the outset. It used as both a discrimination and a classification technique.[73] Because assumptions about the groups have already been made, it is less of an exploratory technique and more of a testing or classification method.[59] Similar to PCA, CDA results also determine linear combinations of variables. For CDA, these linear combinations of the data produce the greatest distance between known groups.[13] For CDA analysis, data are also transformed to the $\log_{10}$ and assumed to be normalized data. A generalized form of the CDA equations are provided by Klecka:[72]

$$f_{km} = u_o + u_1 X_{1km} + u_2 X_{2km} + \ldots + u_p X_{pkm} \qquad \text{Equation 2.9}$$

where f_{km} is the score of the CD function for the case m in the group k, X_{ikm} is the value of the variable X_i for the case m in group k, and u_i are the coefficients of the CD function.[72] The variable u is calculated such that the group means are as dissimilar as possible for the first

CD function. The second function calculates the *u* coefficients to describe the maximum uncorrelated differences (functions perpendicular to each other) between groups. This process is continued iteratively until all of the functions are calculated. In CDA, the analyst determines the assumed number of groups (n). The number of discriminants produced for an analysis is n-1. In addition, there must be at least two samples per group, and the number of variables must be two less than the total number of samples.[64] The group means are described as centroids, around which the individual data points cluster. CDA analyses are calculated based on the Mahalanobis distance (distance between sample and centroid) as described above. The group centroids are compared for similarity or dissimilarity.

Two approaches are used in CDA: concurrent and stepwise. Concurrent CDA analyzes between group variances by all variables simultaneously, and minimizes the differences between group means as compared to the variance within groups. Stepwise CDA analysis starts by calculating the best discriminating variable, then proceeds through the next best discriminating variable in a stepwise fashion.[73] Similar to PCA, there are also tests that can be performed after the analysis on the data to determine best fit for individual samples. The GAUSS software has routines (classification functions) for probability of group membership in the CDA module.

After determination of the discriminant functions, the Wilks' lambda test is used to examine the statistical significance of group separation. In a results report from the GAUSS software, the Wilks' lambda (multivariate analysis of group means) and its significance are reported. For a Wilks' lambda calculation, matrices are calculated for between-group and within-group differences. The determinants of these matrices are used in the Wilks' lambda calculation:

$$\Lambda = \left| \frac{SS_{wg}}{SS_{wg} + SS_{bg}} \right| \qquad \text{Equation 2.10}$$

where SS_{wg} represents within group differences and SS_{bg} represents the between group distances.[74] As Wilks' lambda is an "inverse" measurement, a smaller value of the Wilks' lambda indicates greater separation between the groups. The value for lambda ranges from 0 (greatest difference between groups) to 1 (group centroids are the same).[72] In this dissertation, CDA was used to test the groups identified from the PCA analysis performed earlier, to ascertain the distinctiveness of groups produced by PCA analysis. Plots of the CDA results follow the PCA analysis in individual studies.

OCHRE STATISTICAL MANIPULATIONS

The study focuses on the determination of the trace-element pattern or fingerprint related to the geochemistry of the source. The first step in data analysis is the transformation of the data to the $\log_{10}$ values of the raw elemental data. This is the normal statistical procedure for other data taken from elemental analysis as described above. For the ochre study, multivariate statistics as described were initially applied of the $\log_{10}$ transformed data. An alternate approach, not taken, would have been to standardize the data by normalizing each element to the group mean. Studies have shown the results to be nearly equivalent. Standard statistical routines as described above (zero-value substitution, R-Q mode PCA analysis etc.) were performed using the GAUSS software at MURR.

Initial statistical analysis indicated that the Fe concentration was actually driving the majority of the variance in the total data set content, rather than the trace elements. The trace elements that define the "signature" of a particular ochre source location can be anticipated based on past research. Figure 2.1 shows a principal component plot of initial data taken from the Missouri and Texas ochre study.

PC 3 is on the ordinate and PC2 on the abscissa. Values (eigenvalues) for the PC axes come from the linear transform of the data into multivariate space.

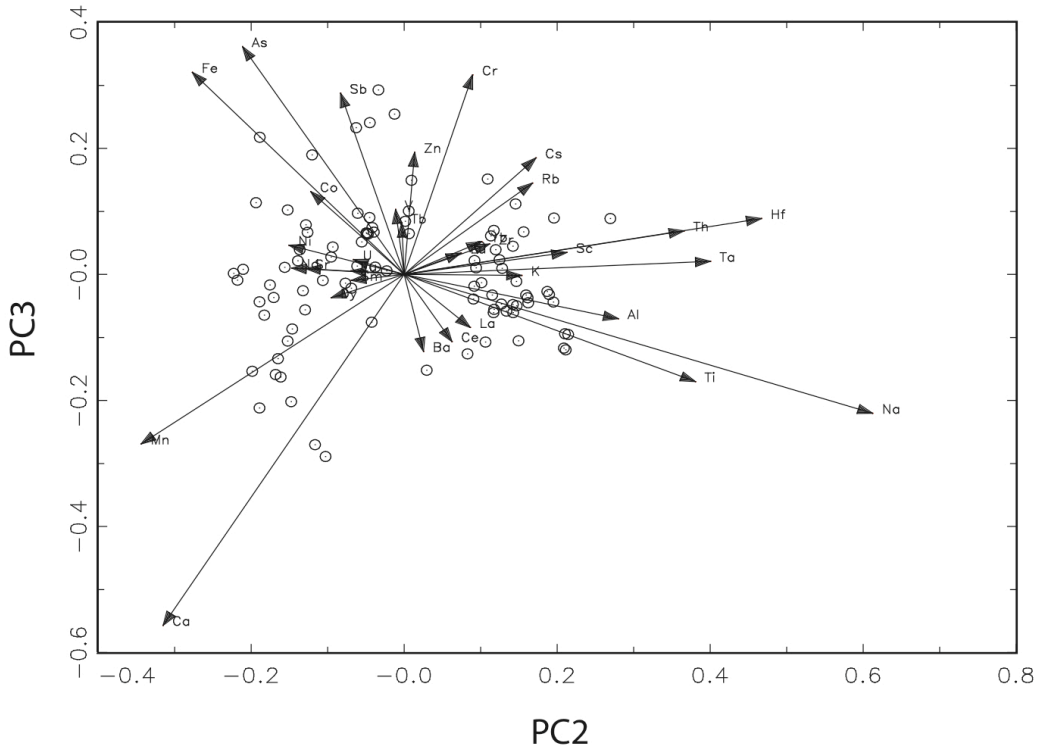

Figure 2.1: R-Q mode PC 3 vs. 2 for combined Missouri and Texas ochre data, indicating influence of Fe on the data.

When the sample identification numbers were referenced to the original data in the plot, it was found that PC1, 2 and 3 are driven by Fe concentration. Samples with high iron are in the same area of the Fe vector of Figure 2.1. Many of the PC plots generated with this data exhibited similar patterns. Despite the $\log_{10}$ normalization, the greater variation in the Fe concentration appears to be influencing the PCA as well as clouding interpretation of the elemental signature of ochre.

Another noticeable aspect of this plot is that the vectors for elements Na, Ti and Al are opposite Fe. This indicates that these are the major elements that make up the rest of the matrix composition of ochre besides Fe, and share an inverse relationship with Fe. Silicon is not routinely measured by INAA at MURR, so values for it are not available. However, it was found through XRF that silicon is one of the other main elements in ochre, as discussed in Chapter 4. Other elements group together in Figure 2.1, suggesting chemical relationships in ochre. An example of the grouping is the rare earth elements and the association of Cs and Rb. This grouping of elements from the same groups of the periodic table suggests geochemical relationships between these elements and it will be discussed in Chapter 4.

This situation of iron dominating the first PCs is less common than for other types of archaeological samples. For instance, obsidian is consistently about 70% silica (SiO_2), although ceramics may have a more varied makeup. There are few archaeological examples where the matrix has marked variability. As explored in Chapter 4, the definition of ochre can be vague. Concentrations of Fe in ochre can differ over a rather wide range, from 1% to nearly 65%. The variation in Fe may obscure the variations in other components such as the trace elements. For instance, if a trace element such as La is in high Fe matrix, after statistical analysis it could appear quite small relative to a La concentration in low Fe matrix.

Ratios to Iron in Ochre

The main goal of the study is to determine the trace element patterns in ochre. As a result, mathematical adjustment to the data was necessary to allow one to explore the trace element data relative to the Fe matrix for every sample. For subsequent statistical analyses of ochre samples, all values were presented as a ratio to Fe. A relationship between two theoretical sources is presented in Equation 2.11.

$$\left(\frac{[La]}{[Fe]}\right)_{source1} \; vs. \; \left(\frac{[La]}{[Fe]}\right)_{source2} \qquad \text{Equation 2.11}$$

Using ratios to Fe will also mitigate the influence of large differences in concentration in Fe across the entire data set for either local or regional studies. Moreover, the transform to ratios does not change the information in the data and in theory, therefore should not affect the resulting interpretation.[75] These ratios were then used in the multivariate statistical analyses as described above. This log-ratio approach (Fe-ratio and subsequent log 10-transform), is similar to other statistical treatment of data reported in the literature where a particular component in all of the samples may act as a diluent or a factor that would affect trace element concentration interpretation.[59] Although this exact method presented here was not found in the archaeometric literature, these types of transforms have been used previously for multivariate analysis and do not affect the interpretation of the data.[75] However, it is slightly different than the log ratio method presented by Baxter et al.[76] and Aitchison et al.[75, 77, 78] In their papers, the ratio of the element of interest to the

standardized value (geometric mean) of the matrix element is used.[76] First, the geometric mean of the *ith* case is defined:[76]

$$g_i = (x_{i1}x_{i2}...x_{ip})^{1/p} \qquad \text{Equation 2.12}$$

where g_i is the geometric mean, x is a sample and p is the variables in a $n \times p$ matrix. The centered log ratio is the following:

$$y_{ij} = \log\frac{x_{ij}}{g_i} \qquad \text{Equation 2.13}$$

where any sample x is divided by the geometric mean g_i.[76] The use of the geometric mean is another way to standardize the data. This version of the log ratio has been used most often with fully compositional data where all elements and oxides sum to 100%. As all of the elements were used in these studies, some variance was influenced by the major matrix elements. In this dissertation, those major matrix elements negatively correlated with iron were removed prior to statistical analysis as discussed in the next section. Furthermore, the elements for which INAA has poor sensitivity (Ni, Zr), as well as other elements with a large number of zeros were eliminated from the analysis. This has the effect of reducing potential problems with elements below limits of detection or those with possible low precision. The data used in this dissertation are elemental data only (not fully compositional), and the method presented is not standardized in the same manner. Instead it uses the simple ratio of the element to iron in each sample as presented in Equation 2.11.

Pearson's Correlation

Ultimately, the goal of the ochre study is to understand the trace elemental fingerprints associated with the individual ochre source. As ochre is made up of other minerals, the trace elemental signature must be associated with the original Fe concentration. In order to extract this association between the trace elements and the Fe concentration, a Pearson's correlation was used. This statistical test reveals the relationship (ideally linear) between two sets of data, and determines whether the variables are proportional to each other. The relationship is modeled by a least-squares linear regression.[67]

$$r_{xy} = \frac{\Sigma(x_i - \bar{x})(y_i - \bar{y})}{(n-1)\sigma_x \sigma_y} \qquad \text{Equation 2.14}$$

where x_i and y_i are individual measurements; $\bar{x}$ and $\bar{y}$ are the sample means, and σ_x and σ_y are the standard deviation of the sample sets.[67] This statistical test can be used to determine an association between the element of interest and Fe. The returned coefficient r from the test is the slope of the line that models the relationship of the variables. The range of values will be between -1 and 1, with 1 being the highest (positive) correlation and -1 being the most negative. The reported score can fall anywhere between these values, with many reported as close to 0, making a clear determination of correlation difficult. The Pearson's results were compared for each element for significance on the 95% confidence interval (α=0.05). Elements with a negative Pearson's score were eliminated from further statistical analyses. These elements are associated with accessory minerals and are not part of the iron oxide signature. This selection of a group of elements for data analysis is an appropriate

method for determining variability in ochre sources as discussed earlier. Results of these data will be discussed in Chapter 4.

CHAPTER 3: INAA AND PIXE ANALYSIS OF CABORN-WELBORN CERAMICS

INTRODUCTION

The Caborn-Welborn (C-W) phase[79, 80] dates to the late Mississippian period (A.D. 1400-1700) and the distribution of C-W sites is centered around the confluence of the Wabash and Ohio rivers in the United States as show in Figure 3.1. To date, more than 80 C-W sites have been recorded within a 60 km long stretch of the lower Ohio Valley in Indiana, Kentucky, and Illinois.[80] The sites range from small farmsteads encompassing less than a quarter of a hectare to large villages that cover more than 14 hectares. C-W sites tend to cluster within three distinct sub-areas in the C-W region: eastern, central, and western. Each sub-area has villages and associated hamlets and/or farmsteads.[80] A further discussion of the archaeological context is discussed in Shergur et al.[81]

In order to assess whether central Mississippi Valley-derived ceramics and Oneota-like ceramics were manufactured from the same clays as other C-W vessels, we investigated the elemental composition of 122 sherds, three daubs, and five clay samples, using instrumental neutron activation analysis (INAA) and particle-induced X-ray emission (PIXE) analysis.

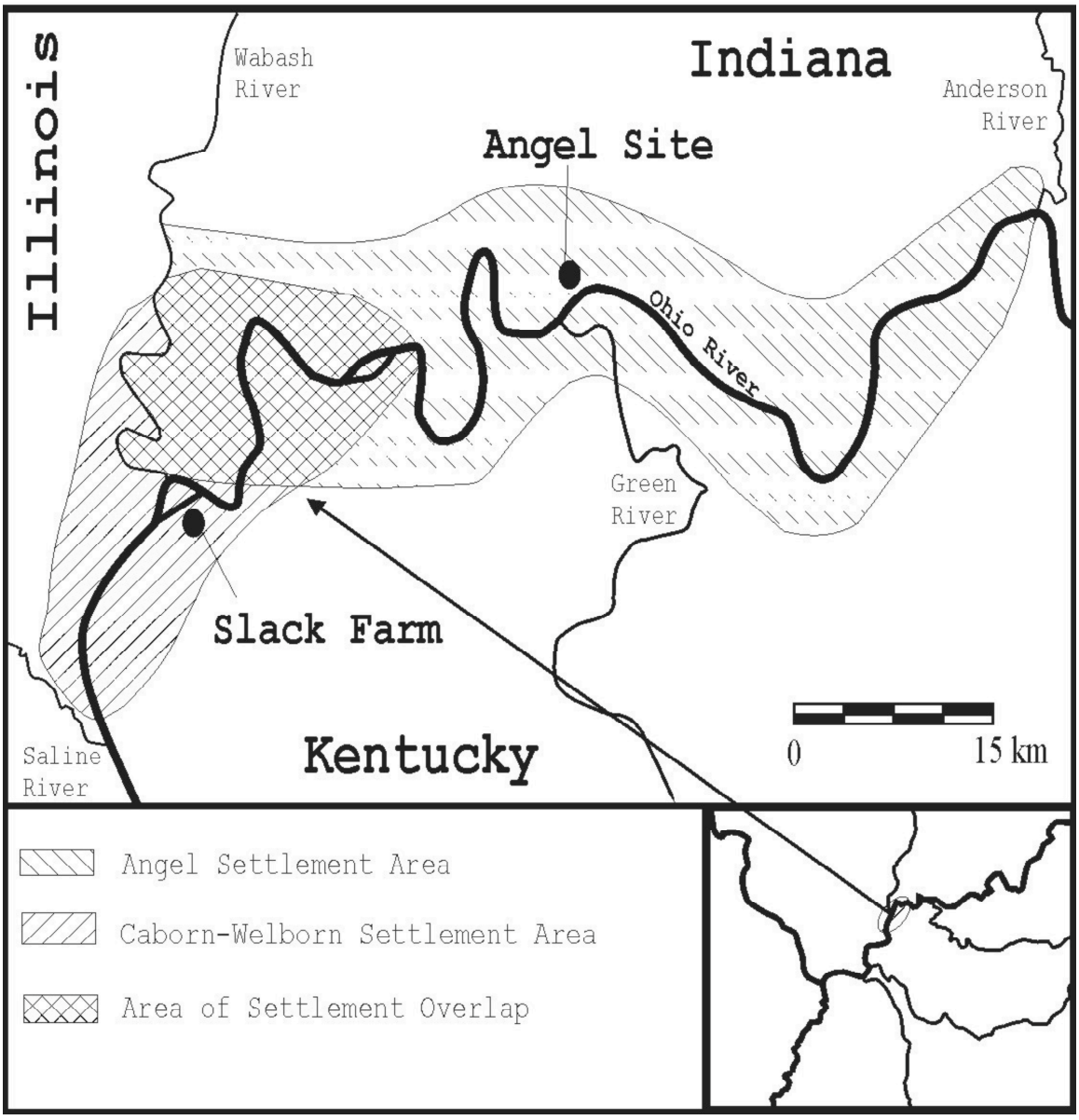

Figure 3.1: The Caborn-Welborn region.

EXPERIMENTAL PROCEDURE

Sample Selection

Ceramic, daub, and clay samples were selected from ten C-W phase sites (Slack Farm [15Un28], Murphy [12Po1], Moore [15Un42], Blackburn [15Un57], Alzey [15He37], Cummings [15He775], Hooper [15Un177], Hart [15He35], Ritz [15He777], and Site [15He110] as shown in Figure 3.2, and from two off-site localities. The largest group of samples (n=55) was recovered from the Slack Farm site, a large centrally located village. In order to characterize the composition of C-W assemblages, all of the major C-W type ceramics and vessel forms were sampled. This included 20 Mississippi Plain jar sherds, 33 Bell Plain bowl and bottle sherds, 28 C-W Decorated jar sherds, seven Kimmswick Plain pan sherds, eight Kimmswick Fabric Impressed pan sherds, one Miscellaneous Incised/Trailed Plate rim, and one Mound Place Incised bowl sherd. In addition to these specimens, three daub fragments and five local clay samples were analyzed.

The Central Mississippi Valley stylistic types selected for analysis were three Campbell Applique jar rims, a Walls Engraved bottle sherd, a Campbell Punctate bottle rim, a Campbell Punctate body sherd, a Campbell Incised rim sherd, a Kent-like Incised jar rim, and a Vernon Paul Applique jar body sherd. Based on a visual inspection of these sherds, the Campbell Punctate bottle rim was thought to be the best candidate for a vessel that was made outside the lower Ohio Valley (CW127). This bottle rim had a small node attached to its neck and is characterized by the Memphis Rim Mode and may have been obtained by Caborn-Welborn people through interaction with Mississippian

groups living in the central Mississippi River valley.[82] Sixteen Oneota-like sherds were also analyzed.

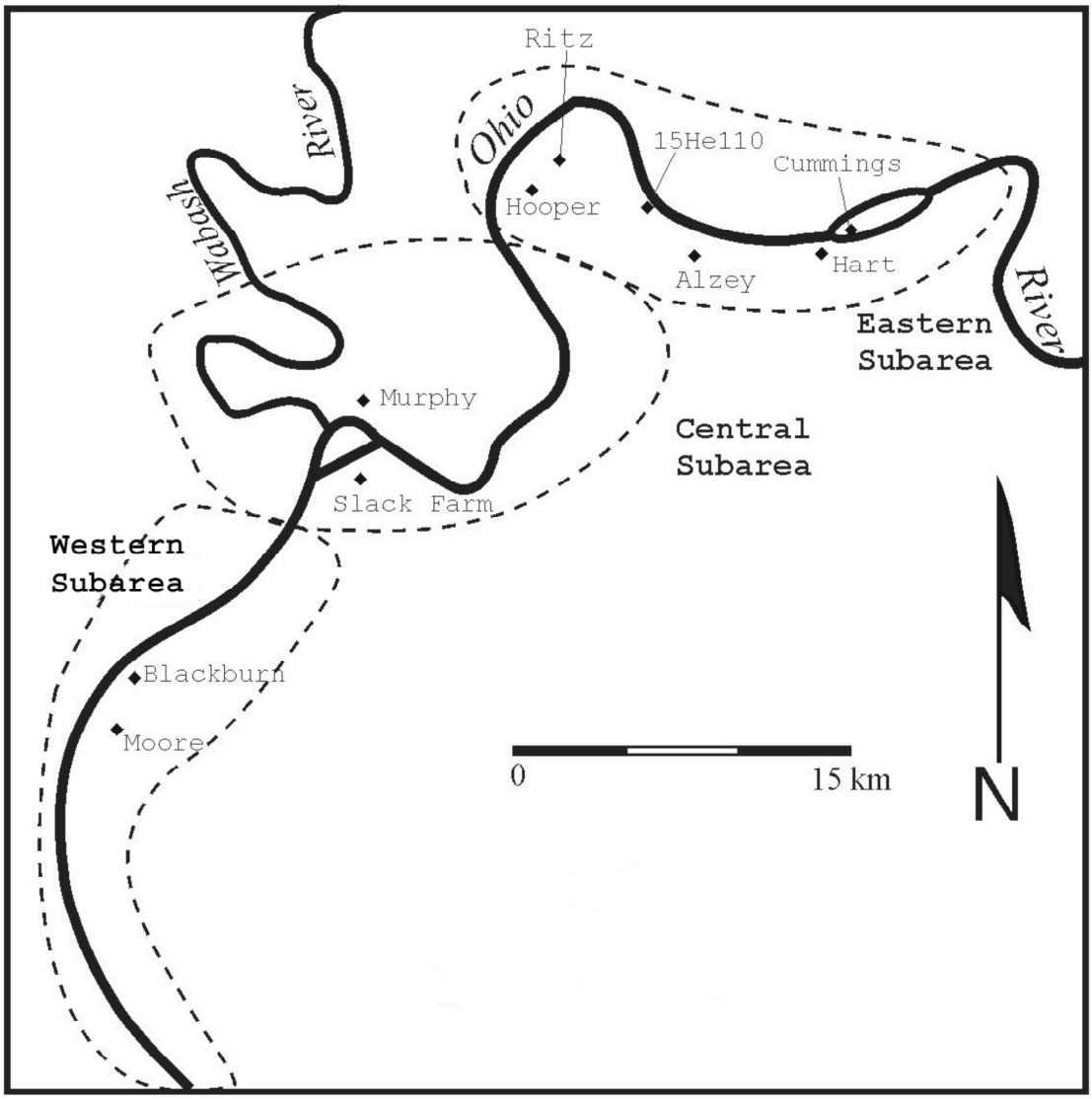

Figure 3.2: The ten Caborn-Welborn phase sites
from which the ceramics were collected.

Sample Preparation

Sample preparation was performed by Jason Shergur. Surface contamination was removed from the sherds using a silicon carbide rotary burr. The "burred" area was then washed with deionized water and stainless steel bone-cutters were used to take the sample. The cut portions were ground with a Brazilian agate mortar and pestle and the powdered samples were dried at 110 ^{o}C for a period of at least 48 hours. Before being ground and powdered, both the clay and daub samples were heated in a muffle furnace at 100 ^{o}C overnight to remove excess moisture. For INAA, approximately 200 mg of powder from each sample was sealed in a pre-cleaned high-purity quartz vial.

Analytical Procedures

Samples and standards were irradiated at the University of Missouri Research Reactor (MURR) for a period of 24 hours. National Institute of Standards and Technology (NIST) standard reference material (SRM) 278 Obsidian Rock was used as the primary comparator standard and SRM 1633b Coal Flyash was used as the secondary standard. At least three samples (~ 100 mg/sample) of each SRM were included in every irradiation. The thermal flux in the irradiation position was estimated at $5x10^{13}$ neutrons cm^{-2} s^{-1}. Following irradiation, two sets of counts were taken on the samples at the University of Kentucky. Seven days after irradiation "mid" counts were acquired for one hour to measure the short-lived nuclides. The samples were then allowed to decay for another three weeks, and three-hour "long" counts were acquired to measure the nuclides with longer half-lives. The gamma-ray spectra were analyzed with the ASAP spectroscopy package from Nuclear Data.

The remaining powder from each pottery sample was pressed into a 25.4-mm diameter pellet for PIXE analysis. The PIXE analyses were performed in order to measure elements not routinely measured by Glascock et al.[13] in a "short" count following a five-second pneumatic tube irradiation. One advantage of PIXE is that it allows measurement of elements such as copper (Cu), gallium (Ga), magnesium (Mg), phosphorus (P) and silicon (Si) that are not routinely measured by INAA. In addition, the PIXE analysis allowed verification of elemental concentrations of analytes that were obtained in both analytical procedures.

A detailed description of the PIXE facility can be found in Blanchard et al.[83] Briefly, protons enter the target chamber by passing through a 7-μm thick Kapton window and X-rays exit through a 2.5-μm thick Mylar window at 45° relative to the beam. The beam, which is at an angle of 23° relative to the sample surface, is swept over the target to irradiate a 16-mm diameter area. The sample chamber is flushed with helium at atmospheric pressure to reduce sample heating and charging, and each sample is irradiated for 15 minutes. For 10 minutes of the 15-minute irradiation, the detector is placed 3.5 cm from the target, a 1900 μm-thick polypropylene filter is placed between the sample and the detector, and the sample is irradiated with a 2.1 MeV proton beam. For the remaining 5 minutes of analysis, the polypropylene filter is removed, the detector is moved further away from the target (7.5 cm), and the sample is irradiated with a 1.6 MeV proton beam. For each bombarding energy, a relative measure of the number of protons striking the target is made by measuring the number of protons that backscatter from the Kapton window. The two spectra are then combined and the thick-target PIXE analysis is performed with a modified version of the

GUPIX PC-based software package.[36] System calibration is performed by analyzing a series of thin-film gravimetric standards from Micromatter, Inc. (Deer Harbor, WA).

RESULTS AND DISCUSSION

Ceramic Composition

The isotopes and gamma rays used in the INAA measurements are listed in Table 3.1 along with the results obtained for the NIST SRM 1633b Coal Fly Ash.

Table 3.1: INAA Results for NIST 1633b Coal Fly Ash Standard Reference Material

Isotope	γ-ray (keV)	Certified[a] (μg/g)	Measured[b] (μg/g)
Mid-Counts			
^{131}Ba	496.3	709 ± 27	800 ± 100
^{51}Cr	320.1	198 ± 5	190 ± 10
^{140}La	1596.2	[94]	90 ± 2
^{177}Lu	208.4	[1.2]	1.2 ± 0.1
^{24}Na	1368.6	2010 ± 30	2000 ± 80
^{147}Nd	531.0	[85]	95 ± 9
^{124}Sb	602.7	[6]	3.8 ± 0.2
^{153}Sm	103.2	[20]	17.4 ± 0.2
^{175}Yb	396.3	[7.6]	7.5 ± 0.3
Long-Counts			
^{141}Ce	145.4	[190]	183 ± 3
^{60}Co	1332.5	[50]	45.4 ± 0.6
^{134}Cs	795.8	[11]	11.1 ± 0.2
^{152}Eu	1408.0	[4.1]	4.19 ± 0.05
^{59}Fe	1099.2	77800 ± 2300	77200 ± 800
^{181}Hf	482.2	[6.8]	7.0 ± 0.1
^{86}Rb	1076.6	[140]	130 ± 10
^{46}Sc	889.3	[41]	40.7 ± 0.5
^{182}Ta	1221.4	[1.8]	1.7 ± 0.1
^{160}Tb	879.4	[2.6]	2.8 ± 0.3
^{233}Th (^{233}Pr)	312.0	25.7 ± 1.3	25.1 ± 0.4
^{65}Zn	1115.6	[210]	260 ± 20

[a] Recommended values are listed in brackets.
[b] Average and standard deviation of the analysis of 7 *ca.* 100 mg samples of the SRM.

Good agreement between the measured and certified values was obtained for every element except Sb and Zn. Antimony is retained in the data set because the value reported for the SRM is only a recommended value. Zinc is also retained in the data set as the Zn concentration values in the ceramics obtained by INAA are in good agreement with the Zn values determined by PIXE.

The concentrations of Al, Ca, Cu, Ga, K, Mg, Mn, Ni, P, Si, and Ti in the ceramic samples were determined by PIXE. A detailed discussion of the accuracy and precision of the PIXE measurements in complex matrices can be found in Wong and Robertson 1993.[22] As the samples were not counted until one week following irradiation, it was not possible to use INAA to measure Ca concentrations because its half-life is on the order of minutes. However, it is necessary to obtain Ca concentration values because Ca is a large constituent of the shell temper.[84] Shell temper is primarily composed of calcium carbonate ($CaCO_3$), and the size and amount of shell temper in a Mississippian ceramic vessel is often related to vessel function.[85] For example, Mississippi Plain jars have larger fragments of shell temper and were fired at lower temperatures than Bell Plain bowls and bottles. If the measured elemental concentrations are not corrected for the shell temper dilution, a misleading variance between the samples will arise due to the concentration of Ca. The concentration of each element (in μg/g) was corrected for shell temper dilution of the ceramic sample using an equation from Steponaitis et al.[85]

$$[Z]_{corrected} = \frac{10^6 \cdot [Z]}{\left(10^6 - 2.5 \cdot [Ca]\right)} \qquad \text{Equation 3.1}$$

The INAA and PIXE database is provided in Appendix I.

Extra-regional Analysis

To determine if ceramics from the C-W region could be distinguished from contemporary ceramics from other regions in the southeastern United States, the results were compared with the work of Steponaitis et al.[85] In this study, the authors were able to assign ceramics from 21 regions to one of four broad geographical areas based on chemical composition (Figure 3.3). A statistical comparison was performed using principal components analysis of the calcium corrected data of values in the two studies using software developed by Glascock[13] and Neff.[61] In order to include the major, minor, and trace elements in the comparison, the analysis was performed on log-10 transformed concentration values. Twenty-one of the 23 elements reported in Steponaitis et al. (1996) were used in the analysis, as values for arsenic and uranium were not considered reliable in the C-W data set.

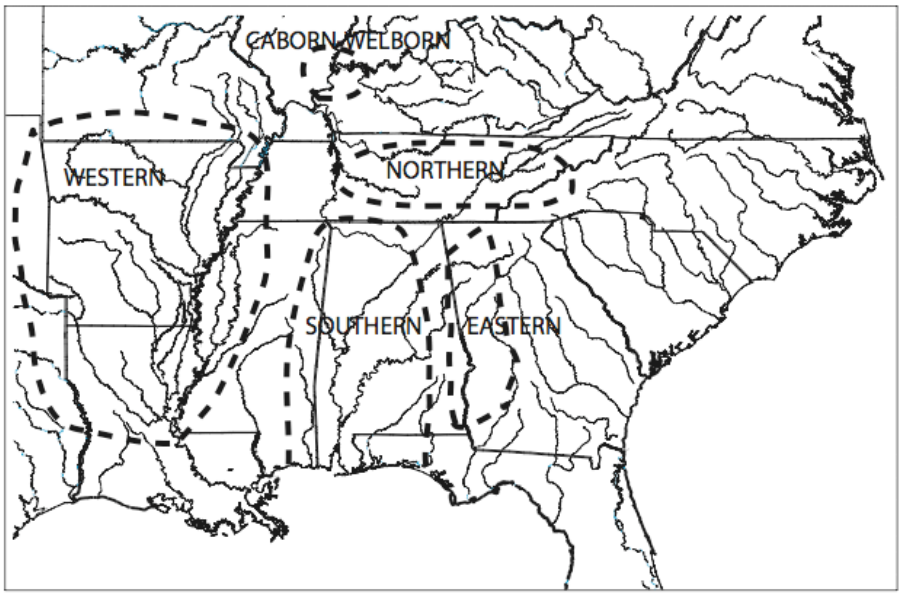

Figure 3.3: The four geographical areas described by
Steponaitis et al. (1996) and the Caborn-Welborn region.

The principal component analysis shows that the C-W samples are a defined, separate group slightly related to the Steponaitis et al. samples. As can be seen in Figure 3.4, there is not a strong overlap of the first two principal components from the C-W data with the published Steponaitis geographic groups. This result is reasonable, because no samples from the Ohio River valley were included in the Steponaitis et al. study. The analysis distinguishes the C-W data from the southern and eastern groups very well. The C-W samples display slight overlap with both the western and the northern groups.

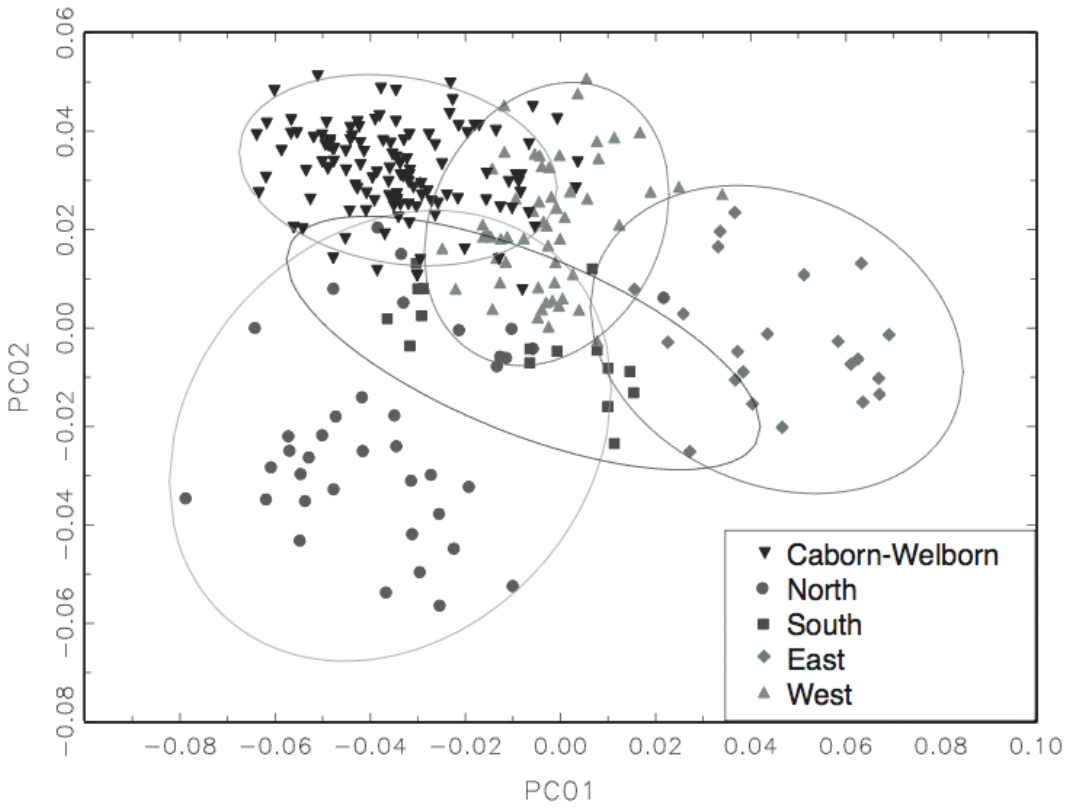

Figure 3.4: Plot of principal component 2 (PC02) vs. principal component 1 (PC01) demonstrating the separation between the Caborn-Welborn group and the groups identified by Steponaitis *et al*. The ellipse confidence intervals are ninety percent.

A posterior classification of the samples compares the C-W group to three Steponaitis subgroups (northern, eastern, and western). This posterior classification takes group dispersion into account using Mahalanobis distances.[13, 61] The southern Steponaitis group was not used in this analysis because it contained only 16 samples that were spread over a large ellipse. While the posterior classification attributes 61% (74/122) of the C-W samples to the northern group and 38% (46/122) to the western group, the probabilities for these attributions are very low (most less than 10%, many less than 1%). These results suggest that the ceramics from the lower Ohio Valley form their own geographically and chemically

distinct group. An additional posterior analysis was performed on the C-W data using a discriminant classification based on the Mahalanobis distance probabilities.[13, 61] This program ascertains how well the groups are defined in terms of each other. In this analysis, the C-W data was considered a separate group. This analysis shows that the C-W data are more closely associated chemically within the C-W group than with the Steponaitis subgroups. Of 122 C-W samples, only eight were potentially placed with other Steponaitis subgroups, and again the probabilities of membership in these eight cases are quite low. This analysis confirmed that the C-W ceramics clustered together and were not placed well in another Steponaitis subgroup.

An additional PCA analysis was performed with the concatenated C-W and Steponaitis data. This statistical analysis was performed to observe how the data behaved when the Steponaitis and C-W sherds were considered to be one large data set. The coefficients from this analysis were applied to the geographic Steponaitis subgroups (northern, southern, eastern, western), and the C-W set itself, and the PC scores were plotted. As shown in Figure 3.5, while the centroids of the groups have shifted, the C-W data is still closest to the northern and western groups.

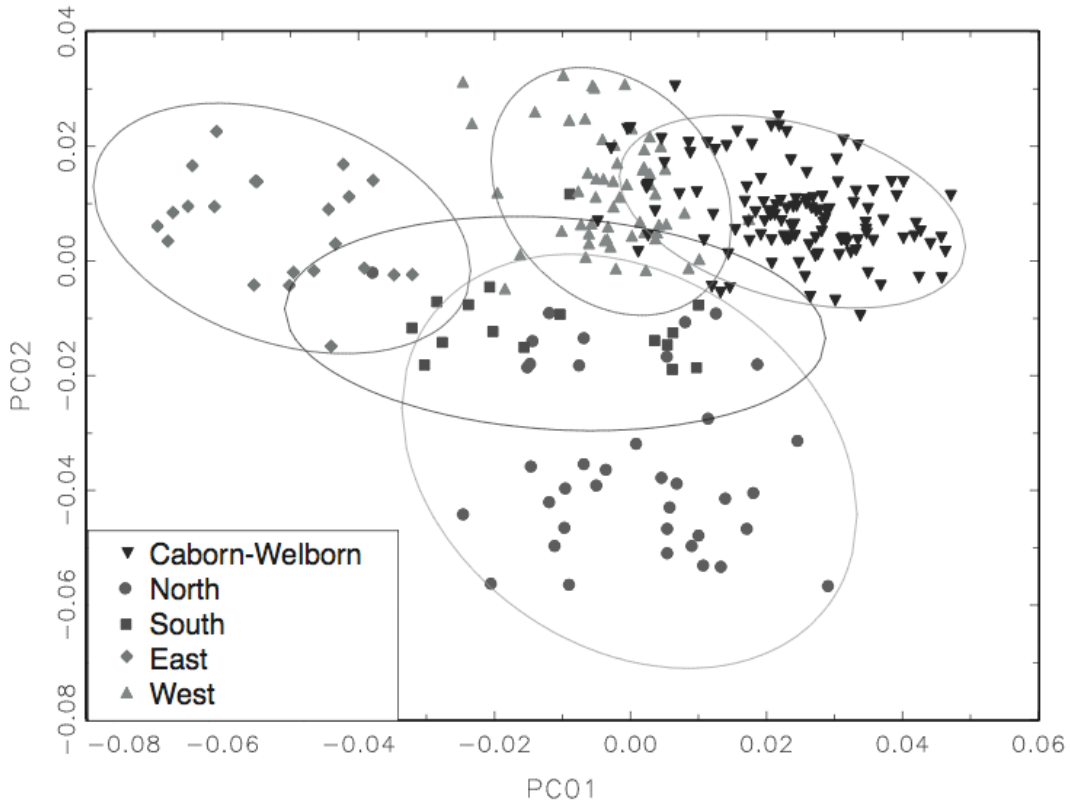

Figure 3.5: Plot of principal component 2 (PC02) vs. principal component 1 (PC01) of concatenated Caborn-Welborn and Steponaitis data sets. The ellipse confidence intervals are ninety percent.

In addition to PCA, the Na and K concentrations of the sherds were used in the original Steponaitis study to distinguish between geographical groups based on mineralogy. According to the paper, these elements are associated with smectite and illite.[85] Comparing the C-W data to Steponaitis et al. data on a bivariate Na-K plot shows that the C-W data are very similar to the western group (Figure 3.6). This suggests that the C-W and the western Steponaitis et al. samples have a very similar mineralogy. These similarities are expected, as the geographical separation between the Ohio River floodplain and the central Mississippi River Valley is small. As such, the clays in both regions may have been derived from similar

alluvial materials. Other elements that show similar patterning in the overlap of C-W and western groups on bivariate plots include Hf, Rb and Fe.

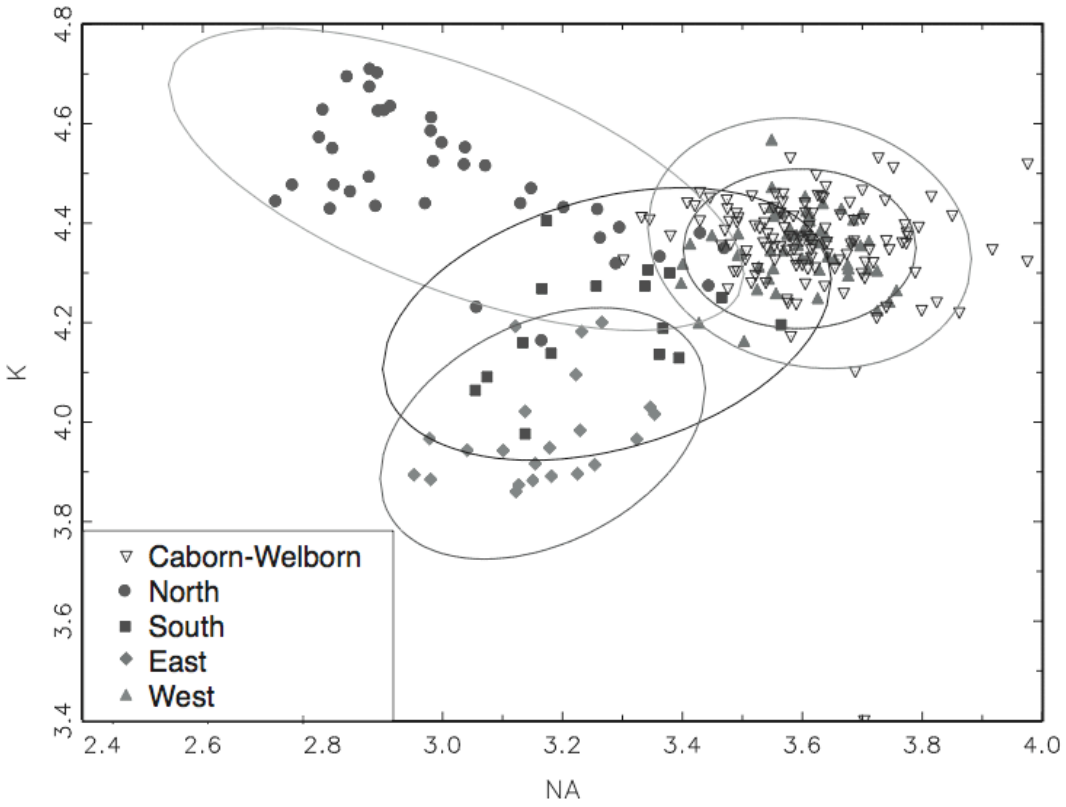

Figure 3.6: Bivariate plot of the $\log_{10}$ of the potassium (K) and sodium (Na) concentrations for the Caborn-Welborn and Steponaitis ceramics. The ellipse confidence intervals are ninety percent.

Intra-regional Analysis

In addition to the extra-regional analysis, an intra-regional analysis also was performed on the C-W data set. This PCA analysis included 32 elements obtained by INAA and PIXE to ascertain if there are subgroups in the C-W data set itself. Elements that accounted for the majority of variance in the principal components included P, Mn, Ta, Sb,

Ba, and Cr (Figure 3.7). This set of elements is different than those responsible for the greatest observed variance in the concatenated Steponaitis et al. and C-W data set comparison. Use of bivariate plots of discriminating elements often provides more information on potential groupings within a data set. As shown in Figure 3.7, P and Cr are the largest orthogonal vectors, indicating the greatest variance within the C-W data. A log-log bivariate plot of the concentrations shown in Figure 3.8 has a large spread in the spatial distribution. However, when sub-area information is added, (as indicated by different symbols in Figure 3.8) these distributions are not necessarily related to sub-area. If there was a relationship between site location and chemical composition, the samples should group together by sub-area (symbol). In this case, it is hard to differentiate between statistical groups, suggesting the sub-areas are indistinguishable within the C-W region based on this information. These results suggest that clays with similar chemical composition were present and were used within the three C-W sub-areas.

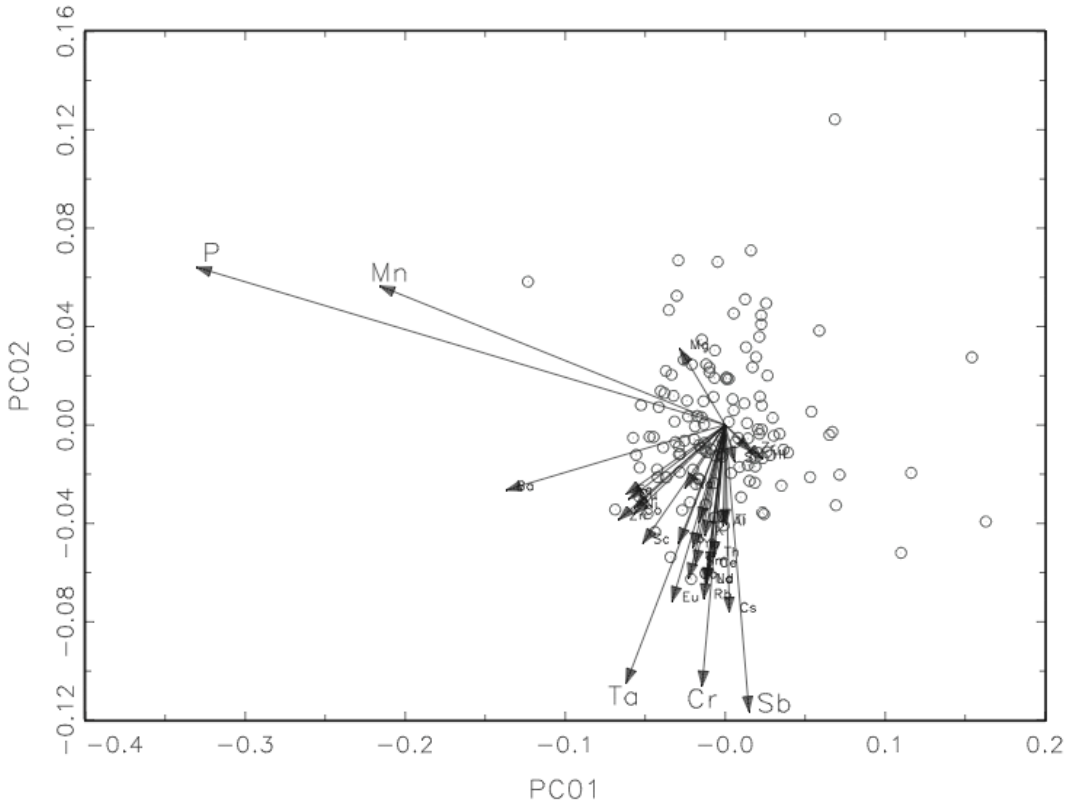

Figure 3.7: Plot of principal component 2 (PC02) vs. principal component 1 (PC01) for all the Caborn-Welborn samples demonstrating the elements responsible for the greatest variance within the data set.

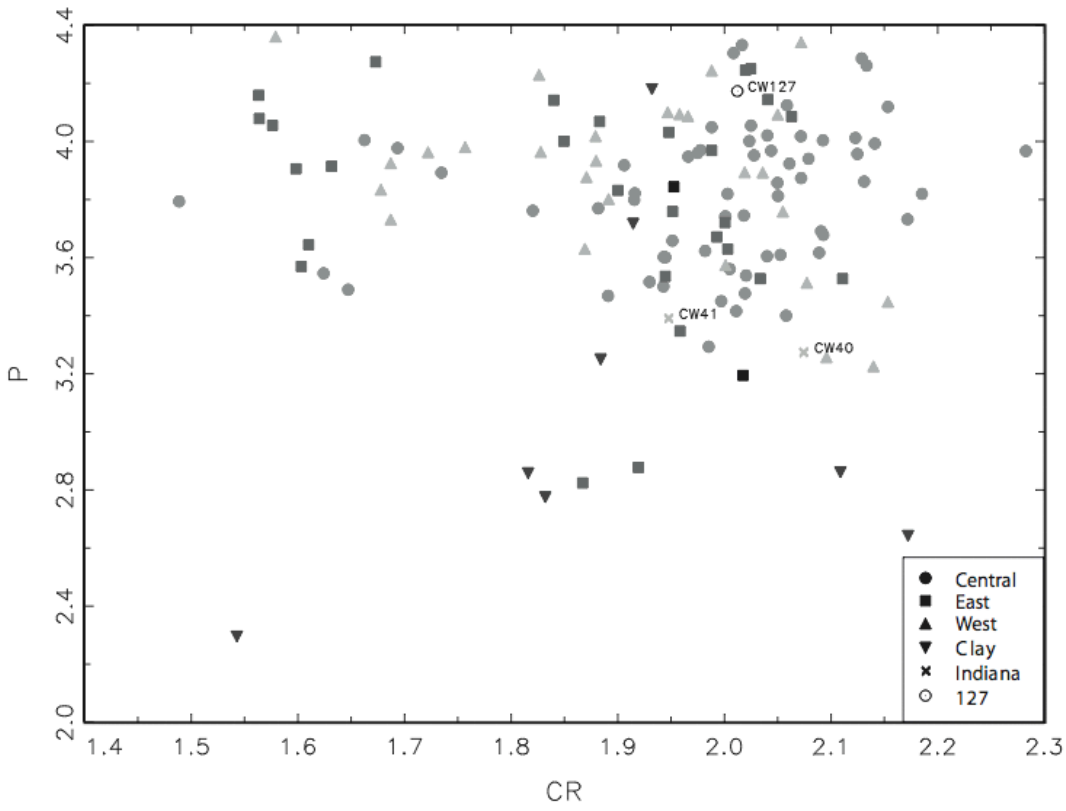

Figure 3.8: Bivariate plot of log-10 concentrations of phosphorus (P) and chromium (Cr) for the Caborn-Welborn ceramics based on sub-area.

Within the C-W data set, additional sub-classifications and analyses were performed based on archaeological information. The data was examined by site and by ceramic type. Throughout the analysis the sample CW127 is highlighted as identified in the introduction. Samples CW40 and CW41 are identified in Figures 3.8 and 3.9. These samples came from Central Indiana and were included in the analysis to ascertain if these samples could be distinguished from C-W types.

The first analysis was performed based on site classification. The samples are primarily derived from four village sites: Murphy (n=13), Slack Farm (n=55), Blackburn (n=14), Moore (n=14), and Alzey (n=10). These site designations are listed in Table 3.2.

Table 3.2: Archaeological site designations for the C-W ceramics, daub, and clay samples*.

Site Name	Site Number	Subarea	Number of Samples
Hart	15He35	Eastern	4
Alzey	15He37	Eastern	10
	15He110	Eastern	2
Ritz	15He775	Eastern	4
Cummings	15He777	Eastern	4
Hooper	15Un177	Eastern	6
Murphy	12Po1	Central	13
Slack Farm	15Un28	Central	55
Moore	15Un42	Western	14
Blackburn	15Un57	Western	14

* Two clays samples were obtained off-site.

For the site analysis, samples were selected from sites of different size and in different areas in the C-W region. The largest sample was taken from the centrally located Slack Farm site. Most of the samples came from surface contexts. An attempt was made to select a variety of ceramic types and to include ceramics that were made locally (based on abundance) as well as those that could potentially represent vessels obtained through interaction with groups living to the north or south of the lower Ohio River valley. Nearly all of the C-W samples, regardless of site, group very closely together and are difficult to distinguish from each other. Sub-areas of the C-W region do not show any significant trends in association with each other. For instance, sites located in the eastern sub-area, which includes Hooper and Alzey, are not more closely related to one another than to samples from sites in the central sub-area, including Murphy and Slack Farm. The Central Indiana samples (CW40 and CW41) do not have any particular association.

In the PCA plot of C-W ceramics based on sub-area (Figure 3.9), the obvious outlier points closest to the large central group belong to clay samples collected from the Murphy site. These samples do not show an association with the larger group of ceramic samples. Two outlier points on the far right of the plot represent clay samples taken from off-site. Despite the small group size, these clays are distinctly different from the ceramic samples. This suggests that the ceramics were made from different clay sources than those sampled in this study. Further studies with additional clay source samples need to be performed in order to ascertain the potential location of the local clay source. The clay samples are also chemically different from daub samples from the Slack Farm site (15Un28). One daub sample seems to be similar to the ceramic samples. The central Indiana examples are

grouped together to the right of the C-W cluster, but not obviously different from C-W examples. In summary, the Central Indiana sherds do not exhibit any associations with the C-W ceramics.

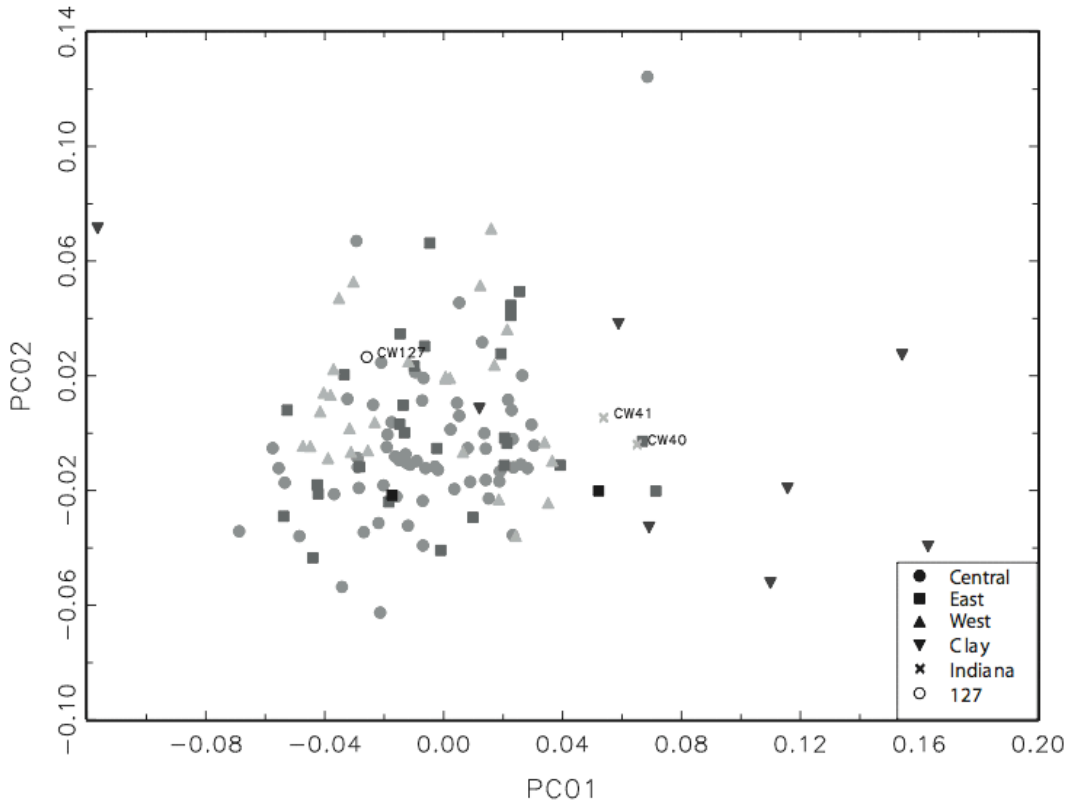

Figure 3.9: Plot of principal component 2 (PC02) vs. principal component 1 (PC01) of Caborn-Welborn ceramics based on sub-area.

A PCA analysis was also performed to determine if chemical differences could be identified that distinguish between the production of Caborn-Welborn ceramic types, central Mississippi Valley derived ceramic types, and Oneota-like ceramics (Figure 3.10). Based on the work of Pollack and Munson (1998:163-202; Pollack 1998), ceramic types from C-W

sites can be assigned to one of these three groups. The ceramics that are most characteristic of these groups are listed in Table 3.3.

Table 3.3: C-W ceramic groupings

Ceramic Groups	Ceramic Types
Central Mississippi	Campbell Punctate, Campbell Incised, Campbell Applique, Kent Incised-like, Walls Engraved, Vernon Paul Applique
C-W (lower Ohio Valley)	Mississippi Plain, Bell Plain, Caborn-Welborn Decorated, Kimmswick Plain, Kimmswick Fabric Impressed, Mound Place Incised, and Miscellaneous Incised/Trailed
Oneota-like	Oneota-like

The PCA analysis shows that most of the samples group closely together, and the centroids strongly overlap.

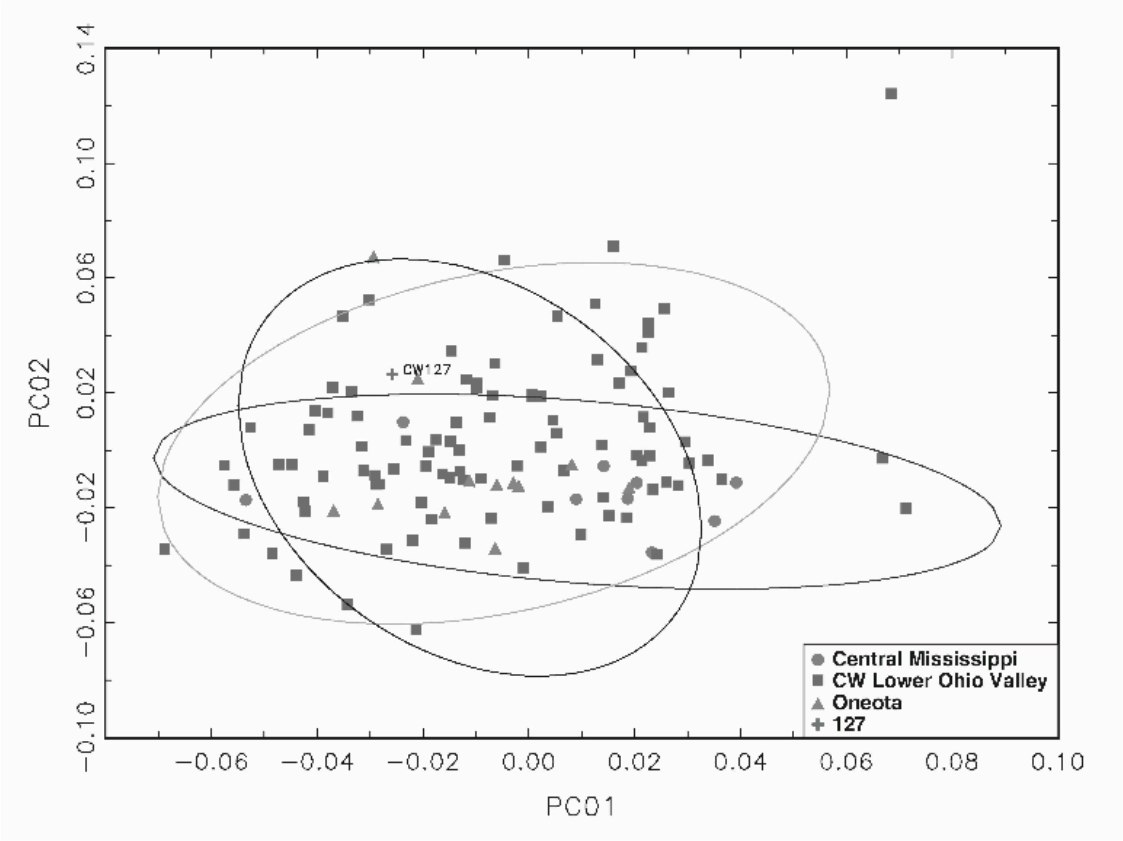

Figure 3.10: Plot of principal component 2 (PC02) vs. principal component 1 (PC01) of Caborn-Welborn ceramics using source classification. The ellipse confidence intervals are ninety percent.

The few outlier points do not suggest a specific trend in one group over another. Using the posterior classification analysis, about a quarter of the lower Ohio Valley samples can be placed with the central Mississippi (23 out of 98 total) and Oneota-like (23 out of 98 total) ceramics, respectively. As mentioned earlier, this method compares the three groups to each other as well as the assignments of the samples to a particular group. In this case, many of the Lower Ohio Valley samples had significant statistical assignments to another group. This suggests that regardless of ceramic group, these ceramics are chemically similar. As

such, the Oneota-like and central Mississippi Valley derived types appear to have been made from locally derived clays. They do not represent vessels obtained by C-W people through interaction with groups living to the north or south of the Ohio Valley. This pattern also holds for specimen CW127, which visually appears to have been associated with a ceramic vessel manufactured in the central Mississippi Valley. Chemically it appears to have been produced from local clays. It should be noted that part of the problem in distinguishing C-W ceramics from central Mississippi Valley ceramic types is due to the similarities identified by the PCA between the ceramics from the lower Ohio Valley and Steponaitis et al.'s western group. As such, it may be difficult to distinguish C-W from central Mississippi valley ceramics without a much larger number of samples. The difficulty in distinction should also affect the comparison of the C-W and Oneota-like ceramics, since clay from areas to the north of the lower Ohio Valley would have been derived from different parent materials and thus should be distinguishable from lower Ohio Valley clays.

CONCLUSIONS

The elemental compositions of 130 C-W sherds, daub, and clay samples were measured using INAA and PIXE. By using the concentrations of 21 elements, the C-W samples were compared to the Steponaitis et al. data set for the southeastern United States. PCA and posterior analysis indicated that although C-W ceramics may be stylistically and compositionally related to Steponaitis et al. samples from the Southeast, they constitute a chemically distinct group. The greatest similarity is between the composition of Steponaitis et al.'s western group and the composition of C-W samples. This is consistent with the relative geographical location of the two regions. Additional similarities in mineralogy

between C-W ceramics and the western group were documented by comparing sodium and potassium concentrations on a bivariate plot.

In an effort to identify potential intraregional variance, similar data analyses were performed using only C-W samples. Based on comparisons by location (subarea), ceramic type, and ceramic group**,** the PCA analysis indicates that the ceramic samples from ten C-W sites are very closely related to each other. With the exception of a few outlying data points, it is difficult to identify differences in the source of clays within the C-W region or those used to manufacture the different ceramic types recovered from C-W sites. This suggests similarities in the sources of raw materials used for ceramic production. It also suggests that none of the central Mississippi Valley-derived types or Oneota-like ceramics analyzed in this study represent vessels obtained through interaction with groups living outside the lower Ohio Valley. In addition, the clay and daub samples analyzed in this study were found to be chemically different from the ceramics.

CHAPTER 4: OCHRE ANALYSIS

ARCHAEOLOGICAL OCHRE- ANCIENT USES AND STUDIES

Ochre and other iron oxide pigments were important materials in many ancient cultures. They were used for both ceremonial and mortuary purposes and played an important role for cultural expression. Pigments made from ochre are often discovered as long-lasting colorful remains in archaeological contexts, from rock art to ochre-dusted bones in burials,[86] to ancient paint artist palettes or decorated pottery.[87, 88] These striking minerals are found in the famous rock art paintings such as the prehistoric cave art at Lascaux, France, and other caves in Australia, [26, 89, 90] to modern paintings and frescoes.[25] In addition, iron oxide pigments can be found decorating clothing hides,[91] as pigments in ceramic slips and glazes,[92, 93] and they are found frequently dusted over bones in burials in many parts of the world (including the Paviland ochre found in Great Britain).[86, 94] Other documented uses include as a preservative for skin, bone, and wood as well as a polishing abrasive.[95] In addition, ethnographic studies document the use of ochre as part of medicine.[88]

Ochre is a long-lasting colorful material that is generally impervious to weathering and extreme conditions. For ancient people, ochre and other iron oxides provided a range of vivid and stable pigments that could be used in both water-based (blood) and organic (fat or egg protein) binders.[96] There is evidence for both processing and heat treatment of ochre to create particular colors and other characteristics.[97] A descriptive anthropological report on ochre use from Qazfeh Cave, Israel, is presented by Hovers et al.[98] A general ethnographic overview of decorative, medicinal, and ceremonial uses of ochre in North America has been compiled by Ellis et al.[99] and Mrzlack.[88]

SUMMARY OF PREVIOUS ANALYTICAL OCHRE STUDIES

Studies connecting ochre and their sources are rare compared to provenance studies of other materials such as ceramic and obsidian. A review of the literature finds several studies of ochre by Raman spectroscopy. Ochre has also been studied by other elemental analysis methods such as PIXE and scanning electron microscopy energy dispersive spectrometry (SEM-EDS). By far, the majority of the existing methods used to study ochre and iron oxides in the archaeological and chemistry literature are mineralogical, microscopic, or diffraction studies, instead of elemental analysis.

General studies

Several studies in the chemistry and geological sciences literature present analytical studies not directly related to the archaeological applications of ochre examination. However, these studies have indirect applications to the investigations of ochre mineralogy, crystallography and behavior in the natural environment. Some of the techniques employed include Mössbauer spectroscopy, X-ray diffraction (XRD), Raman spectroscopy, and magnetic susceptibility methods.

A Mössbauer paper[100] on red and yellow ochre investigated natural iron oxides to understand the conversion of ferrous to ferric iron, and iron hydroxide and oxyhydroxide transformation into iron oxides. This study also pinpointed the temperature at which goethite converts to hematite. Mössbauer spectroscopy was also used to investigate the oxidation state and the type of binder used with the iron oxide pigments.[101]

Mineralogical methods

Most previous works have focused on identifying the mineralogical content of paints, pigments, and ochres, instead of the elemental composition. Rather than sourcing, these papers address such issues as pigment use and classification, mineralogical identification, study of ancient pigment technologies, possibility of heat treatment of pigments, and oxidation state.

The studies include investigations of the technology of painters at Lascaux using PIXE by Menu et al.,[26] SEM-EDX, PIXE and TEM analysis of pigments and technology of Paleolithic painters by Chalmin et al.,[89] Raman examination of rock art in Quercy, by Smith et al.,[102] Raman analysis of ancient Egyptian pigments, by David et al.,[103] Raman and PIXE analysis of Eritrean rock art by Zoppi et al.,[104] Raman analysis and XRD of iron oxide pigments from Italian ceramic fragments compared to modern pigment samples by Clark and Curri,[92] and examination of black Paleolithic pigments by TEM and micro-XANES by Chalmin et al.[105] Edwards[106] gives a summary of Raman investigations of pigments up until 2005. Smith and Clark[107] published a general review article on Raman spectroscopy which covers rock art and associated pigments. An investigation of rock art iron oxide pigments was carried out by Scott et al.,[108] and includes analyses by thin section, polarized light microscopy (PLM), XRF, XRD, and Fourier transform infrared microscopy (FTIR). Most of the analyses confirmed the use of hematite and goethite as the pigment materials as well as the identification of unusual green and blue pigments.

Elemental Analysis

In general, there are fewer studies on the elemental analysis of ochre than spectroscopic studies. Most are based on SEM-EDS analysis, while others are based on PIXE. Very few are based on INAA with the exception of Erlandson et al.[109] and Mrzlack,[88] and Popelka-Filcoff.[110-113] Some general studies are the sourcing of the Paviland ochre by XRF and petrography by Young et al.[94] Weinstein-Ilani et al.[114] describe the possible sourcing of ochre from the El-Wad cave in Israel by SEM-EDS. A general summary of the physical and chemical methods that have been used to analyze pigments was compiled by Rowe.[115]

Australia:

Several investigators have examined Australian ochre, both in ancient and modern contexts. In Australia, ethnographic studies and interviews with Aboriginal people about sources and use of ochre have occurred more often than in the United States or other parts of the world.

Mineral magnetic analysis of ochre was used by Mooney et al.[116] to characterize ochre from known sites. Smith et al.[117] used the oxygen-isotope ratios in quartz to determine the provenance of Australian ochre. Jercher and co-authors[118] used Rietveld XRD and XRF to determine the mineralogy and elemental composition of modern Aboriginal ochre. Goodall et al.[119] found subgroups within a data set of ochre obtained from Fern Cave, using photoacoustic spectroscopy (FTIR-PAS), PIXE and proton-induced gamma-ray emission spectroscopy (PIGE). The latter study suggested that the concentrations of elements in the ochre artifact were related to the ochre source and were not affected by diagenetic effects. [119]

A few elemental studies of Australian ochre have also been performed. David et al.[120] used PIXE on 69 ochre samples from Northern Australia. They suggest that ochre from Australia could be traced to their original geological sources. They described several statistical methods used to identify the differences between sources, including a cluster analysis and a multi-dimensional scaling. The main variation in the samples appeared to be based on major elements, which included Fe, Ca, Ti and Cr. However, the data were not calibrated relative to a precise elemental standard and assumptions were made about the major oxide composition of the ochre.[120]

Other investigators have researched ethnographic and historical literature to investigate the ancient mining sources in Australia. Clarke[121] analyzed ochre from the Wilgie Mia ochre mine to study particle size and elemental composition. He also interviewed local Aboriginal people concerning the uses of ochre from this particular source. The use of iron oxide pigments on cave walls was investigated by electron probe microscopy.[121]

Clarke and North[122] describe the analysis of pigments in rock art from Kakadu National Park. While the trace elements of individual pigments were not identified, the authors consider this to be important for future work. The main focus of the paper was on the use of SEM-EDX (energy dispersive X-ray analysis) to describe the mineralogy and ancient technology used to mix the pigments for conservation and preservation, although ICP-MS was used to determine many trace elements.[122]

Europe and Worldwide

Other works on ochre analysis have been reported around the world. Young[94] wrote a summary of ochre found with the "Paviland Lady", a burial discovered in Wales. Ochre examples, iron ore, and manganese ore were investigated by XRF, petrography, as well as digested for ICP-MS analysis. Associations with possible source locations were based on patterns in the elemental content of the ochre as well as suggestions of mixing of pure iron ore with clays and other materials.[94]

A few studies have been published concerning the analysis of pigments from prehistoric cave art in Europe. Menu et al.[26] described the technologies used by ancient people in the famous caves of Lascaux and elsewhere. They suggest a differentiation between the source pigment materials existed due to trace elemental patterns measured by PIXE.

Users of iron oxide pigments were known in Europe and the Middle East during the Middle Ages and Renaissance periods. These types of iron oxide based pigments have been most commonly studied for religious paintings and frescoes from the time period.[123] Both composition and technological studies have been performed on these types of pigments. Grygar et al.[124] used SEM and EDX, XRD and voltammetry to identify the pigments used in Baroque paintings. They also identified K and Ti as potential indicators of source based on the fact that these elements were related to geological weathering and other changes.[124]

United States

In contrast to the work in Australia, few studies on the characterization of ochre from sources in North America have been conducted. Erlandson et al.[109] described the use of

PIXE analysis on samples from eight ochre sources in western North America (California, Oregon, Alaska, and Wyoming) and demonstrated that the elemental signature from these measurements satisfied the provenance postulate.[109] Although the conclusions are based on only one or two samples per source, this work suggests that these sources might be differentiated from one another based on their major, minor, and trace-element content. Mrzlack[88] recently published a master's thesis based on the use of PIXE to characterize ochre artifacts from a cave in Alaska. She concluded that ochre from the cave came from the same source, and may be related to sources in Oregon.

An independent study by Ellis et al.[99] reports on the INAA and inductively coupled plasma optical emission spectroscopy (ICP-OES) analysis of ochre artifacts from Texas. They describe several pilot studies that elucidated information on the intra- and inter-source variability in the data set. The authors analyzed worked nodules found in four Texas archaeological sites by ICP-OES (inductively coupled plasma optical emission spectrometry) and INAA. Within the study, they investigated intra-sample variation and found that some elements were affected by weathering of the sample. In addition, the authors concluded that INAA is an optimal technique for studying the trace elemental composition of ochre and also understanding variations within ochre.

ANCIENT OCHRE SOURCES

Unlike other artifact types, there is very little in the literature concerning ancient ochre sources in the United States. There are only a few documented ancient ochre sources in the United States, most notably Sunrise Mine in Wyoming.[95, 125] In the Erlandson study, ochre samples were selected from known or suspected ancient source locations. Two of the

source locations were from known archaeological sources (Sunrise Mine, Wyoming, and Redwood Quarry, California).[126, 127] In 1999, one sample from Sunrise Mine and three from Redwood Quarry were analyzed by PIXE and INAA. The samples came from locations where archaeologists believe prehistoric people may have procured the raw ochre to process for cultural use.[109]

While some of the cultural implications of ochre are known based on the use of raw minerals and artifacts found in archaeological sites, very little is known about the procurement and processing of ochre by indigenous people. It is possible that ancient people sought particular sources of ochre for specific characteristics, and that ochre was exchanged along ancient routes. In addition, people may have processed the iron-based pigment to obtain a particular particle size, or added binders as part of the pigment processing.[89] Given their prominence and prevalence in archaeological sites, it is necessary to understand the chemistry of ochre before engaging in studies of artifact sourcing and ancient technology.

Unlike some other artifact classes such as ceramics, identifying ancient ochre sources can be extremely difficult. In the case of ceramics, the discovery of a kiln or ceramic "wasters" identifies the production site of ceramics. Clay sources, on the other hand, are more difficult to identify, especially if the landscape has changed over time.

In the case of ochre, a small amount of this intensely pigmented material can color many artifacts or cultural objects. It is also feasible that smaller amounts of ochre could travel for miles as an exchange good. Mrzlack[88] suggests several social mechanisms: direct procurement, embedded procurement, and exchange. By understanding the movement of ochre materials from sources through geochemical and statistical analysis, insights into these exchange patterns and others may be elucidated.

The only clearly documented known ochre mining site in the United States is the Sunrise Mine site (Hell Gap site, also known as Powars II).[95] In a study of the Sunrise Mine site in Wyoming, Tankersley et al.[95] identified an ancient ochre quarry now on the site of a modern mine. The site contains both specular and earthy hematite, with specular being the dark gray and shiny species and earthy being the red, soil-like species. The authors suggest that its location and quality of ochre material made the mine an important source during Paleo-Indian times.[95] In addition, they connected some Paleo-Indian ochre-stained artifacts from the Hell Gap with the Powars II site based on mineralogy, suggesting that aboriginal people sought ochre from the Sunrise Mine for particular characteristics or cultural significance.[95, 125] Ancient tools stained with ochre have been found in the original mining areas. Stafford et al.[128] also investigated one of the sources studied by Erlandson et al.[109]

Erlandson et al.[109] investigated ochre from the Redwood site. Archaeologists documented this site earlier, located in modern Oakland, California. Evidence for ochre mining and processing included the ochre pits, evidence of fire, and areas for mixing and grinding the pigment. At the time it was recorded, it was as one of the few hematite mines extant in California.[126, 127]

For Missouri, a possible archaeological source of ochre was identified near Leslie, Missouri by W.H. Holmes.[129] Holmes, from the Smithsonian Institution, documented in 1904 what he thought to be "aboriginal" activity at the "modern" mine site. His conclusions stemmed from a system of tunnels carved through the iron ore as well as the discovery of many stone implements. Holmes did not suggest for what purpose native people may have used the ochre; he only observed that it must have been important to the ancient people.[129]

OCHRE GEOCHEMISTRY AND MINERALOGY

The geochemistry and geological characteristics of ochre and iron oxides will be discussed in a very general manner, because there is no specific information regarding the sources or artifacts sampled in this study. However, trends in the geochemistry and other properties have been investigated in other research[96, 130-144] and the relevant material is presented here.

Definition of Ochre

The definition of ochre is vague, as ochre can vary in mineralogical content from a pure iron oxide to a dilute mixture of iron oxide and other minerals. Ochre is typically composed of two common forms of iron oxide: Fe_2O_3 (hematite) and $FeO(OH)_x$ (goethite), mixed with clays, silicates, and other minerals, such as MnO_2. Technically, the term "ochre" is not equivalent to either hematite or goethite, because ochre is made up of these iron oxides and other iron minerals and other surrounding materials.[99] Red ochre is made up of the mineral hematite (α-Fe_2O_3) and is 70 weight percent Fe. Yellow ochre (goethite or limonite) has the general chemical formula α-$FeO(OH)_x$ where the iron content can vary by hydroxide content but is nominally 63 weight percent Fe.[145] Robertson defines ochre as "ferruginous oxides and hydroxides, generally manganese-poor, which are spatially and genetically associated with sulphide orebodies".[146]

Ochre is found in a variety of geological contexts including "sedimentary, igneous, metamorphic rocks, and weathered products, soils and unlithified sediments derived from any of these rock types".[99] One source describes ochre as material that contains 10-50% iron oxides for goethite and up to 90% for hematite.[96] From an archaeological perspective,

however, many related iron oxide minerals are often considered ochre based on visual observation, physical characteristics, and uses rather than by chemical or spectroscopic analysis.

Ochre Formation

Ochre and related ocherous materials are found in igneous, sedimentary and metamorphic contexts [137] as primary or weathered products of the original material. As the third most abundant crustal element, iron can be found in nearly every rock to some extent, and thus soils and ochre due to weathering.[96] In general, iron oxides are found worldwide in many contexts, thus providing materials used by prehistoric people across space and time. Goethite is found as the result of weathering of iron-containing minerals such as magnetite and siderite.[147] In some locations, such as Missouri, ochre and iron oxides can be found in both igneous and sedimentary formation in very close geographic proximity. In Missouri, hematite and limonite is often found surrounded by broken cherts and sandstone.[144] Other elements substitute in iron oxides, a common element being aluminum, which preferentially substitutes in goethite over hematite. [96] Several types of geological formations host ochreous deposits. Diagenesis of these deposits can lead to nodules of ochre or "soil-like" ochre powders. Soils with very low concentrations of iron can be highly colored despite the low concentration of Fe.

Color

Ochre ranges in color from deep purple to light yellow, but the most common colors are a blood red for those with high hematite content and yellow for those with high goethite

content.[146] One source describes the color differences between yellow and red ochre as related to both the Fe(III) ion as well as the charge transfer between the Fe^{3+} and OH^- and O^{2-} groups.[137] Another source indicates that color is also related to the particle size and shape of the goethite or hematite.[96] Crystalline hematite with particle size of about 1 micron has a purple coloring, while sub-micron particle sizes tends to create the red hues.[123] A study by Marshall et al. confirms that color is related to particle size, especially for the darker-hued ochre.[148] Particle size of the material also seems to be important in the definition and uses of ochre. Due to its small particle size and thus a large surface area to volume ratio, ochre granules and particles stick to the surfaces quite readily and thus deeply color the surface with only small amounts of material.[137] Substitution of other elements, mostly transition metals, has also been demonstrated to alter the hue of iron oxides, as described by the "Munsell value". Increasing amounts of Cr, Co, and Ni cause a red shift, while V and Mn cause a green shift.[96, 147] Other authors mention Mg and Ti as common substituting elements in hematite.[101] Marshall also asserts that changes in ochre color are due to concentrations of Cu in the ochre.[148]

Heat treatment

As mentioned earlier, heat can be used to change the color of ochre. In general, iron hydroxides can be converted to the oxide complement by heating. Chemically, this occurs as a rearrangement of the cations and loss of hydroxides.[96] The most common example of this transformation is the change from goethite (yellow) to hematite (red), which occurs in nature. It has been speculated that indigenous people in several cultures heated ochre to change its color. Evidence of this kind of ochre processing is apparent at several sites.[97] Goethite

dehydrates into hematite by heat treatment. It has been suggested that ancient people observed this transition and exploited it. One group of authors asserts that this change in color from yellow to red ochre occurs with a heating to 280- 400° C, [114] although some authors report this transition occurring as low as 125° C.[135] However, it is important to point out that ochre of different colors may in fact be from the same site and appear different visually due to dehydration of the mineral or by heat treatment.

INORGANIC CHEMISTRY AND STRUCTURE OF IRON OXIDES

The two most common forms of iron oxide used during ancient times were goethite and hematite, although other less common minerals and pigments such as magnetites have also been investigated. Most iron oxide materials are formed by the direct precipitation of Fe(II) and Fe(III) solutions or transformation of another mineral by dissolution or re-precipitation. While there are many possibilities for iron oxide formation, goethite and hematite are the most thermodynamically stable minerals and are the most common.[96] In general, the structure of the iron oxides is the octahedral structure with Fe as the central ion and O^{2-} or OH^- as the ligands.[96] In the Fe(III) state, iron oxides are always in the high spin (unpaired d electrons). In the ground state, the 5d electrons are unpaired, with the notation of $^6S_{5/2}$.[96]

Goethite

In general, the crystal arrangement is orthorhombic, has hexagonal close packing of anions, and has antiferromagnetic properties. Goethite has a parallel structure to diaspore (α-AlOOH). It is also thermodynamically the most stable under ambient conditions. Due to its

stability, goethite is frequently found in most iron oxide formations.[96] In humid areas, it is the most common stable soil iron oxide. Surrounding materials include hematite, calcite, quartz and others.[147]

Hematite

Hematite crystals are rhombohedral and hexagonal, and can be weakly ferromagnetic or antiferromagnetic. It is the oldest iron oxide known and frequently found worldwide, based on its stability under ambient conditions. It is also based in the hexagonal close packing arrangement of anions, but instead is in the corundum (α-Al_2O_3) structure. Hematite can be found as a red earth or shiny, silvery ore (specular hematite) among others. Hematite also has a very high tinting strength as compared to goethite, and a very small amount of hematite can cause an identifiable color change.[96] It is found in similar contexts to goethite, and is often surrounded with chert and other accessory minerals. It is the primary mineral in Precambrian iron formations.[135]

Solubility

Iron in the +3 state for both goethite and hematite, has a low solubility compared to Fe(II). Fe(III) oxides, however, dissolve slowly over time. Iron oxides in general are the least soluble in the pH 7-8 range, and more soluble at extreme pH values. This is due to the fact that iron oxides are amphoteric, forming cationic and hydroxo compounds in acidic solution, and anionic and hydroxo compounds in basic media.[96] However, the addition of other ligands such as chloride, phosphate, and citrate to the iron oxide compounds changes the solubility of the entire compound.[96]

Although Fe(III) is fairly insoluble, Fe(II) is more soluble. One of the more common processes for iron oxides in the natural environment is reduction of Fe(III) to Fe(II).[96] In sedimentary formations, reducing and acidic conditions enhance the precipitation of iron.[99] Within iron oxide sites, the minerals undergo changing oxidation states, and therefore dissolve Fe(II) and re-precipitate back as the Fe(III) state. In addition, bacteria and other organisms have been found to aid in the precipitation of iron materials.[135] Hematite is more commonly found in sediments subject to diagenesis.[123] However, the distribution of Fe and other elements in the resulting soils or rocks should follow similar patterns as the parent rock.[96] In general, iron oxides especially those in the Fe(III) state, have a very low solubility, very small crystal size, a high specific surface area ($>100\ m^2\ g^{-1}$) and vibrant colors.[96] Other authors suggest that the solubility of certain elements in hematite mines is related to the surrounding water pH.[142]

As a general rule, iron oxides have a very small particle sizes, ranging from tens of nanometers to a few microns. Thus, they have a large surface to volume ratio. In reactions with water, hydroxylation is one of the first and fastest reactions. As more water is absorbed, the water molecules hydrogen bond to the surface OH groups on the iron oxide. These hydroxyl groups are considered the reactive groups in iron oxides.[96]

Because ochre and other minerals associated with hematite and goethite are so ubiquitous in archaeological contexts and occur in many types of formations, understanding the geochemistry of ochre sources is important for interpreting its role in the archaeological record.

DEFINING OCHRE SOURCES

While the aforementioned studies suggest that it may be possible to source ochre through elemental analysis, these investigations involved a very limited number of samples and it is apparent that there is a clear need for a systematic study of the variation in elemental content and geochemistry of ochre from a large sample set. This study investigates the systematic sampling and elemental analysis of ochre to determine the "Fe oxide element signature" of a given ochre source, and to determine whether this signature can be clearly distinguished from sources by region. Prior studies of ochre characterized limited numbers of samples from sources in North America.[88, 95, 109, 128, 149] More thorough and comprehensive studies are necessary to examine the inter- and intra-source variation within a potential ochre source.

The objective of this study was to identify the inherent variation of the major, minor, and trace-element signatures of ochre source materials. A subsequent multivariate analysis demonstrates whether or not ochre materials satisfy the provenance postulate and how these ochre sources can be distinguished from one another. This work is an initial step in the development of an elemental database for ochre materials. The database can be further augmented to provide a more detailed and accurate picture of ochre variability. Ultimately, the main objective of chemical characterization of ochre is the development of a database for sourcing ochre artifacts similar to those established for ceramics, obsidian and other archaeological materials created by Glascock et al.[13]

EXPERIMENTAL METHODS

The following description of the experimental methods is the same for each of the studies on ochre. Despite the different provenance of the samples, they were prepared and analyzed under the same conditions.

Most of the ochre samples in this study were analyzed by INAA and XRF in order to obtain a comprehensive characterization of the material. Prior to this study, there had not been a comprehensive trace element analysis of ochre. Thus, it was unknown which elements might be important for chemical characterization and sourcing analysis. Certain elements can be measured in XRF that are not possible in INAA and vice versa. For that reason, most of the samples in this study were prepared and analyzed by both methods.

The ochre material was first processed by drying the sample at 100^0C in an oven overnight to remove moisture. Solid ochre was not pulverized prior to drying. Powdered ochre samples were dried in porcelain crucibles. It was clear upon processing the ochre in the laboratory that some samples thought to be ochre in the field were actually large pieces of other minerals such as quartz covered in a thin layer of Fe oxide. These non-ochre samples were difficult to process, and were not a good representation of the ochre present at the source. Therefore, some of these non-ochre samples were eliminated from the analysis. This situation occurred with samples that were in more of a "chunk" form and does not apply to the "soil-like" ochre examples.

After drying, the raw ochre sample was crushed with a rock hammer into smaller pieces (< 0.25 inch particle size). An alumina vessel and ball were used in a mixer mill to crush these pieces into a fine powder for analysis. Following a 15-minute powdering cycle, the alumina vessel was subjected to two five-minute cycles of grinding with high-purity

quartz glass to clean the alumina vessel and ball between ochre samples. After the quartz cleaning cycles, the alumina vessel and ball were rinsed with de-ionized water to minimize potential cross-contamination between samples. The cleaning cycle of two quartz-grinding steps was experimentally determined to reduce the possibility of cross-contamination. This was evaluated by analyzing the quartz by XRF, and by comparing the results of incremental quartz cleaning steps by the Student's t-test. The resulting powdered ochre sample was used for both INAA and XRF analysis. These powders were again dried at 100 ^{0}C overnight before preparation for either INAA or XRF.

For some ochre with limited amounts of material available, an alternative method was used to prepare the samples for INAA only. Each sample was broken into smaller pieces with a rock hammer if necessary, but those provided as powder were not crushed with the hammer. Instead of the mixer mill routine, the crumbled sample was then pulverized into a powder using a Brazilian agate mortar and pestle. The mortar and pestle was cleaned between each sample by washing both pieces with de-ionized water with a small amount of Alconox powder. The mortar and pestle were then rinsed again in de-ionized water and wiped clean with Kimwipes. This is an established methodology used for ceramic preparation in other INAA analyses of ceramic used at the Archaeometry Laboratory.

The INAA analysis followed standard laboratory procedures developed by Glascock[13] for geochemical samples. For the short counts, about 60 mg of sample was irradiated in 1.2 mL high-density polyethylene vials, using the MURR pneumatic tube system for five seconds at a thermal flux of approximately 8.0×10^{13} neutrons cm^{-2} s^{-1}. After a decay of 25 minutes, the samples were counted for 720 seconds on a 25% relative efficiency high resolution HPGe detector. For the mid-count and long-count measurements, about 60 mg of

sample was sealed in high purity quartz vials and irradiated for 24 hours at a thermal neutron flux of approximately 5.2 x 10^{13} neutrons cm^{-2} s^{-1}. After a decay period of seven days, the "mid" count data was acquired for 2,000 seconds. After decay of an additional three weeks, the "long" count data were acquired for 10,000 seconds on automated sample changers. The comparator standards used in the INAA measurements were NIST SRM 1633a (Fly Ash) and SRM 688 (Basalt), and the quality control standards were NIST SRM 278 (Obsidian Rock) and Ohio Red Clay.[13]

The samples were prepared for XRF analysis by mixing approximately 3 grams of finely ground sample with approximately 0.7 grams of X-ray Mix (Chemplex) in a virgin polycarbonate vial for 15 minutes on a mixer mill. The resulting mixture was then pressed into a 32-mm diameter pellet. The XRF measurements were made on a X-LAB 2000 instrument , manufactured by Spectro, using a combination of three excitation targets with a Pd anode; molybdenum for Cr – Y and Hf – Th (35 kV, 4.4 mA), aluminum oxide for Zr – Nd (52 kV, 5.7 mA), and highly-oriented pyrolytic graphite for Na-V (15 kV, 13 mA). The concentrations were determined using a combination of the Compton and fundamental parameters models. Calibration of the XRF method was made using over 70 pressed-pellets of standard reference materials. Pressed pellets of NIST SRM 2689 Coal Fly Ash and NIST SRM 690 Iron Ore and Ohio Red Clay were used as quality control samples for the XRF analysis. SRM 690 has a very high Fe concentration, and is low in other elements. In fact, very few other elements besides Fe are certified by NIST for this standard. Therefore, SRM 690 is used to validate the Fe values in high Fe samples (>50% Fe), as calibration of the XRF is not adjusted for very high concentrations of Fe. Since Ohio Red Clay and SRM 2689 are low Fe, they were used to confirm all other elements in the analysis as well as samples with

lower iron values. Table 1.8 lists the results of the XRF analysis of the standard reference materials.

Splits of the same ochre material were analyzed by both INAA and XRF as the two techniques compliment each other in the elements that can be quantified in ochre samples. Table 4.1 lists those elements analyzed by both INAA and XRF.

Table 4.1: Elements routinely measured by INAA and XRF in ochre samples

INAA	Al, As, Ce, Co, Cr, Dy, Eu, Fe, Hf, K, La, Lu, Mn, Na, Nd, Sb, Sc, Sm, Th, Ti, U, V, Yb, Zn
XRF	Al, As, Ba, Cr, Cu, Fe, K, P, Pb, Rb, Si, Y, Zn, Zr

DATA ANALYSIS AND TRENDS IN OCHRE

As discussed above, ochre is hard to define from a mineralogical standpoint. Therefore, comparing materials found on archaeological sites to a given definition or even to each other becomes difficult, if not impossible. Many red-brown materials on archaeological sites are called ochre, and perhaps most of them fall under this broad definition of ochre materials. In this wide range of materials identified as "ochre", the range of concentrations of iron is wide as well as that for other elements. For the characterization and provenance studies, a method was needed that could take into account the wide variation in the iron oxide content in the raw material itself. As discussed in the Chapter 2, normalization of the data was performed by computing a ratio of the element concentration to the Fe concentration in each sample. Therefore, elements of interest can be directly compared from sample to

sample as the Fe concentration relationship between samples becomes relative rather than absolute. This approach allows a direct comparison of the trace elemental composition of the ochre without being affected by extremely high or low Fe concentrations in the individual samples.[113, 150]

In addition, other data manipulations were performed before statistical analysis as discussed in Chapter 2. First, individual elements were removed that were below limits of detection or not measured by INAA reliably, which included Ni, and Zr, and Cs, Rb, Lu, Sr, Ta, and Tb for certain geographic regions. Since ochre is made up of iron minerals admixed with clays, aluminosilicates and other minerals, the Fe concentration across the data set of ochre ranged anywhere from 0.5 to 70 weight percent, depending on local geochemistry and choice of field sample. In the case of low iron, the elements composing the clays and minerals such as K, Si, and Al made up the difference in the sum total of the sample. In order to include the major, minor, and trace elements in the comparison, and to also take into account the non-normal distributions of the individual elements, the analysis was performed on $\log_{10}$ transformed concentration ratio values.[13]

A two-tailed Pearson's correlation test was applied to the data relative to Fe concentration to ascertain which elements were significantly positively or negatively correlated with Fe. It is assumed that the elements associated with Fe are related to the Fe oxide signature and to the origin sample, whereas the elements not associated with, or negatively correlated with, Fe are related to elements that replace Fe, which essentially behave as diluents to the ochre.

The results of the Pearson's correlation identified the elements negatively correlated with Fe. Significant values were evaluated in both the 95% and 90% confidence interval.

Elements identified as being highly negatively correlated (and therefore diluents) by INAA included Al and Na, and those identified by XRF include Al, Ba, Si, and Zr. Geochemically, this group of elements comprises major components of the other minerals present with the Fe oxides and therefore these are possible diluents to the samples. Elements significantly positively correlated were included in the multivariate analyses.

A statistical comparison of the XRF and INAA data for the following studies was performed using the GAUSS software developed by Glascock and Neff with additions by William Grimm, 2004. [13, 61] Such data analyses included cluster analysis, principal components analysis (PCA), and canonical discriminant analysis as described in Chapter 2.

OCHRE PROJECTS

The ochre projects described below used similar approaches for each application of the methods and interpretation.[110-113] All of the studies used the same sample preparation and analysis methods. However, the objectives for each study were slightly different. The following sections describe the archaeological background and rationale for the analytical approach and analysis. Next, the results of the statistical analysis and the data interpretation are presented. At the end of the section, a discussion that summarizes results of the ochre studies is described.

SAMPLING

Each ochre study had different objectives and questions, therefore, the sampling strategies were different for each case. Each study is discussed separately in terms of the ochre sampling and the strategies used in each of the studies and the reasoning behind the ochre sampling.

Ochre Sources in Southeastern Missouri

Samples were selected for this study with a number of objectives in mind. It is unknown if any of the iron oxide sources in southeastern Missouri were used during ancient times as a source of ochre. However, ochre sources are easily accessible and they provide materials with distinctive colors and large distributions of Fe-bearing minerals compared to other minerals in the Missouri landscape. Popelka-Filcoff and Descantes systematically collected the Missouri samples from abandoned iron mines on Mark Twain National Forest property and private property in 2004.[151]

Southeastern Missouri hosts both igneous and sedimentary iron ore formations. All of the areas sampled in this study came from sedimentary formations.[152] The igneous formations are significantly older than the sedimentary formations in geological time, and are generally more profitable commercially (for example the mining locations of Pilot Knob, and Iron Mountain).[134] The smaller sedimentary formations were also exploited commercially for iron ore from the mid 19th through early 20th centuries, but were often quickly exhausted. Unlike igneous formations, the sedimentary mines are susceptible to weathering and other environmental diagenetic changes.

The sources were selected on the basis of archaeological surveys of historical mine sites. Once on site, samples were systematically collected from the rims and sides of the mine pits to avoid possible disturbances deep within the mine pit. Up to 20 samples were collected per source, and at each sub-location sampling included at least five samples. This sampling method allows an evaluation of the provenance postulate. [13, 52] The source locations and their characteristics are described in Table 4.2 and shown in Figure 4.1.

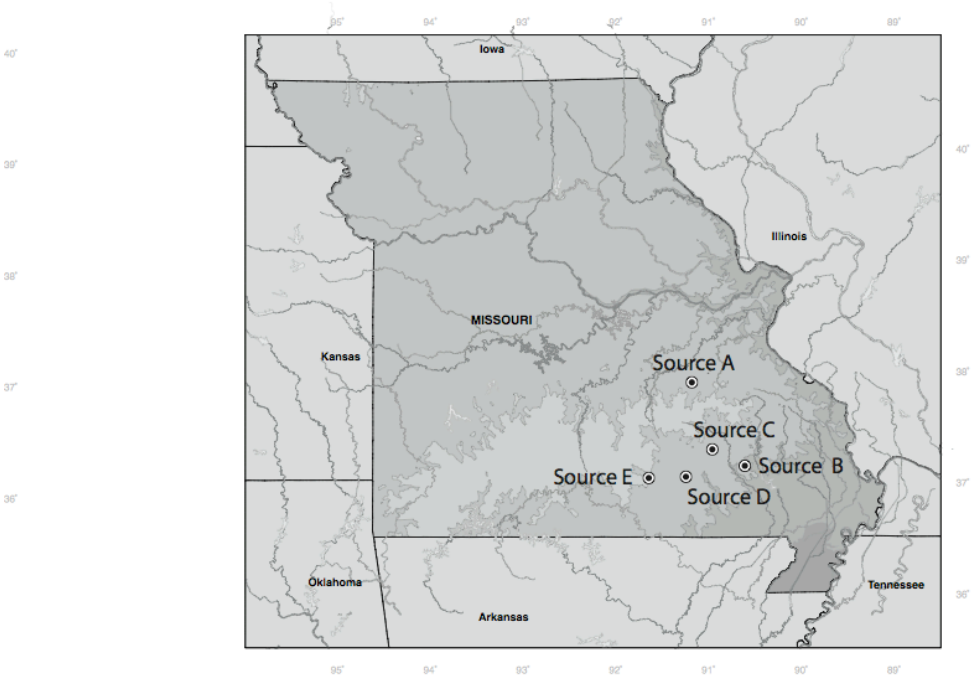

Figure 4.1: Map of ochre sampling locations around southeastern Missouri

Table 4.2: Details and characteristics of ochre samples and sources

Site	Source Name	Location	Missouri County	Number of Samples Analyzed
A	Meramac Spring Park	I	Phelps	4
		II		5
		III		3
		IV		5
		V		4
B	Private Property	I	Wayne	5
	(near site 511 (USFS)	II		5
		III		5
		IV		0
C	Site 741(USFS)	I	Wayne	5
	Bald Eagle Mine	II		5
		III		0
		IV		0
D	Site 810 (USFS)	I	Wayne	3
E	Road Cut, Big Spring	I	Carter	5
		II		5
		III		5
		IV		5

Results

Appendix II has the elemental data for Missouri ochre. Figure 4.2 shows good agreement between INAA and XRF for measurements of iron.

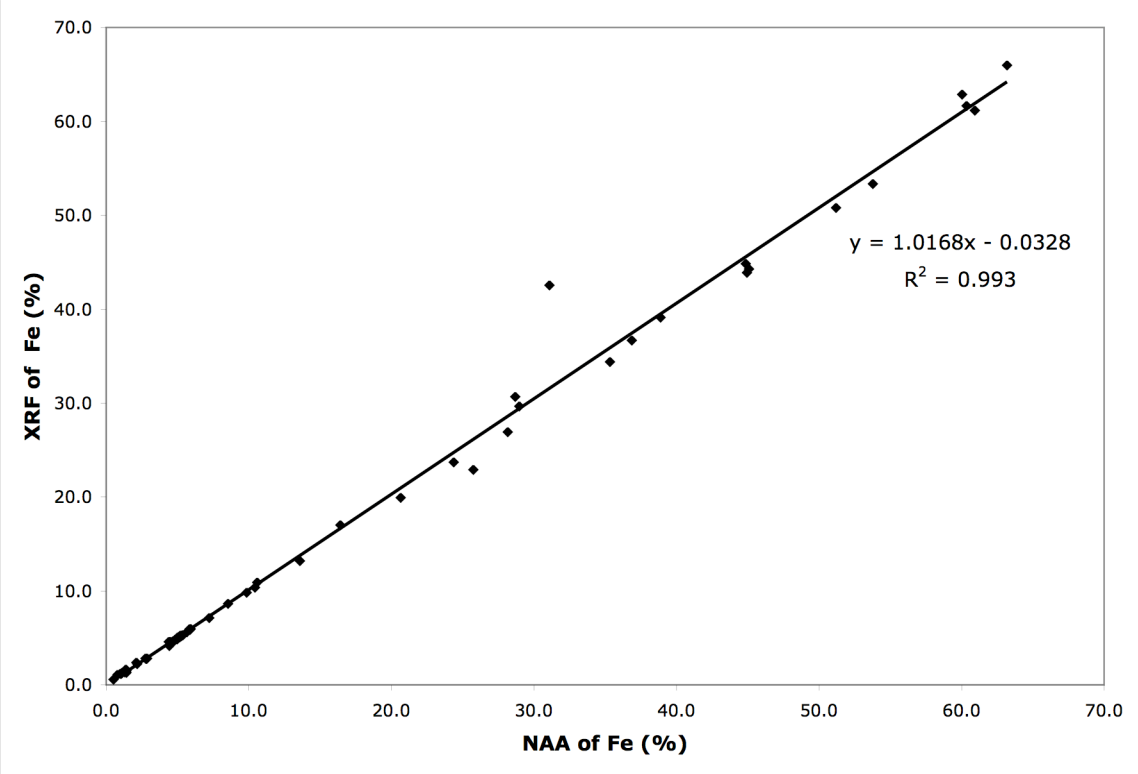

Figure 4.2: Correlation between INAA and XRF in the measurement of Fe

Other elements that also had excellent correlation measured both by INAA and XRF include: Al, As, Ba, Cr, K, Rb, and Zn. There was not good agreement for the values for Cr between INAA and XRF. This is probably due to an analytical error caused by the fast neutron reaction interferences on the high Fe when using INAA for which a correction was not made. Figure 4.3 shows the PCA analysis of Missouri ochre by INAA.

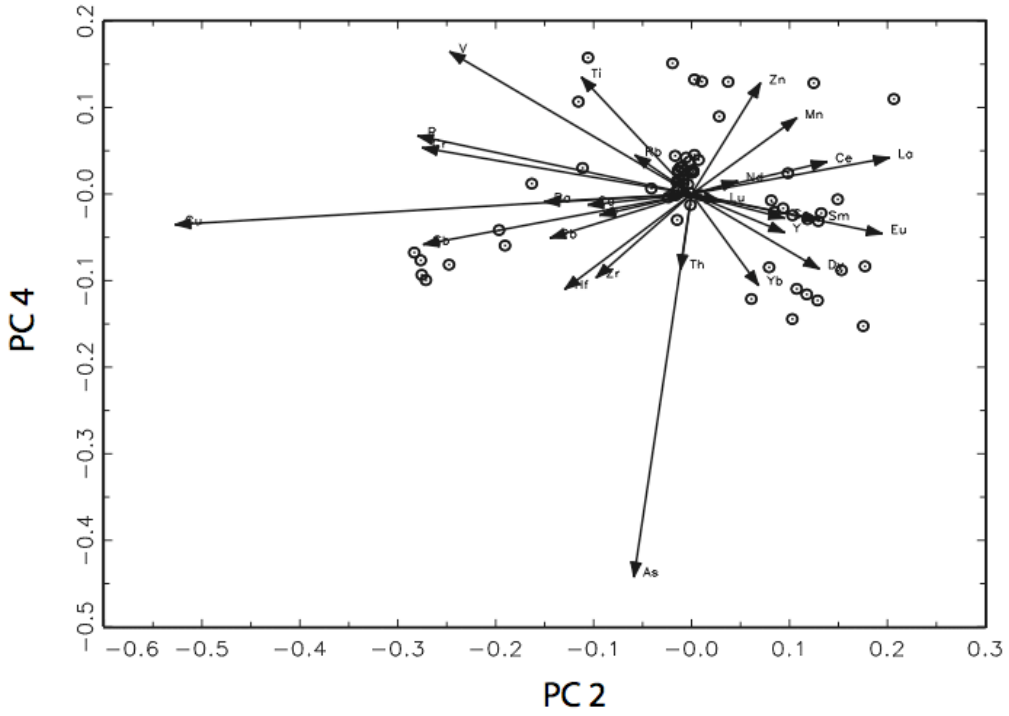

Figure 4.3: Principal component 4 vs. principal component 2 for the concatenated $\log_{10}$ elemental data of INAA and XRF (R-Q mode). Elements are presented as a ratio to Fe.

Principal components 4 and 2 were used in this analysis as the plot of these two components displays the elements that drive the variance most clearly. Despite the operation to normalize Fe content by use of a ratio, and even the elimination of Fe from the calculations, principal component (PC) 1 (79 % of the variance) seems to be most influenced by Fe concentration as discussed in Chapter 2. This result was observed in a similar study performed in Australia, although the authors did not use a ratio transform.[119] Therefore, the first principal component was not used to investigate the elements related to the ochre signature independent of Fe concentration. Principal components 1 through 5 describe 94%

of the total variance for the data set. While the other principal components are not presented here, they demonstrated similar trends to those observed for PC 4 and 2. Elements with the longest vectors were aggregated from the plots of combinations of PC 1 through 5. These elements were then used in the elemental bivariate plots described below.

Trends in the PC plot (Figure 4.3) indicate a general grouping of the individual samples associated with their source sampling. In addition, vectors for elements from the same group in the periodic table often point in the same direction in the PC plot. A clear example of this are the correlated vectors representing Hf and Zr, which may represent quartz composition.

Element ratios with the longest vectors in PC space, and thus greatest variance in the data set include: Cu, Eu, As, P, V, and Sb. These element ratios were plotted in several combinations in bivariate plots to investigate which pairs of element ratios were able to separate subgroups of the southeastern Missouri ochre samples. To satisfy the provenance postulate, inter-source variation must be greater than intra-source variation. In this case, the sources are the individual locations of sampling (Sources A, B, C, D and E). Figure 4.4 is a bivariate plot of $\log_{10}$(Sb/Fe) vs. $\log_{10}$(Eu/Fe).

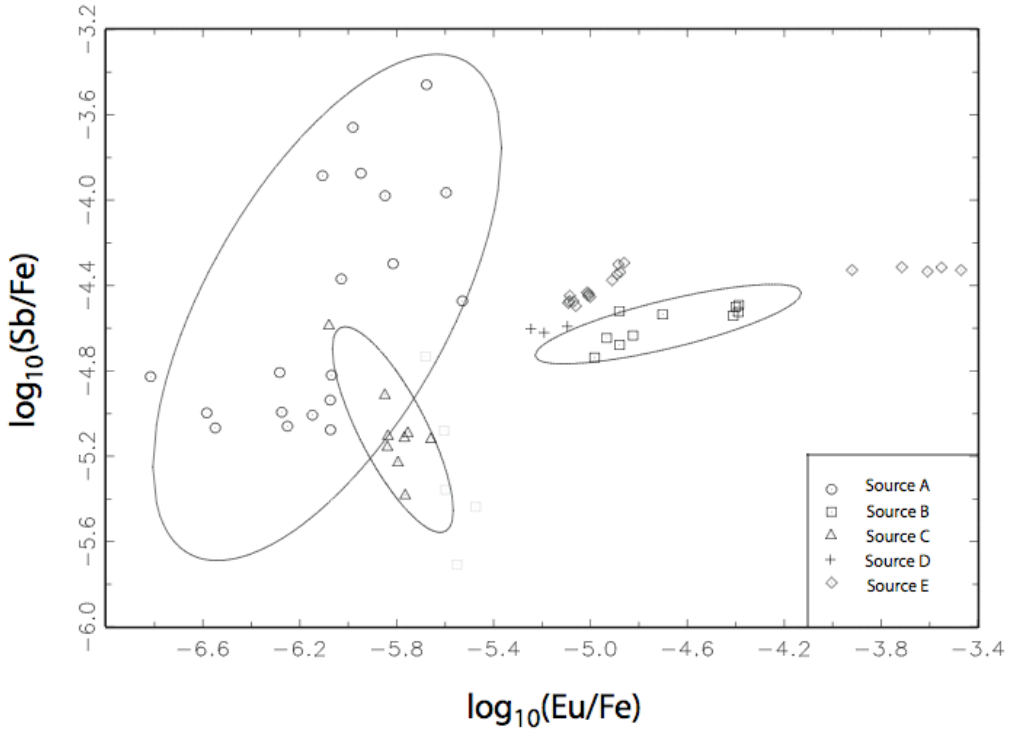

Figure 4.4: Bivariate Plot of $\log_{10}$[Sb/Fe] vs. $\log_{10}$[Eu/Fe], with individual sources identified. Confidence ellipses are 90 percent.

Figure 4.4 demonstrates some of the clearest distinctions between sampling sources and is representative of other similar bivariate plots. Ellipses on the plot are 90% confidence intervals. While there is some overlap of groups, many groups form a distinct cluster. As in Figure 4.4, a bivariate plot of $\log_{10}$(P/Fe) vs. $\log_{10}$(Cu/Fe) also demonstrates clear separation between the sources (Figure 4.5).

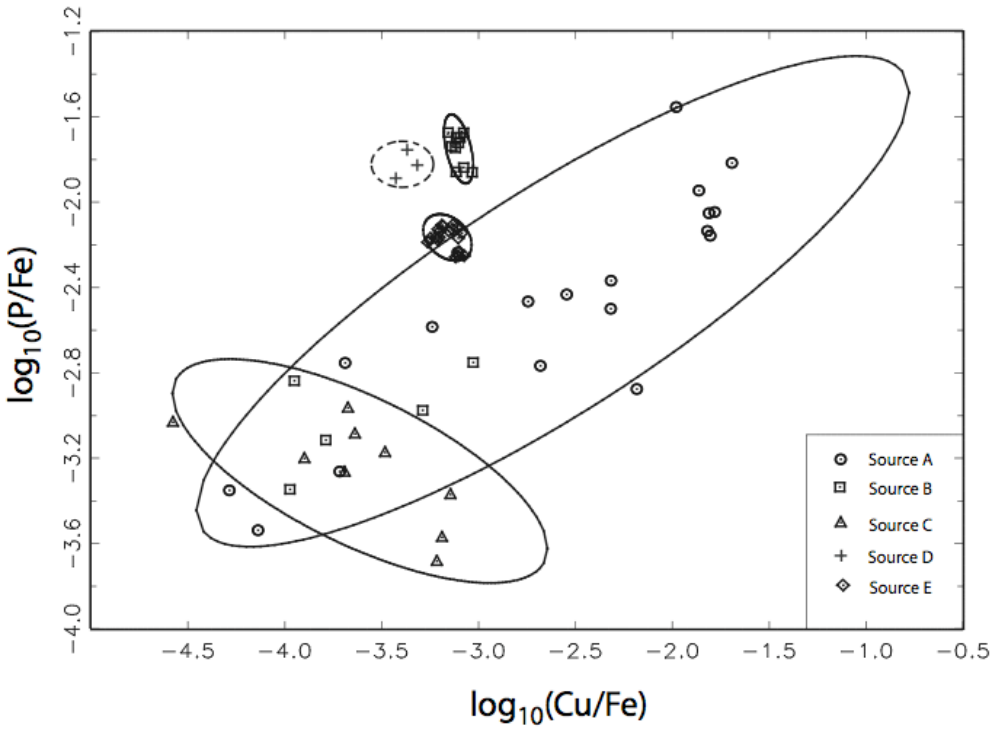

Figure 4.5: Bivariate plot of $\log_{10}$[P/Fe] vs. $\log_{10}$[Cu/Fe] with individual sources identified. Confidence ellipses are 90 percent.

The elements in Figure 4.5 are those analyzed by XRF and not routinely analyzed by INAA. These elements also display variance and grouping of the ochre, but in a different arrangement than that of Figure 4.4. As seen in Figure 4.3, elements in the same group in the periodic table also show similar trends in the composition of ochre. Figure 4.6 is a plot of $\log_{10}$(Sm/Fe) vs $\log_{10}$(Eu/Fe) demonstrating a linear relationship between elements from the same group of the periodic table, in this case, the rare earth elements. This element correlation is to be expected in many geological materials.

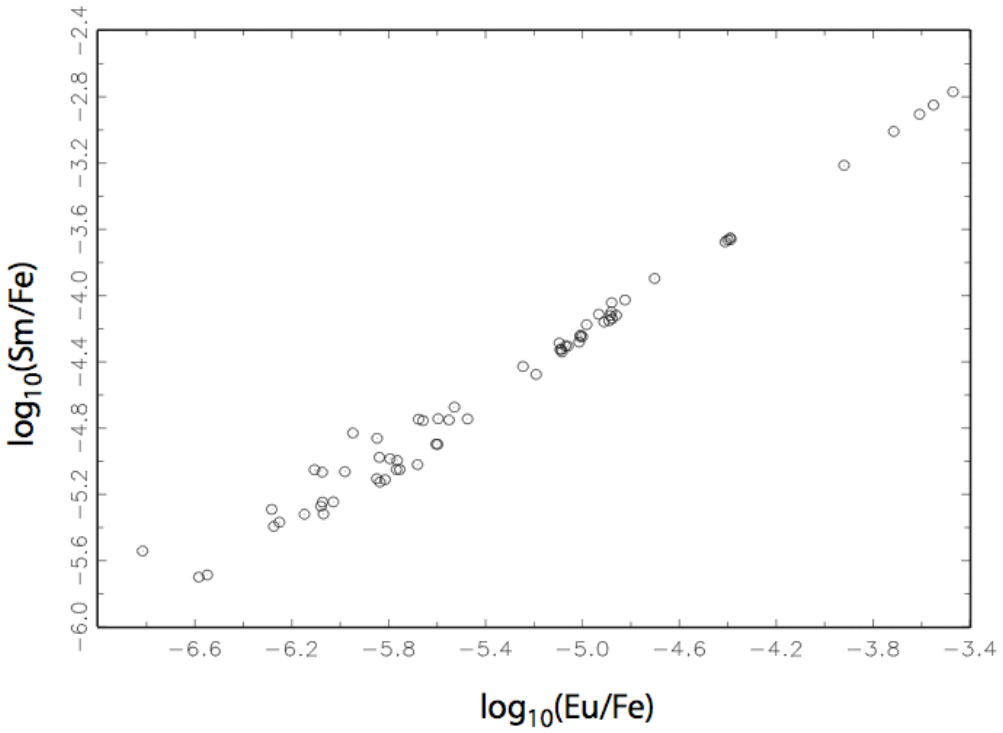

Figure 4.6: Bivariate plot of $\log_{10}$[Sm/Fe] vs. $\log_{10}$[Eu/Fe] indicating linear trends in these elements in ochre.

Discussion

In the majority of bivariate plots, samples from source A were widely distributed. Ideally, samples taken from locations only meters apart should have similar geochemical signature. In the case of source A, however, the location is now a privately owned park, which was heavily mined for iron ore during the late 19th and early 20th centuries. At the actual sampling locations, there were piles of Fe-oxide and other minerals throughout. It is conceivable that despite sampling in a close geographic location, the entire site has been heavily disturbed with tons of material moved throughout the decades of mining. Therefore, sampling may not be representative of a particular location. Sources B, C, and D are also

similar to source A in terms of geography, history, and disturbance. These sources are located on National Forest and private land. They were identified by Mark Twain National Forest Service archaeologists as sites where historical iron ore mining was performed.[151] Several of these sources were old mine pits filled with modern trash. Although sampling was done on the "rims" of the sources, disturbance was evident throughout. In the case of source B, three distinct sub-locations were sampled including a field, a creek bed, and a site with obvious remnants of mining activity, several hundreds of meters apart.

In contrast, samples from sources B, C, and D on the bivariate plots (Figures 4.4 and 4.5), group together in tighter clusters than source A, although there is still some spread within the clusters. However, within sources B and C, sub-source differences can be seen. For example, one sub-source location is distinct but still included within the source B ellipse. One group of B samples is more closely associated with source A than B. Source D is only defined by three samples due to problems with the field sampling in which the selected samples turned out not to be ochre. A suggested region on the bivariate plots is indicated, but at least four samples are needed to calculate a probability ellipse. Source C samples are closely related to each other but no obvious sub-groups are observed. Samples from source C appear to be possibly associated with source A in the bivariate plots, but can be seen to be a distinct group from source A.

Source E has a slightly different history and yields very different results from sources A through D. All 20 samples for source E were taken from a road cut from sub-locations a meter or so apart. The material in the road cut exhibited a very strong red-orange color in contrast to the surrounding soils. These samples were more "soil-like" rather than the other samples from sources A-D, which tended to be rocks or nodules of iron mineral material.

This can clearly be seen in the elemental data, where samples from Source E are 5% Fe in contrast to other sources, where the samples are anywhere from 10 to 55% Fe. In all bivariate plots, samples from source E generally cluster very closely together. One E subgroup is distinctly separate, yet associated with the other samples from source E. Throughout the permutations of elemental bivariate plots, it was seen that this small group of samples were consistently higher in all of the rare earth elements, which can be clearly seen on the $\log_{10}$(Sb/Fe) vs. $\log_{10}$(Eu/Fe) plot (Figure 4.4). Source E is an excellent example of a less disturbed source location that yields a more easily defined chemical signature as well as a tighter group in the PC and bivariate plots

Source A is chemically distinct from Sources B and E. This distinction indicates that inter-source variation is seen in this data set and that sources geographically diverse also can be discriminated in elemental plots. Variation in these sources, inter-source or intra-source, can be attributed to local geochemistry of the iron-bearing materials. The mining disturbance may cloud results of the sampling, but ideally, the chemical "signature" of the five broad sources can be identified from the elemental patterns.

In general, the variation in ochre seems to occur in the transition metals and rare earth elements. Other major components such as K and Si reflect the inverse relationship between these elements and Fe. As Fe concentration decreases, these elements tend to increase as they are the major elements in the composition of the other rock or earthy materials in ochre. Those elements identified as being significantly positively correlated by the Pearson's correlation include transition metals as well as elements from groups 4 and 5 of the periodic table. In general, the rare earth elements are positively correlated with Fe, however the correlation is small and not statistically significant. It is logical that transition metals and

rare earth elements vary in ochre materials and are related to the Fe oxide signature, as many are closely related to Fe chemically and in oxidation/reduction trends.

Figure 4.6 demonstrates that elements in the same periodic group exhibit similar trends in ochre. While $\log_{10}$(Sm/Fe) vs $\log_{10}$(Eu/Fe) is shown in this work, other pairs of elements also demonstrate similar trends. Understanding these trends, among others will help elucidate trace element behavior within Fe minerals overall.

Conclusions

This study provides insight into sampling methodology and ways to characterize multiple locations within an ochre source. The elements identified in this study may not be universal for differentiating between other source locations, but provide the beginnings for an analytical database for ochre.

By analyzing iron minerals from systematically selected Fe-bearing mineral sources in southeastern Missouri, it can be seen that a Fe-oxide signature exists for the areas sampled, and that ochre materials can feasibly be sourced. Despite significant site disturbances and environmental changes, this study found that source location of the ochre materials could be distinguished by elemental analysis. Disturbance in the sources from "modern" mining should be taken into account for this project as well as any other studies concerning provenance of iron-bearing pigments. In an ideal situation, samples would be taken from sources used by aboriginal people that had not been disturbed by modern practices. For an understanding of the archaeological context, the history or ethnohistory of a source is necessary to understand use of the source and possible changes over time.

This study also illustrates the importance of meticulous sampling and choice of sources. One sample is unlikely to be representative of the entire source. Multiple samples from each location in addition to multiple sampling locations are necessary to comprehensively characterize an ochre source. Although the sources of ochre may be hard to distinguish due to some internal variation, it is possible to geochemically characterize regions.

The broad definition of ochre encompasses many types of iron minerals in several geological contexts. As a result of this diversity, iron concentrations will vary dramatically. To account for this variability, ratios of analyzed elements to Fe were used to minimize variation due to Fe concentration. A combination of INAA and XRF provides characterization of the important elements used in understanding sourcing of ochre. These elements broadly belong to the transition metals and rare earth elements, implying a connection between these elements to and the variance of Fe minerals.

This study demonstrates the power of using a combination of the Pearson's two-tailed correlation test and multivariate statistics (PCA analysis), for characterizing ochre. The Pearson's analysis identified elements associated with surrounding minerals (negatively correlated with Fe) and elements associated with the Fe oxide signature (positively correlated with Fe). Multivariate statistics of elements with a positive correlation with Fe were used to describe the variance in the elements within the data set. The results of this study demonstrate that ochre satisfies the provenance postulate in that inter-source variance is greater than intra-source variance. Their "chemical fingerprints" can distinctly identify samples from meticulously sampled, tightly grouped locations.

The five sources in southeastern Missouri provide a foundation for future ochre analytical studies. Similar studies that characterize ochre sources as well as artifacts need to be completed to fully understand ochre geochemistry and provenance.

Ochre Artifacts from Jiskairumoko, Peru

This section describes the analysis of 65 archaeological ochres from different contexts from the Terminal Archaic-Early Formative site of Jiskairumoko, Peru. INAA was conducted to evaluate the heterogeneity of the elemental compositions of ochre artifacts used by residents of Jiskairumoko. Jiskairumoko is located in the Lake Titicaca basin (Figure 4.7). Excavations at Jiskairumoko (Figure 4.8) represent the first systematic archaeological study conducted in the Lake Titicaca Basin of an open air Archaic Period residential site.

Figure 4.7: Geographic location of Jiskairumoko

Table 4.3. Contexts, Dates and Associations for Ochre at Jiskairumoko

Ochre context	*^{14}C Date B.C.*	*Associations*
Drop zone from heat treatment in Pithouse 1	3385–3078	Clay lined hearth inside a structure not far from deer bones.
1 palette and 1 abrader	2473–2119 2072–1878	On edge of and next to Pithouse 2
Ground dust at base of Burial 3	1883–1680	Older adult female buried with a lapstone
Ochre stained manos associated with Burial 4 and ochre stained lapstone from just above burial.	No direct dates	Unsexed adult buried with burned and unburned faunal remains from at least two individuals one adult and one juvenile
Ground dust at base of Burial 5	No direct dates	Individual buried with numerous red chert flakes placed at distal end of interment.
External ochre stain outside Rectangular Structures 1 and 2	No direct dates	Rock-soil feature and split rock altar
Ochre stained animal bones	No direct dates	Rock-soil feature and split rock altar
Ochre stained manos, groundstone fragments found in rock pavement.	No direct dates	Rock pavement, perhaps related to cooking

The site is located in the Rio Ilave drainage in the southwestern basin. [97, 153] Further information on the detailed archaeology of the site was provided by Craig and included in Popelka-Filcoff et al. [110] Key contexts where ochre was encountered at Jiskairumoko are listed in Appendix III.

Project Goals

There were several objectives for the analysis of the Jiskairumoko ochre. The chemical variability of ochre artifacts must be determined in order to evaluate its potential role in ancient exchange and regional inter-community interaction. Ideally, it would be valuable to know if ochre is a non-local resource and where it comes from (e.g. if the source is local or not, and whether multiple sources were used). The primary sources of ochre in the region have not been located, making precise sourcing studies impossible. However, an exploratory study of ochre chemical variability is warranted for several reasons. There is little knowledge about the chemical variability of ochre sources, the reporting of results will increase this understanding. Chemically variable groups may suggest use of either different sources or different portions of a variable source. Are there chemical differences in ochre remains recovered from different contexts of Jiskairumoko's multi-component occupation? Multiple structure types are located at the site and ochre is found in association with each kind. Are these ochres chemically similar or is there high variability? The site's earliest residential context bears evidence of thermal processing of ochre. There is also ochre in later secondary refuse heaps. Is there large variation in composition in the ochres found in the thermal processing context? Some have suggested that color of ochre, (perhaps a result of thermal treatment) is independent of geographic location.[137] Do the ochres found in this early residential context appear chemically similar to ochres recovered in secondary refuse contexts? By understanding the chemical composition of ochre in different contexts, variability in use and procurement of the material can be explored.

Ochre Sampling

A total of 65 ochre samples were recovered from a range of excavated contexts at Jiskairumoko. The samples were analyzed by INAA and the results are presented in Appendix III.

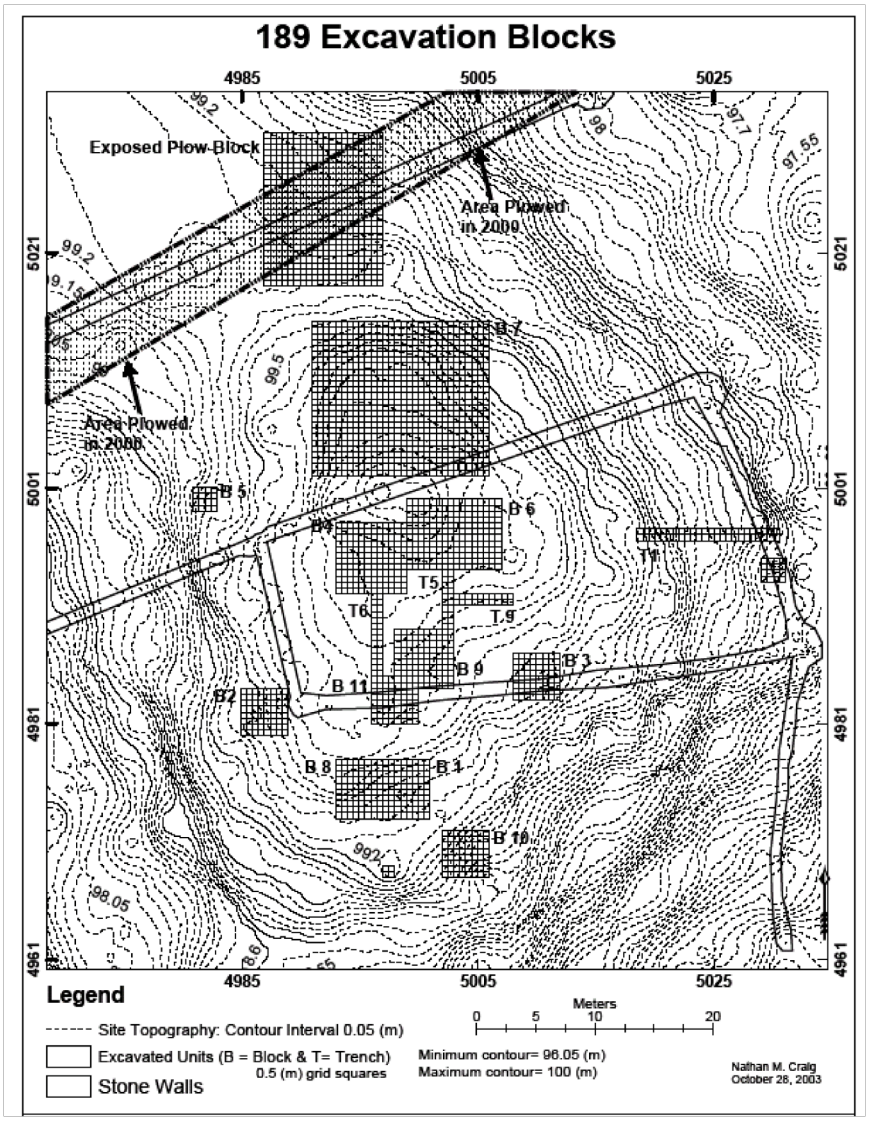

Figure 4.8: Jiskairumoko site map

Ochre samples were recovered as both singular lumps and powdered material. Only ochre masses were analyzed to prevent any possible contamination issues. Samples ranged in color from yellow to dark brown, with varying shades of red and red-brown in between. These color variations may indicate differing iron concentrations or particle sizes, and may be due to inherent impurities in the mineral,[95] or heat treatment. Appendix III lists the examined samples and their Munsell values.

Samples were obtained from pithouse floor assemblages, the perpendicular debris arc found next to the hearth of a Late Archaic pithouse, later expedient hearth features situated in secondary pithouse fill, secondary debris fill in pithouses, from along the edges of later rectangular structures, and from an exterior ritual area.

Statistical Treatment of Data

The raw concentration data were subjected to several mathematical and statistical transformations. The ratio of the element of interest to Fe helps offset inherent variation in Fe across the data set. A $\log_{10}$ transform is a standard statistical conversion for elemental data. This transformation reduces the "weighting effect" from comparing very small to very large concentrations in the data.[13] More details on the calculations and reasoning behind these transforms can be found elsewhere.[113]

Although INAA can routinely measure approximately 30 elements in geological samples by the methods described, several elements were below the detection limits, or were otherwise unreliable elements for ochre. For this study, 16 elements were used: As, Ce, Co, Cr, Dy, Eu, La, Mn, Nd, Sb, Sc, Sm, Sr U, V, Yb and Zn. These elements are similar to other ochre studies as those related to the "Fe-oxide signature" and not the surrounding minerals.[113]

Statistical Operations

An initial study of the data was undertaken using cluster analysis (Clustan software) to identify possible clusters and groups within the elemental data. The cluster analysis included the use of a hierarchical tree diagram to display the results. Distances were calculated using a squared Euclidean distance. The linkage between groups was calculated by the increased sum of squares. The results of the cluster analysis outlined five distinct groups, henceforth referred to as Groups 1, 2a, 2b, 3a, and 3b.

An R-Q mode PCA was also performed on the data set to evaluate the elements in the data set contributing to the variance as discussed in Chapter 2. PC plots graphically indicate a linear combination of original variables, oriented in the direction of greatest variance. PC space also displays the elements with the greatest variation by graphically displaying them with the longest vectors.

In addition, a CDA was performed on the groups defined by the cluster analysis. This statistical procedure was performed to evaluate group differences as defined by the cluster analysis. CDA analysis assumes that the groups are different and calculates the equations describing the greatest difference between the groups.[13]

Results of Sample Variance

The concentrations for Fe ranged from as low as 4 weight percent to as high as 67 weight percent, with a majority of the samples in 35–50% Fe range. The mathematical transform of the elemental ratio to Fe helped to normalize the data for this range of Fe concentration in the samples. After the transformation and PC analysis, several observations were made. Principal components 1–8 described 95% of the cumulative variance for the data

set. Figure 4.9 is a plot of PC 2 vs PC 4 as an example of one of several possible permutations.

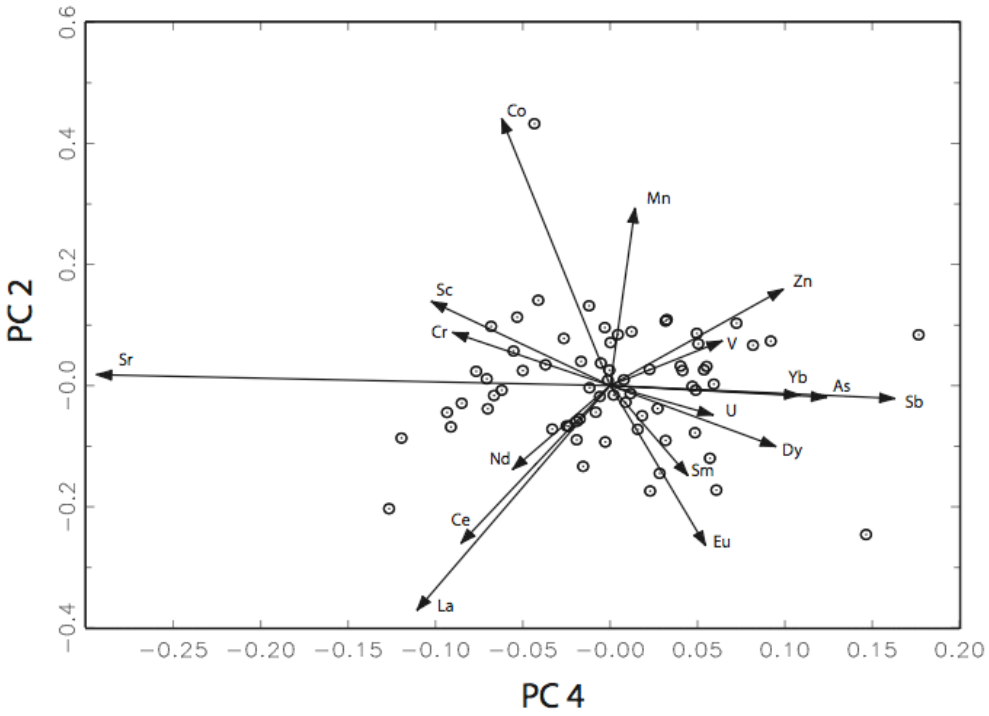

Figure 4.9: R-Q mode principal components plot (PC 2 vs. PC 4) demonstrating elements that drive variance in Jiskairumoko ochre

On this plot, the longest vectors represent the most remaining variance in this two dimensional PC space. Element ratios with the longest vectors in the various permutations of PC bivariate plots in total included: Sr, Co, Mn, Zn, Eu, Sm, Ce and La. Bivariate plots of these elements were explored to ascertain which pairs of elements could be used to visually describe group associations.

The cluster analysis identified five discrete groups based on the trace element chemistry of the selected ochre samples. These five groups were examined several ways to discern possible relationships between the variation in the elemental comparison of the artifacts and possible archaeological significance.

Bivariate plots based on archaeological context were examined to investigate potential contextually specific groupings (Figures 4.10–13). Artifacts were divided into several groups based on archaeological context and plotted according to $\log_{10}$[Sm/Fe] vs $\log_{10}$[Co/Fe] (Figure 4.10), $\log_{10}$[Eu/Fe] vs $\log_{10}$[Zn/Fe] (Figure 4.11). The third elemental bivariate plot was grouped according to cluster analysis and plotted by $\log_{10}$[Eu/Fe] vs $\log_{10}$[Mn/Fe] (Figure 4.12). Figure 4.12 indicates visual grouping of the samples in an elemental plot, with some samples associated in a large group, but other clusters are both visually and statistically distinct.

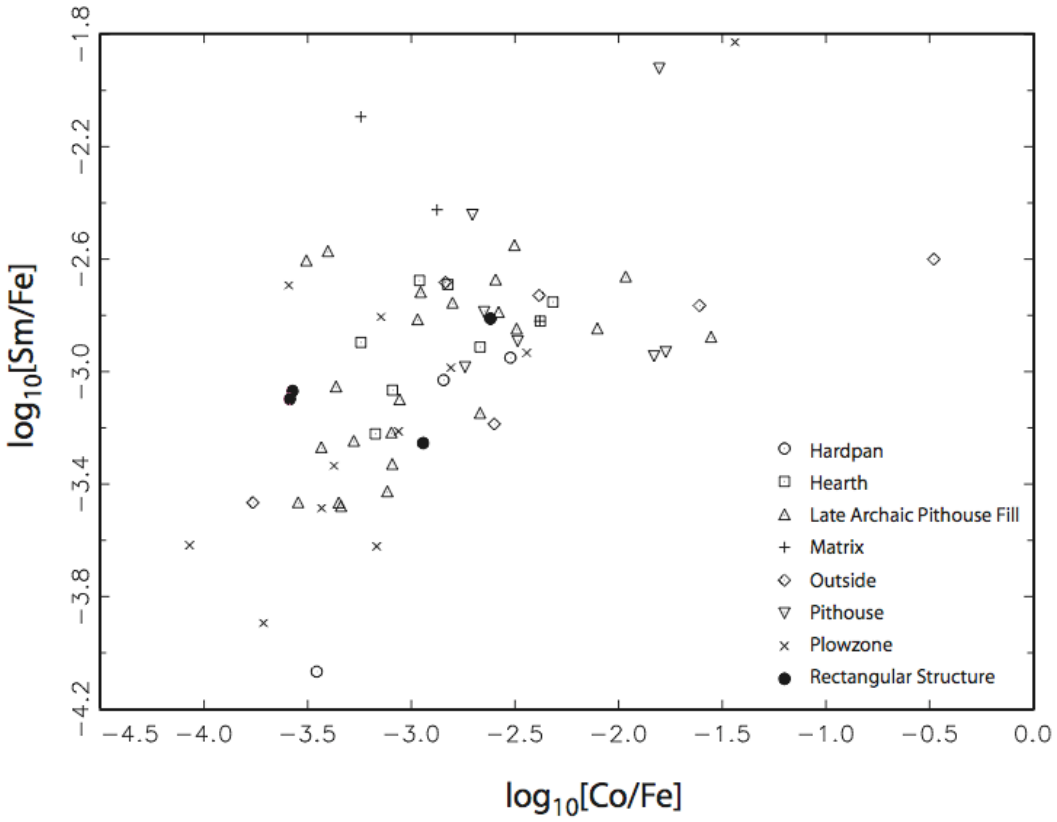

Figure 4.10: Bivariate plot of $\log_{10}$ [Sm/Fe] vs $\log_{10}$ [Co/Fe].
Samples are plotted by groups as determined by context.

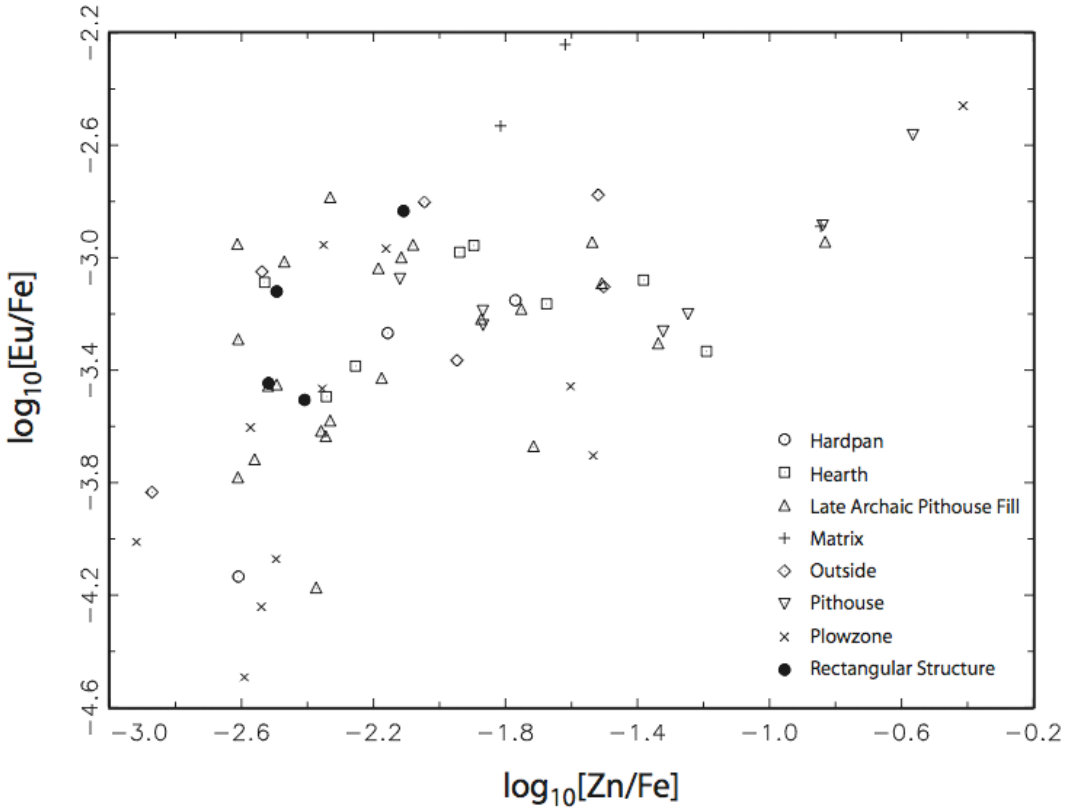

Figure 4.11: Bivariate plot of $\log_{10}$ [Eu/Fe] vs $\log_{10}$ [Zn/Fe].
Samples are plotted by groups as determined by context.

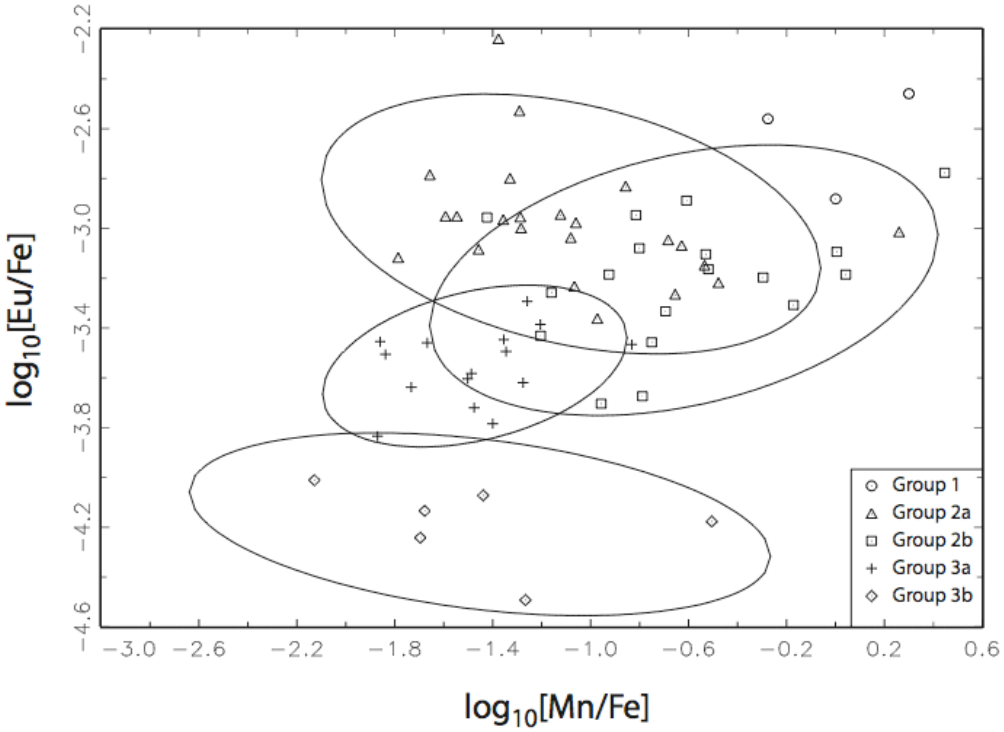

Figure 4.12 Bivariate plot of $\log_{10}$ [Eu/Fe] vs $\log_{10}$ [Mn/Fe].
Samples are plotted by groups as determined by a cluster analysis.
Group 1 did not have enough samples to form an ellipse.

Canonical discriminant analysis (Figure 4.13) indicates that by using CD1 and CD2, groups defined by the hierarchical cluster analysis are well defined and have analytical merit. Group 2a, 2b, and 3a appear to be associated in one central aggregation, while Group 3b is somewhat separated from this central concentration. Group 1 emerges as a distinct cluster that is very different from the others.

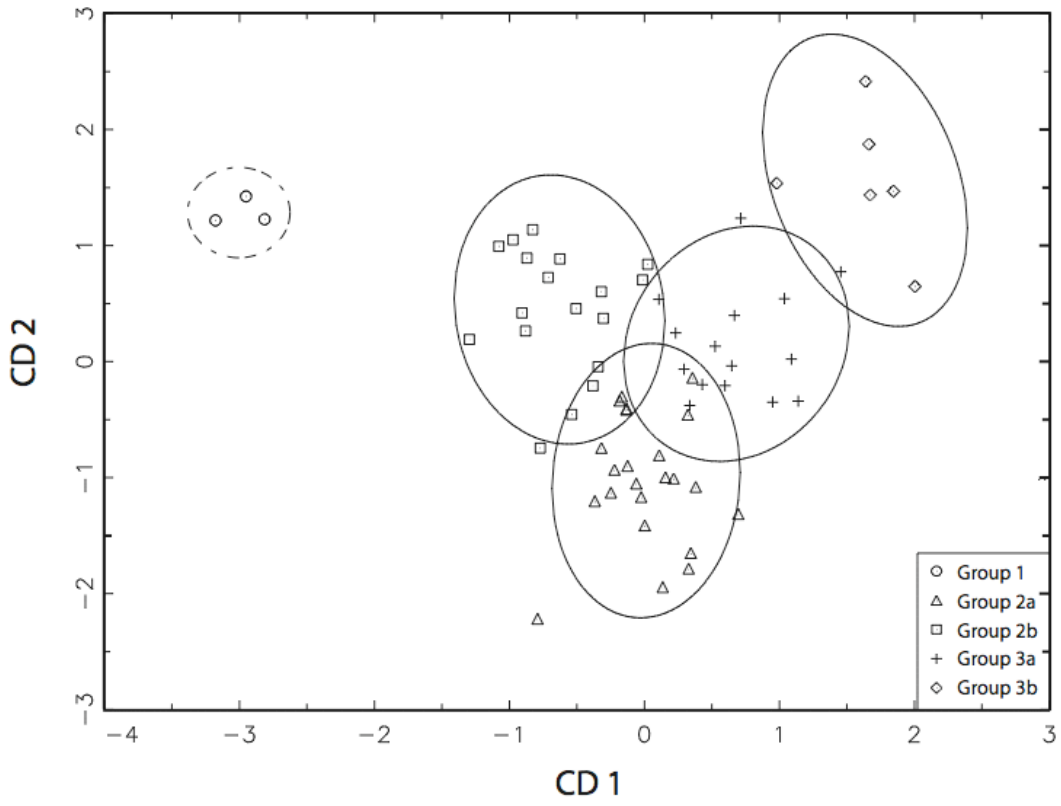

Figure 4.13: Canonical discriminant analysis plot (CD2 vs CD1).
Samples are plotted by groups as determined by a cluster analysis.

The groups found in this project display variation in their chemical composition. Because sources were not analyzed in this study, the variation in sources cannot be quantified. However, the variation in groups implies different procurement practices or variation within the procurement site. Depending on the source and the geochemistry of the region, different elements and element groups can be used to characterize the sources and artifacts. Sub-source variation in the major source may also be present.[113] It can be seen from these data that the trace element analysis of ochre is helpful for understanding its variability. The following section will discuss archaeological interpretation of the variation in ochre composition at the site of Jiskairumoko.

Archaeological Interpretation

In considering archaeological interpretation of the results from chemical characterization the five questions described in the project goals were addressed in a collaboration with Dr. Nathan Craig.[110]

1) What is the overall variability of ochre? Variability is present, but it is not large. Given the paucity of ochre chemical characterization studies, evaluating the degree of variability is problematic. Hierarchical clustering suggests the presence of five groups, which were corroborated by canonical discriminant analysis. Groups 1 and 3b appear to be the most dissimilar from the majority of samples. Groups 2a, 2b, and 3a may comprise a single heterogeneous cluster.

2) Are there chemical differences in ochre remains recovered from different contexts? Variability is present, but does not appear to be context-specific. The majority of samples are scattered throughout, as seen in Figures 4.10 and 4.11. The samples that comprise this aggregation come from all of the depositional contexts sampled at Jiskairumoko. Ochre sampled from the different archaeological contexts at Jiskairumoko is not chemically distinct.

3) Are ochre artifacts from different household structures chemically similar or different? Ochre artifacts from different structures are chemically similar. Samples 368 and 320 are very close together in CD space as well as the $\log_{10}$[Sm/Fe] vs $\log_{10}$[Co/Fe] and $\log_{10}$[Eu/Fe] vs $\log_{10}$[Zn/Fe] bivariate diagrams (Figure 4.10 and 4.11). Sample 368 comes from a sealed context at the base of the Late Archaic pithouse while sample 320 was recovered from the edge of a large rectangular structure. Both samples come from clear and unambiguous contexts. However, they are very similar chemically indicating that either the

same source or the same portion of a heterogeneous source was used throughout the span of Jiskairumoko's occupation.

4) Is there large variation in the ochre from the thermal processing area? Figures 4.10-12 and the CD plot (Figure 4.13) indicate that there is considerable chemical variability in the samples taken from the hearth in the base of the Late Archaic pithouse and from the hearth-associated debris arc. This variability suggests that ochre in this activity area was obtained either by 1) trips to different parts of a single source or 2) exchanges for ochre from different sources or 3) mixing of ochre with other materials. It is not likely that the thermal treatment of the ochre significantly altered the trace chemical signature of the ochre. The chemical variation between of ochre artifacts in this context suggests use of different portions of a single source or multiple sources are represented. This information serves as an additional line of evidence indicating that the debris arc next to the hearth was not the outcome of a single behavioral episode. Instead, it represents habitual hearthside activity.

5) Is the ochre from this context similar to ochre found in secondary refuse? Elemental and CD space plots all indicate chemical similarities between ochre artifacts recovered from the central hearth and debris arc encountered at the base of the Late Archaic pithouse. The occurrence of chemically similar ochre artifacts in both contexts provides additional evidence that secondary refuse deposits were formed by cleaning hearths and removing debris from inside structures.

Several other observations can be made from Figures 4.12 and 4.13. Group 1 exhibits the greatest distance in CD space. This group consists of samples from the plow zone, deep within the fill of Pithouse 3, and a stain outside Pithouse 3. Group 1 may represent a source, or portion of a source, that was not generally preferred by occupants of Jiskairumoko. None

of the samples forming Group 1 were recovered from early occupational contexts at Jiskairumoko, although none can be attributed to later contexts with confidence. Samples comprising Group 3b are all from plow zone contexts except for samples 315 and 342. The latter two samples are not from early contexts. Thus, Groups 1 and 3b, which are the most chemically distinct, do not appear to include any samples recovered from early contexts. For example, none of the ochre from Late Archaic pithouse contexts is members of either Group 1 or 3b. These two groups may represent two portions of a single heterogeneous source or two different sources that were not preferred by residents of Jiskairumoko.

Conclusions

Although the artifacts could not compared to the ochre sources from the region, some tentative conclusions about the variability of ochre and its use at Jiskairumoko can be drawn. Chemically distinct groups of ochre were found from Jiskairumoko. Major elements, such as Fe, Mn, and others, are important as the trace elements, such as the rare earth elements, in studying ochre variability. Viewed in a number of different dimensions and transformations, a majority of ochre samples appear to form a single rather heterogeneous congregation that comprises all of the depositional contexts that were sampled. Ochre use within any given depositional context is comprised of members of more than one statistically defined group. The clusters consist of samples from multiple depositional contexts. Without locating and characterizing a range of ochre sources it is impossible to determine if these reflect multiple sources or a single heterogeneous source. Later in time, either two additional portions of a source or two additional sources may have come into use. Additional work locating and characterizing Andean ochre sources is needed.

Ochre Sources from the Tucson Basin, Arizona

In order to identify the original source of any ochre from a given archaeological site, the geochemical sources must be characterized. The characterization of sources from a region helps to provide information about local or regional exchange in raw materials, in this case, iron oxide minerals. This section describes the intensive sampling and instrumental neutron activation analysis (INAA) of ochre from the Western Tucson Basin, Arizona and the subsequent multivariate analysis of the data. This study has several goals, including characterizing variance in ochre geochemistry within and between sources, identifying the important elements in characterization of ochre, and establishing a database for further comparison. The overall objectives are to explain the geochemistry of ochre in the region of Tucson, Arizona as well as understanding ancient ochre procurement.

Description of Sources

Ochre sources in the West Tucson Basin, Arizona have been identified through fieldwork by archaeologists and geochemists at Desert Archaeology Inc. as likely places for ochre procurement.

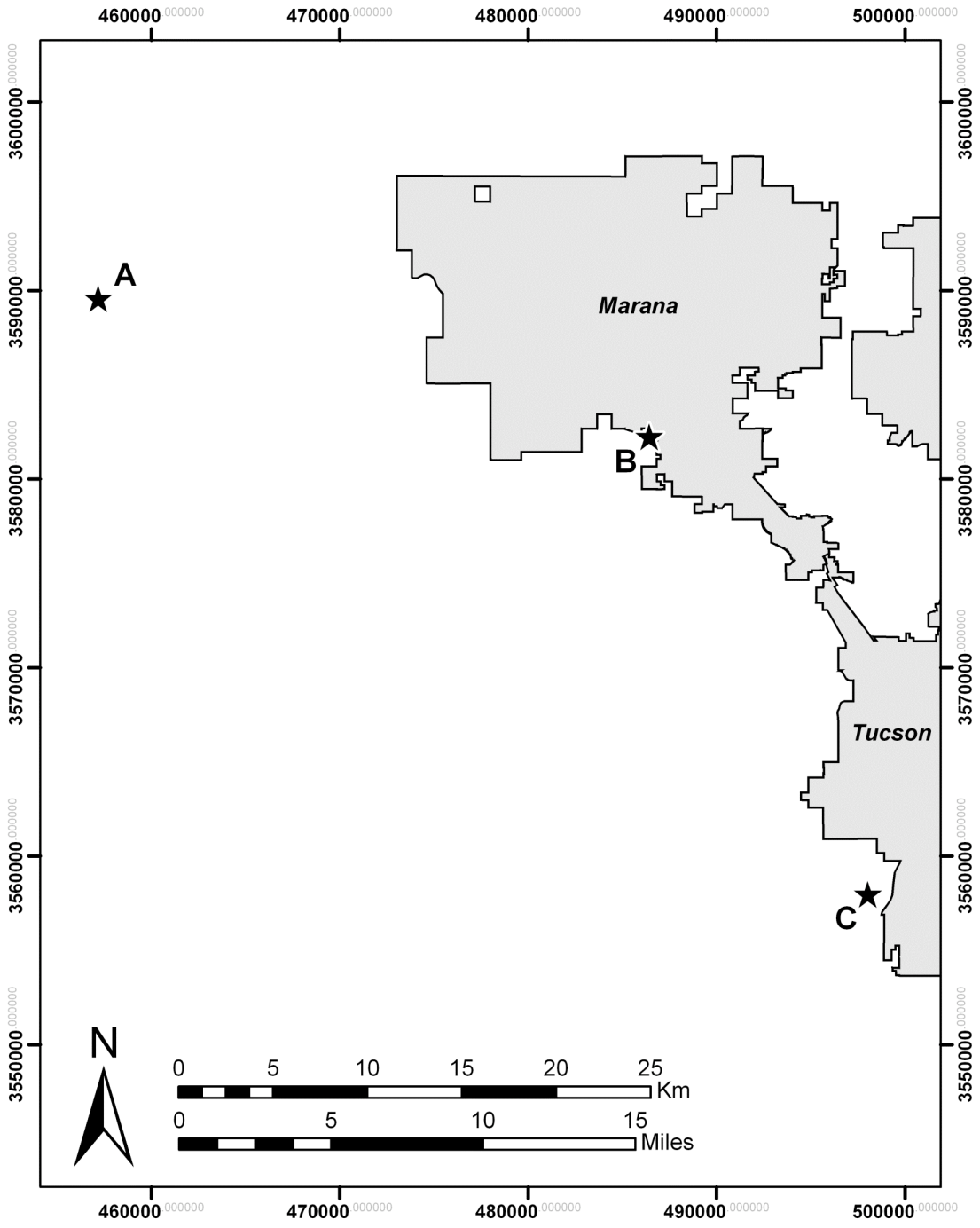

Figure 4.14: Locations of ochre sampling for Arizona.
A. Ragged Top, B: Rattlesnake Pass, C: Beehive Hill

Archaeological evidence suggests that sites nearby were processing areas for ochre from these sources. Exactly 120 ochre samples were collected from three locations: Beehive Hill, Rattlesnake Pass, and Ragged Top. Of these, 100 were processed for analysis by instrumental neutron activation analysis. The sampled sources were carefully documented and described from a geological perspective. (Appendix IV)

The material at Beehive Hill is generally described as an iron-rich soil forming on colluvium covering the hills in the surrounding area. The color of the oxide material is a light orange-red. The material from Rattlesnake Pass includes both colluvium as well as possible gypsum materials hosting the hematite deposits. These materials are particularly friable and crumbly, with a color in the light orange-red shades. Ragged Top is identified as a possible hematite source, made up of iron-rich, harder sedimentary rock. This iron oxide material tends to be darker than the other two sources, with tendencies into the red-brown shades. It is likely that these deposits are mostly hematite, because this is the prevalent mineral in sedimentary formations in drier climates.[123]

Sampling

Three main sources (Beehive Hill, Rattlesnake Pass, and Ragged Top) were selected to fully characterize the individual source, and to investigate differences between sources, and the degree of homogeneity within a source. Samples were collected and documented by Desert Archaeology, Inc. staff, during the summer of 2005. Sampling distances between Beehive Hills 1 and 2 were on the order of 1-2 km. Sampling distances between the Beehive Hill group and the other two groups (Rattlesnake Pass and Ragged Top) were on the order of

15-45 km. Thus, this sampling provides information concerning ochre differences on both a local and regional scale.

For each of the sub-sources within the three main sources, there were five individual sub-samples taken. Multiple sampling allowed a more complete characterization of the source as well as a more complete and correct statistical evaluation of the sources. The methodology allowed thorough characterization of each source, especially for understanding the variation within the source. In order to possibly trace artifacts or other archaeological ochre materials to these original sources, the differences between sources must be greater than within the variation the sources, thus validating the provenance postulate.[52]

Sampling was also performed to ascertain the differences within sources. For instance, Group 1041 (245-249) was taken in a confluence zone between Beehive Hill #1 and #2. This sample was taken to establish the relationship between this region and the two Beehive Hill areas. It was anticipated that this sample would fall midway between the two sub-sources. (Figure 4.14)

Statistical Analysis

Data processing followed established routines described elsewhere.[113] From the total data set, only elements that could be measured reliably by INAA in a majority of the samples (i.e. not below detection limits) were used for the analysis. A Pearson's correlation was used to determine which elements were associated with Fe, and which were associated with the surrounding minerals. Only those elements that were positively correlated with Fe in the Pearson's analysis within the 90% confidence interval were used in further analysis, leaving a group of 17 elements for data analysis. For each element, the data used in subsequent

mathematical analyses was computed as a ratio to Fe in the sample. This ratio was used to normalize any weighting in the analysis due to very large or very small concentrations in Fe across the data set. The large variance in Fe resulted from the presence of other geological material in the ochre samples. The Pearson's results as well as the ratio helped to determine elements associated with Fe in the iron oxides, henceforth referred to as the Fe-oxide signature of the material. The calculated values were then $\log_{10}$ transformed for use in statistical analysis. Multivariate analysis (principal components and canonical discrimination analysis) followed to analyze and quantify variance in the data set.

Results

Iron concentrations in the Arizona sample set varied from 8 to 81 weight percent with the majority of values in the range of 20 to 40 weight percent. The majority of samples have iron values consistent with other ochre materials examined in other studies, thus no samples were rejected based on Fe concentration. There is no apparent trend between the concentration of Fe in the samples and the source location, as all sources analyzed have a wide spread of Fe concentration. PCA was performed and the results were examined.

In this data set, principal components 1-6 were found to describe 97% of the total variance. By using a combination of the two-dimensional plots of PC 1 through 6, the elements that describe the greatest variance across the data were gathered. These elements include: As, Sb, Zn, Co, Mn, Eu, Lu, and Cr.

Discussion

Figure 4.15 displays the results of the principal components analysis for principal component (PC) 4 vs 2 as a representative example of other PC plots.

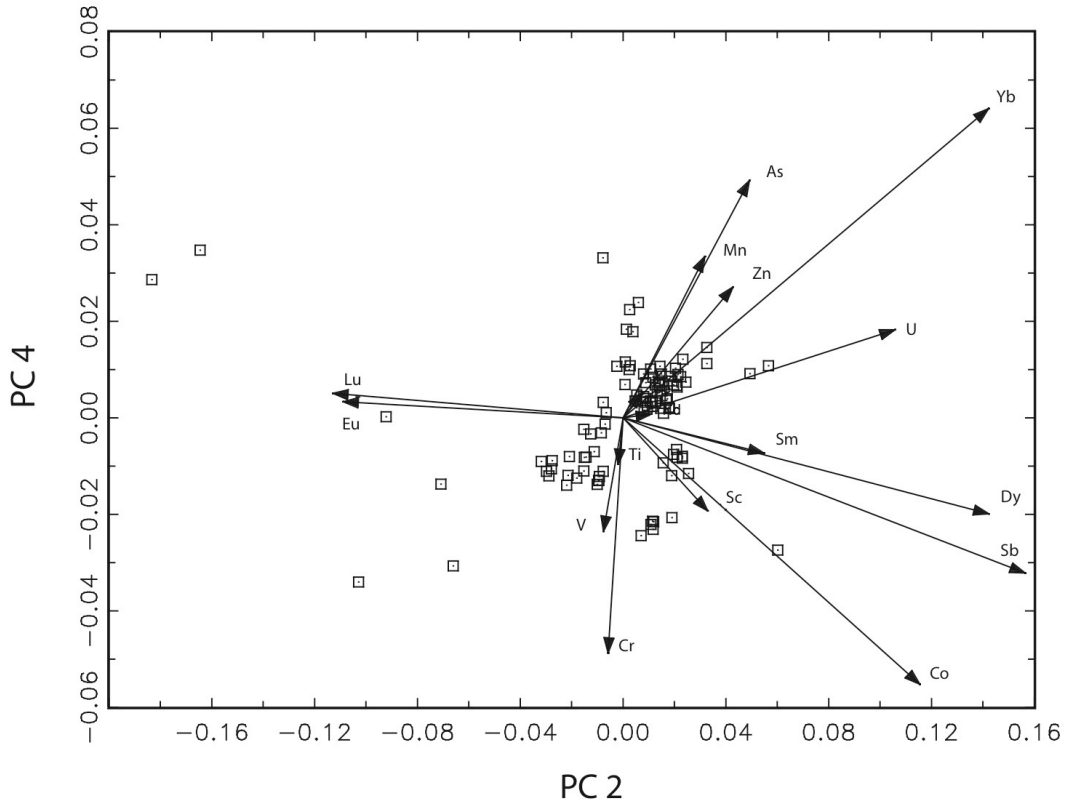

Figure 4.15: R-Q mode principal component (PC) plot of PC 4 vs PC 2 demonstrating elements that drive the variance in this sample set.

Similar to ochre from other regions of North America, the discriminatory elements generally fall into the transition metals and rare earth elements.[110, 113, 150] It has been suggested that some or all of these elements may substitute in the Fe(III) oxide lattice,[96] thus leading to signatures in the ochre that are characteristic of the source despite weathering and

other environmental changes. Figure 4.16 displays a bivariate plot of $\log_{10}$[Sb/Fe] vs. $\log_{10}$[As/Fe].

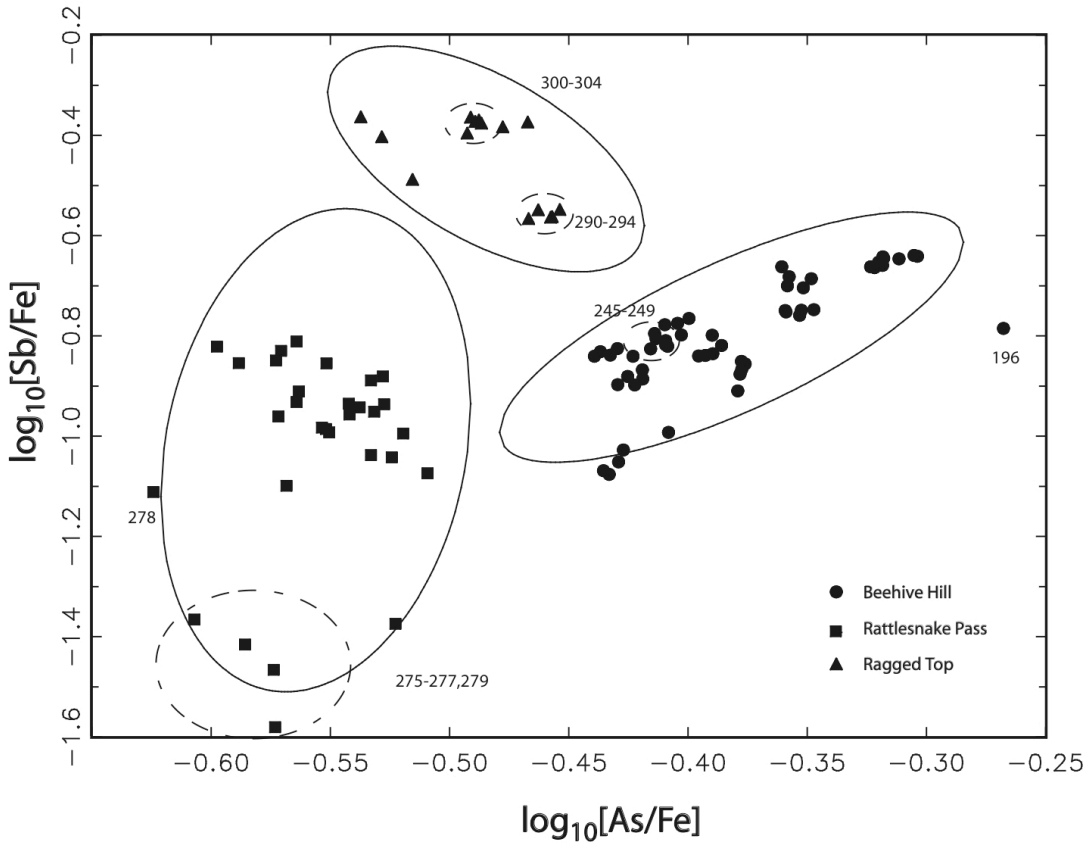

Figure 4.16: Log_{10}[Sb/Fe] vs. $\log_{10}$[As/Fe] demonstrating dispersion of groups. Confidence ellipses are 90%. Dashed ellipses do not indicate statistical significance.

This plot provides a clear example of other bivariate plots of pairs of element ratios that also demonstrate source grouping. The groups from Beehive Hill, Rattlesnake Pass, and Ragged Top can be easily distinguished from one another, demonstrating that this pair of element ratios can be used to distinguish between the major source areas on a regional scale. In addition, sub-sampled areas can also be observed as smaller clusters clearly in the groups,

suggesting that intra-source differences can be characterized. Figure 4.17 plots $\log_{10}$[As/Fe] vs. $\log_{10}$[Mn/Fe].

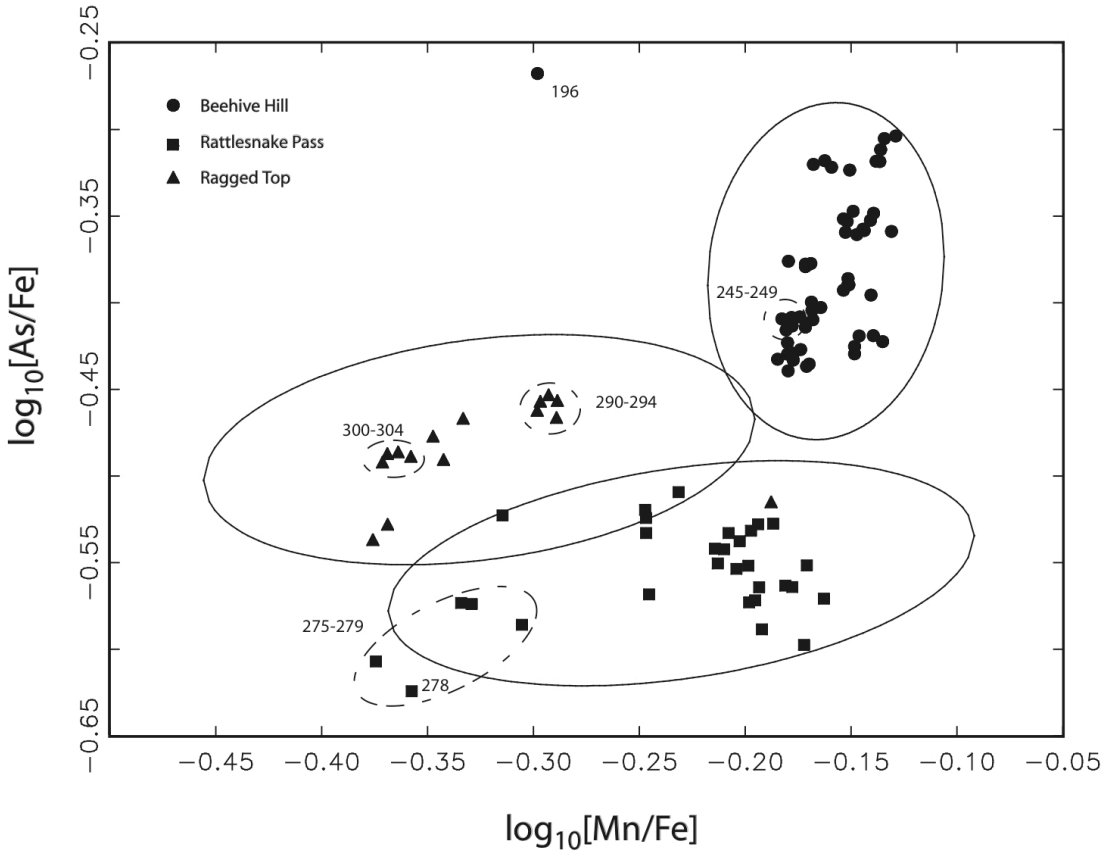

Figure 4.17: Log_{10}[As/Fe] vs. $\log_{10}$[Mn/Fe]. Confidence ellipses are 90%. Dashed ellipses do not indicate statistical significance.

While the groups have shifted, the distinction between the groups is still clear. Some of the sub-sampling regions in the individual sources are also slightly more cohesive than in Figure 4.16. Among all of the bivariate plots, arsenic was routinely found to be an element useful for identifying sub-sampled areas. While arsenic appears to be an element than could consistently differentiate the geographic groups, antimony also is a strong discriminator in this data set.

A few of the outliers in Figures 4.15 and 4.16 were examined in detail. Sample 278 had an extremely low Fe concentration of 8 weight percent, and a corresponding low concentration of Zn (12 weight percent). The remainder of the sample was made up of Ca (24 percent) and perhaps Si and other materials which could not be measured by INAA, although could be quantified in an XRF study. Its closest source affiliation is Rattlesnake Pass. A cluster of samples 275-279 were taken from a location at a topographically lower area. From its appearance in the field, these samples were thought be "desert rose" or related to barite and gypsum crystals. This cluster, although affiliated with Rattlesnake Pass, tended to form its own widely spaced cluster a distance away from the main group of Rattlesnake Pass. While elemental analysis cannot determine mineralogy, the higher concentration of Ca and slightly lower concentration of Fe suggest that this mineralogical assessment is likely. Despite the difference in mineralogy, between gypsum/barite and hematite, it can still be seen that the Fe-oxide signature can be identified and associated with the group.

Sample 196 also fell outside of the confidence ellipse, with an abnormally high value of As and low value of Co. Nevertheless, it is still more closely associated with Beehive Hill than any other source. Samples 245-249 do not have appear to favor either Beehive Hill #1 or #2, but instead form a subgroup with the larger group that describes both sites. From an initial investigation, this group situated at the confluence of Beehive Hill #1 and #2 does not appear to be influenced from its geographic location between the hills, and appears to display characteristics of both hills.

Sample 289 was the only sample that could be processed from a sub-sampling region on Ragged Top. It is associated with other Ragged Top samples in most plots. However, in a plot of $\log_{10}$[As/Fe] vs $\log_{10}$[Mn/Fe] (Figure 4.17), it is higher in Mn than other Ragged

Top samples, placing it in Rattlesnake Pass source group. Since there is only one sample for this sub-source, it is difficult to make definitive conclusions about this sub-source.

Samples 300, 302 and 304 were the only samples processed from another sub-sampling region. In most of the bivariate plots (Figure 4.16-18), these samples cluster together and are separated from samples from the other sub-sampling regions. With three samples, it can be stated with greater confidence another true sub-region probably exists in the of Ragged Top data.

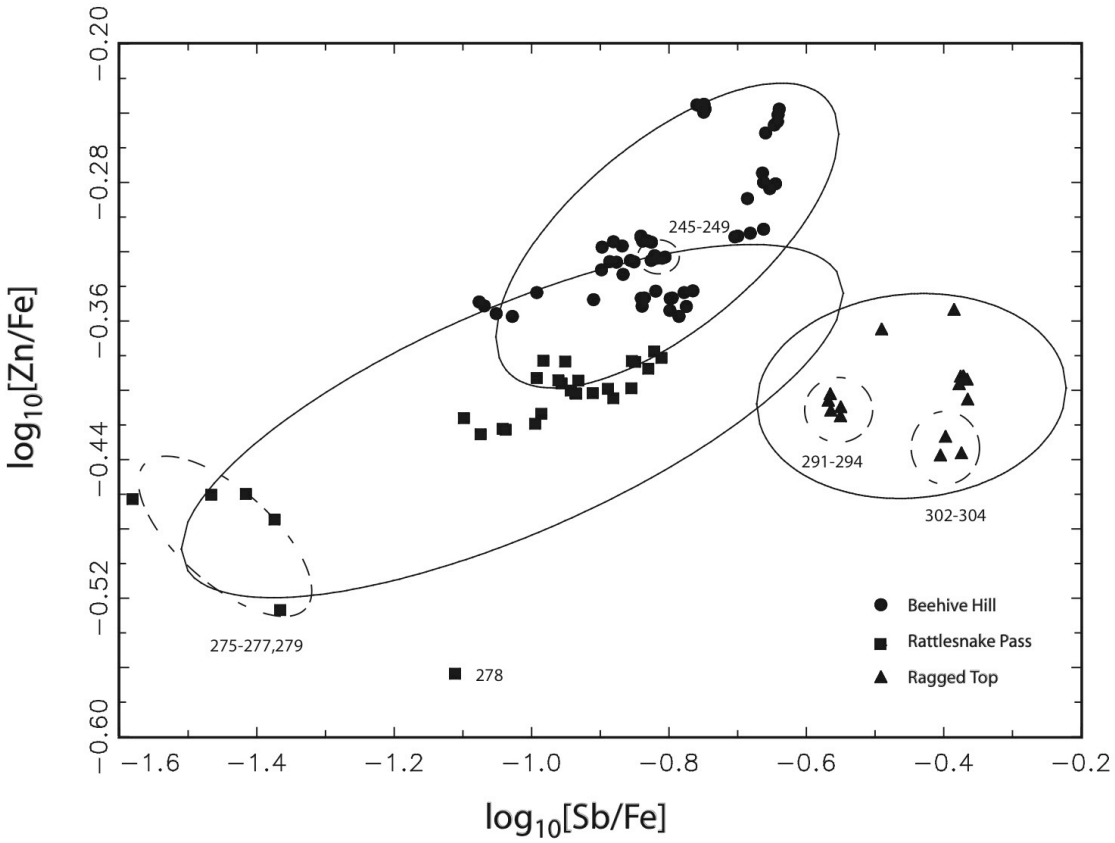

Figure 4.18: Log_{10}[Zn/Fe] vs. log_{10}[Sb/Fe]. Confidence ellipses are 90%. Dashed ellipses do not indicate statistical significance.

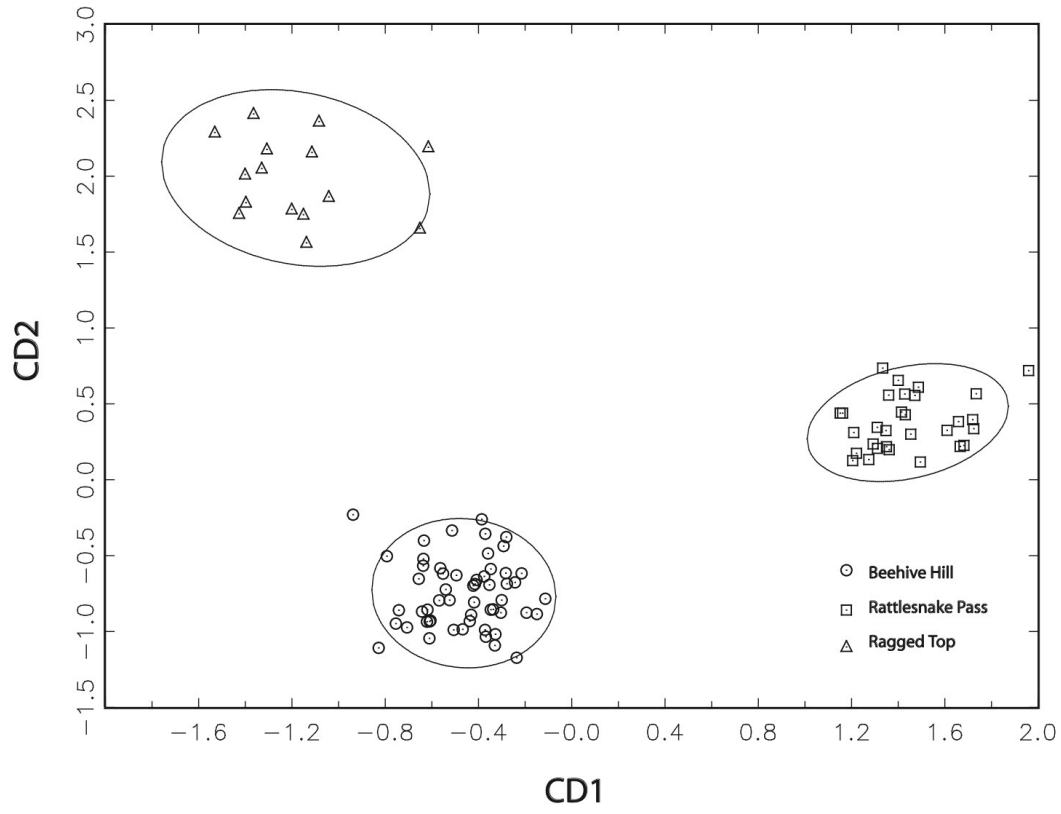

Figure 4.19: Canonical discriminant 2 vs. canonical discriminant 1 for Arizona ochre. Confidence ellipses are 90%.

The results of the canonical discriminant analysis are presented in Figure 4.19. The plot of CD 2 vs CD 1 demonstrates that Ragged Top, Rattlesnake Pass and Beehive Hill are statistically different groups. A post-classification analysis using Mahalanobis distance calculations tested the definition of the source groups. It was found that each 100% of the samples were attributed to their respective groups, confirming the distinctiveness of each of the sources Beehive Hill, Rattlesnake Pass, and Ragged Top. The Wilk's lambda result is 0.0019, indicating a high degree of discrimination between groups. The p value is 0.0000 indicating discrimination of groups within the 90% confidence interval. This CDA analysis corroborates earlier discussion of the three sources as geochemically distinct entities.

Conclusions

The work on Arizona ochre sources presents an interpretation of compositional data from INAA and multivariate statistics for a selected group of geological sources from the Western Tucson Basin, Arizona. Through principal components analysis, elements that drive the variance were identified. Some of the variables were selected for display in bivariate plots. These elements generally are members of the transition metals and rare earth element groups, similar to those found in other studies as important to discriminate between ochre. Element ratios such as As/Fe and Sb/Fe demonstrated clear distinction between groups in bivariate plots. In addition, As provided further distinction of the sub-sampled regions within the sources.

Through the use of multivariate statistics, the three sources of Beehive Hill, Ragged Top, and Rattlesnake Pass were investigated for both within and between source variation. From a geochemical perspective, the three groups of are distinctly different iron oxide sources. This is demonstrated through presentation of the data in elemental space in several pairs of diagnostic elements. The canonical discriminant analysis also demonstrated that the three identified geographic groups are statistically different and have unique elemental signatures. Both statistical analyses indicate that the sources, even those in close geographic proximity, have a distinct geochemistry that satisfies the provenance postulate and allows differentiation between the sources. The ability to characterize the sources on a kilometer scale is important for understanding both the variance in iron oxide ochre across a given landscape as well as identifying sources which may have been used in ancient times.

North American Ochre

This study had several goals: first, to present and perform a meta-analysis of all the INAA data for ochres from North America to date. The second goal is to perform multi-variate analyses of the data to understand variability in the data set. The third goal is to document the important trace element indicators for ochre sources in North America. Fourth, the study aims to interpret possible comparisons or connections between the sampled sources and artifacts; and fifth, to discuss possible archaeological conclusions from the elemental analysis.

Statistical Analysis

Data processing followed the routines described elsewhere.[113] From the total data set, only elements that could be measured reliably by INAA (i.e. not below detection limits) were used for the analysis. A Pearson's correlation was used to determine which elements were associated with Fe. Only those that could positively be associated with Fe in the Pearson's analysis within the 90% confidence interval were used in further analysis. Thus a group of 17 elements were used for data analysis. For each element, the data used in subsequent mathematical analyses was computed as a ratio to Fe in the sample. Multivariate analysis by principal components and canonical discrimination analysis followed to analyze and quantify variance in the data set.

Artifacts and Sources

Knowledge of the provenance of ochre specimens is important for any study is important for the ultimate analysis and discussion. Whether in an archaeological or

geological context, the original location of the ochre is central to understanding its possible uses, movement and exchange in ancient communities. For this study, artifacts and sources were treated by separate analyses. Similar to other archaeological materials, such as ceramics, in many cases the artifact may be quite different from the raw material due to ancient processing. During prehistoric times, ochre was treated by heating it, mixing it with binders, or mixing pigments together for a particular quality or effect. Therefore, raw materials and human-altered materials were be treated separately for statistical sourcing studies. The original materials were analyzed by the same analytical parameters as the artifacts to eliminate any other possible variation in the study and allow for direct comparison between sources and artifacts where possible. Tables 4.4 and 4.5 outline the source and artifact information for each site.

Table 4.4: Ochre Sources investigated in this study

Location	Number of Samples	Researcher
Southeastern Missouri	65	Popelka-Filcoff et al., 2005
Western Tucson Basin, Arizona	100	Miksa and Wallace, 2005
Various California	23	Erlandson et al., 1999
Various Oregon	9	Erlandson et al., 1999

Table 4.5: Ochre Artifacts investigated in this study

Location	Number of Samples	Researcher
W. Central Texas (McCullogh County)	35	Ellis et al. 1997
Southeastern Alaska	7	Mrzlack, 2002

Sources

The sources studied are presented in Table 4.4, and come from Missouri, California, Oregon and Arizona. While fragmentary INAA data exists from other locations around

North America, all comparisons were made with multiple samples per state or source. This provides a more complete comparison and improved statistical interpretation. In some cases such as Missouri and Arizona, the sources were more thoroughly sampled, whereas in Oregon and California, the sources are represented by only one sample per source.

All data sets were concatenated into a single large data set for the introductory analysis. Elements used in the analysis included: As, Ce, Co, Cr, Eu, Mn, Nd, Sb, Sc, Sm, U V, Yb and Zn. These elements are those that can be measured reliably by INAA as well as those most likely to be associated with the Fe-oxide signature.[113] Appendix V has the elemental data for some of the ochre material studied. Other data used in this study has been published elsewhere.

A principal components analysis was performed to determine the elements that are responsible for variance in the concatenated data set. The elements most responsible included: Eu, Sb, Cr, As and Mn. This data set appears to have the same elements that differentiate sources as found in other studies, namely transition metals and rare earth elements.[113, 150] For sources, principal components 1-7 describe the variation in 96% of the data set. Similar to other ochre studies, despite the ratio to Fe, PC 1 tends to be driven most strongly by Fe concentration. Other principal components demonstrated elements that drove the variance in the sample set more clearly than PC 1, so these were used instead. Figure 4.20 plots PC 3 vs 2 and shows the samples and the vectors representing the elements. Elements mentioned above have the longest vectors, indicating the greatest variance.

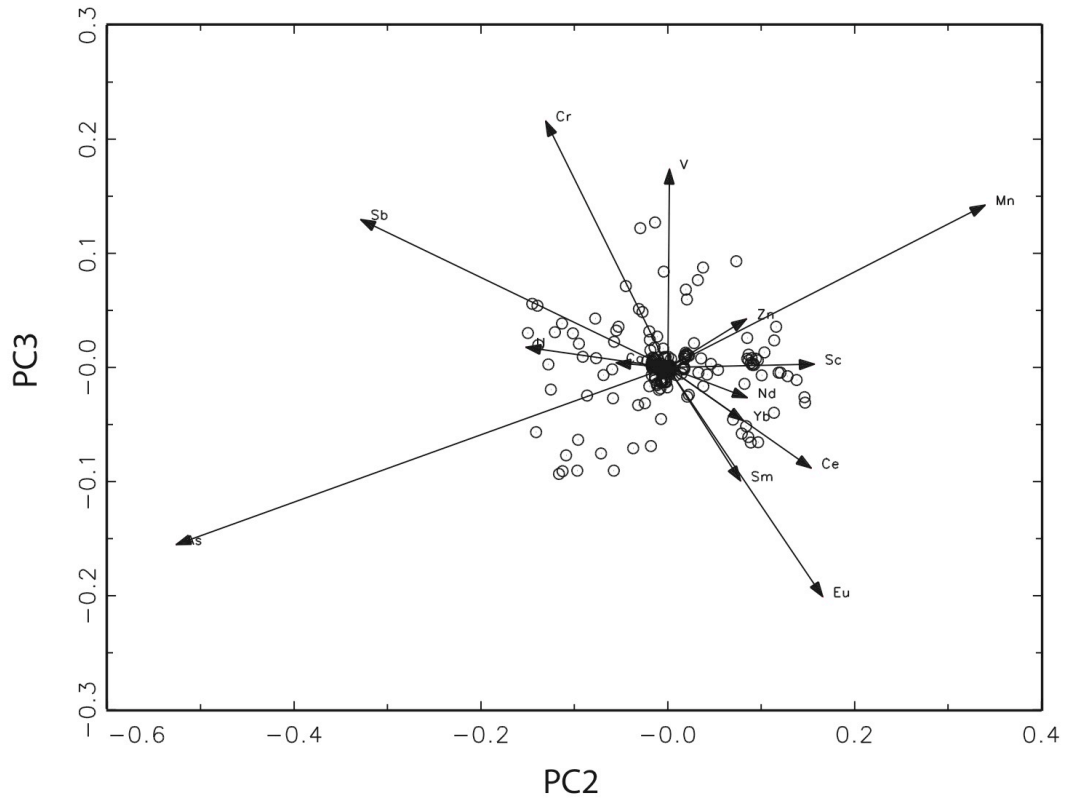

Figure 4.20: R-Q mode principal components 3 vs. 2 for ochre source data. Vectors indicate direction and magnitude of variance.

Figure 4.21 is a plot of $\log_{10}$[As/Fe] vs. $\log_{10}$[Sb/Fe] for all data from North American sources.

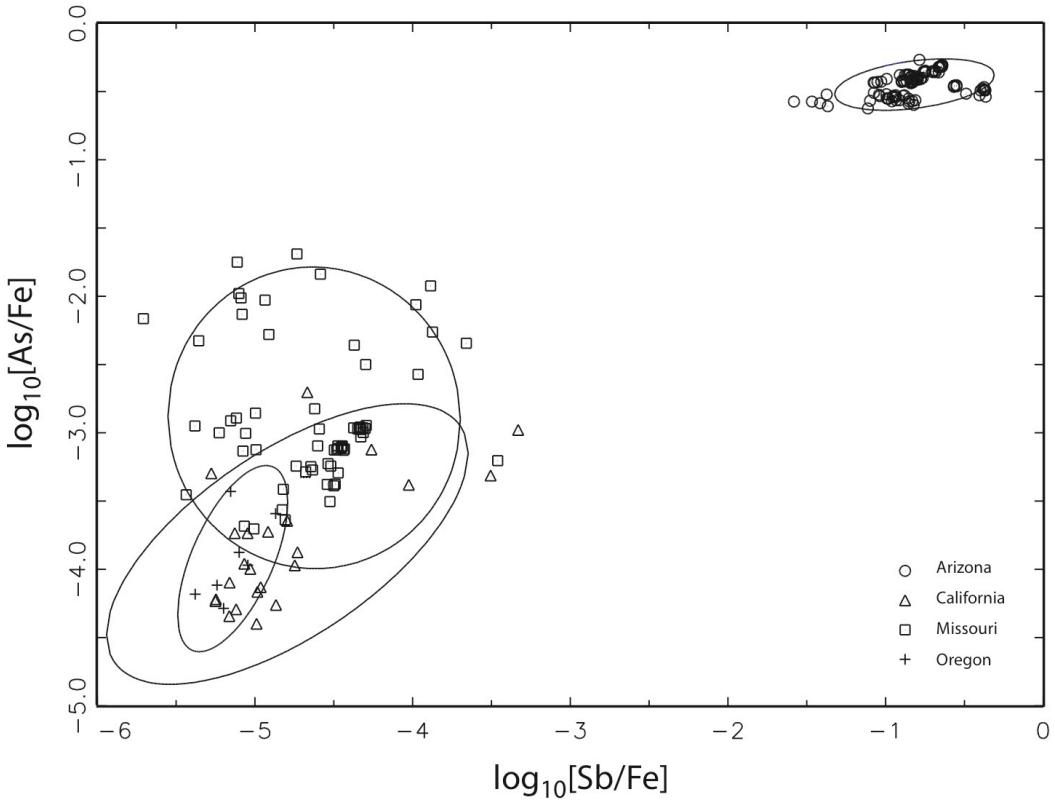

Figure 4.21: Plot of $\log_{10}$[As/Fe] vs. $\log_{10}$ [Sb/Fe]. Confidence ellipses are 90%.

The geochemical results reflect the sampling of the sources and location of the sources. Samples from Arizona were collected methodically from sources within about 40 km apart at the maximum. The samples cluster tightly together within the 90% confidence ellipse. Within the main group of the sources, it can also be observed that small clusters within the sources indicate individual sources as well as sub-sampling regions within the sources. The samples from Missouri, California and Oregon represent samples taken from sources further apart from each other. The Missouri samples were collected from several counties in southeastern Missouri over distances of several miles. In addition, the source sites were used historically as iron mines and therefore quite disturbed, however, small clusters of sub-

sampled areas can also be seen. For more information see Popelka-Filcoff et al.[113] Samples from California and Oregon were taken from sites several counties apart, usually with only one or two samples per source.[109] Therefore, the ellipses represent a larger sampling area with fewer samples. There appears to be overlap within the Missouri, Oregon and California sources on this plot and other related plots. However, using a posterior classification based on Mahalanobis distances for the California, Arizona and Missouri samples (the Oregon data set was too small), nearly all samples were associated with their respective groups (180 out of 188 cases or 96%).

Oregon and California seem to be geochemically related, which follows the geographical relationship. The association of Missouri with these two groups appears less likely from a geographic standpoint. However, the original formations of the ochre material were perhaps a similar type of geological or mineralogical formation. As compared to the Missouri, California and Oregon sources, the samples from Arizona are considerably higher in rare earth elements, antimony, chromium and arsenic. These elements follow the pattern of transition metals and rare earth elements as discriminatory elements for ochre.[113, 150] Although the source ellipses for some groups are spread out, and tend to overlap each other, sources in ochre can be identified on a large geographic scale.

A canonical discrimination analysis (CDA) was performed on the Missouri, California and Arizona source data as shown in Figure 4.22.

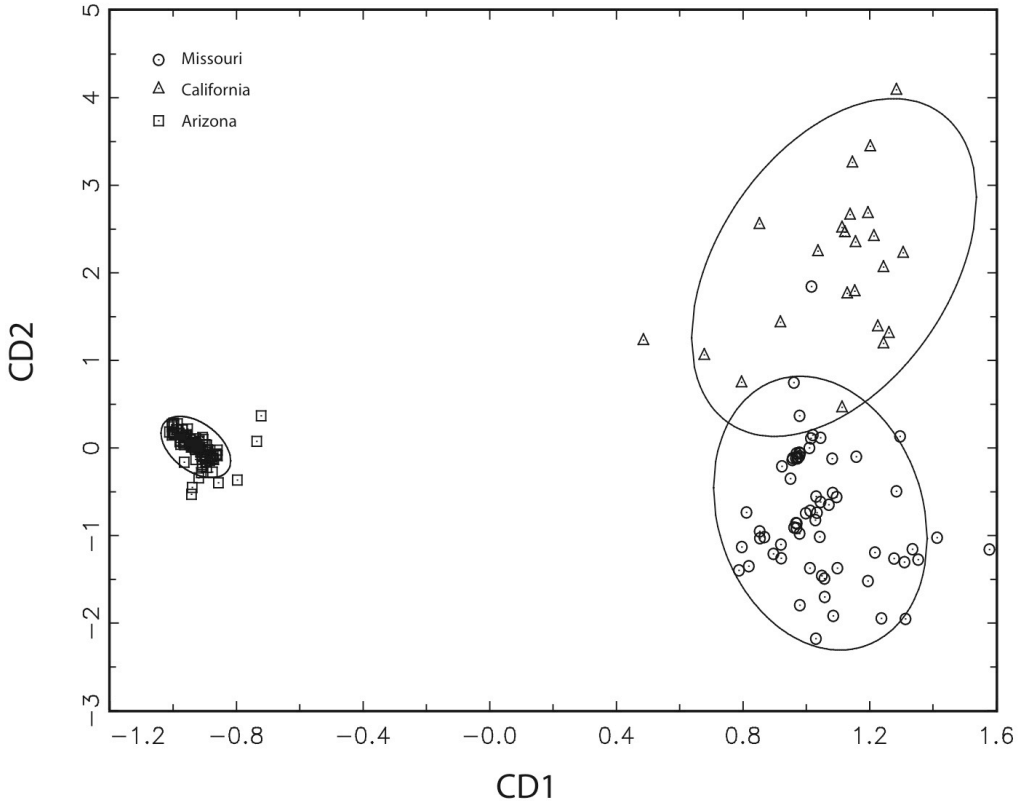

Figure 4.22: Plot of canonical discriminant 2 vs 1 for North American sources (Missouri, California and Arizona only) demonstrating separation between the groups. Confidence ellipses are 90%.

The sample set from Oregon was too small to be included in this type of statistical analysis. CDA analysis assumes that the groups are different and calculates discrimination functions describing the largest difference between the groups.[13] This assumption would be appropriate for this type of investigation, as the ochre groups are considered geographically and presumably geochemically distinct. The results of the canonical discriminant analysis are shown in Figure 4.22. As verified in the figure, ochre from Arizona is distinctly different than California and Missouri. This confirms the results seen in the bivariate plots discussed earlier. Ochre from sources in California and Missouri are still separated in the canonical

discriminant plot, but appear to be more similar to one another than to the Arizona ochre source. Although the 90% confidence ellipses are close to each other, Missouri and California form discrete groups.

Artifacts

The artifact data used in this study came from two locations. The first was an ochre found in a cave context in Alaska.[88] The second group is from four sites excavated in Texas.[99] Information about these sites is presented in Table 4.5. The same elements for artifacts were used for sources in the data analysis. In this concatenated data set, principal components 1 through 5 describe 99% of the variance in the data set. The elements that emerged from the PC analysis included Eu, Sb, Cr, As, Dy and Mn. Figure 4.23 plots PC 3 vs 2 demonstrating both the samples and the element vectors driving the variance.

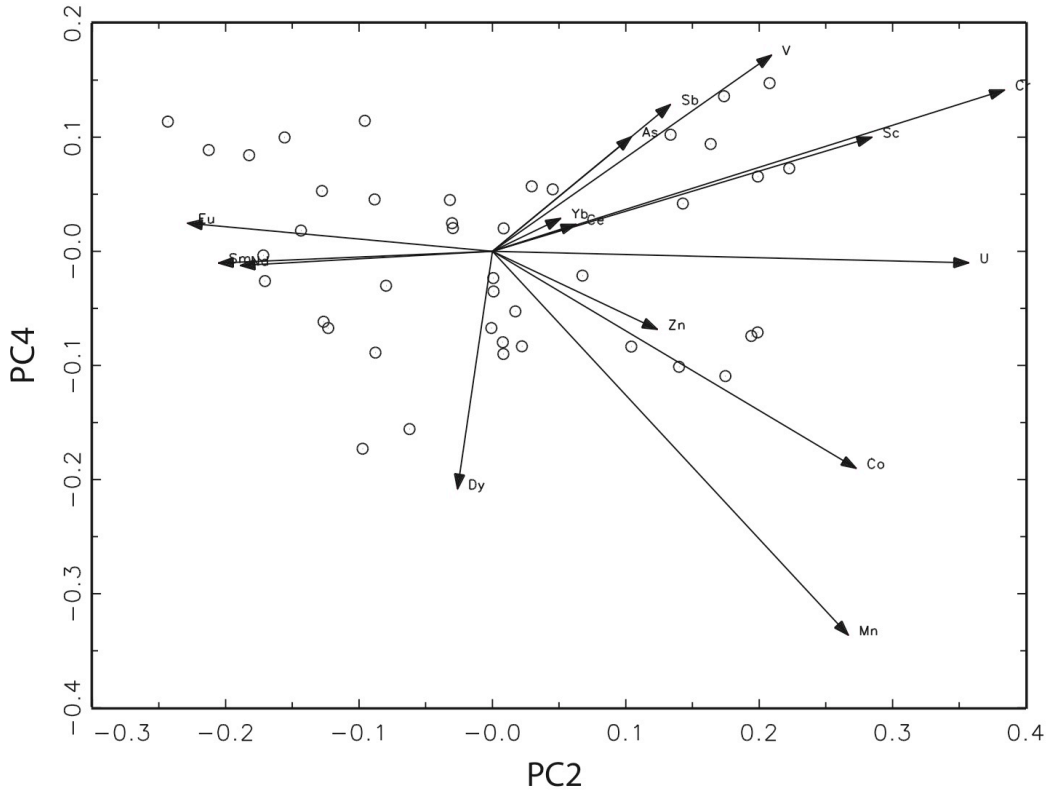

Figure 4.23: Principal components 4 vs. 2 for ochre artifact data (R-Q mode analysis). Vectors indicate direction and magnitude of variance.

The longest vectors represent the elements presented above. As with data for sources, the rare earth elements, antimony, and arsenic appear to discriminate the groups in ochre analysis. Posterior classification analysis was not used on these data, as the Alaska artifact sample set was too small. If more artifacts are analyzed in the future, these groups should be better defined.

Figure 4.24 plots $\log_{10}$[Dy/Fe] vs $\log_{10}$ [Cr/Fe].

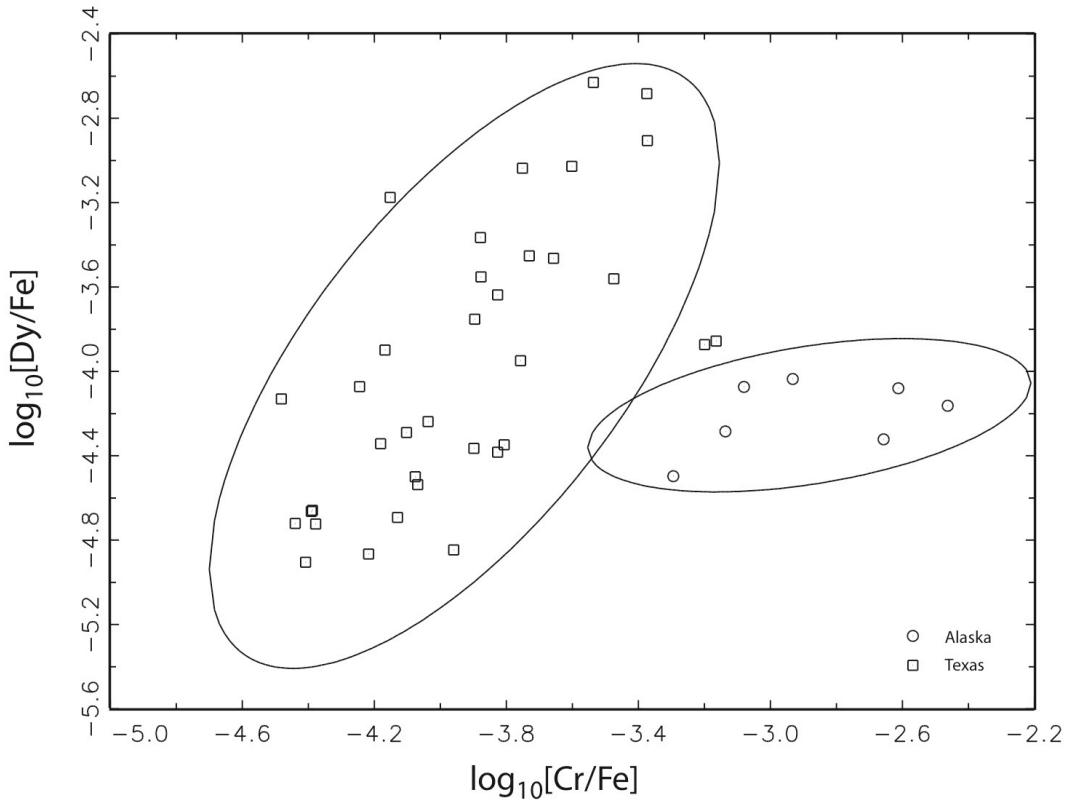

Figure 4.24: Plot of $\log_{10}$[Dy/Fe] vs. $\log_{10}$ [Cr/Fe]. Confidence ellipses are 90%.

Although only two groups are plotted, they are distinctly different. Since the data from only two archaeological sites are plotted, it is difficult at this point to draw solid archaeological conclusions. It is not surprising given different geochemistry and distance, artifacts from such different geological and geochemical associations would be different. This could be attributed to a difference in original sources as well as a difference in artifact uses. Ochre could also be an ancient exchange good, similarly to other types of artifacts. Artifacts, similar to sources, can be differentiated geochemically and appear to follow the provenance postulate.

Although the group dispersion and the confidence ellipses appear to be large, the scale of the plot is quite small. With the addition of other artifact groups, the separation and comparison of other groups will possibly change the group associations.

Conclusions

This meta-analysis of elemental ochre studies from the United States indicates that ochre satisfies the provenance postulate. Sources of ochre can be characterized from a particular region, and artifacts can be distinguished from source material. Ochre sources and artifacts can be characterized through trace elemental analysis. By using Fe ratios and statistics, elements important for distinguishing ochres were found independently of Fe concentration. Principal components analysis identifies important elements that can differentiate ochre groups.

As elemental ochre projects develop, more information added to this database will extend the understanding of ochre sourcing, characterization of sources and artifacts, and the beginning of sourcing studies with ochre material. More data is needed to establish the identity of sources and connections to artifact material, but this combined database provides a solid foundation for future elemental ochre studies.

ELEMENTS IN OCHRE

After analyzing ochre in these studies from around the world, several trends became apparent. First, the elements negatively associated with Fe were nearly always the same, and are assumed to be a part of the accessory minerals surrounding the ochre. The Pearson's test identified these easily. It probably can be assumed that these elements are the same across

data sets in general, but the Pearson's test should be performed on each data set to confirm this result. As ochre comes from several different geochemical contexts, the accessory minerals may change from location to location. In addition, an elemental definition of ochre was found through this data. While it does not describe the mineralogical content, a better elemental characterization of materials called "ochre" can be found.

The elements found to be associated with Fe, as well as important for distinguishing sources, generally were members of the first row transition metals and rare earth elements, with the addition of As and Sb. Different combinations of these elements were found for specific locations and studies, but generally these elements were members of these larger groups. A summary of these elements is compiled in Table 4.6.

Table 4.6: Table of elements found to be significant in each study

Study	Elements
Missouri (Southwest)	Cu, Eu, As, P, V, and Sb
Peru (Jiskairumoko)	Co, Mn, Zn, Eu, Sm, Ce, and La
Arizona	As, Sb, Zn, Co, Mn, Eu, Lu, and Cr
North America	Eu, Sb, Cr, As, and Mn

Similar important element groups agree with another paper produced independently in the INAA analysis of hematite from Africa.[150] While more studies need to be done to fully characterize ochre from sites worldwide, this work indicates that the elements in Table 4.6 are the major participants in the individual geochemical signature of ochre sources.

Since transition metals and rare earth elements (REE) appear to be the signature elements for ochre, additional research was done to explore these relationships. In the case of transition metals, a possibility for this trend includes similar atomic radii for these elements to Fe. In addition, similar oxidation states and electronic configurations (depending

on the ion), make substitution of these elements more likely. It is probable that the elements with similar size substitute for Fe in the octahedral structure of the iron oxide. Even though the material may be subject to diagenesis, the patterns in the parent rock (originating from the source) are likely to be reflected in the ochre material that is sampled and analyzed. As discussed earlier, substitution of transition metals in ochre may also lead to color changes in the ochre. While the exact nature and concentration cannot be determined by visual characteristics alone, various attributes may lead to general conclusions about the sample. The amphoteric qualities of iron also lead to interesting trends. At low pH, iron may tend to act like a hard acid and therefore substitution of other small radius, high charge atoms such as the lanthanides may be more likely. At higher pH, iron may act as more of a soft acid, with larger atomic radii and lower charges, with the substitution of As, Sb and other soft acids more likely.

Trends in rare earth elements (REE) in iron oxides can also be explained. REE tend to be strongly electropositive, and prefer ionic rather than covalent bonding. Most REE are in the +3 oxidation state although other oxidation states exist for Ce and Eu. REE also are affected by the lanthanide contraction, where there is a decrease of atomic volumes with the increase of atomic number across the group. This is due to imperfect shielding of electrons, increasing effective nuclear charge with increasing atomic number, due to the reduction in size of 4f subshell.[154]

Rare earth elements can substitute for the following cations: Ca^{2+}, Y^{3+}, Th^{4+}, U^{4+} Mn^{2+}, and Zr^{4+}. Eu^{2+} can substitute for Pb^{2+}, Ca^{2+}, Sr^{2+}, and Na^{+}. For the lanthanides, the unfilled 4f orbitals are shielded by the 6s orbital. Therefore REE have similar electronic structures, and group together in minerals; and no REE are found alone.[154] This statement is

also supported by the results from the statistical analyses. For the PCA plots, the REE vectors generally went in the same direction and with similar magnitude. This trend was also reflected in the bivariate plots, where REE produced similar patterns in the plots. If one of the REE was plotted against another, a clear high correlation linear trend was seen. (Figure 4.6)

REE in minerals follow several patterns related to substitution in minerals. Some authors claim it is related to coordination number. In the case of generally octahedral iron oxides, there is a distribution of REE with both lighter and heavier elements present.[154] In sedimentary formations, such as those that produce clays, also carry the REE concentration patterns, even in the diagenetic process.[154]

The above geochemical literature supports the trends observed in ochre analysis. Transition metals, As, Sb and rare earth elements appear to reflect the original source of the iron oxide, despite effects from diagenesis. These results, along with those found by Kiehn et al.[150] support the assertion that ochre can be traced back to its original source by its geochemical patterns.

For most samples analyzed in this study, the Fe concentrations varied from low percent values to nearly 70 weight percent. The rest of the sample was made up of oxygen (comprising the oxides for most elements), elements negatively correlated with Fe (Al, Ca, K, Na, Ti, Si) and trace values of other elements (comprising the geochemical signature).

CONCLUSIONS:

General conclusions can be drawn from the elemental analysis of ochre. Unlike some spectroscopic studies performed earlier, this study is unique in that it is a collection of elemental studies performed on ochre to understand geochemical variability and

archaeological implications. This project sought to understand whether ochre can be traced back to its original source, and to discover the trace elemental fingerprint indicative of its original geochemistry. The research found that ochre is related to its source by geochemistry and it that does fulfill the model of the provenance postulate for discerning inter- and intra-source variability.

By using several sampling methods, sources of ochre were characterized for their internal variability. By using local, regional, and national approaches to the data variability, general conclusions can be drawn about the variability of ochre and its possible role in ancient exchange networks. Certain studies dealt only with the characterization of the sources, while others sought to understand the relationships in ochre artifacts. The artifact studies concentrated on the variability of ochre from a particular site. The North American meta-analysis combined data from several studies, divided into a source specific study and an artifact specific study. The source versus artifact sampling is an important distinction for future ochre studies.

The results of the ochre studies led to a more complete database of elemental analysis for ochres worldwide. While some elemental data has been produced and published from Australia ochre, and a few small studies on North American ochre, this study considerably augments the prior amount of ochre elemental data produced and established new data for comparison in future studies. In addition, the use of the log-ratio method was found to be a useful approach for ochre analysis. The log-ratio method for analysis is an appropriate strategy for understanding a data set with an inherent large amount of variability in the sample matrix, independent of the variation that can be used to fingerprint sources. A

possible future analysis is to use a normalization of the data (ratio to the element mean) to ascertain if this produces interpretable results.[76]

It was also shown that by using established multivariate analyses for archaeometric analysis such as cluster analysis, PCA and CDA, conclusions about ochre variability and ochre sources can be found. Archaeological conclusions concerning the variation in the data sets can be interpreted on a variety of scales, from regional to a national scale. Deductions concerning ochre procurement and exchange are in the early stages and provide a foundation for future work in this area.

Another result of the multivariate statistical analysis, specifically PCA, is that elements important in ochre analysis were identified. While there were no specific elements that could be used for ochre worldwide, the major groups of elements were identified. Generally, the elements that can be used to differentiate ochre sources include the rare earth elements, first row transition metals, arsenic, and antimony. Similarly to other artifact groups, a group of characteristic elements may be region specific. INAA appears to be the method with the most range and sensitivity for these groups of elements compared to XRF, although XRF can identify many of these elements and others at higher detection limits. The numbers and types of samples studied were variable in this study, however for future studies the elements analyzed should not be limited to the groups mentioned above. Future projects should measure as many elements as possible understand similarities and differences between data sets, although the rare earth metals, transition metals, As, and Sb should be elements of interest.

In addition to the archaeological implications, basic ochre elemental composition was determined for samples from sites and sources around the world. While not all components

of ochre can be identified with this analysis, a better definition of ochre composition can be created. While the specific definition may not apply to every material called "ochre", a general range of concentrations of elements and oxides were found through this study. A possible future project might be the X-ray diffraction (XRD) of the same samples to correlate the mineralogical components with the elemental composition.

From this foundation, more elemental studies of ochre can be completed using similar experimental methods. It has been demonstrated that ochre data, similar to other artifact groups, can be tested using the provenance postulate for characterization of sources. Additional data not only provides a larger database, but also provides a comparison to the results described here for future studies. Further investigation of ochre sources can be completed on regions worldwide to characterize ochre sources more fully. Future projects incorporating the data for use of comparisons between sources and artifacts can lead to further conclusions about the participation of ochre in exchange or the use of the material in everyday and ceremonial applications. An important part of the study design for future project is the characterization of the ochre as a source material or an artifact.

Appendix: Tables provide the elemental data for all samples presented in this chapter. Other ochre with known provenance was also sampled and analyzed from the United States and worldwide. However, there was not enough of one site or one source to perform statistics or make solid conclusions related to the ochre geochemistry.

CHAPTER 5: PXRF APPLICATIONS IN ARCHAEOLOGY

Portable X-ray fluorescence spectrometry (PXRF) has been used in geological and environmental applications such as determining the composition of soils, investigating the heavy metal contamination of soils, and metal alloy analysis. A review of PXRF in environmental applications can be found in Melquiades et al.[155] Zwicky and Lienemann describe a comparison between laboratory-based wavelength dispersive XRF (WD-XRF) and portable energy-dispersive XRF (P-ED-XRF) for quantitative results.[156] In addition, PXRF techniques have several applications in metal analysis for both industry as well as archaeology.

A review of the development and application of PXRF can be found in Piorek.[49] A general overview of the components and technology can be found in Bichlmeier et al.[50] These studies also cover a wide range of the different types of instrumentation provided by several manufacturers, from hand-held devices to component based instruments.[46] Advances in miniature X-ray sources as well as thermoelectrically-cooled, high-precision detectors have allowed improved resolution as well as smaller PXRF instrumentation for many applications. There has also been discussion in the literature about microcapillary optics for μ-PXRF and smaller spot sizes for analysis.[157] These small spot sizes are particularly important for the analysis of small areas such a pigment lines or detail in the bulk artifact. The literature also covers various types of X-ray sources (radioactive vs. X-ray tube) and detectors, as well as software for quantification.[158-161] Zarkadas et al. describe the PXRF system in use at the Demokritos Lab in Greece for archaeometric applications.[162]

Similar to the other methods presented in this dissertation, the focus for PXRF studies is on the elemental analysis of artifacts. From these compositional studies, interpretations of

artifacts and ancient exchange routes can potentially be identified. Examples of previous PXRF archaeometric studies on glass include Islamic examples from Egypt,[163] analysis of historical glass and jade and painting on glass,[164] and analysis of Limoges enamels for possible forgeries.[165] PXRF has been extensively used on metals, including tin residues from smelting and gold coins,[166] layers in gold pigment from a Giotto fresco,[167] and analysis of ancient gold jewelry from a museum collection.[168] Ceramics, stone and pigments are also types of artifacts that have been analyzed extensively by PXRF: dolerite stone axes from England,[169] paintings and metal alloys,[170] Spanish paintings and frescoes,[171] analysis of paintings to detect forgeries,[172] and trace elemental analysis of pottery.[42] However, there are many more cases in the literature of the application of PXRF to art and archaeology. A general article on the application of several types of μ-PXRF for analysis in art and archaeology is covered in Janssens et al.[9] as well as Moioli et al.[9, 173]

This work describes the development and application of a PXRF for the investigation of Peruvian obsidian for sourcing. Detailed background information on the archaeological context behind the obsidian project can be found in the article by Craig et al.[174]

General Considerations for PXRF

Historically, the three most useful multi-elemental techniques for obsidian analysis and sourcing are INAA,[175] XRF,[176] and laser ablation inductively coupled plasma-mass spectrometry (LA-ICP-MS).[177] INAA has several advantages, including higher precision, higher sensitivity, and higher accuracy than XRF. INAA is also more matrix-independent and less susceptible to geometric effects than XRF. However, INAA requires access to a reactor facility, longer analytical time, and the destruction of a small fragment of the artifact

for analysis. The main advantage of XRF is that it is a non-destructive, rapid, multi-elemental analysis technique. While ICP-MS yields detection limits similar to or better than INAA, it is rarely applied to obsidian analysis as it requires sample dissolution, which can be difficult with obsidian, which has high silica content and requires treatment with hydrofluoric acid for complete dissolution. Laser ablation ICP-MS (LA-ICP-MS) requires minimal sample preparation and the damage to the artifact is negligible, but standardization is often difficult, and accuracy and precision are poor compared to INAA. LA-ICP-MS was not used in this dissertation.

As mentioned in the methods chapter, PXRF has several advantages for archaeometry. First, a portable unit can be transported easily to the archaeological site, field area or museum, lessening potential for loss or destruction of artifacts during travel. Export of artifacts from some countries can be both difficult and expensive because of strict, bureaucratic export laws. In this case, it is more efficient to bring the instrumentation to the artifacts. Because PXRF instrumentation is relatively low cost compared to other multi-elemental analysis techniques, it is more accessible to more facilities and researchers.

PXRF can be performed on artifacts *in situ*, or the artifact can be brought to the PXRF and analyzed directly, generally with negligible sample preparation. This ability allows analysis of artifacts without drilling or sampling of the artifact, which is particularly important for museum samples that are culturally significant. In addition, less sample preparation also saves time and reduces the possibility of contamination of the sample. PXRF analysis is relatively fast; depending on the sample matrix and the type of analysis, multi-element analysis at the major, minor, and trace level can be performed in a matter of minutes. Because measurements are generally done in non-vacuum conditions, limits of

detection for PXRF are often higher than conventional XRF, which is frequently performed under vacuum, and many of the lower Z elements such as those below Ca cannot be measured with PXRF. In general, most PXRF systems can measure elements from 20<Z<92 depending on the application and matrix.[49]

The background information and advantages for PXRF are covered in the methods section (Chapter 1) of this dissertation, and the instrumental methods and precision and accuracy will be discussed in this chapter. As PXRF is a relatively new technique at MURR, this section of the dissertation will focus more on establishing the method for valid archaeometric analysis rather than the interpretation of the analytical results. This study compares the results for a given set of obsidian from Peru that had also been previously analyzed by standard XRF and INAA.

CASE STUDY: PERU OBSIDIAN SAMPLES

This study focuses on obsidian which has been used throughout the world for a variety of purposes.[174, 178] Obsidian is a best-case scenario for chemical sourcing and identification due to its homogeneity and unique source profiles, thus providing a good case study for development of the PXRF for elemental analysis and sourcing. Obsidian is a volcanic glass formed during volcanic events when the lava cools rapidly and does not crystallize. As a result of the process of volcanic eruption, obsidian is, in most cases, homogenous, for bulk as well as surface analytical archaeometric analyses. Obsidian can be chemically fingerprinted based on trace elements that are characteristic of the source. In some cases, obsidian can even be traced to specific volcanic eruptions.[64] Most obsidian

sources are known and the chemical fingerprints have already been characterized with high precision by INAA, XRF and other methods.[64 175, 177, 179]

For this study, 68 artifacts were available for analysis. These samples had been exported earlier and analyzed by a lab-based XRF at the Archaeological XRF Laboratory at the University of California, Berkeley.[169] Later, a portion of the same samples were analyzed[180] by INAA at the Archaeometry Laboratory at the University of Missouri Research Reactor (MURR). These samples were chosen for analysis by PXRF to allow a comparison with the other established methods (XRF and INAA). The purpose was to evaluate the ability of MURR's PXRF system to analyze and characterize obsidian artifacts as well as to identify the original sources of the artifacts (as established by the other methods). This study seeks to establish whether PXRF can be used in artifact sourcing studies as a comparable, field-portable method to established archaeometric laboratory methods such as XRF and INAA.

Instrumentation and Analysis Parameters

The PXRF setup consists of an X-ray source, a detector, a MCA, sets of collimators for the X-ray source, an aluminum collimator for the detector, a laptop computer, and two small laser pointers (for alignment of the sample with the X-ray beam). The system is relatively compact, and can easily be transported in a single case.

The main components of the instrumentation (X-ray source and detector) are designed by Amptek Inc. and are discrete components. This arrangement allows for many possible configurations of the instrumentation depending on the application.

The X-ray source for this instrument is an Eclipse II, made by Oxford Instruments and distributed by Amptek Inc. The X-ray source has a tungsten (W) filament cathode, which is designed for repeated on/off cycles for recurring measurement applications and is internally cooled. The Eclipse II has a silver (Ag) anode (target) and a thin (125 μm) Be end window. The tube has a variable voltage potential from 1-30 kV, and current from 0-100 microamperes. The X-ray source comes with an AC external power source and controller.[181]

The detector is an Amptek XR-100CR, consisting of a high performance X-ray detector, preamplifier, and Peltier cooled Si-PIN photodiode with a 13 mm^2 active area. The diode is 300 μm thick and has a 25 micron-thick Be window. With a 12 μs shaping time it provides a full-width-half-maximum resolution of 149 eV for the Kα line of Mn (5.9 keV).[181]

The MCA (Amptek MCA8000A) has 16k of data storage channels allowing storage for up to 128 different spectra. The electronics also include a pulse height digitizer, as well as a low level discriminator. In combination with the Amptek PMCA software, acquisition and identification of elements in the X-ray spectra can be accomplished. The software is Windows (PC) compatible, and in this experiment, was installed on a Dell laptop computer for measurements in Peru. A channel-to-energy calibration was set up in advance for all subsequent measurements based on multiple thin-film standards. The PMCA has a built-in library of element K, L, and M lines and routines for identification of peaks and regions of interest in the spectrum. After calibration, the software automatically calculates the peak counts, area and full width half maximum (FWHM) for peak resolution. The software automatically suggests elements for each peak based on the energy of the peak. In addition, multiple spectra can be displayed at the same time for comparison. The XRS-FP module of

the software allows deconvolution and calculations on the spectra as well as quantitative analysis.[181]

The X-ray source, detectors, sample holders and laser pointers were attached to a table that aligns the components in the appropriate distance and geometry. Several experiments were performed to ascertain the suitable angles between the X-ray source and detector and the distance between the components to achieve the optimal peak-to-background for the elements of interest.

Spot size

While the system was designed to allow multiple analysis spot sizes through the use of collimators, the smallest analysis spot size is 10 mm diameter. This analysis area was chosen as a balance between a smaller spot size for analyzing smaller artifacts and a large enough spot to collect data in a reasonable amount of time. The spot size should not be too small, as the collimation of the X-ray beam may eliminate too much X-ray intensity to fluoresce the sample at high enough count rates. Once this dimension was determined, the sizes of the collimators around the X-ray source and the distance from the sample to the X-ray source and the detector were calculated.

Collimators

As specified from the manufacturer, the divergence of the generated X-rays results in a wide solid angle (130°) from the beryllium window. A collimator was necessary to define the area irradiated by the source. A copper collimator was designed to fit as a small, lightweight modified cylinder over the end of the X-ray source. This collimator was

designed to be light and machined to protect the fragile end window of the X-ray tube as well as not put any unnecessary weight on the end of tube. It was calculated that at least 0.47 mm of Cu was necessary to attenuate 99% of 30 keV Ag X-rays, using the basic attenuation equation:

$$I = I_o e^{-[(\mu/\rho)x]} \qquad \text{Equation 5.1}$$

where I represents transmitted intensity, I_o incident intensity, μ the absorption coefficient (material and energy dependent), ρ the density and x the thickness of the material. The μ/ρ (cm^2/g) values were taken from tabulated values from the NIST website.[182] To achieve a 10 mm diameter X-ray beam, the copper collimator was designed with a 5 mm aperture. Another collimator was also designed with a 7 mm aperture to create a slightly larger spot size on the sample. The final 2 mm of each collimator was tapered to accommodate the detector. Although the end was tapered, there is still enough material to attenuate the Ag X-rays. In practice, it was found that even though the Cu collimator was cut away at the end, a significant Cu peak appeared in the spectra due to the fluorescence of Cu by the Ag X-rays from the source. Initially this was remedied by an additional "jacket" of shaped Teflon around the collimator to attenuate the Cu X-rays. This jacket of Teflon was found to be effective in blocking the Cu X-rays, but became bulky when the X-ray source needed to be close to the detector in closer geometries. The sum of the copper and Teflon collimators also began to present possible weight problems on the fragile end of the X-ray tube. Ultimately, the Teflon covers were removed, and the copper collimators were professionally plated with a thin layer of silver on all surfaces, which was enough to reduce the copper peak to

background levels. A calculated value of 2.03 x 10^{-4} mm of Ag is needed to attenuate 99% of the 7.6 keV copper X-ray. This method not only eliminated the possibility of Cu peaks in the resulting spectra, but did not add any other artifact peaks that may have come from the collimator material. Since the outer coating was made of silver, any possible fluorescence of this coating would only add into the possible silver peak from the tube itself and not create any other confounding peaks or spectral abnormalities.

An experiment was performed to determine the exact spot size of the X-ray beam after the collimation of the beam. This was found by essentially photographing the X-ray exposure using the same X-ray to sample holder distance on the table setup. Instead of placing a sample, the back of a Hasselblad medium-format camera with high-speed photographic scientific grade film was attached to the sample holder of the PXRF. All experiments were performed in a darkroom. After each exposure to the X-ray radiation, the film was then advanced for the next frame. Photographs were taken for one second and two seconds incrementally with the maximum time being ten seconds. The negatives were then developed in a commercial laboratory. An example of a frame can be seen in Figure 5.1.

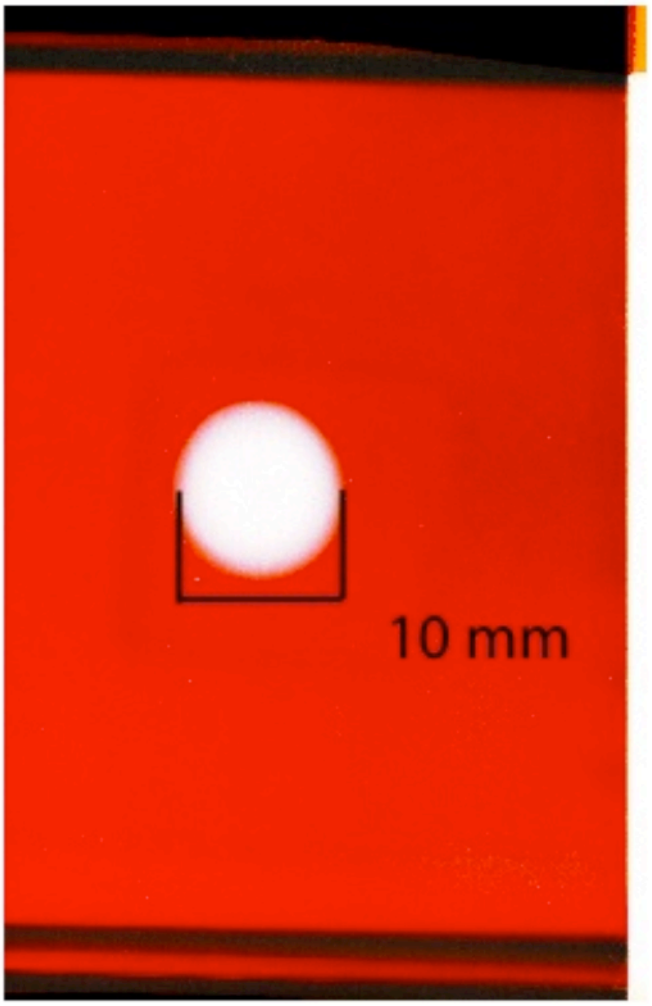

Figure 5.1: Example frame of exposed photographic film documenting the spot size of the collimated X-ray beam.

The negatives were measured to assess the beam size of the PXRF. It was found that regardless of the exposure time, the spot size remained at 10 mm, exactly as calculated and planned in the PXRF geometric setup. This experiment both verified the beam size as well as allowing a way to ascertain the area analyzed on a given sample.

A small aluminum collimator was designed and placed on the end of the detector cylinder, (Figure 5.2). It was found experimentally that the aluminum in the collimator did

not fluoresce appreciably to affect the spectrum or subsequent quantitative analysis, but instead helped to minimize the detection of scattered X-ray events. The aperture of the collimator hole is 1 mm. With the addition of the collimator, it was found that the count rate was diminished, but the peak-to-background ratio was not significantly affected in the elements of interest. The finished collimator also has a slit cut into it to accommodate any additional critical absorption filters that might be necessary in the analysis.

Instrument Geometry

Several experiments were performed to determine the appropriate angle between the source and detector. With the source normal to the sample and keeping all other experimental variables the same, the relative angle between the source and detector was changed approximately 15 degrees at a time, over the range from 15 degrees to 90 degrees. For each position, the net and gross counts were recorded for iron and copper. These experiments were performed prior to the silver plating of the collimator, so the goal was to find the optimum geometry that achieved the highest peak to background ratio of Fe and the lowest of Cu. The results of the experiment demonstrated that at small source to detector angles, an increase in both Compton and Rayleigh scattering was observed. At smaller angles it is also more likely for the detector to see X-rays from the source itself, despite collimation of the source. At larger angles the Fe peak became smaller overall (both peak and background), and the Cu peak became quite large. In addition, the Cu peak to background ratio was relatively high. This result is to be expected as the X-ray source was fluorescing the bare copper collimator with a direct path. After the collimator was plated with silver later in the study, this copper peak disappeared from the resulting spectra. From

this study based on Fe, the peak-to-background ratio was found to be at a maximum at about 45 degrees between the source and detector, and at a minimum at close geometry (23 degrees) and at a distant geometry (85 degrees). Therefore, the setup for the instrument was chosen to be 45 degrees for all measurements although variation in the peak-to-background ratio occurs depending on the specific element.

All of the above factors were taken into account when designing the table used to align the components in a precise and replicable manner. This aluminum table was precisely machined and designed to hold the components correctly, without being heavy or having too much aluminum near the analytical area, reducing any possible Al fluorescence. (Figure 5.2) The consistency of the placement of the components is important due to the irregularity of the sample sizes and shapes. Further specifications for the table design stipulated that the source should be normal to the object surface. Several sample holders were designed to gently and securely hold the object, while also being small so as not to add extra fluorescence into the analytical spectra. The sample holders were made all of the same dimensions, out of Lexan to minimize extraneous fluorescence. Source-holder apertures of varying sizes were used to accommodate samples of varying sizes. Figure 5.2 shows the X-ray source, detector, table, sample holder and laser pointer when arranged in a typical setup.

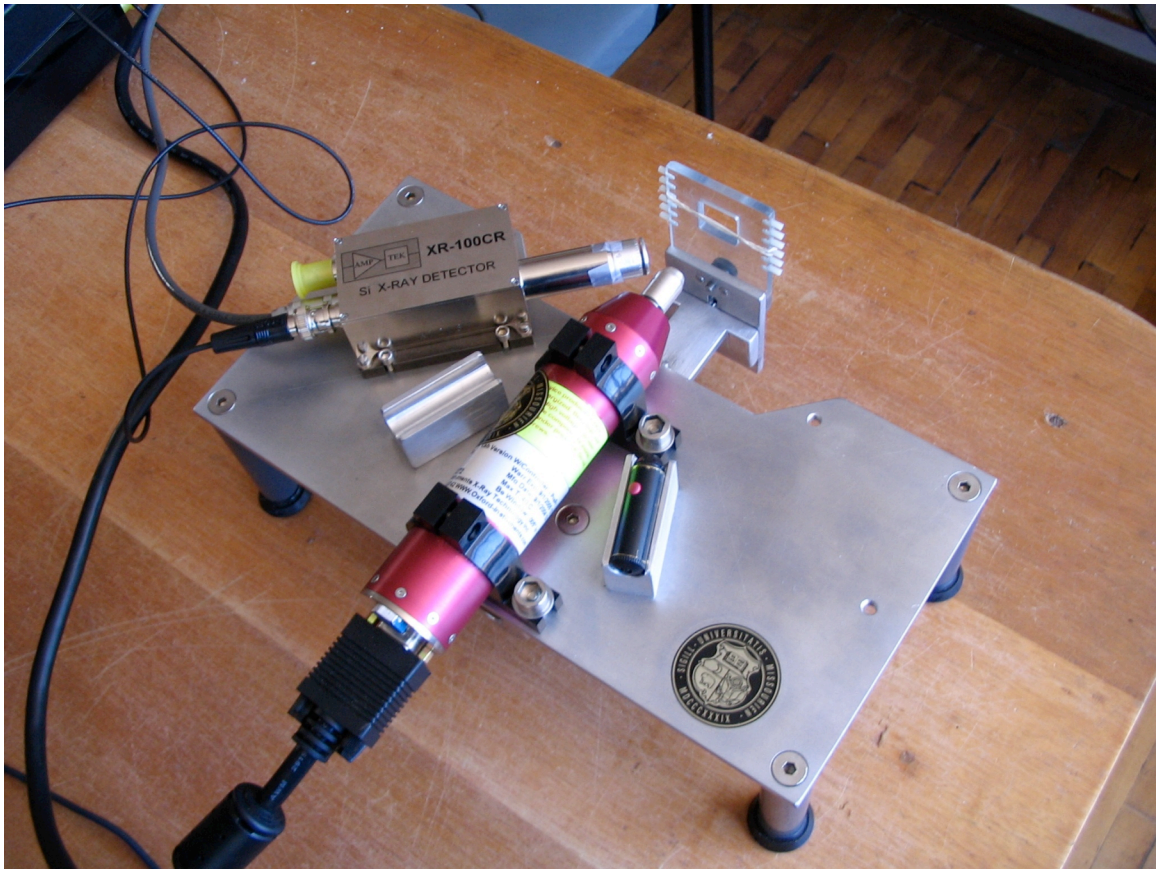

Figure 5.2: Picture of PXRF set–up

Figure 5.3 shows the power sources associated with the X-ray source and detector.

Figure 5.3: X-ray and detector power sources and multi-channel analyzer (MCA)

Individual samples were placed in the sample holder of the PXRF system, at a distance of 20 mm from the front of the X-ray tube. Along the side of the sample holders are plastic studs that hold, with a series of rubber bands, the samples from the back of the sample holder plate. The sample holder can be adjusted in the x- and y- direction for the optimal analysis position. For each analysis, a smooth surface on the sample was selected to minimize surface effects and scatter and increase the count rate.

Small laser pointers were set up in such a way to intersect on the sample surface to aid in alignment of the sample with the X-ray beam. The area analyzed on each sample was 10 mm in diameter. Obsidian samples were analyzed using an X-ray source voltage of 25

keV, and 20 micro-amps current. A counting time of 200 seconds was used on each sample. In general, with the appropriate collimators on the source and detector, and the correct X-ray source settings, the count rates were generally around 1600-1800 counts per second. For each sample, the current settings were also adjusted to minimize the dead time on the detector, keeping it less than 20%, and ideally even less than 10% if possible to minimize sum peaks. The highest setting on the X-ray tube is 30 keV. The manufacturers do not recommend operating the source at this high voltage for long periods of time. Therefore, to analyze elements with X-ray energies higher than 30 keV, the appropriate L- and M- lines were used instead of the K-lines.

CALIBRATION

Thin film standards of single and multiple elements on Mylar films (Micromatter, Inc.) were used for the calibration of the instrument. Elements and compounds used in the thin film analysis included: V, Mn, Cr, SrF_2, Pb, Au, Ag, Ti, Co, Ni, ZnTe, Fe, BaF_2, and Cu. Thickness of deposition on the thin films ranged from 43.9 $\mu g/cm^2$ to 53.2 $\mu g/cm^2$. Based on these thin-film standards, coefficients were created in the software for channel-to-energy calibration. Results from the analysis of these thin-film standards could also be used for a possible future empirical calculation of concentrations.

EXPERIMENTAL SETUP

Matrix-matched standards in obsidian can be used to set up calibrations for a particular matrix. The software also has the capability of standardless (i.e. fundamental parameters) analysis. FP analysis was used for obsidian analysis as described later in this

chapter. Standards and quality controls used in the analysis included polished samples of obsidian from known and previously analyzed obsidian sources (Alca, Chivay and Quispisisa, Pachuca, El Chayal, Ixtepeque, San Martin, Otumba, and Obsidian Cliff). These standards were used at the beginning and end of the daily sample collection to assure stability of the system and detect changes in calibration during the sample run.

For a given measurement sequence, the tube was allowed to warm up by operating it for about 20 minutes before acquiring data. It was found in initial simple experiments, that both the dead time and the signal produced varied considerably as the instrument warmed up in the first 20 minutes. Despite the fact that the documentation indicated that it was not necessary to warm up the instrument, it became apparent that either the electronics or the X-ray tube or both needed to be warmed up prior to acquiring reproducible data.

SAMPLE ANALYSIS

Obsidian samples were analyzed with no advance preparation, additional sampling or treatment. Any cleaning was simply to wash and remove dirt and surface residue. This had been done prior to cataloguing the archaeological samples. Because the samples were complex artifact points, they varied in size, shape, and thickness, depending on the point style and technical ability of the craftsperson. It was calculated that the minimum thickness of the sample (assuming a 70% SiO_2 matrix and 99% attenuation) would be 3.2 mm (3200 microns) using the 25 keV Ag peak from the source as was used in the experimental procedure. Any X-ray penetration beyond the 3.2 mm was considered in the "infinite thickness" range. However, the elements measured would be from a shorter range as Si is the lowest Z element measured as well as the least dense. Penetration depth for the elements

measured ranged from 2.51 x 10^{-3} mm (2.51 microns) for Rb and 4.89 x 10^{-4} (0.489 microns) mm for Zr. The highest fluorescent X-ray measured was for Sr, with a K_β of 15.87 keV. Its attenuation in SiO_2 requires 2.01 x 10^{-2} mm. However, it has been calculated elsewhere that 50% of the depth of penetration provides the fluorescence signal.[183] Therefore, the majority of the signal from obsidian originates in the first 1-10 microns of the artifact. It was also assumed that the obsidian sample is homogenous due to its inherent composition, and that the spot size analyzed was directly representative of the bulk of the sample composition.

For each analysis, the sample was placed in the sample holder with the flattest and smoothest side to the beam in order to optimize the signal count and decrease the possibility of error due to scatter from the artifact itself. In most cases, the sample was large enough and flat enough to achieve the desired count rate (as compared to the polished, flat standard obsidian material). In some cases, the sample was too small for analysis, which was reflected by how it fit in the sample holder as well as the resulting data. The smaller samples often suffered from scattering of X-rays from the edges of the sample. Poor results of a small sample were observed by a low count rate (significantly lower than 1600 counts per second). Often, a minor adjustment of the sample in the holder corrected the problem, but for a small fraction of the artifacts, the data collected was questionable compared to others primarily due to size limitations of the artifact. Figure 5.4 shows an obsidian artifact being analyzed. As seen in the figure, minimal preparation is needed and the sample is held gently but firmly in the sample holder.

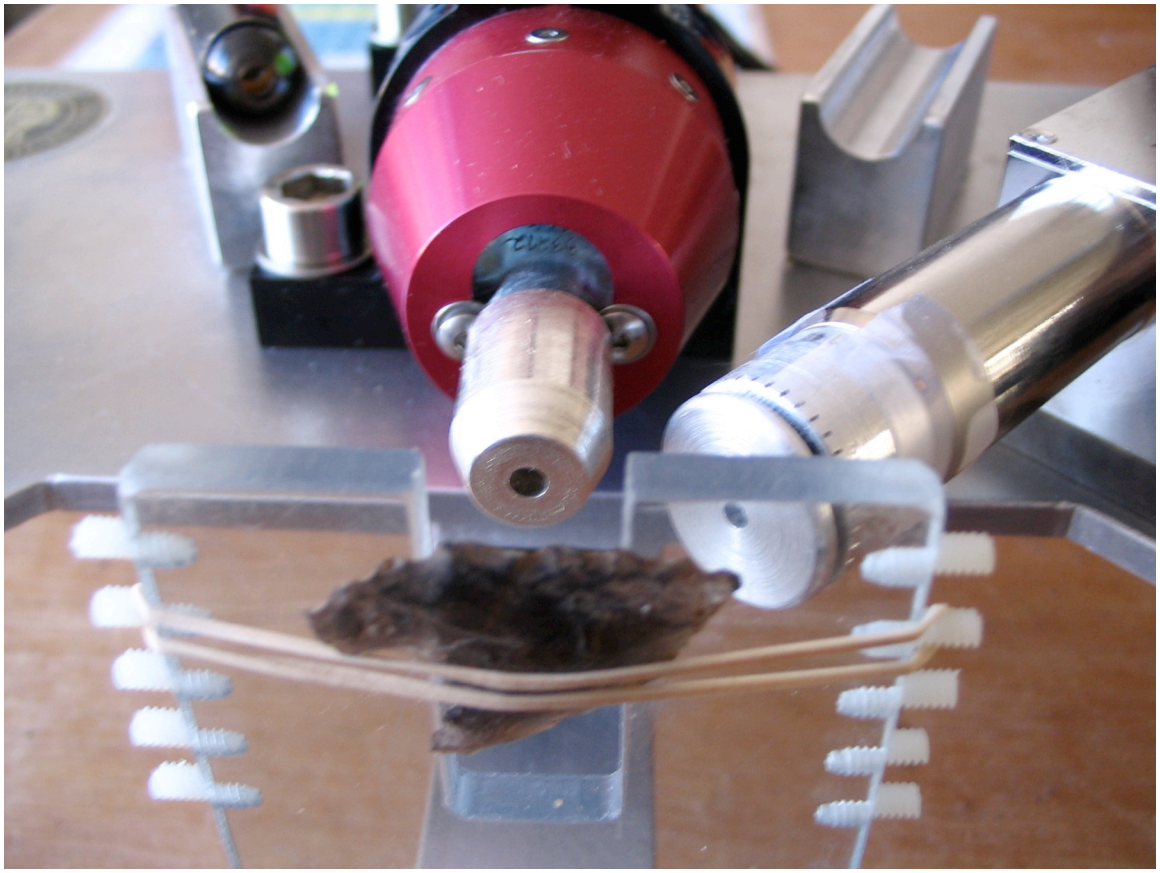

Figure 5.4: PXRF Analysis of Peruvian Obsidian

QUANTITATIVE RESULTS

Quantitative PXRF results can be strongly affected by analysis of irregular surfaces. One author reports that concentrations from a highly irregular surface are generally lower due to the effective distance between the source and sample and the sample to detector will generally be larger. As a result of the inverse square law ($1/r^2$), this extra distance makes both the source and fluoresced X-ray signals weaker.[51]

For obsidian, six elements (Sr, Rb, Zr, Zn, Fe and Mn) were measured in all samples. It had been determined earlier from prior INAA studies that these elements could be used to

differentiate obsidian from various sources in the region. Figure 5.5 demonstrates an example spectrum for obsidian from the Chivay source.

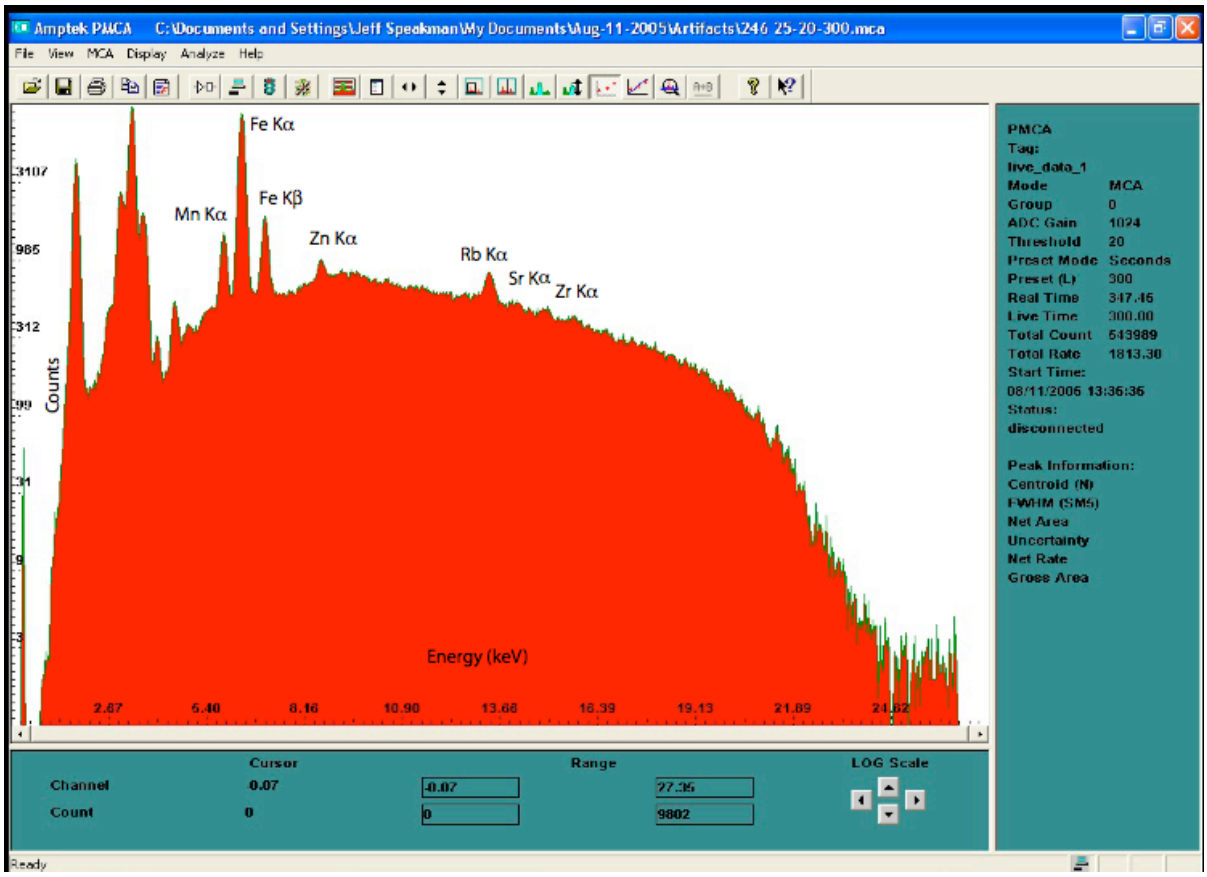

Figure 5.5: Example spectrum of obsidian from the Chivay source by PXRF

The instrumentation and software were advertised to have the capability for both fundamental parameters and empirical calculations for quantitative analysis.[47] Although calibration and standards were used to set up an empirical analysis with matrix-matched standards, at the end of the experiments, it was determined that the calculated results were based entirely on fundamental parameters calculations rather than a combination of

fundamental parameters and empirical approaches. Analysis of the data was completed using the fundamental parameters model only. The XRF-FP software, provided by Amptek and CrossRoads Scientific, identifies peaks and calculates quantitative data for the elemental compositions of the samples.[181]

The software provided with the instrument also appeared to perform quantitative calculations based on the ratio of the Compton to Rayleigh scatter peaks. However, after attempting several calculations with this method it was also determined that that module was non-functional and thus results from this method will not be presented.

For the fundamental parameters analysis, the quantitative results were calculated based on data provided by the software for X-ray interactions. The data were calculated using a sum to 100%, assuming a SiO_2 content of approximately 70%, which has been established to be the average for most obsidian examined in the past. This assumption allows the remaining element oxides to sum to 100%.

Evaluation of Quantitative Analysis

Before proceeding to the archaeological analysis of the project, the analytical capabilities of the Amptek PXRF were evaluated for its precision, accuracy, and reliability as an analytical instrument and method.

Detection limits

Detection limits for each element were calculated using the PMCA program that was provided with the Amptek PXRF system. The Peaksearch option was used to identify and fit the peaks of the six elements of interest from a Chivay obsidian standard spectrum as

compared to a software library of peak energies. Values from the peak fitting were used to calculate the background for each peak. The Peasksearch option also provides uncertainty (in percent) for each peak fitting. Peak uncertainties (second row of table) were determined by PMCA software, and uncertainty values correspond to peak fit after peak fitting by the software. Lower uncertainty values indicate better peak shape, higher peak counts relative to background, and other factors, contributing to a better peak fit by the software. Limits of detection were calculated as three times the square root of the background counts for each peak of interest. Limits of quantification (LOQ) are calculated as 10 times the square root of the background counts for each peak of interest.[184] Table 5.1 provides the values of uncertainty (as determined by the PMCA software for peak fitting) and limits of detection for the elements in the obsidian study.

Table 5.1: Peak uncertainties and limits of detection for the elements in the study

	Sr	Rb	Zr	Zn	Fe	Mn
keV	14.16	13.39	15.77	8.64	6.4	5.9
Uncertainty (%)	5.0	5.9	8.7	8.6	0.5	1.5
LOD (ppm)	6	25	15	2	30	21
LOQ(ppm)	21	82	51	8	100	69

From the table, it can be seen that the limits of detection are fairly low, although the uncertainty for some peaks can be attributed to high background relative to the peak in that region of the spectrum. For Fe and Mn, the values for Chivay (presented in the next section) are several orders of magnitude above LOQ. However, for Sr, Rb, Zr and Zn, reported values are 2 to three times the LOQ, still allowing quantification but this difference is reflected in the higher uncertainties in the peak fitting.

Precision

In order to assess the precision of the method for obsidian, quality control data was taken from the daily analysis of obsidian from known sources. These quality controls were prepared with material from the known source, glued into a plastic backing and polished to a flat surface. As PXRF is a non-destructive methodology, these obsidian standards can be used over and over again with no degradation of the standard. Table 5.2 presents the measured concentrations, standard deviation and relative standard deviation of the three quality controls used in this study. Numbers after each standard (i.e. Alca-3) indicate individual examples of the quality control.

Table 5.2: Precision of obsidian quality controls by PXRF. All values are in ppm.

	Sr	**Rb**	**Zr**	**Zn**	**Fe**	**Mn**
Alca-1-1	86	149	135	33	5122	476
Alca-2-1	80	142	123	30	5164	461
Alca-3-1	96	152	131	31	5125	465
Alca-4-1	104	157	144	32	5107	456
Alca-1-2	120	166	120	30	5111	452
Alca-2-2	88	142	130	30	5148	462
Alca-4-2	83	165	125	29	5121	477
Alca-5-2	122	174	89	35	5117	463
Alca-1-3	67	136	132	35	5155	475
AVERAGE	**94**	**154**	**125**	**32**	**5130**	**465**
STDEV	19	13	16	2	20	9
RSD (%)	19.7	8.3	12.4	7.4	0.4	1.9
Chivay-1-1	48	248	125	32	4876	671
Chivay-2-1	69	231	93	32	4896	679
Chivay-3-1	71	238	127	29	4838	697
Chivay-4-1	52	257	133	32	4830	695
Chivay-1-2	79	245	142	35	4826	673
Chivay-2-2	42	257	107	29	4883	683
Chivay-4-2	86	304	136	35	4769	670
Chivay-5-2	53	247	92	35	4869	705
Chivay-1-3	79	285	130	35	4782	690
AVERAGE	**64**	**257**	**121**	**33**	**4841**	**685**
STDEV	16	23	19	3	45	13
RSD(%)	24.9	9.1	15.6	7.9	0.9	1.8
Quis-1-1	126	172	109	26	5177	390
Quis-2-1	148	198	144	30	5111	369
Quis-3-1	159	198	147	27	5103	366
Quis-4-1	151	200	120	29	5109	390
Quis-1-2	144	178	128	29	5147	373
Quis-2-2	167	194	127	26	5104	382
Quis-4-2	151	199	149	28	5098	375
Quis-5-2	150	189	118	26	5144	374
Quis-1-3	149	180	117	27	5159	368
AVERAGE	**149**	**190**	**129**	**28**	**5128**	**376**
STDEV	11	11	15	2	29	9
RSD(%)	7.5	5.7	11.3	5.5	0.6	2.4

From the six elements measured, strontium appears to have a higher relative standard deviation, especially at lower concentrations. The next highest element % RSD occur for Zr and Zn. These high % RSD values may be related to the low peak-to-background ratio for these elements. Although the reported values for these three elements are above the limits of detection as well as the limits of quantification, the high background, especially in the higher Z elements is likely the cause of higher % RSD. Although the FP quantitative analysis can correctly identify and quantify these elements, it may not be able to consistently model and calculate the peaks correctly due to the high background. Otherwise, with the exception of Zr, the relative standard deviations for the rest of the elements are below 10%, indicating that the PXRF methodology is consistently precise for obsidian applications. The quality control data were taken over a period of two weeks in the field, also indicating the reliability of the method over a longer period of time.

Accuracy

As there is no certified standard for obsidian, accuracy comparisons are made between PXRF performed with the MURR instrument and INAA data acquired at MURR. As seen in the following table, there is a good correlation between the INAA and PXRF values, signifying PXRF as a relatively accurate method for obsidian. Table 5.3 lists these values including the p values for the z-score analysis of the data.

Table 5.3: Averages, standard deviations and percent relative standard deviations for the Chivay obsidian standard by PXRF and INAA, including z-scores analysis. All concentration values are in ppm.

	Sr	**Rb**	**Zr**	**Zn**	**Fe**	**Mn**
MURR- INAA (n=18)						
AVG	49	245	134	35	4883	707
STDEV	11	3	8	6	89	10
% RSD	22	1	6	18	2	1
MURR-PXRF (n= 9)						
AVG	64	257	121	33	4841	685
STDEV	16	23	19	3	45	13
% RSD	25	9	16	8	1	2
P value	0.0	0.0	0.0	0.5	0.0	0.0
Z score	3.0	2.3	-2.6	-0.7	-3.6	-4.8

The z-scores analysis performed using a two-tailed analysis with an α of 0.05 (95% confidence interval), and the assumption that the means, including standard deviations are the same.

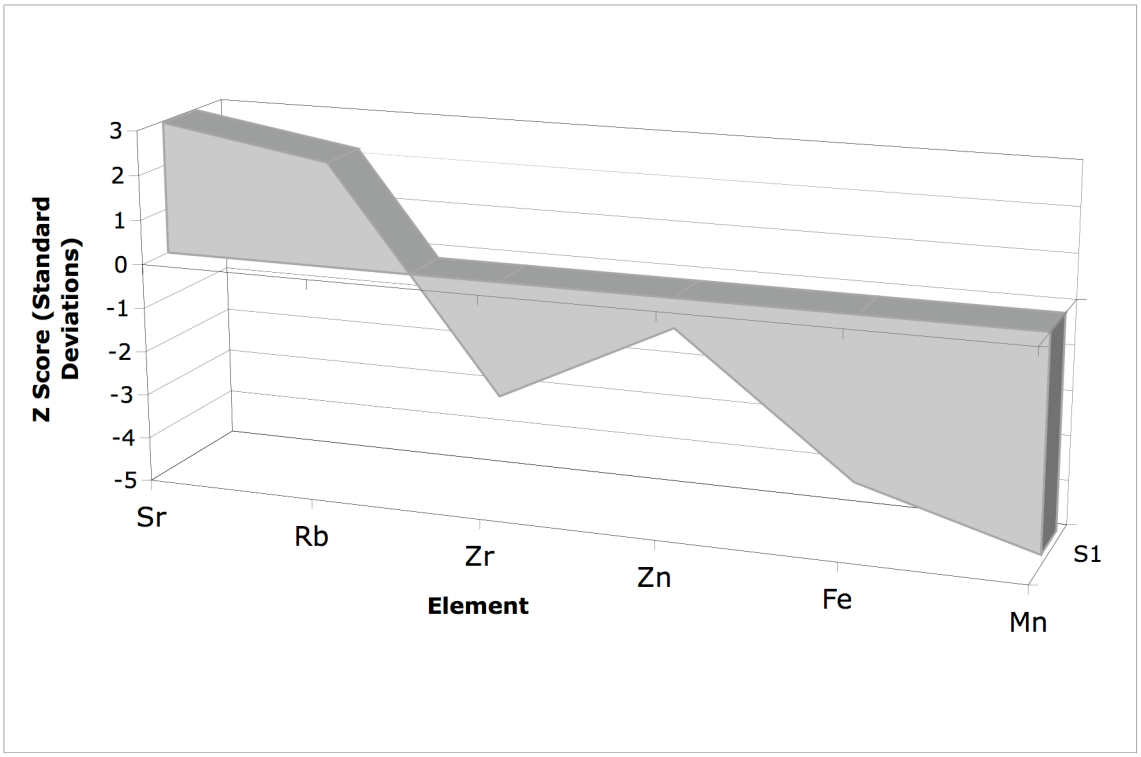

Figure 5.6: Z scores for the six elements measured by PXRF compared to INAA in Chivay obsidian

For all of the elements but Zn, the means for INAA and PXRF are not the same, and the z scores are larger than 2 standard deviations. It also appears that the trend in z scores increases with atomic number of the element. This may be related to the background calculations of the FP method as INAA is independent of atomic number.

A comparison for the data acquired from the MURR PXRF, the MURR INAA and the Berkeley XRF on artifacts is presented in Figure 5.7. A table of the data results is presented in Table 5.4.

Table 5.4: Averages, relative standard deviations and standard deviations for Chivay obsidian artifacts by XRF, PXRF and INAA. All values are in ppm.

	Sr	Rb	Zr	Zn	Fe	Mn
Berkeley-XRF						
Average	46	241	82	40	6380	682
% RSD	7	5	6	11	5	9
Standard Deviation	3	12	5	4	290	59
MURR-PXRF						
Average	63	256	112	33	4860	677
% RSD	24	8	21	9	1	3
Standard Deviation	15	21	24	3	45	18
MURR- INAA						
Average	49	245	134	35	4883	707
% RSD	22	1	6	18	2	1
Standard Deviation	11	3	8	6	89	10

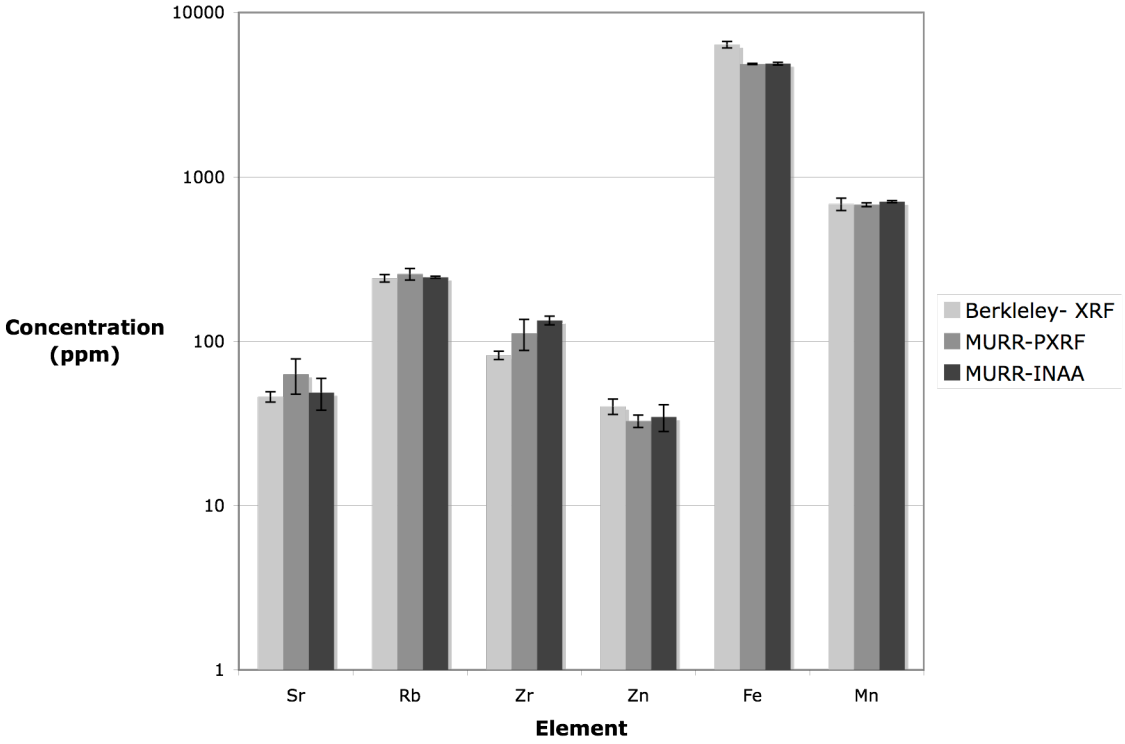

Figure 5.7: Graphical comparison of results for obsidian from the Chivay source for PXRF, INAA and XRF.

The data used in this figure came from the 66 analyzed artifacts attributed to Chivay from Peru. Ideally, since all are from the same source, there should be little variation between the artifacts, and all methods should be able to attribute the artifacts to this source based on the chemical fingerprint described by the six signature elements. As seen in Figure 5.7, the data show that each of the three methods agree very closely. The values from the MURR-PXRF and MURR-INAA agree more closely with each other rather than with the Berkeley XRF data. Despite the challenges in calibrating the PXRF, the FP quantification produced better results than expected. Although the agreement between the values is not perfect, the signature of the obsidian is evident, and this is the most archaeologically important fact for obsidian sourcing. Deviations in agreement between methods can be

easily normalized through a ratio for direct comparison between data. This normalization is common practice in archaeometric studies performed in different laboratories with different instruments and under different analytical conditions. In fact, the data demonstrate that there is also relatively low relative standard deviation, again supporting evidence for a highly precise methodology. Figure 5.6 also provides the error bars for each measurement, and as mentioned before, these errors are quite small.

Figure 5.8 is a plot of Mn vs. Rb, two elements commonly used to distinguish obsidian from the area. Three sources are identified: Chivay, Quispisisa and Alca. This plot includes the measured standards by PXRF (diamonds) and the artifacts measured by PXRF (diamonds). Averages of other data for standards are presented for INAA (triangles) and XRF (squares).

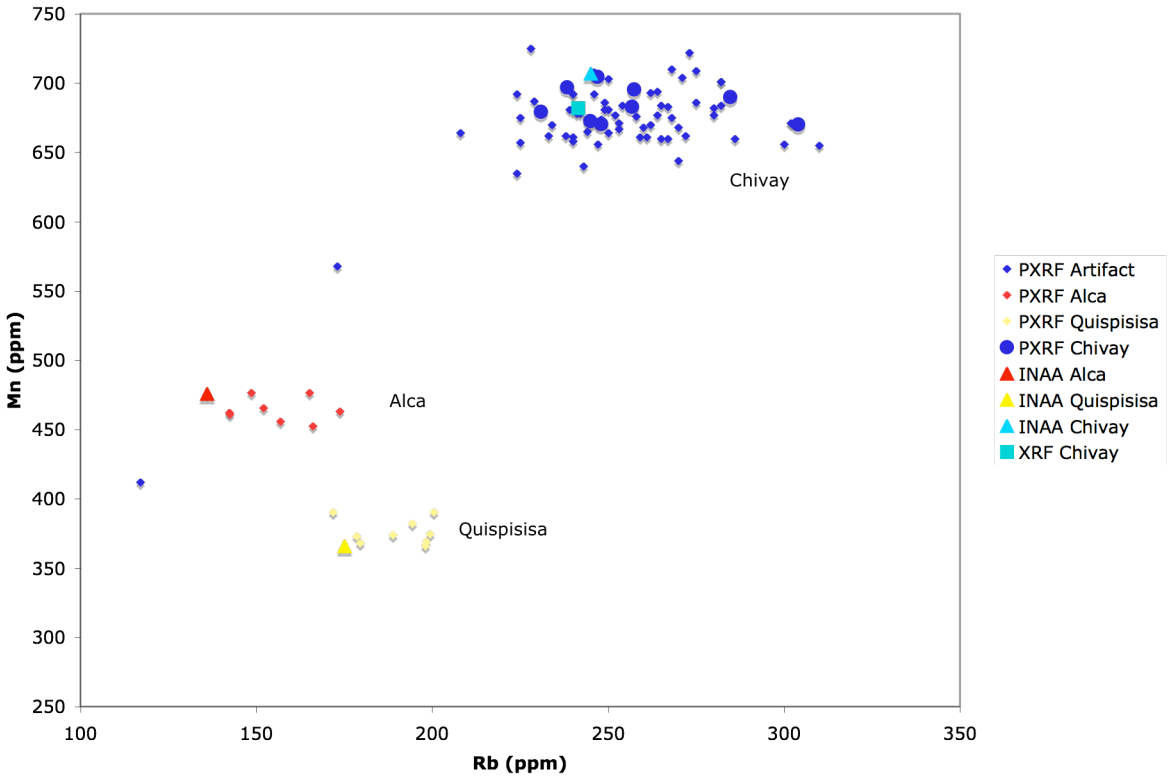

Figure 5.8: Plot of Mn vs. Rb demonstrating separation between obsidian sources for Peruvian obsidian by three analytical methods

This plot demonstrates that by using Mn and Rb, the three major obsidian sources in Peru can be clearly distinguished. These differences also hold up for combinations of other elements used in this study, and Mn and Rb are provided as an example. The figure also shows that the majority of artifacts investigated in this study clearly are from the Chivay source except for the two outliers discussed earlier. Assemblages for each source material are grouped close together to define the cluster. INAA and XRF data are presented as averages only, and agree with the clusters defined by PXRF. If more data points for INAA and XRF were provided, it is likely that they would form more tightly clustered groups reflecting better precision due to lack of X-ray scattering off uneven artifact surfaces. The larger spread in data for artifacts from Chivay is a reflection of the variability in size and

surface contours of the artifacts as opposed to the polished surface of the artifacts used in XRF. PXRF is more susceptible to these size and surface effects than INAA. Regardless of the group data spread, from an archaeometric perspective, the artifacts can be correctly attributed to the correct obsidian source.

Sources for error include the size of the artifact and possible scattering interactions of the beam with the artifact. In addition, artifacts that were close to the spot size of the X-ray beam often produced low count rates and less accurate data. Additional sources of error may occur in the instrumentation and software itself, and include calibration errors, detector counting error statistics, statistical errors for peak fitting, and small changes in source and detector voltages among others. In general, the agreement between PXRF and INAA was better for the standards, which had large flat surfaces as compared to the artifacts which could be smaller, with irregular surfaces. All data from the obsidian investigated by PXRF are presented in Appendix VI.

Conclusions

The results of the PXRF found that a majority (66 of the 68) obsidian samples analyzed were assigned to the Chivay source.[174] The remaining two samples are from an unknown source, possibly the Alca source.[174] The close geographic proximity of Chivay to Jiskairumoko makes it a logical regional source for obsidian for the site and a reasonable hypothesis for the greater percentage of Chivay obsidian found at Jiskairumoko. The archaeological implications for archaeological interactions and exchange are discussed elsewhere.[174]

The analytical results from the PXRF data agree with the XRF and INAA analysis, demonstrating that the PXRF is suitable for use in sourcing archaeological obsidian. This study demonstrates that PXRF using FP quantification is both precise and accurate enough for sourcing archaeological obsidian in this case. The data produced from this technique can "fingerprint" obsidian from a given source, as well as be used in obsidian comparison databases.

Future studies with this instrumentation can be planned on other obsidian projects that may or may not use the elements discussed above. The PXRF can be used to identify sources of artifacts at archaeological sites and museums, and thus reconstruct ancient exchange of this valuable ancient commodity. Due to its portability, PXRF may also be used in the field to identify new obsidian sources. As the software is developed further, the FP analysis can be optimized for obsidian analyses. In addition, empirical XRF methods and standards can be developed, as well as Compton/Rayleigh scatter peak ratios for quantitative analysis using the same instrumentation already constructed and demonstrated in this study.

Appendix I: INAA and PIXE combined data for the Caborn-Welborn ceramics.
Data are presented in ppm values.

ANID	SAMPID	SITE	TYPE	SOURCE	GROUPS	SUBGROUP
CW01	15un28 859-3	28	8	3	Slack Farm	Slack Farm
CW02	15un28 337-27	28	8	3	Slack Farm	Slack Farm
CW03	15un28 1929-41	28	8	3	Slack Farm	Slack Farm
CW04	15un28 1004-51	28	2	3	Slack Farm	Slack Farm
CW05	15un28 292-7	28	2	3	Slack Farm	Slack Farm
CW06	15un28 667-1	28	2	3	Slack Farm	Slack Farm
CW07	15un28 429-1	28	2	3	Slack Farm	Slack Farm
CW08	12Po1 141.722.1	1	4	3	Murphy	Murphy
CW09	12Po1 141.427.1	1	4	3	Murphy	Murphy
CW10	15un28 805-10	28	16	4	Slack Farm	Slack Farm
CW11	15un28 929-24	28	16	4	Slack Farm	Slack Farm
CW12	15un28 805-9	28	16	4	Slack Farm	Slack Farm
CW13	15un28 716-23	28	16	4	Slack Farm	Slack Farm
CW14	15un28 445-6	28	4	3	Slack Farm	Slack Farm
CW15	15un28 667-17	28	4	3	Slack Farm	Slack Farm
CW16	15un28 16-3	28	16	4	Slack Farm	Slack Farm
CW17	15He110 42-2	110	2	3	Cummings	Alzey
CW18	15He110 25-1	110	2	3	Cummings	Alzey
CW19	15un28 267-6	28	16	4	Slack Farm	Slack Farm
CW20	15un28 787-28	28	4	3	Slack Farm	Slack Farm
CW21	15He777 44-5	777	8	3	Cummings	Cummings
CW22	15He777 27-1	777	4	3	Cummings	Cummings
CW23	15He777 45-7	777	8	3	Cummings	Cummings
CW24	15He777 42-1	777	4	3	Cummings	Cummings
CW25	15un42 33-4	42	4	3	Blackburn	Moore
CW26	15un42 32-8	42	8	3	Blackburn	Moore
CW27	15un42 131-1	42	20	2	Blackburn	Moore
CW28	15un42 252-10	42	2	3	Blackburn	Moore
CW29	15un42 33-26	42	4	3	Blackburn	Moore
CW30	15un42 244-1	42	4	3	Blackburn	Moore
CW31	15un28 284-6	28	24	2	Slack Farm	Slack Farm
CW32	15un28 125-54	28	4	3	Slack Farm	Slack Farm
CW33	15un28 928-25	28	4	3	Slack Farm	Slack Farm
CW34	15un28 503-2	28	3	3	Slack Farm	Slack Farm
CW35	15un28 27-6	28	4	3	Slack Farm	Slack Farm
CW36	15un28 523-32	28	24	2	Slack Farm	Slack Farm
CW37	15un28 928-10	28	21	2	Slack Farm	Slack Farm
CW38	15He37 221-2	37	8	3	Cummings	Alzey

CW39	15He37 311-1	37	4	3	Cummings	Alzey
CW40	12H25 5-7-67.134				Central Indiana	
CW41	12H25 8-13-66.205				Central Indiana	
CW42	12Po1 142.438.11	1	30		Murphy - Daub	Murphy
CW43	12Po1 142.444.8	1	30		Murphy - Daub	Murphy
CW44	12Po1 142.430.6	1	30		Murphy - Daub	Murphy
CW45	15un57 308-1	57	4	3	Blackburn	Blackburn
CW46	15Un57 275-1	57	3	3	Blackburn	Blackburn
CW47	15un57 210-1	57	4	3	Blackburn	Blackburn
CW48	15un57 361-3	57	2	3	Blackburn	Blackburn
CW49	12Po1 141.204.1	1	19	3	Murphy	Murphy
CW50	12Po1 141.222.1	1	3	3	Murphy	Murphy
CW51	12Po1 141.522.1	1	8	3	Murphy	Murphy
CW52	12Po1 141.555.1	1	1	3	Murphy	Murphy
CW53	12Po1 141.327.1	1	1	3	Murphy	Murphy
CW54	12Po1 141.263.1	1	8	3	Murphy	Murphy
CW55	12Po1 141.827.2	1	8	3	Murphy	Murphy
CW56	12Po1 141.427.1	1	4	3	Murphy	Murphy
CW57	15He775 6.35	775	3	3	Cummings	Cummings
CW58	15He775.6.7	775	3	3	Cummings	Cummings
CW59	15He775 4.14	775	26	2	Cummings	Cummings
CW60	15He775 6.18	775	3	3	Cummings	Cummings
CW61	15UN42 32-9	42	8	3	Blackburn	Moore
CW62	15UN42 252-11	42	3	3	Blackburn	Moore
CW63	15UN42 32-1	42	1	3	Blackburn	Moore
CW64	15UN177 33-39	177	3	3	Cummings	Hooper
CW65	15UN177 33-1	177	4	3	Cummings	Hooper
CW66	15UN177 34-15	177	24	2	Cummings	Hooper
CW67	15UN177 33-9	177	8	3	Cummings	Hooper
CW68	15UN57 308-1	57	4	3	Blackburn	Blackburn
CW69	15UN57 268-1	57	8	3	Blackburn	Blackburn
CW70	15UN57 143-2	57	8	3	Blackburn	Blackburn
CW71	15He35 15-23	35	8	3	Cummings	Alzey

CW72	15He35 15-4	35	3	3	Cummings	Alzey
CW73	15He35 15-52	35	8	3	Cummings	Alzey
CW74	15He35 15-15	35	8	3	Cummings	Alzey
CW75	15UN28 468-1	28	16	4	Slack Farm	Slack Farm
CW76	15UN28 382-35	28	4	3	Slack Farm	Slack Farm
CW77	15UN28282-16	28	24	2	Slack Farm	Slack Farm
CW78	15UN28 267-11	28	16	4	Slack Farm	Slack Farm
CW79	15He37 291-1	37	3	3	Cummings	Alzey
CW80	15He37 144-1	37	3	3	Cummings	Alzey
CW81	15He37 103-1	37	3	3	Cummings	Alzey
CW82	15He37 141-1	37	3	3	Cummings	Alzey
CW83	15He37 206-1	37	4	3	Cummings	Alzey
CW84	15He37 211-1	37	8	3	Cummings	Alzey
CW85	15He37 123-2	37	4	3	Cummings	Alzey
CW86	15He37 276-3	37	8	3	Cummings	Alzey
CW87			31		Clay 1	
CW88			31		Clay 2	
CW89	15un177 34-12	177	4	3	Cummings	Hooper
CW90	15un177 33-4	177	4	3	Cummings	Hooper
CW91	15un42 33-1	42	4	3	Blackburn	Moore
CW92	15un42 223-1	42	8	3	Blackburn	Moore
CW93	15un42 33-45	42	3	3	Blackburn	Moore
CW94	15un57 137-2	57	1	3	Blackburn	Blackburn
CW95	15un57 151-1	57	4	3	Blackburn	Blackburn
CW96	15un57 244-1	57	8	3	Blackburn	Blackburn
CW97	15un57 368-1	57	4	3	Blackburn	Blackburn
CW98	15un57 371-1	57	3	3	Blackburn	Blackburn
CW99	15un28 125-26	28	4	3	Slack Farm	Slack Farm
CW100	15un28 644-2	28	4	3	Slack Farm	Slack Farm
CW101	15un28 915-2	28	1	3	Slack Farm	Slack Farm
CW102	15un28 265-38	28	4	3	Slack Farm	Slack Farm
CW103	15un28 904-50	28	4	3	Slack Farm	Slack Farm
CW104	15un28 510-1	28	4	3	Slack Farm	Slack Farm
CW105	15un28 90-1	28	3	3	Slack Farm	Slack Farm
CW106	15un28 720-22	28	3	3	Slack Farm	Slack Farm
CW107	15un28 28-11	28	8	3	Slack Farm	Slack Farm
CW108	15un28 125-1	28	1	3	Slack Farm	Slack Farm
CW109	15un28 328-13	28	8	3	Slack Farm	Slack Farm
CW110	15un28 31-3	28	4	3	Slack Farm	Slack Farm
CW111	15un28 945-2	28	3	3	Slack Farm	Slack Farm
CW112	15Un28 945-1	28.00	3.00	3.00	Slack Farm	Slack Farm
CW113	15un28 985-33	28	8	3	Slack Farm	Slack Farm
CW114	15un28 779-10	28	24	2	Slack Farm	Slack Farm
CW115	15un28 764-12	28	18	2	Slack Farm	Slack Farm
CW116	15un28 446-36	28	16	4	Slack Farm	Slack Farm
CW117	15un28 977-1	28	16	4	Slack Farm	Slack Farm

CW118	15un28 444-12	28	8	3	Slack Farm	Slack Farm
CW119	15Un28 413-102	28.00	8.00	3.00	Slack Farm	Slack Farm
CW120	15un28 908-18	28	16	4	Slack Farm	Slack Farm
CW121	15un28 915-8	28	8	3	Slack Farm	Slack Farm
CW122	15un57 168-1	57	3	3	Blackburn	Blackburn
CW123	15un42 174-1	42	1	3	Blackburn	Moore
CW124	15un28 508-27	28	16	4	Slack Farm	Slack Farm
CW125	15un28 444-15	28	8	3	Slack Farm	Slack Farm
CW126	15un57 260-1	57	22	3	Blackburn	Blackburn
CW127	15un42 226-1	42	23	2	Blackburn	Moore
CW128	15un28 919-115/daub	10	30	30	Daub	Slack Farm
CW129	15un28 1096-7/daub	10	30	30	Daub	Slack Farm
CW130	15un28 1004-75/daub	10	30	30	Daub	Slack Farm

ANID	Al (%)	Ba	Ce	Co	Cr	Cs	Cu	Eu	Fe (%)
CW01	8.01	1992	97.3	14.6	123.2	6.64	43.84	1.97	4.18
CW02	9.46	2906	110.7	11.9	94.4	7.27	34.19	2.15	4.01
CW03	9.07	1536	105.7	11.4	101.1	7.47	27.97	1.97	4.55
CW04	10.14	2032	102.8	8.4	114.4	7.19	31.16	2.09	3.95
CW05	10.57	2711	117.2	15.1	101.9	8.89	53.59	2.33	4.29
CW06	9.29	2500	92.5	12.6	80.5	6.32	27.60	1.65	4.24
CW07	7.83	1698	84.9	8.1	54.3	4.96	18.97	1.65	2.79
CW08	9.89	2095	100.0	13.0	88.0	6.50	29.12	1.82	3.09
CW09	12.19	2184	88.6	6.3	89.3	8.38	48.41	1.78	3.06
CW10	9.34	2341	109.5	10.4	76.1	7.67	32.96	2.22	4.21
CW11	9.86	2206	106.5	8.5	95.9	6.82	38.57	2.16	3.44
CW12	10.39	2228	119.9	11.9	148.4	7.99	42.09	2.47	3.58
CW13	9.82	1958	114.2	10.4	66.1	7.53	38.86	2.24	4.81
CW14	10.06	1503	106.3	15.3	114.3	7.57	33.38	1.86	3.73
CW15	9.24	2186	89.9	13.8	82.3	7.35	34.20	1.60	4.99
CW16	8.65	1533	113.2	15.8	87.6	7.45	33.83	2.11	4.78
CW17	10.60	1429	118.0	16.2	90.0	9.87	40.48	2.37	4.91
CW18	10.32	1268	114.2	7.5	104.1	9.39	28.37	2.04	4.10
CW19	10.26	2456	110.8	9.7	135.2	7.11	28.67	2.25	3.79
CW20	10.05	2832	105.6	10.9	96.6	7.00	39.29	2.04	3.13
CW21	9.26	1623	96.8	9.0	69.2	6.00	29.00	2.12	3.02
CW22	9.64	1403	102.4	9.4	83.0	7.97	39.58	2.01	3.19
CW23	8.96	1546	115.6	12.6	70.7	7.81	22.40	2.19	3.92
CW24	9.93	1825	114.6	11.0	76.4	7.83	31.30	2.32	3.62
CW25	8.00	1761	84.1	19.3	74.0	7.31	31.75	1.57	4.49
CW26	8.65	1787	102.3	22.3	108.6	7.49	51.67	2.11	4.59
CW27	9.68	1364	98.6	9.8	137.9	8.26	38.28	2.10	4.70
CW28	8.43	2196	103.1	13.0	112.2	6.44	40.78	2.05	4.42
CW29	9.28	2262	107.3	19.1	88.5	8.03	34.01	2.20	4.44
CW30	9.03	2908	110.3	15.1	97.3	6.66	26.84	2.23	4.70
CW31	11.24	4342	110.1	15.0	135.9	8.16	57.25	2.26	4.39
CW32	9.53	2072	98.7	10.7	191.7	5.90	20.04	2.15	4.36
CW33	8.78	1460	100.1	12.7	77.8	7.94	27.23	2.02	4.63
CW34	10.81	2572	122.1	16.1	92.4	10.09	64.13	2.39	4.27
CW35	9.38	2172	96.6	13.4	119.9	7.55	44.84	1.95	4.45
CW36	10.32	2016	102.0	11.7	123.7	7.43	41.58	2.07	3.43
CW37	10.22	2004	109.3	12.0	99.3	7.64	46.51	2.26	3.15
CW38	10.42	3330	116.3	18.7	97.3	8.14	48.81	2.35	4.52
CW39	10.97	2414	114.9	18.7	79.4	8.04	35.93	2.25	4.33
CW40	8.84	1308	89.2	5.5	118.6	5.65	37.81	1.88	3.99
CW41	9.58	1391	85.8	5.1	88.6	5.34	41.80	1.82	3.33

CW42	10.67	759	91.1	6.7	67.9	9.59	24.83	1.62	3.11
CW43	2.91	4953	42.4	8.0	85.5	2.73	80.22	1.49	11.26
CW44	10.67	1053	115.4	8.1	65.4	9.78	25.63	2.23	2.97
CW45	7.68	1371	91.6	8.6	57.1	4.09	22.59	1.64	3.07
CW46	9.14	1514	102.3	13.4	75.8	6.09	34.27	2.08	2.42
CW47	9.60	2244	109.9	16.4	67.0	5.90	39.33	2.31	4.43
CW48	9.31	1311	112.6	10.9	142.3	8.06	29.24	2.44	5.03
CW49	11.52	2223	101.4	8.5	100.2	9.19	23.45	1.94	3.75
CW50	12.62	1843	92.7	7.5	94.9	9.20	36.68	3.58	3.42
CW51	9.15	1266	108.8	9.3	82.4	4.35	16.29	1.92	4.28
CW52	13.47	2460	135.7	12.3	133.2	12.98	45.02	2.40	5.06
CW53	13.89	2195	114.5	9.4	118.0	9.27	28.34	2.24	4.15
CW54	13.42	2408	122.6	17.3	122.7	9.58	55.03	1.31	4.62
CW55	11.12	1957	101.8	8.3	112.2	8.85	50.22	2.18	3.76
CW56	5.62	1100	39.0	3.3	44.4	3.89	36.76	0.84	1.42
CW57	14.24	2105	132.2	15.0	129.1	10.68	50.68	1.88	4.52
CW58	11.70	1609	125.2	17.5	108.0	10.09	48.44	2.04	4.86
CW59	10.69	1778	107.1	11.9	98.4	7.58	29.69	1.88	4.03
CW60	12.11	1710	95.6	10.7	100.1	6.80	32.94	2.21	3.59
CW61	9.57	1518	80.9	10.1	74.2	6.37	25.13	1.59	3.66
CW62	10.03	1335	81.7	10.0	77.8	6.40	32.93	1.70	3.89
CW63	12.07	1688	91.3	14.9	90.8	6.93	43.05	1.84	4.38
CW64	12.45	1301	102.6	14.9	88.0	7.83	32.75	1.85	4.50
CW65	12.55	1221	108.5	11.8	100.7	6.96	28.29	1.93	3.97
CW66	11.88	1074	97.8	10.0	90.8	7.06	43.02	1.77	3.27
CW67	12.18	1472	81.8	11.2	73.6	6.13	53.71	1.65	2.68
CW68	9.89	1259	88.3	9.8	75.7	4.52	29.17	1.46	2.99
CW69	11.65	1592	99.8	17.5	92.4	6.48	44.88	1.47	4.89
CW70	11.74	1676	102.6	14.7	104.5	7.72	39.17	1.95	4.74
CW71	13.72	5092	126.6	11.2	105.8	8.66	44.83	2.43	4.21
CW72	15.62	3118	129.5	14.9	115.6	8.88	30.55	2.35	5.46
CW73	13.24	3320	118.3	13.0	104.6	8.36	40.04	1.89	4.41
CW74	13.35	3682	127.7	16.5	88.7	9.21	43.59	0.89	4.70
CW75	13.68	2735	120.5	16.9	49.4	9.31	65.09	2.43	4.13
CW76	10.66	1254	87.8	14.9	42.1	7.27	27.25	1.76	4.21
CW77	14.56	2783	103.8	11.9	46.0	9.83	56.92	2.35	4.45
CW78	8.86	2372	94.1	40.6	30.8	4.63	22.31	0.61	4.92
CW79	13.36	3283	124.7	17.6	47.1	9.97	41.94	1.07	5.13
CW80	9.63	2257	94.1	14.4	36.6	6.09	37.05	1.39	4.23
CW81	10.44	1404	82.1	12.7	40.7	5.44	28.91	1.23	3.74
CW82	10.05	2004	97.7	14.6	39.7	7.39	44.16	1.25	4.27
CW83	12.48	2019	108.2	14.0	109.8	7.41	26.71	0.96	3.90
CW84	13.79	1883	104.6	10.8	42.8	8.27	40.28	2.20	4.05

CW85	10.73	2562	106.0	15.1	36.6	6.52	16.59	1.51	3.80
CW86	11.65	3328	102.1	19.5	37.7	7.12	38.86	2.01	4.87
CW87	9.07	570	85.2	10.9	34.9	6.94	23.29	0.76	3.39
CW88	14.96	398	155.2	13.4	148.6	15.34	13.60	1.15	1.65
CW89	10.17	1017	82.2	11.2	89.4	6.88	27.60	0.91	2.94
CW90	11.16	1400	90.0	11.0	40.1	7.54	30.76	0.84	3.01
CW91	9.03	1800	74.8	11.9	37.9	5.83	31.37	2.10	4.08
CW92	13.57	2118	109.0	15.7	52.7	9.21	65.51	3.24	5.63
CW93	11.93	1541	101.0	8.5	48.6	7.62	40.59	1.84	3.58
CW94	12.66	1886	108.3	17.9	47.6	8.56	33.38	1.91	4.99
CW95	13.14	1630	104.7	19.6	48.6	6.61	43.67	1.92	4.88
CW96	11.51	1687	94.9	12.1	67.2	7.89	40.16	1.32	3.57
CW97	12.66	2532	108.3	14.3	118.0	6.64	37.12	1.08	3.51
CW98	13.42	1435	120.4	20.0	124.6	10.34	57.88	1.75	5.96
CW99	8.97	2261	155.9	30.2	142.3	7.17	32.64	2.80	7.30
CW100	10.98	2048	117.7	23.9	100.7	7.98	46.74	2.65	3.35
CW101	11.37	2540	131.3	17.6	138.4	11.58	26.13	3.02	4.76
CW102	10.57	2616	118.2	14.0	110.6	7.82	28.87	1.97	4.46
CW103	11.22	2450	116.0	6.0	112.1	8.39	5.67	1.09	4.61
CW104	10.62	3980	119.6	7.8	103.9	6.84	35.73	1.39	3.06
CW105	12.62	3774	133.7	37.9	134.5	9.47	71.66	3.24	5.01
CW106	10.53	2839	114.4	12.8	105.9	8.44	44.95	2.14	3.31
CW107	11.03	2449	115.7	13.6	104.3	8.65	34.61	1.76	4.38
CW108	14.30	2041	149.8	25.9	153.2	13.14	35.36	3.41	5.24
CW109	9.99	2908	111.4	14.1	97.3	6.91	39.08	2.28	4.12
CW110	12.02	3327	114.3	10.6	118.0	9.21	38.81	1.75	4.33
CW111	11.81	2040	115.9	23.5	112.9	8.74	25.76	3.35	4.15
CW112	11.34	2162	115.5	21.1	109.6	8.90	23.98	2.13	4.05
CW113	14.82	2495	135.7	19.8	132.6	10.65	39.08	2.36	5.15
CW114	11.73	1950	96.0	13.7	104.5	8.30	52.79	2.47	3.41
CW115	11.87	3084	109.1	11.0	102.5	8.05	16.42	1.85	5.10
CW116	11.87	2920	120.5	12.2	115.0	8.56	32.62	2.59	4.08
CW117	11.38	2728	120.9	13.4	109.7	7.88	38.17	2.22	4.38
CW118	10.27	1989	97.0	14.5	85.0	7.47	47.57	2.14	2.73
CW119	10.90	2044	99.9	13.8	87.7	6.83	41.82	2.18	2.76
CW120	11.29	3001	122.5	12.4	123.7	10.43	54.26	2.47	4.75
CW121	10.30	2961	118.5	8.9	106.5	9.12	36.30	1.70	5.04
CW122	10.32	1659	117.1	15.1	119.5	9.23	34.92	1.93	6.00
CW123	8.99	1528	112.4	14.3	113.4	8.66	25.83	3.10	5.17
CW124	9.61	3461	115.1	17.7	105.5	7.83	37.37	2.32	3.68
CW125	11.15	1711	112.7	19.5	104.8	8.12	40.68	3.12	3.41
CW126	9.63	1206	118.4	6.7	100.2	7.44	40.15	1.32	3.70
CW127	9.19	2252	88.6	16.2	102.8	6.19	35.30	1.51	5.04

CW128	8.52	578	111.5	10.4	82.1	5.89	25.90	1.32	4.63
CW129	7.71	1485	103.5	25.3	76.5	5.38	19.61	2.09	4.09
CW130	10.09	1095	111.2	21.2	128.4	7.53	25.50	1.87	4.51

ANID	Ga	Hf	K (%)	La	Lu	Mg	Mn	Na	Nd
CW01	19.82	5.97	1.99	51.54	0.57	5599	836	5005	53.44
CW02	27.32	6.91	2.18	57.15	0.66	7539	556	4381	28.65
CW03	22.48	5.96	2.13	55.11	0.60	5553	668	3197	32.27
CW04	27.19	5.76	2.30	56.17	0.58	3690	730	3425	34.34
CW05	40.56	4.86	2.27	60.65	0.69	4044	1229	2918	37.97
CW06	13.24	5.69	2.47	47.90	0.54	7456	840	6221	29.88
CW07	21.10	6.41	1.75	44.21	0.50	4225	945	6671	0.00
CW08	27.99	5.78	2.60	50.39	0.58	5381	319	3850	39.72
CW09	23.47	4.85	2.78	47.40	0.50	4142	713	3687	0.00
CW10	22.66	6.40	2.78	58.91	0.62	6240	654	4776	47.83
CW11	24.43	6.64	2.46	59.29	0.70	6418	854	3377	38.19
CW12	0.00	6.82	2.36	62.77	0.75	7989	636	3941	58.55
CW13	31.39	6.77	2.34	60.43	0.77	6245	766	3839	54.29
CW14	27.08	5.48	2.38	53.08	0.57	5804	896	4045	0.00
CW15	20.28	4.84	2.32	47.22	0.52	6814	1084	4854	53.50
CW16	19.05	5.78	2.32	57.06	0.67	6796	628	3978	46.03
CW17	38.96	5.49	2.12	53.34	0.72	8614	1148	2003	65.69
CW18	26.05	5.84	1.74	59.64	0.58	3723	572	3764	0.00
CW19	30.59	6.34	2.59	59.82	0.67	5925	730	2146	49.39
CW20	17.57	6.80	2.30	55.40	0.62	9002	662	5851	39.78
CW21	25.91	6.20	1.91	55.75	0.62	4842	599	3457	53.73
CW22	19.71	5.48	2.91	53.71	0.55	6516	491	2685	48.89
CW23	30.22	5.53	1.86	59.49	0.65	4794	483	2991	50.61
CW24	22.97	6.09	2.02	59.57	0.63	7311	574	3106	46.99
CW25	22.73	5.65	2.11	45.37	0.55	10085	1475	5074	51.11
CW26	21.14	6.33	2.15	54.70	0.68	7879	1727	4119	67.89
CW27	27.18	5.86	2.05	54.60	0.59	6859	764	4504	51.15
CW28	28.25	5.39	1.98	55.72	0.60	5873	993	3325	49.47
CW29	28.68	5.62	2.35	57.53	0.64	5839	1716	3559	50.10
CW30	23.73	6.19	2.13	58.65	0.64	5390	1141	3872	77.97
CW31	30.75	5.28	2.22	59.59	0.60	6349	892	3211	58.57
CW32	19.67	7.75	2.41	53.46	0.64	6890	621	5949	90.11
CW33	28.98	6.02	2.05	52.82	0.64	6418	608	4178	50.45
CW34	30.44	5.22	2.37	65.25	0.66	4589	796	5968	61.09
CW35	22.40	5.79	2.29	51.89	0.57	8077	831	4799	0.00
CW36	19.45	5.92	2.93	55.18	0.61	6627	569	5008	63.61
CW37	31.93	7.01	2.61	68.73	0.71	6565	456	7080	62.69
CW38	31.57	6.52	2.54	61.56	0.68	6798	1612	3009	66.63
CW39	39.24	8.05	2.87	60.62	0.70	8521	959	4224	64.38
CW40	21.84	7.24	1.62	50.31	0.57	2021	279	5293	54.34
CW41	21.64	6.69	1.71	48.52	0.60	2500	327	5495	50.71

CW42	29.67	28.27	2.56	48.74	0.51	6994	185	2213	44.39
CW43	0.00	4.38	0.83	34.10	0.46	30515	16495	3516	0.00
CW44	29.63	6.27	2.83	60.55	0.64	5380	80	2790	89.04
CW45	11.49	9.53	1.26	48.12	0.58	3356	348	4873	50.43
CW46	19.40	3.48	2.07	57.56	0.62	5129	712	3891	69.46
CW47	24.44	6.28	2.04	60.46	0.67	4665	1330	4067	72.98
CW48	17.33	7.08	1.82	62.01	0.66	5194	622	4667	56.95
CW49	19.64	5.36	2.28	55.66	0.57	6944	697	3017	50.28
CW50	27.85	4.39	2.52	21.27	0.39	4588	922	3447	64.81
CW51	19.65	9.30	1.49	61.68	0.64	3760	330	3815	62.80
CW52	38.58	6.66	2.29	74.70	0.77	2155	1034	5926	52.18
CW53	47.57	5.38	2.63	62.64	0.66	6543	673	3087	67.62
CW54	45.80	6.56	2.89	66.18	0.72	5514	1089	3700	55.15
CW55	27.37	7.20	2.62	58.29	0.56	3291	693	4599	55.14
CW56	18.34	2.18	1.17	22.36	0.25	11763	408	1737	20.05
CW57	43.97	5.55	2.73	73.65	0.74	8128	791	2636	69.54
CW58	20.35	5.83	2.53	66.12	0.68	4801	680	3097	58.28
CW59	19.65	6.89	2.23	59.53	0.65	8020	312	4120	60.98
CW60	27.81	6.11	2.38	64.02	0.64	7109	637	2397	59.89
CW61	25.30	4.54	2.01	44.65	0.47	10183	5328	3061	43.26
CW62	19.95	4.71	2.47	45.54	0.54	10356	384	3716	40.95
CW63	29.15	5.73	2.70	50.33	0.58	11236	1715	3561	43.96
CW64	30.27	5.84	2.58	57.96	0.59	8717	538	3114	47.98
CW65	29.06	6.99	2.44	59.67	0.68	5876	522	2959	73.17
CW66	25.46	6.77	2.63	53.26	0.57	6937	476	4142	74.37
CW67	31.91	6.42	2.64	45.66	0.52	16526	539	3656	50.37
CW68	21.52	9.14	1.87	14.91	0.41	5143	511	217	39.90
CW69	23.25	6.11	2.65	55.84	0.55	8753	1410	4026	63.42
CW70	29.19	6.33	2.83	58.03	0.61	10559	1285	4314	52.35
CW71	22.48	7.51	2.99	69.46	0.73	9388	699	4352	74.12
CW72	29.49	7.73	3.40	72.10	0.80	9190	800	5331	61.24
CW73	22.34	6.91	3.14	66.75	0.69	10159	563	4199	61.35
CW74	27.66	5.94	2.86	69.93	0.83	8336	576	3282	53.97
CW75	38.50	5.07	2.76	18.48	0.77	11121	769	2558	65.76
CW76	22.13	9.16	2.23	48.31	0.61	8190	1293	8266	37.26
CW77	42.78	6.58	2.84	59.44	0.69	8196	646	4284	15.00
CW78	17.95	8.11	1.68	52.77	0.58	6455	5096	6301	47.11
CW79	36.79	6.11	2.69	66.59	0.72	8670	1075	3446	44.80
CW80	17.94	9.34	2.00	50.62	0.63	8454	454	6140	37.59
CW81	29.08	8.35	2.50	53.50	0.60	13368	589	5899	32.93
CW82	27.03	7.63	2.10	52.69	0.63	11242	631	5221	45.72
CW83	17.07	5.42	2.55	61.01	0.63	7482	435	2683	66.96
CW84	37.13	5.81	2.89	58.73	0.63	10546	741	3587	49.90

CW85	15.94	7.59	2.34	56.63	0.66	6527	707	4107	37.32
CW86	18.33	5.59	2.49	55.98	0.64	10256	868	3317	53.98
CW87	13.73	8.93	2.31	46.09	0.60	10830	162	5639	41.59
CW88	33.25	6.31	2.22	79.22	0.60	7490	36	1351	52.25
CW89	18.85	6.68	2.23	45.33	0.59	6619	629	5152	23.57
CW90	24.72	5.91	1.91	51.88	0.66	8808	704	3274	39.40
CW91	19.11	5.79	1.96	42.87	0.50	9047	702	5059	35.73
CW92	33.61	5.99	2.46	62.67	0.70	15486	1112	4349	51.30
CW93	33.26	6.94	2.32	55.97	0.63	9302	521	5492	31.27
CW94	33.62	6.33	2.55	60.41	0.68	10621	1270	4854	63.20
CW95	2.58	8.55	2.85	56.62	0.67	9872	1622	6534	50.74
CW96	23.81	7.08	2.12	51.60	0.64	11602	400	3579	41.70
CW97	26.76	6.14	2.80	59.02	0.65	7763	659	2980	41.31
CW98	32.96	6.77	3.26	67.79	0.76	14802	585	5644	54.15
CW99	9.19	11.84	3.31	49.97	0.49	26270	1988	9456	57.28
CW100	29.11	6.91	2.31	55.49	0.55	7918	1000	4377	52.91
CW101	34.54	6.42	2.08	64.67	0.58	5234	649	3982	57.34
CW102	28.29	6.12	2.26	57.36	0.60	7058	579	3657	76.70
CW103	9.06	6.03	2.57	58.58	0.63	10937	600	5035	56.74
CW104	9.15	7.52	2.40	59.17	0.63	6404	467	3481	57.24
CW105	40.91	5.92	2.77	65.11	0.66	3325	1293	4021	49.04
CW106	28.45	6.29	2.11	56.87	0.58	6662	741	9431	69.94
CW107	28.67	6.06	2.23	58.60	0.63	8996	388	3855	61.98
CW108	44.25	6.75	2.80	76.12	0.92	5448	775	5470	76.50
CW109	20.00	7.42	2.12	56.79	0.59	5193	506	4589	37.68
CW110	28.64	5.04	2.69	57.63	0.58	8962	575	2987	52.76
CW111	22.25	6.07	2.37	58.26	0.58	7530	457	3785	62.54
CW112	18.34	6.27	2.26	59.85	0.56	6980	511	3575	77.29
CW113	39.71	6.04	3.41	68.82	0.73	11126	1537	3800	77.20
CW114	18.93	5.05	2.23	49.43	0.50	6754	816	5563	53.65
CW115	36.73	6.09	2.27	55.74	0.57	10084	624	4144	67.46
CW116	38.49	6.44	2.48	61.04	0.61	11133	552	4079	62.54
CW117	22.51	6.89	2.60	66.30	0.66	8355	811	3718	90.68
CW118	21.01	6.42	2.22	52.02	0.51	5910	425	3747	49.26
CW119	28.12	6.89	0.25	54.79	0.57	4072	502	5052	52.79
CW120	29.76	5.20	2.18	63.88	0.65	8553	994	4724	49.26
CW121	30.79	5.88	2.04	60.34	0.65	7217	1275	3352	63.22
CW122	25.91	6.47	1.88	61.81	0.67	12097	480	4332	67.62
CW123	21.21	6.85	1.66	60.05	0.63	7783	723	7278	78.59
CW124	29.90	6.16	1.90	57.29	0.61	7699	313	4028	68.92
CW125	26.87	5.78	2.25	55.89	0.61	7510	731	3472	55.91
CW126	26.97	7.09	1.73	60.99	0.68	8784	331	3889	57.57
CW127	22.76	5.38	1.77	46.62	0.47	7728	825	3753	44.74

CW128	28.39	9.64	2.18	57.06	0.75	7050	1280	4523	55.94
CW129	24.41	10.66	1.95	39.60	0.37	6750	603	3097	46.44
CW130	16.92	7.04	1.99	51.28	0.59	8280	541	5677	47.83

ANID	Ni	P(%)	Rb	Sb	Sc	Si(%)	Sm	Ta	Tb
CW01	32.36	0.491	129.49	1.29	17.15	24.93	8.51	1.03	1.16
CW02	35.44	0.913	140.90	1.52	18.27	27.52	9.43	1.28	1.79
CW03	26.38	0.364	151.04	1.60	18.28	25.19	8.75	1.17	1.04
CW04	37.94	1.332	144.72	1.49	18.05	27.84	9.22	1.14	1.29
CW05	58.16	2.015	157.12	1.85	23.51	20.75	9.72	1.13	1.34
CW06	37.23	0.828	111.27	1.33	15.83	28.89	7.42	1.14	1.13
CW07	28.42	0.780	94.29	1.07	13.76	27.67	7.12	0.91	1.12
CW08	35.24	0.399	126.95	1.42	17.40	29.31	8.35	1.14	1.17
CW09	32.58	0.455	169.97	1.71	18.99	34.18	7.17	1.05	0.98
CW10	45.17	0.588	150.29	1.64	20.33	25.03	9.60	1.16	1.74
CW11	34.30	0.420	138.88	1.42	18.57	27.96	9.39	1.18	1.17
CW12	61.11	0.539	179.48	1.80	21.70	26.73	10.70	1.34	2.00
CW13	37.08	0.577	138.40	1.70	19.52	28.16	10.09	1.30	1.39
CW14	37.42	0.251	128.30	1.69	18.21	27.80	8.30	1.22	1.32
CW15	33.74	0.629	133.02	1.60	16.40	26.81	7.33	1.10	0.87
CW16	43.66	0.316	135.52	1.68	19.00	26.14	9.37	1.19	1.61
CW17	48.65	0.678	150.93	2.14	22.16	24.53	9.15	1.21	2.01
CW18	27.20	0.159	140.11	2.00	22.16	23.29	9.10	1.23	1.17
CW19	33.28	0.727	136.14	1.57	18.44	28.40	9.85	1.16	1.81
CW20	43.89	0.197	136.72	1.55	17.90	28.61	9.33	1.14	1.29
CW21	35.98	1.386	105.71	1.40	18.10	24.95	9.12	1.22	1.86
CW22	41.36	0.075	133.69	1.89	18.32	24.90	8.88	1.12	1.68
CW23	37.74	1.002	125.82	1.80	20.47	21.61	9.73	1.28	1.64
CW24	45.94	1.171	109.69	1.84	19.16	24.69	10.34	1.11	1.41
CW25	31.08	0.423	118.95	1.52	15.29	27.14	6.72	1.05	0.93
CW26	59.24	0.775	150.42	1.49	18.97	26.33	8.91	1.15	1.26
CW27	46.12	0.167	144.70	1.69	19.35	28.99	9.07	1.14	1.60
CW28	47.94	1.229	152.43	1.44	20.17	21.99	9.20	1.06	1.22
CW29	50.97	1.251	156.70	1.65	20.14	25.93	9.65	1.14	1.28
CW30	58.58	1.739	134.17	1.48	19.74	24.62	9.79	1.20	1.62
CW31	55.03	1.824	160.40	1.74	22.76	23.78	9.63	1.11	1.24
CW32	48.63	0.927	125.29	1.22	16.28	32.63	9.45	1.18	1.29
CW33	46.20	0.294	162.57	1.73	19.18	24.88	8.73	1.11	1.18
CW34	54.32	0.886	191.94	2.14	23.38	25.16	10.82	1.14	1.80
CW35	55.00	0.871	155.68	1.61	18.46	28.80	8.50	1.12	1.19
CW36	39.41	0.477	150.12	1.63	19.23	28.33	9.23	1.15	1.34
CW37	44.88	0.282	169.43	1.65	19.83	29.67	11.70	1.23	1.43
CW38	48.77	0.931	167.84	1.77	21.33	27.15	10.25	1.16	1.76
CW39	53.93	0.678	159.98	1.72	19.54	33.81	10.24	1.30	1.41
CW40	27.42	0.188	99.40	1.31	16.88	25.35	8.30	0.91	1.13
CW41	27.36	0.246	99.62	1.23	15.81	27.06	8.00	0.94	1.31

CW42	26.23	0.060	185.81	2.14	19.46	26.85	7.37	1.11	0.89
CW43	69.31	1.526	0.00	0.63	170.62	13.13	7.14	0.00	1.13
CW44	34.71	0.073	206.37	2.26	19.77	29.08	9.94	1.29	1.76
CW45	25.26	0.949	87.36	1.01	16.34	24.87	7.99	1.20	0.97
CW46	45.78	0.851	215.67	0.36	6.93	25.38	9.58	0.33	0.53
CW47	34.80	1.680	110.75	1.51	18.59	23.82	10.13	1.11	1.22
CW48	26.81	0.278	116.66	1.99	9.50	27.42	10.41	0.60	1.42
CW49	33.03	0.552	156.48	0.83	22.19	22.72	8.53	1.13	1.20
CW50	42.08	0.932	163.48	1.75	20.28	23.47	3.68	0.37	1.54
CW51	32.50	0.663	90.51	0.51	16.10	24.37	9.64	1.17	1.46
CW52	46.88	0.905	212.45	1.29	28.99	25.03	11.46	3.14	1.56
CW53	45.56	1.040	177.10	0.85	24.79	27.30	9.52	1.54	1.40
CW54	56.37	0.414	212.64	0.98	25.32	27.75	10.97	1.44	1.31
CW55	44.53	0.649	178.92	0.91	22.63	27.28	9.38	2.44	1.25
CW56	18.92	0.309	81.58	0.35	8.87	13.29	3.40	0.99	0.50
CW57	61.09	0.336	186.74	0.83	26.51	28.91	12.44	1.65	1.72
CW58	40.36	0.336	155.61	0.83	24.57	24.49	11.00	2.21	1.32
CW59	32.42	0.469	146.41	0.77	20.08	25.99	10.68	1.74	1.43
CW60	39.59	0.525	130.92	0.84	17.88	24.32	11.15	0.12	1.46
CW61	34.66	0.747	118.86	0.67	15.69	20.41	7.55	1.61	0.97
CW62	41.00	0.628	127.45	0.78	16.00	26.42	8.00	1.08	1.11
CW63	34.19	1.232	130.15	0.75	18.38	29.11	7.88	1.74	1.27
CW64	53.15	0.343	119.73	0.58	19.20	28.38	9.43	1.42	1.66
CW65	45.63	0.427	118.72	0.66	20.42	27.51	10.33	0.95	1.50
CW66	50.45	0.222	123.33	0.72	18.35	29.77	9.35	1.80	1.33
CW67	54.45	0.067	111.24	0.64	14.11	34.10	7.89	1.73	1.44
CW68	30.11	1.034	77.59	0.33	15.21	28.84	2.73	1.60	1.10
CW69	56.79	1.214	118.47	0.59	18.84	28.60	9.24	1.56	1.32
CW70	44.82	0.776	141.01	0.80	20.42	30.49	9.61	2.09	1.33
CW71	42.85	1.779	164.83	0.77	22.65	35.43	11.79	2.97	1.72
CW72	78.48	1.218	188.29	1.12	24.29	39.69	12.43	2.57	1.87
CW73	53.06	1.758	147.33	0.70	21.55	34.63	11.28	2.44	1.55
CW74	54.78	1.075	178.93	0.67	24.19	29.26	11.56	1.35	1.92
CW75	59.86	0.948	186.39	0.70	24.41	27.34	11.04	0.16	1.43
CW76	34.65	0.352	62.39	0.67	16.94	35.36	7.19	1.05	0.95
CW77	58.20	1.011	68.43	0.73	23.55	32.74	9.37	1.32	1.20
CW78	61.76	0.622	84.27	0.67	11.50	33.51	8.35	0.55	1.28
CW79	60.17	1.876	175.27	0.68	23.70	29.15	10.99	0.97	1.56
CW80	38.80	1.441	106.80	0.73	16.61	29.34	8.61	1.01	1.15
CW81	48.42	0.441	87.85	0.61	14.69	33.00	8.64	0.60	1.12
CW82	38.15	0.805	127.87	0.54	17.80	28.65	8.69	0.72	1.63
CW83	40.77	1.394	127.78	0.51	20.53	24.73	10.47	0.61	1.42
CW84	42.77	0.822	171.25	0.65	20.84	30.39	10.11	1.34	1.79

CW85	46.13	1.199	141.17	0.42	17.83	27.95	9.64	0.10	1.37
CW86	49.16	1.137	140.27	0.55	17.50	29.50	9.39	1.18	1.66
CW87	20.35	0.020	125.59	0.58	14.69	31.46	7.66	0.57	1.06
CW88	34.48	0.044	185.12	1.25	23.53	26.63	8.33	0.79	0.92
CW89	23.94	0.574	139.45	0.43	16.37	25.90	8.00	0.79	1.19
CW90	49.49	0.371	136.20	0.40	18.08	25.77	9.07	0.53	1.31
CW91	32.38	2.276	90.85	0.70	14.17	25.79	6.10	1.28	1.12
CW92	43.95	0.912	157.04	0.63	23.44	30.57	11.08	1.76	1.65
CW93	24.13	0.835	136.00	0.65	19.77	33.67	8.76	1.11	1.42
CW94	48.06	0.676	155.19	0.56	21.51	31.53	9.98	1.34	1.43
CW95	43.67	0.535	146.07	0.65	17.71	40.47	9.21	1.42	1.33
CW96	43.31	0.913	145.11	0.65	19.42	29.67	8.40	1.03	1.29
CW97	46.54	2.178	129.78	0.49	19.89	26.48	9.65	0.81	1.60
CW98	44.36	0.179	171.51	0.68	22.94	35.74	11.37	1.23	2.07
CW99	33.80	1.316	203.14	0.76	24.97	29.09	7.73	1.70	1.55
CW100	44.85	0.659	159.11	0.82	19.98	26.76	8.66	1.40	1.24
CW101	36.94	0.983	208.58	1.15	27.30	21.18	10.08	1.43	1.46
CW102	36.57	0.928	167.12	0.84	21.80	24.54	9.67	1.28	1.46
CW103	53.55	0.720	167.32	0.78	21.48	27.81	9.64	1.37	1.44
CW104	38.08	2.147	160.11	0.69	20.39	24.84	9.38	1.46	1.35
CW105	44.69	1.929	198.86	1.00	26.34	24.24	10.82	1.39	1.59
CW106	48.17	1.133	173.16	0.93	20.93	24.02	8.79	1.38	1.27
CW107	48.57	0.556	189.33	0.90	21.14	27.77	10.01	1.34	1.44
CW108	54.10	0.660	237.91	1.38	30.60	28.49	12.48	1.61	1.35
CW109	35.84	1.119	151.77	0.62	19.09	24.79	9.28	1.44	1.32
CW110	38.37	0.747	202.21	0.89	23.21	24.25	9.28	1.29	1.33
CW111	32.83	0.407	181.32	1.05	22.77	26.43	9.05	1.35	1.06
CW112	35.10	0.403	177.20	0.93	22.48	25.42	9.23	1.33	1.26
CW113	74.17	1.028	206.94	1.11	27.22	30.89	11.27	1.41	1.30
CW114	41.14	0.300	177.42	0.93	19.93	27.86	7.69	1.21	1.09
CW115	45.15	0.260	185.02	0.89	20.48	29.69	9.16	1.32	1.30
CW116	39.72	0.838	193.20	0.99	22.89	28.25	10.30	1.30	1.42
CW117	42.81	1.049	186.01	0.99	21.47	27.91	11.09	1.47	1.48
CW118	32.07	0.328	168.08	0.65	16.56	27.98	7.99	1.34	1.10
CW119	33.89	0.400	165.36	0.76	17.64	29.29	8.36	1.31	0.94
CW120	44.20	1.009	209.54	1.04	24.92	21.98	10.47	1.31	1.39
CW121	42.29	0.896	195.31	1.10	21.38	23.49	9.69	1.35	1.32
CW122	32.08	0.323	176.25	1.09	23.79	24.63	10.45	1.28	1.22
CW123	18.83	0.568	148.77	0.89	21.78	22.63	10.37	1.26	1.46
CW124	31.39	1.001	167.96	0.73	21.18	22.80	9.64	1.32	1.05
CW125	54.02	0.345	174.26	0.90	20.99	25.48	9.59	0.13	1.14
CW126	39.97	0.372	121.83	0.74	19.91	23.40	10.75	1.38	1.57
CW127	26.81	1.489	96.96	1.11	18.15	21.36	7.13	1.21	0.82

CW128	36.18	0.525	196.32	0.95	16.09	27.72	9.82	1.42	1.30
CW129	35.62	0.179	132.13	0.83	14.49	27.85	9.90	0.14	1.03
CW130	45.75	0.073	194.46	1.92	21.85	23.65	10.77	1.51	0.94

ANID	Th	Ti	Yb	Zn	Zr
CW01	13.28	5024	3.37	219.4	159.9
CW02	14.40	5846	4.32	225.1	0.0
CW03	13.96	4981	3.80	198.8	0.0
CW04	13.80	6009	4.06	226.0	280.7
CW05	15.92	4749	3.71	275.9	0.0
CW06	12.60	5445	3.61	184.5	0.0
CW07	10.75	4329	2.70	188.1	225.5
CW08	13.58	5484	3.68	171.4	203.7
CW09	13.06	5350	2.94	220.9	0.0
CW10	14.58	5444	3.83	258.7	163.5
CW11	14.63	7063	4.08	203.4	188.5
CW12	16.27	5389	4.63	304.1	0.0
CW13	15.19	5852	4.12	198.7	228.9
CW14	14.58	5837	3.62	188.6	0.0
CW15	12.63	5622	3.35	180.6	0.0
CW16	15.15	5165	4.03	218.9	149.5
CW17	16.45	5176	4.23	245.5	0.0
CW18	15.83	5218	3.90	160.2	0.0
CW19	14.58	6041	3.74	203.0	0.0
CW20	13.96	5417	3.85	228.9	273.1
CW21	13.69	5178	3.92	228.6	212.3
CW22	13.53	5124	3.89	187.4	210.3
CW23	15.44	4698	3.46	209.0	253.0
CW24	14.22	4964	4.01	209.4	143.1
CW25	13.99	4256	3.00	174.5	186.4
CW26	14.63	5341	3.89	242.7	235.0
CW27	15.17	5566	4.22	224.5	189.6
CW28	15.42	5142	3.63	242.4	89.0
CW29	15.62	5424	3.88	308.3	170.1
CW30	15.24	5316	4.11	230.2	179.7
CW31	15.94	5296	4.01	261.2	127.3
CW32	13.25	6225	4.09	186.2	227.1
CW33	14.19	4814	3.77	206.5	217.8
CW34	16.90	5201	4.37	246.2	257.3
CW35	13.04	5728	3.62	250.0	0.0
CW36	14.20	5763	3.96	203.4	188.3
CW37	15.44	5805	4.39	251.3	302.4
CW38	16.21	5589	4.60	242.8	217.0
CW39	15.81	6687	4.46	201.7	232.3
CW40	14.12	3949	3.87	194.8	240.3
CW41	14.10	4488	3.79	190.9	147.3

CW42	13.97	4802	3.23	152.7	0.0
CW43	4.50	1397	3.15	541.8	0.0
CW44	16.81	5980	4.16	185.8	218.2
CW45	14.39	5147	3.68	136.5	316.1
CW46	14.45	5435	3.76	55.8	0.0
CW47	14.54	5520	4.43	161.8	197.9
CW48	16.87	5517	3.93	213.6	199.8
CW49	15.20	5665	3.50	197.6	117.7
CW50	13.82	5426	2.31	212.3	165.6
CW51	14.88	5345	4.24	142.1	315.6
CW52	19.74	7282	4.51	231.5	236.3
CW53	17.21	6543	3.56	190.5	148.4
CW54	17.69	6395	4.49	250.4	189.8
CW55	16.25	5931	4.17	228.7	269.9
CW56	6.31	2589	1.53	96.5	111.2
CW57	18.52	6872	4.67	212.3	180.4
CW58	18.52	6225	4.38	204.0	330.3
CW59	14.98	4882	4.42	215.2	232.6
CW60	13.85	4421	4.20	184.4	157.4
CW61	11.58	4090	3.17	176.3	142.0
CW62	12.17	4450	3.19	198.4	171.5
CW63	13.81	8132	3.63	226.9	145.8
CW64	14.56	6798	3.69	151.0	123.7
CW65	15.51	6879	4.42	165.7	202.6
CW66	14.32	5964	3.96	183.9	241.8
CW67	11.92	8328	3.66	151.1	174.9
CW68	13.68	6479	2.47	131.1	278.4
CW69	14.25	6502	3.74	210.7	192.3
CW70	15.49	5877	4.02	208.9	202.7
CW71	17.41	7751	5.07	250.2	258.2
CW72	18.92	9152	4.73	234.4	223.9
CW73	16.18	7966	4.86	219.7	328.3
CW74	17.42	6658	4.69	200.1	246.9
CW75	16.61	5748	4.56	268.4	137.7
CW76	15.46	5853	3.74	218.4	320.2
CW77	16.46	6833	3.95	224.7	243.4
CW78	10.47	5332	3.85	93.5	274.7
CW79	17.41	7231	4.78	207.0	215.6
CW80	13.94	5200	3.90	193.6	274.6
CW81	12.44	5960	3.80	170.4	278.8
CW82	14.81	5424	3.80	216.3	237.6
CW83	14.87	5285	4.45	167.3	190.7
CW84	15.16	6838	4.17	218.2	221.7

CW85	14.59	6303	4.10	189.0	248.9
CW86	13.99	6496	4.02	212.8	231.1
CW87	12.17	5390	3.65	129.0	298.1
CW88	16.66	7090	3.43	83.7	258.3
CW89	12.54	4556	3.75	183.1	226.0
CW90	13.43	4792	1.76	237.9	190.3
CW91	13.19	4776	2.82	175.6	197.2
CW92	17.00	6055	4.46	297.7	187.4
CW93	15.53	6031	3.85	191.2	224.5
CW94	15.74	6820	4.57	237.0	165.8
CW95	14.88	7502	3.94	179.1	269.7
CW96	15.34	5821	3.68	180.0	114.8
CW97	14.91	6129	4.35	182.4	200.3
CW98	16.86	7294	4.73	245.0	271.7
CW99	22.28	5081	3.76	259.1	409.5
CW100	16.37	5986	4.01	164.4	181.6
CW101	18.84	5464	4.37	198.8	215.2
CW102	16.12	5435	4.20	195.1	211.3
CW103	16.28	6099	4.37	192.4	235.5
CW104	16.05	6053	4.39	222.8	271.0
CW105	18.53	6550	4.53	257.3	269.4
CW106	16.64	5620	4.37	195.1	210.2
CW107	15.74	6092	4.76	239.1	202.1
CW108	20.95	7692	5.12	184.4	212.2
CW109	15.21	5681	4.45	176.6	224.4
CW110	16.24	5071	3.91	193.0	124.6
CW111	16.77	5919	3.98	157.3	263.8
CW112	16.81	5798	4.22	158.2	167.3
CW113	19.27	6852	5.18	242.2	222.2
CW114	14.57	5329	3.35	173.0	168.5
CW115	15.15	5939	4.35	194.0	192.9
CW116	17.13	5798	4.56	224.1	251.8
CW117	16.70	6380	5.11	199.0	234.9
CW118	13.58	5996	3.69	128.7	214.5
CW119	13.99	6527	4.04	143.1	251.0
CW120	17.39	5330	4.64	274.8	254.4
CW121	16.00	5568	4.51	189.6	250.7
CW122	17.80	4984	4.65	223.1	199.1
CW123	16.34	4883	4.64	85.0	251.8
CW124	15.83	5045	4.74	246.5	222.7
CW125	15.54	5628	4.24	183.3	228.4
CW126	15.89	5051	4.74	167.1	270.4
CW127	15.31	4143	3.54	150.2	194.7

CW128	14.58	5880	4.17	119.4	323.1
CW129	13.43	5630	2.90	113.5	347.2
CW130	16.52	5600	4.39	113.3	275.8

Appendix II: Elemental data for southern Missouri ochre sources in this study.
The first section is INAA data only, the second XRF data only.
Values are presented as ppm unless noted with percent (%).

ANID	Site ID	Site Location	Munsell
JDR099	A-I-1	Meramac Park, Phelps County, Missouri	2.5YR 6/4
JDR100	A-I-2	Meramac Park, Phelps County, Missouri	2.5YR 6/6
JDR101	A-I-3	Meramac Park, Phelps County, Missouri	7.5YR 6/4
JDR102	A-I-4	Meramac Park, Phelps County, Missouri	2.5YR 5/4
JDR103	A-II-1	Meramac Park, Phelps County, Missouri	7.5YR 8/4
JDR104	A-II-2	Meramac Park, Phelps County, Missouri	10YR 8/6
JDR105	A-II-3	Meramac Park, Phelps County, Missouri	10YR 7/8
JDR106	A-II-4	Meramac Park, Phelps County, Missouri	10YR 8/4
JDR107	A-II-5	Meramac Park, Phelps County, Missouri	10 YR 8/6
JDR108	A-III-1	Meramac Park, Phelps County, Missouri	5YR 5/6
JDR109	A-III-2	Meramac Park, Phelps County, Missouri	5YR 5/6
JDR110	A-III-4	Meramac Park, Phelps County, Missouri	2.5YR 3/6
JDR112	A-IV-1	Meramac Park, Phelps County, Missouri	7.5YR ¾
JDR113	A-IV-2	Meramac Park, Phelps County, Missouri	5YR 4/4
JDR114	A-IV-3	Meramac Park, Phelps County, Missouri	7R 3/2
JDR115	A-IV-4	Meramac Park, Phelps County, Missouri	
JDR116	A-IV-5	Meramac Park, Phelps County, Missouri	5YR 6/4
JDR117	A-V-1	Meramac Park, Phelps County, Missouri	10R 5/6
JDR118	A-V-2	Meramac Park, Phelps County, Missouri	5YR 5/4
JDR119	A-V-3	Meramac Park, Phelps County, Missouri	2.5YR 3/6
JDR121	A-V-5	Meramac Park, Phelps County, Missouri	2.5YR 4/4
JDR122	B-I-1	Doug Wood Property, Wayne County, MO	5YR 6/4
JDR123	B-I-2	Doug Wood Property, Wayne County, MO	5YR 6/4
JDR124	B-I-3	Doug Wood Property, Wayne County, MO	7.5YR 8/4
JDR125	B-I-4	Doug Wood Property, Wayne County, MO	2.5YR 6/4
JDR126	B-I-5	Doug Wood Property, Wayne County, MO	5YR 6/4
JDR127	B-II-1	Doug Wood Property, Wayne County, MO	5YR 5/8
JDR128	B-II-2	Doug Wood Property, Wayne County, MO	10YR 7/6
JDR129	B-II-3	Doug Wood Property, Wayne County, MO	10YR 7/6
JDR130	B-II-4	Doug Wood Property, Wayne County, MO	10R 7/8
JDR131	B-II-5	Doug Wood Property, Wayne County, MO	10 YR 6/6
JDR132	B-III-1	Doug Wood Property, Wayne County, MO	7YR 7/6
JDR133	B-III-2	Doug Wood Property, Wayne County, MO	10YR 7/6
JDR134	B-III-3	Doug Wood Property, Wayne County, MO	7.5Y 8/6
JDR135	B-III-4	Doug Wood Property, Wayne County, MO	7YR 8/6
JDR136	B-III-5	Doug Wood Property, Wayne County, MO	7.5 YR 7/6
JDR137	C-I-1	Site 741, Wayne County, MO	7.5YR 5/6
JDR140	C-I-4	Site 741, Wayne County, MO	5YR 5/8
JDR142	C-I-6	Site 741, Wayne County, MO	10YR 7/6
JDR144	C-I-8	Site 741, Wayne County, MO	10YR 8/4
JDR145	C-I-9	Site 741, Wayne County, MO	10YR 7/6
JDR147	C-II-1	Site 741, Wayne County, MO	7.5YR 5/6

JDR148	C-II-2	Site 741, Wayne County, MO	
JDR149	C-II-3	Site 741, Wayne County, MO	5YR 5/8
JDR150	C-II-4	Site 741, Wayne County, MO	5YR 4/6
JDR151	C-II-5	Site 741, Wayne County, MO	5YR 5/8
JDR162	D-I-2	Site 810, Wayne County, MO	5YR 6/6
JDR162B			5YR 6/6
JDR163	D-I-4	Site 810, Wayne County, MO	5YR 6/6
JDR164	D-I-5	Site 810, Wayne County, MO	5YR 6/6
JDR165	E-I-1	Big Spring, Carter County, MO	7.5 YR 6/6
JDR166	E-I-2	Big Spring, Carter County, MO	7.5 YR 6/6
JDR167	E-I-3	Big Spring, Carter County, MO	7.5 YR 6/6
JDR168	E-I-4	Big Spring, Carter County, MO	7.5 YR 6/6
JDR169	E-I-5	Big Spring, Carter County, MO	7.5 YR 6/6
JDR170	E-II-1	Big Spring, Carter County, MO	7.5YR 7/6
JDR171	E-II-2	Big Spring, Carter County, MO	7.5YR 7/7
JDR172	E-II-3	Big Spring, Carter County, MO	7.5YR 7/8
JDR173	E-II-4	Big Spring, Carter County, MO	7.5YR 7/9
JDR174	E-II-5	Big Spring, Carter County, MO	7.5YR 7/10
JDR175	E-III-1	Big Spring, Carter County, MO	7.5 YR 6/6
JDR176	E-III-2	Big Spring, Carter County, MO	7.5 YR 6/6
JDR177	E-III-3	Big Spring, Carter County, MO	7.5 YR 6/6
JDR178	E-III-4	Big Spring, Carter County, MO	7.5 YR 6/6
JDR179	E-III-5	Big Spring, Carter County, MO	7.5 YR 6/6
JDR180	E-IV-1	Big Spring, Carter County, MO	7.5 YR 6/6
JDR181	E-IV-2	Big Spring, Carter County, MO	7.5 YR 6/6
JDR182	E-IV-3	Big Spring, Carter County, MO	7.5 YR 6/6
JDR183	E-IV-4	Big Spring, Carter County, MO	7.5 YR 6/6
JDR184	E-IV-5	Big Spring, Carter County, MO	7.5 YR 6/6

Missouri NAA data

anid	Al (%)	As	Ba	Ca (%)	Ce	Co	Cr	Cs
JDR099	0.58	9	0.0	0.000	1.3	0.4	21.6	0.0
JDR100	0.90	13	148.5	0.000	0.9	0.6	34.5	0.0
JDR101	0.81	57	0.0	0.000	3.4	7.6	12.2	0.0
JDR102	1.49	22	45.2	0.000	5.6	1.2	16.3	0.0
JDR103	1.06	242	0.0	0.000	2.8	34.1	246.6	0.3
JDR104	0.95	1177	36.2	0.000	5.2	32.6	143.7	0.3
JDR105	4.74	1272	55.8	0.000	6.0	34.9	478.0	0.4
JDR106	0.64	99	0.0	0.000	0.9	8.8	71.1	0.2
JDR107	0.87	418	55.5	0.000	3.4	11.8	87.6	0.3
JDR108	1.05	458	116.6	0.076	1.6	54.3	46.5	0.0
JDR109	1.02	385	0.0	0.000	11.8	107.6	290.7	0.0
JDR110	2.34	1704	55.2	0.000	24.3	354.7	283.0	0.4
JDR112	1.01	119	0.0	0.000	19.1	91.4	329.8	0.0
JDR113	0.74	233	0.0	0.000	17.7	142.2	148.0	0.0
JDR114	0.75	131	18.7	0.000	17.6	11.5	152.9	0.3
JDR116	0.79	339	0.0	0.000	2.8	5.9	26.4	0.0
JDR117	0.80	17	0.0	0.000	2.0	1.0	31.1	0.0
JDR118	0.74	331	0.0	0.000	27.3	56.1	72.3	0.0
JDR119	0.71	166	0.0	0.000	7.1	9.7	351.4	0.0
JDR121	0.84	285	0.0	0.000	12.3	17.7	33.8	0.0
JDR122	5.71	12	473.2	0.344	75.9	15.6	64.8	3.1
JDR123	6.81	12	608.8	0.315	80.9	16.4	67.1	3.4
JDR124	1.75	3	0.0	0.000	11.7	1.3	9.6	0.6
JDR125	6.05	9	512.2	0.371	82.0	12.7	68.4	3.5
JDR126	6.19	12	537.9	0.338	81.0	12.9	68.5	3.4
JDR127	3.03	9198	0.0	0.000	16.8	45.4	31.5	0.0
JDR128	2.24	2079	0.0	0.000	25.6	62.1	38.2	0.0
JDR129	0.92	1218	0.0	0.000	21.7	13.6	18.9	0.0
JDR130	1.94	1128	0.0	0.000	12.5	3.0	43.8	0.6
JDR131	1.96	157	0.0	0.000	21.7	64.8	91.8	0.5
JDR132	2.20	6	12.0	0.000	10.9	1.0	23.0	0.9
JDR133	2.39	7	151.6	0.000	169.0	3.1	16.6	0.9
JDR134	1.89	6	0.0	0.000	10.3	0.8	15.3	0.8
JDR135	2.11	4	46.3	0.000	11.0	0.8	12.8	0.8
JDR136	1.92	6	0.0	0.000	15.7	1.5	17.1	0.9
JDR137	2.78	232	0.0	0.000	24.5	10.6	12.1	0.8
JDR140	1.42	4208	0.0	0.000	16.5	2.0	77.4	0.7
JDR142	2.18	57	34.2	0.000	24.1	4.2	6.5	0.3
JDR144	0.95	105	0.0	0.000	4.0	4.8	11.0	0.0
JDR145	0.87	106	0.0	0.000	3.5	6.0	14.2	0.0

JDR147	2.44	6542	0.0	0.000	20.4	18.0	40.7	0.0
JDR148	2.19	3024	0.0	0.000	17.3	21.3	27.5	0.3
JDR150	2.52	2037	51.6	0.000	28.3	4.9	55.2	0.0
JDR151	2.09	3701	0.0	0.000	18.1	16.9	54.0	0.0
JDR162	2.12	11	0.0	0.000	10.8	0.4	23.1	0.6
JDR162B	1.88	9	0.0	0.000	7.2	0.3	18.6	0.4
JDR163	2.44	21	0.0	0.000	9.0	0.5	21.3	0.5
JDR164	2.57	14	0.0	0.000	13.9	0.5	19.7	0.6
JDR165	10.57	57	283.9	0.079	287.6	111.5	86.5	8.0
JDR166	10.75	50	282.7	0.113	335.2	118.3	100.5	8.4
JDR167	10.56	57	156.1	0.144	314.5	92.9	94.1	8.1
JDR168	10.22	56	241.4	0.237	247.3	87.3	82.6	7.9
JDR169	9.83	51	304.3	0.158	283.9	79.2	87.5	7.7
JDR170	9.18	53	220.9	0.098	78.8	11.1	72.4	6.6
JDR171	9.08	51	262.4	0.000	85.3	11.4	72.7	6.9
JDR172	10.27	54	217.0	0.052	81.6	11.6	79.1	7.5
JDR173	9.63	52	238.9	0.000	81.5	11.6	76.1	7.0
JDR174	10.49	58	215.6	0.084	91.0	12.2	79.1	7.7
JDR175	10.38	38	211.7	0.128	38.6	7.2	83.4	8.4
JDR176	10.00	38	157.5	0.090	40.3	7.3	82.1	8.4
JDR177	9.87	39	160.8	0.056	38.8	7.1	80.3	8.2
JDR178	9.57	40	164.7	0.095	38.5	7.3	81.1	8.1
JDR179	10.37	39	146.9	0.056	37.2	7.3	80.8	8.2
JDR180	11.36	45	224.6	0.101	43.9	9.2	83.2	8.9
JDR181	12.20	44	169.8	0.136	47.3	8.8	82.8	9.5
JDR182	11.82	45	145.9	0.000	47.5	8.6	83.7	9.2
JDR183	12.03	47	181.0	0.000	46.2	8.9	82.0	9.3
JDR184	11.76	44	174.2	0.043	47.2	9.0	82.5	9.1

anid	Dy	Eu	Fe(%)	Hf	K (%)	La	Lu	Mn
JDR099	0.000	0.030	1.43	0.135	0.00	0.52	0.000	2
JDR100	0.000	0.024	1.48	0.149	0.00	0.45	0.024	3
JDR101	0.000	0.054	2.12	0.642	0.00	1.45	0.022	10
JDR102	0.268	0.130	4.39	0.726	0.00	2.55	0.024	5
JDR103	0.386	0.050	4.43	1.213	0.15	1.16	0.123	14
JDR104	0.582	0.077	9.86	2.253	0.18	1.93	0.135	57
JDR105	1.305	0.115	13.59	5.002	0.44	2.25	0.163	54
JDR106	0.000	0.000	2.18	0.603	0.06	0.31	0.073	6
JDR107	0.071	0.069	4.83	1.662	0.19	1.34	0.031	16
JDR108	0.529	0.098	10.43	0.268	0.00	0.55	0.050	25
JDR109	1.137	0.272	51.19	0.559	0.00	4.40	0.034	116
JDR110	3.153	0.824	53.77	0.534	0.00	9.88	0.235	329
JDR112	1.908	0.427	60.03	0.718	0.00	10.84	0.187	45
JDR113	1.916	0.515	60.34	0.397	0.00	10.66	0.111	94
JDR114	0.531	0.178	63.18	0.331	0.00	8.02	0.000	28
JDR116	0.285	0.064	24.38	0.648	0.05	1.39	0.031	6
JDR117	0.136	0.038	7.23	0.664	0.00	0.83	0.000	13
JDR118	0.930	0.379	44.95	0.239	0.00	11.92	0.000	219
JDR119	0.436	0.093	60.93	0.932	0.00	2.48	0.000	18
JDR121	0.363	0.161	28.69	0.170	0.00	5.00	0.000	89
JDR122	4.887	1.068	2.75	12.924	1.80	33.09	0.479	1000
JDR123	4.504	1.145	2.87	13.981	1.66	35.05	0.500	917
JDR124	0.362	0.101	0.51	1.721	0.19	13.27	0.079	44
JDR125	4.917	1.145	2.81	13.880	1.97	34.95	0.493	843
JDR126	4.962	1.154	2.82	13.730	1.63	34.38	0.488	849
JDR127	3.834	0.940	45.09	0.624	0.00	7.81	0.151	187
JDR128	4.416	0.700	28.16	2.151	0.12	15.97	0.524	139
JDR129	2.378	0.650	25.75	1.345	0.08	13.78	0.291	79
JDR130	1.545	0.462	16.42	2.220	0.32	7.39	0.225	129
JDR131	5.070	1.504	44.86	0.844	0.29	20.52	0.717	1622
JDR132	0.369	0.111	1.06	1.506	0.23	9.95	0.066	46
JDR133	0.435	0.167	1.27	1.351	0.00	13.11	0.041	880
JDR134	0.509	0.116	0.99	1.329	0.13	9.97	0.055	30
JDR135	0.499	0.105	0.80	1.364	0.13	11.69	0.087	45
JDR136	0.422	0.168	1.12	2.483	0.09	21.86	0.042	42
JDR137	1.064	0.355	20.66	1.616	0.22	14.43	0.112	99
JDR140	0.921	0.241	28.97	2.805	0.39	10.90	0.048	21
JDR142	0.387	0.098	4.45	0.757	0.20	4.67	0.085	46
JDR144	0.000	0.124	8.55	0.000	0.00	1.16	0.101	47
JDR145	0.530	0.170	10.59	0.125	0.00	1.04	0.117	59
JDR147	2.608	0.629	36.87	1.377	0.18	8.43	0.080	46

JDR148	2.171	0.547	31.08	1.253	0.04	6.97	0.096	57
JDR150	2.383	0.551	38.88	3.440	0.11	9.12	0.288	47
JDR151	1.897	0.515	35.33	1.084	0.09	6.84	0.083	46
JDR162	0.000	0.080	1.42	1.731	0.00	7.31	0.054	17
JDR162B	0.000	0.055	1.05	1.416	0.00	5.29	0.017	15
JDR163	0.614	0.089	1.38	2.063	0.00	5.79	0.028	24
JDR164	0.622	0.105	1.30	1.848	0.00	9.57	0.022	23
JDR165	33.713	12.775	5.19	4.832	1.13	410.07	1.842	988
JDR166	44.873	18.310	5.40	5.304	1.31	583.17	2.374	1025
JDR167	38.524	14.824	5.28	5.023	1.21	479.88	2.111	852
JDR168	17.469	6.322	5.26	5.618	0.92	204.17	1.011	699
JDR169	25.448	9.818	5.10	5.579	1.01	325.67	1.408	655
JDR170	3.108	0.644	4.67	6.091	1.04	22.90	0.413	168
JDR171	2.700	0.619	4.76	5.533	0.97	23.22	0.342	176
JDR172	2.609	0.654	5.08	5.407	0.90	23.85	0.381	179
JDR173	2.780	0.646	4.87	5.231	1.08	23.94	0.342	173
JDR174	2.868	0.652	5.31	4.837	1.16	23.78	0.387	187
JDR175	2.739	0.531	5.20	7.486	0.83	25.52	0.247	156
JDR176	2.519	0.500	5.09	7.640	0.84	26.66	0.330	159
JDR177	2.523	0.497	4.98	7.628	0.86	25.63	0.362	156
JDR178	2.536	0.489	5.01	7.724	0.73	24.85	0.326	161
JDR179	2.459	0.499	5.15	7.338	0.75	24.71	0.335	149
JDR180	2.468	0.482	5.66	5.845	0.96	26.69	0.336	201
JDR181	2.486	0.511	5.88	5.597	1.10	27.87	0.273	208
JDR182	2.300	0.485	5.92	5.212	1.20	27.30	0.297	203
JDR183	2.526	0.481	5.85	5.551	0.90	27.52	0.254	207
JDR184	2.101	0.476	5.88	5.312	0.91	26.80	0.279	208

anid	Na	Nd	Ni	Rb	Sb	Sc	Sm	Sr
JDR099	0.031	3.04	0.0	0.00	4.95	0.12	0.256	0.0
JDR100	0.032	0.00	0.0	0.00	0.78	0.11	0.146	0.0
JDR101	0.024	2.18	0.0	0.00	2.30	0.34	0.382	0.0
JDR102	0.027	5.73	0.0	0.00	1.48	0.29	0.933	0.0
JDR103	0.034	0.00	39.2	0.00	5.92	1.31	0.657	0.0
JDR104	0.036	4.04	0.0	11.77	12.84	1.56	0.876	0.0
JDR105	0.027	4.21	0.0	20.29	1.57	3.14	1.168	0.0
JDR106	0.034	0.00	0.0	0.00	4.77	0.56	0.189	0.0
JDR107	0.032	0.00	0.0	9.07	5.07	1.24	0.665	0.0
JDR108	0.027	0.00	0.0	0.00	4.45	0.84	0.594	0.0
JDR109	0.025	13.11	699.3	0.00	5.20	3.99	2.073	0.0
JDR110	0.021	18.31	521.0	0.00	27.10	10.30	4.163	0.0
JDR112	0.025	11.25	252.3	0.00	5.91	11.70	2.878	0.0
JDR113	0.027	14.95	421.2	0.00	9.12	12.47	2.896	0.0
JDR114	0.027	5.58	0.0	0.00	5.41	1.00	1.303	0.0
JDR116	0.032	0.00	0.0	0.00	2.45	1.05	0.488	0.0
JDR117	0.026	0.00	0.0	0.00	1.13	0.73	0.371	0.0
JDR118	0.029	11.58	475.1	0.00	3.77	0.99	2.549	0.0
JDR119	0.024	0.00	143.5	0.00	9.06	0.76	1.752	0.0
JDR121	0.026	14.22	122.4	0.00	2.50	0.65	1.229	0.0
JDR122	0.526	28.13	0.0	80.30	0.79	8.63	5.794	0.0
JDR123	0.543	53.80	0.0	83.70	0.91	9.21	6.244	118.3
JDR124	0.027	4.76	0.0	6.56	0.15	1.92	0.645	0.0
JDR125	0.571	34.21	0.0	82.79	0.84	9.09	6.269	119.3
JDR126	0.579	32.03	0.0	79.08	0.91	9.00	6.149	88.2
JDR127	0.023	15.44	110.4	0.00	8.34	3.24	4.295	0.0
JDR128	0.029	10.67	202.2	0.00	2.33	7.75	3.574	0.0
JDR129	0.027	11.28	0.0	0.00	1.13	3.73	3.255	0.0
JDR130	0.027	11.11	0.0	11.03	0.32	9.97	2.920	0.0
JDR131	0.027	33.91	220.3	0.00	1.64	37.65	8.092	0.0
JDR132	0.024	5.18	0.0	10.53	0.19	1.80	0.711	0.0
JDR133	0.028	6.83	0.0	10.00	0.38	2.26	1.012	0.0
JDR134	0.027	6.27	0.0	7.05	0.22	1.73	0.765	0.0
JDR135	0.027	5.33	0.0	9.54	0.17	1.61	0.725	0.0
JDR136	0.029	10.19	0.0	10.64	0.26	2.15	1.054	0.0
JDR137	0.032	12.40	0.0	20.64	0.86	7.08	2.085	0.0
JDR140	0.033	8.46	0.0	0.00	7.53	6.01	1.552	0.0
JDR142	0.035	4.05	0.0	10.13	0.34	3.98	0.782	0.0
JDR144	0.033	3.15	0.0	0.00	0.60	9.94	0.903	0.0
JDR145	0.037	5.94	0.0	0.00	0.63	11.53	1.094	0.0
JDR147	0.033	11.75	0.0	0.00	2.85	6.60	3.293	0.0

JDR148	0.035	8.04	0.0	0.00	2.54	5.58	2.773	0.0
JDR150	0.036	10.05	0.0	0.00	4.77	6.32	3.048	0.0
JDR151	0.036	0.00	0.0	0.00	2.79	6.04	2.648	0.0
JDR162	0.032	3.24	0.0	5.15	0.35	3.03	0.529	0.0
JDR162B	0.033	1.98	0.0	3.58	0.29	2.30	0.390	0.0
JDR163	0.035	0.00	0.0	6.05	0.33	3.09	0.460	0.0
JDR164	0.034	5.23	0.0	8.47	0.33	3.63	0.674	0.0
JDR165	0.061	367.10	204.2	101.25	2.41	14.06	64.593	0.0
JDR166	0.075	595.28	281.5	100.34	2.54	15.53	91.695	0.0
JDR167	0.065	477.44	289.6	96.76	2.56	14.22	74.677	0.0
JDR168	0.068	190.37	153.0	91.52	2.47	13.65	32.182	0.0
JDR169	0.076	290.97	199.2	93.81	2.47	13.24	49.883	0.0
JDR170	0.068	17.22	59.5	87.71	2.38	12.47	3.562	0.0
JDR171	0.065	16.89	0.0	85.06	2.38	12.86	3.615	0.0
JDR172	0.065	18.78	0.0	92.92	2.28	13.44	3.579	0.0
JDR173	0.066	17.77	77.8	87.46	2.24	13.09	3.547	0.0
JDR174	0.064	18.41	0.0	90.14	2.24	14.17	3.676	0.0
JDR175	0.059	14.85	0.0	90.39	1.89	10.56	2.819	0.0
JDR176	0.062	13.85	0.0	84.61	1.86	10.38	2.946	0.0
JDR177	0.061	13.34	71.2	80.27	1.75	10.24	2.814	0.0
JDR178	0.058	14.86	0.0	80.81	1.79	10.07	2.833	0.0
JDR179	0.057	15.04	0.0	73.19	1.90	10.19	2.699	0.0
JDR180	0.075	17.71	0.0	92.19	1.90	13.02	2.813	0.0
JDR181	0.065	15.19	0.0	98.68	1.88	14.13	2.909	0.0
JDR182	0.066	17.61	49.5	85.84	1.99	14.14	2.801	0.0
JDR183	0.059	16.07	0.0	96.82	2.09	13.75	2.674	0.0
JDR184	0.062	17.05	94.6	93.29	1.94	13.81	2.776	0.0

anid	Ta	Tb	Th	Ti	U	V	Yb	Zn	Zr
JDR099	0.000	0.000	0.16	0	1.39	18.2	0.00	3.5	0.0
JDR100	0.000	0.000	0.56	276	0.79	14.6	0.00	8.9	0.0
JDR101	0.029	0.000	0.45	249	1.57	53.3	0.18	8.2	0.0
JDR102	0.000	0.091	0.63	0	2.71	18.9	0.22	0.0	0.0
JDR103	0.160	0.000	2.16	916	5.78	144.7	0.44	8.9	84.0
JDR104	0.342	0.000	2.92	1809	6.82	107.4	0.40	14.0	91.0
JDR105	0.382	0.000	5.59	1948	8.68	434.8	1.09	13.1	146.7
JDR106	0.035	0.000	0.56	83	1.56	48.4	0.00	4.3	0.0
JDR107	0.272	0.000	2.12	1408	5.58	72.4	0.21	7.3	76.4
JDR108	0.000	0.000	0.80	255	2.48	47.2	0.48	0.0	0.0
JDR109	0.000	0.000	0.73	0	9.71	781.8	0.28	263.8	0.0
JDR110	0.000	0.516	2.40	0	6.82	1217.5	1.55	50.6	0.0
JDR112	0.000	0.000	2.72	671	11.97	799.1	0.78	137.9	0.0
JDR113	0.000	0.000	1.23	0	11.36	797.1	0.84	213.4	93.1
JDR114	0.108	0.000	1.36	472	4.10	129.7	0.00	0.0	0.0
JDR116	0.127	0.000	0.90	734	2.01	81.4	0.22	12.5	0.0
JDR117	0.000	0.037	1.69	0	2.01	75.5	0.00	7.5	0.0
JDR118	0.000	0.000	0.72	0	8.86	220.0	0.21	76.0	0.0
JDR119	0.000	0.000	2.92	734	16.77	284.2	0.00	47.7	0.0
JDR121	0.000	0.000	0.23	0	5.03	140.5	0.00	63.2	0.0
JDR122	1.023	0.748	9.97	4282	3.33	74.1	3.35	55.3	293.4
JDR123	1.153	0.678	10.71	4606	3.14	85.8	3.77	59.1	306.8
JDR124	0.110	0.065	1.73	271	1.57	12.6	0.31	8.1	47.8
JDR125	1.121	0.811	10.78	5798	4.25	100.3	3.13	53.3	309.0
JDR126	1.085	0.763	10.66	5215	3.37	92.7	3.44	54.7	328.2
JDR127	0.000	0.554	3.49	349	5.34	28.9	2.08	63.5	122.7
JDR128	0.237	0.579	4.63	2118	11.92	36.5	2.76	82.8	95.6
JDR129	0.000	0.549	2.91	524	5.90	36.5	1.55	43.3	0.0
JDR130	0.237	0.325	3.82	954	7.03	29.4	0.93	62.7	52.6
JDR131	0.000	1.140	6.62	0	16.85	104.7	3.24	433.4	154.4
JDR132	0.156	0.070	2.43	782	1.23	27.5	0.32	7.7	49.4
JDR133	0.199	0.082	3.63	0	1.18	23.8	0.37	8.1	37.4
JDR134	0.161	0.074	2.50	703	1.30	20.3	0.34	7.8	46.6
JDR135	0.150	0.093	2.27	680	1.42	24.3	0.30	7.6	28.3
JDR136	0.204	0.058	2.94	598	1.59	25.0	0.34	13.9	51.7
JDR137	0.382	0.000	4.50	1339	5.52	27.7	0.80	36.5	120.3
JDR140	0.394	0.273	4.71	2101	7.83	47.5	1.11	0.0	92.8
JDR142	0.111	0.000	2.19	1014	3.28	18.2	0.27	15.0	86.2
JDR144	0.000	0.000	1.09	265	4.21	22.2	0.31	21.2	53.5
JDR145	0.000	0.191	1.29	0	4.92	27.5	0.44	34.6	0.0
JDR147	0.161	0.309	3.97	1243	9.79	46.7	1.39	29.5	0.0

JDR148	0.302	0.320	2.76	802	6.91	25.5	1.38	37.2	0.0
JDR150	0.437	0.526	5.91	1574	10.90	75.3	1.33	0.0	177.0
JDR151	0.114	0.378	4.04	918	6.94	48.7	1.28	26.4	0.0
JDR162	0.244	0.041	4.21	757	1.13	24.8	0.18	6.8	54.5
JDR162B	0.185	0.000	3.10	655	0.77	27.0	0.19	7.4	70.7
JDR163	0.199	0.000	3.88	513	1.17	28.6	0.47	8.3	66.8
JDR164	0.231	0.000	4.80	751	1.46	30.9	0.34	5.6	54.0
JDR165	1.014	7.306	14.23	3465	5.60	168.4	16.74	96.5	300.5
JDR166	1.106	9.952	14.75	4609	4.30	190.1	21.48	103.0	377.7
JDR167	1.087	8.555	14.43	3392	3.89	166.2	18.99	98.8	377.6
JDR168	1.098	3.678	14.23	3152	6.10	176.7	9.07	81.8	264.9
JDR169	1.184	5.548	13.96	3773	4.75	159.8	12.73	83.8	240.6
JDR170	1.136	0.508	13.28	4215	6.27	138.9	1.90	64.9	199.0
JDR171	1.033	0.698	13.77	3306	6.09	137.4	1.96	70.4	153.5
JDR172	1.065	0.455	14.36	3563	6.60	148.6	1.97	79.6	133.4
JDR173	1.006	0.370	13.88	3822	6.34	150.9	2.05	78.5	124.5
JDR174	1.057	0.463	14.99	3676	6.46	146.5	1.87	75.6	126.4
JDR175	1.327	0.473	15.36	4381	4.47	148.6	1.71	73.5	203.3
JDR176	1.326	0.395	15.22	4199	4.47	141.2	2.06	72.1	175.1
JDR177	1.332	0.427	15.10	3971	4.57	122.5	1.82	67.2	186.8
JDR178	1.258	0.414	14.69	4332	4.38	147.4	1.96	67.2	161.8
JDR179	1.322	0.396	14.73	3955	4.11	143.1	2.04	73.8	138.0
JDR180	1.233	0.273	15.80	3852	4.92	148.6	1.74	86.0	178.3
JDR181	1.252	0.362	16.75	3669	4.71	149.0	1.77	88.3	159.9
JDR182	1.275	0.325	16.45	3991	5.05	149.9	1.53	88.2	103.2
JDR183	1.241	0.383	16.16	4240	4.72	161.8	1.74	83.1	111.1
JDR184	1.188	0.408	16.45	4199	4.99	133.9	1.88	92.1	134.4

Missouri XRF Data

ANID	Al [%]	Si [%]	P [%]	S [µg/g]	Cl [µg/g]	K [%]	Ca [%]	Ti [%]
JDR099	0.55	> 43.94	< 0.002	< 20	152.9	0.092	0.017	0.010
JDR101	1.04	38.93	0.059	343	122.7	0.082	0.020	0.015
JDR102	1.91	37.85	0.026	971	54.0	0.111	0.018	0.020
JDR103	0.73	41.98	0.039	< 20	36.3	0.203	0.023	0.081
JDR104	0.74	35.52	0.089	202	70.7	0.304	0.022	0.178
JDR105	6.31	26.46	0.208	315	37.7	0.481	0.041	0.256
JDR106	0.50	> 43.37	0.016	< 20	65.3	0.124	0.012	0.030
JDR107	0.62	41.44	0.034	33	60.1	0.261	0.013	0.148
JDR108	1.12	34.51	0.118	1018	56.7	0.102	0.097	0.037
JDR109	1.44	6.99	0.162	< 9.1	7.6	0.192	< 0.003	0.029
JDR110	2.80	4.72	0.230	466	28.6	0.294	0.017	0.060
JDR112	0.85	1.13	0.106	106	21.2	0.314	< 0.003	0.083
JDR113	0.95	1.57	0.157	560	16.3	0.255	< 0.003	0.036
JDR114	1.04	2.69	0.018	48	< 4.8	0.297	< 0.003	0.037
JDR115	1.94	2.43	0.200	312	8.4	0.252	< 0.003	0.049
JDR116	0.18	30.62	0.013	285	52.8	0.149	0.027	0.081
JDR117	0.81	39.75	0.027	< 20	69.9	0.101	0.006	0.015
JDR118	0.56	17.63	0.077	< 8.9	36.3	0.186	0.015	0.030
JDR119	0.88	3.76	0.027	15	24.8	0.402	< 0.004	0.090
JDR121	0.76	17.79	0.098	< 6.3	46.3	0.152	0.013	0.013
JDR122	6.25	32.48	0.055	210	32.0	1.858	0.369	0.504
JDR123	7.38	33.98	0.052	168	22.9	2.006	0.382	0.544
JDR124	3.08	40.25	0.007	< 20	43.2	0.276	0.029	0.062
JDR125	6.64	34.14	0.056	45	9.7	2.058	0.367	0.550
JDR126	6.76	33.85	0.051	18	6.3	2.003	0.375	0.543
JDR127	3.85	10.47	0.020	196	24.8	0.302	0.020	0.072
JDR128	2.07	26.10	0.030	78	35.6	0.285	0.033	0.144
JDR129	1.19	28.49	0.020	< 20	73.1	0.217	0.068	0.107
JDR130	2.95	24.05	0.029	1004	37.8	0.578	0.020	0.119
JDR131	1.48	7.88	0.065	241	38.5	0.423	0.024	0.067
JDR132	4.07	35.86	0.022	< 20	45.9	0.375	0.038	0.086
JDR133	4.11	36.75	0.018	< 20	57.7	0.253	0.021	0.095
JDR134	3.34	38.01	0.014	< 20	83.0	0.287	0.026	0.083
JDR135	3.71	37.79	0.015	< 20	69.1	0.263	0.026	0.085
JDR136	4.53	35.23	0.024	< 20	73.1	0.326	0.020	0.106
JDR137	3.21	28.00	0.022	< 20	34.6	0.377	0.005	0.188
JDR140	1.19	22.47	0.018	183	42.3	0.566	0.010	0.225
JDR142	2.50	40.66	< 0.002	47	37.6	0.245	0.023	0.089
JDR144	0.42	41.36	< 0.002	46	28.6	0.100	< 0.003	0.014
JDR145	0.41	39.24	< 0.002	92	33.2	0.097	0.009	0.013
JDR147	2.45	14.69	0.025	216	10.5	0.264	< 0.003	0.112
JDR148	2.06	11.31	0.026	248	< 6.2	0.236	< 0.003	0.061
JDR149	2.42	20.83	0.022	179	< 4.9	0.236	< 0.003	0.081
JDR150	3.19	16.72	0.036	112	42.0	0.367	< 0.004	0.188
JDR151	2.30	18.03	0.019	152	21.5	0.254	0.008	0.083
JDR162	3.95	37.44	0.018	< 20	38.5	0.134	0.018	0.087

JDR163	4.04	36.32	0.024	< 20	7.4	0.138	0.016	0.091
JDR164	4.24	37.02	0.019	< 20	43.2	0.158	0.015	0.094
JDR165	10.49	26.54	0.039	103	49.4	1.415	0.141	0.452
JDR166	10.71	26.76	0.040	75	32.6	1.410	0.151	0.486
JDR167	10.49	27.14	0.036	97	27.2	1.481	0.140	0.474
JDR168	10.46	27.98	0.039	94	23.8	1.226	0.172	0.482
JDR169	10.15	27.38	0.040	53	31.4	1.291	0.131	0.480
JDR170	9.47	29.99	0.033	69	23.5	1.157	0.077	0.455
JDR171	9.64	30.17	0.028	70	25.3	1.149	0.074	0.442
JDR172	10.28	29.07	0.028	101	31.2	1.137	0.080	0.464
JDR173	9.87	30.03	0.027	95	34.7	1.135	0.076	0.451
JDR174	10.21	28.31	0.030	78	28.9	1.175	0.082	0.444
JDR176	11.16	27.27	0.034	62	22.7	0.969	0.095	0.498
JDR177	11.21	27.19	0.034	49	11.8	0.951	0.094	0.483
JDR178	11.23	27.34	0.034	56	45.3	0.955	0.090	0.503
JDR179	10.88	27.10	0.033	42	39.9	0.928	0.088	0.482
JDR180	11.88	26.26	0.044	34	23.9	1.084	0.094	0.466
JDR181	12.32	26.04	0.044	< 20	6.7	1.087	0.094	0.470
JDR182	12.20	25.46	0.041	19	16.1	1.051	0.084	0.471
JDR183	12.19	26.20	0.043	29	16.6	1.075	0.097	0.469
JDR184	12.10	25.67	0.045	24	11.1	1.072	0.081	0.468

ANID	V [µg/g]	Cr [µg/g]	Mn [%]	Fe [%]	Ni [µg/g]	Cu [µg/g]	Zn [µg/g]
JDR099	9.20	73.2	< 0.001	1.511	3.0	93.60	8.80
JDR101	54.20	349.0	< 0.001	2.391	18.9	221.90	13.80
JDR102	17.80	62.6	< 0.001	> 4.604	6.8	34.30	7.30
JDR103	108.50	190.0	< 0.001	> 4.161	41.9	684.70	12.00
JDR104	137.60	157.0	0.004	> 9.845	50.0	> 1631	18.60
JDR105	525.00	618.0	0.005	> 13.20	73.1	> 2752	22.90
JDR106	33.80	101.0	< 0.001	2.243	27.1	329.50	10.70
JDR107	72.50	93.3	< 0.002	> 4.796	28.8	757.70	13.30
JDR108	38.60	48.0	< 0.002	> 10.38	59.5	> 1432	14.80
JDR109	> 1257	639.0	0.006	> 50.81	768.0	> 2460	296.00
JDR110	> 1917	599.0	0.029	> 53.36	645.0	> 2591	62.60
JDR112	> 1552	768.0	< 0.007	> 62.87	341.0	123.00	152.00
JDR113	> 1514	343.0	< 0.006	> 61.66	593.0	348.00	252.00
JDR114	284.00	325.0	< 0.007	> 65.99	< 32	46.00	29.60
JDR115	> 1239	740.0	< 0.006	> 58.96	562.0	272.00	257.00
JDR116	73.80	43.9	<.003	> 23.73	17.2	46.80	16.00
JDR117	67.50	135.7	< 0.002	> 7.136	11.1	206.20	12.80
JDR118	339.00	136.5	0.021	> 43.91	354.0	936.00	108.80
JDR119	597.00	820.0	< 0.007	> 61.17	196.0	31.50	60.60
JDR121	197.10	53.3	< 0.004	> 30.69	92.5	516.00	81.00
JDR122	131.50	508.0	0.101	2.818	31.6	21.10	54.60
JDR123	121.70	127.6	0.095	2.825	26.4	21.80	62.10
JDR124	< 6.9	96.6	0.005	0.582	4.5	4.70	9.00
JDR125	123.60	188.0	0.085	2.802	24.7	22.50	56.90
JDR126	127.10	104.7	0.085	2.812	26.1	20.50	54.90
JDR127	36.50	83.2	0.014	> 44.30	89.0	47.90	70.90
JDR128	69.80	82.9	0.008	> 26.93	152.9	144.70	93.10
JDR129	56.50	272.0	0.004	> 22.93	32.8	41.90	46.70
JDR130	37.00	335.0	0.015	> 17.02	8.5	153.90	67.90
JDR131	155.00	188.0	0.177	> 44.86	137.0	50.20	422.00
JDR132	24.50	325.0	0.004	1.213	6.5	8.90	9.60
JDR133	58.30	298.0	0.092	1.418	9.4	10.60	10.10
JDR134	15.60	476.0	0.004	1.207	8.6	7.60	10.30
JDR135	20.90	380.0	0.004	1.097	8.1	6.30	10.70
JDR136	34.00	504.0	0.005	1.327	12.4	7.80	13.20
JDR137	< 20	113.2	0.009	> 19.95	32.9	43.80	50.00
JDR140	63.30	106.5	< 0.004	> 29.67	17.6	36.60	23.80
JDR142	< 9.8	15.9	0.003	> 4.615	8.0	31.90	17.40
JDR144	< 9.4	< 17	0.002	> 8.653	8.2	55.30	28.80
JDR145	17.60	< 19	0.005	> 10.92	11.8	64.50	35.30
JDR147	81.40	187.0	< 0.004	> 36.70	69.8	121.20	42.20
JDR148	57.50	116.6	< 0.005	> 42.57	78.0	71.50	45.80
JDR149	< 21	80.2	< 0.004	> 30.72	68.0	93.00	45.60
JDR150	139.10	151.9	< 0.005	> 39.13	< 14	10.30	15.10
JDR151	79.80	271.0	< 0.004	> 34.40	64.5	72.00	32.20
JDR162	28.20	373.0	0.002	1.316	6.0	5.30	8.70

JDR163	< 8.4	394.0	0.002	1.654	5.7	5.90	11.70
JDR164	29.20	317.0	0.002	1.355	5.5	6.30	10.70
JDR165	265.10	128.0	0.104	> 5.275	101.8	40.30	86.10
JDR166	309.70	157.0	0.109	> 5.331	124.2	39.50	91.40
JDR167	288.20	137.0	0.091	> 5.290	100.9	41.40	90.50
JDR168	225.20	68.6	0.071	> 5.212	80.3	36.80	81.70
JDR169	243.30	122.0	0.068	> 5.088	95.8	37.50	83.30
JDR170	174.20	79.1	0.017	> 4.663	54.3	38.30	67.80
JDR171	179.70	101.3	0.018	> 4.709	48.4	37.80	69.20
JDR172	184.80	87.1	0.018	> 5.090	60.7	38.70	73.90
JDR173	186.00	82.1	0.016	> 4.851	61.9	38.30	72.00
JDR174	189.50	93.5	0.017	> 5.277	68.3	44.70	76.10
JDR176	147.60	152.0	0.016	> 5.090	39.6	31.30	71.40
JDR177	154.20	109.5	0.014	> 4.873	43.0	28.10	66.80
JDR178	163.40	100.8	0.016	> 5.078	44.1	30.10	69.60
JDR179	152.40	126.3	0.015	> 5.099	42.8	28.20	67.90
JDR180	174.30	143.0	0.018	> 5.638	54.6	36.60	81.60
JDR181	206.20	110.2	0.020	> 5.882	65.2	36.40	87.00
JDR182	182.50	101.0	0.019	> 5.970	65.8	37.00	84.30
JDR183	202.70	88.9	0.021	> 5.963	59.4	36.80	91.20
JDR184	185.80	95.8	0.021	> 5.912	59.1	38.50	84.90

ANID	Ga [µg/g]	As [µg/g]	Sr [µg/g]	Y [µg/g]	Zr [µg/g]	Ba [µg/g]	Pb [µg/g]
JDR099	2	9.5	6.6	< 0.8	< 2.2	22.3	45.8
JDR101	2.9	58.3	7	1.7	28.2	19.4	21.8
JDR102	2.3	22.5	23.1	1.2	32.5	41.7	86.3
JDR103	3.7	213.1	5.2	2.5	35.5	30.8	56.3
JDR104	2.7	> 1165	7	1.9	71.1	41.6	259
JDR105	13.5	> 1240	7.8	7.5	232.1	55.6	15.1
JDR106	2.4	97.2	4.7	< 0.8	15.1	25.4	25.6
JDR107	2.2	> 422.2	6	< 0.9	42	38.7	152.6
JDR108	5.3	> 454.7	35.6	3.7	6.6	93.5	71.5
JDR109	8.3	371.4	3	6.4	16.7	24.1	57
JDR110	9.1	> 1793	10.2	21.8	24.9	41.6	365
JDR112	< 8.0	102	17.1	9.6	32.6	14.5	286
JDR113	< 7.7	249	17.6	7.6	9.8	17.6	509
JDR114	12.5	127.1	11.6	3.9	18.6	14.3	101
JDR115	< 9.1	208	6	15.1	20.2	< 4.8	878
JDR116	2.8	270.6	5.3	2.8	33.6	26.6	147.4
JDR117	2.2	12	3.4	0.7	24.2	13.8	17.7
JDR118	6.7	311.8	27.1	4.7	13.9	36.1	49
JDR119	< 6.5	137	4	2.4	40.9	23.6	295
JDR121	< 2.9	290.7	36.4	3	13.8	33.3	9.1
JDR122	13.3	9.7	94.2	28.7	515	591.3	25.2
JDR123	14.6	9.3	99	29	547.9	658.4	25.1
JDR124	3.8	2.1	5.8	3.1	68.6	37.3	7.6
JDR125	12.8	7.9	102.7	29.7	557.4	621.5	24.1
JDR126	14.2	10.8	99.4	29	554.1	670.8	21.9
JDR127	5.1	> 8116	8.4	16.5	29.3	33.1	85.6
JDR128	5.2	> 1812	18.2	30.7	86.7	30.4	59.9
JDR129	7.1	> 1016	32.3	13	46.6	31.6	34
JDR130	7	> 1073	4.5	5	114.9	31.2	52.5
JDR131	6.7	140.8	2.3	41.8	26.6	25.5	51
JDR132	3.8	5.6	4.9	3.4	39.6	28.7	6
JDR133	5.2	7	6.1	3.7	49.7	209.9	55.2
JDR134	3.8	5.5	5.8	3	46.4	27.9	7.9
JDR135	4.6	5.2	6.4	3.4	42.4	32.3	6.9
JDR136	4.7	6.7	7.4	3.4	41.4	39.5	6.2
JDR137	9	209.5	9.4	7.1	68.7	34.6	37.4
JDR140	11.7	> 4138	23.3	5.9	122.5	49.9	79.5
JDR142	5.1	56.6	11.5	2.4	29.1	34.3	21.1
JDR144	2.7	100.5	3.4	2.3	6.6	31.1	71.5
JDR145	2.7	105.8	2.9	3	6.6	24.7	69.9
JDR147	13.3	> 6147	11	10	57	30.1	64.9
JDR148	< 4.1	> 3063	5.9	16.2	34.3	17.3	105.6
JDR149	11	> 2823	7.8	9.4	38.5	22.7	80
JDR150	6.3	> 1969	12.6	10.4	138.8	30.6	106.7
JDR151	10.3	> 3335	7.8	9.2	42.9	20.6	56.6
JDR162	4.3	9.6	5.9	1.7	51.3	27	8.6

JDR163	5.9	20.7	5.8	2.3	70.2	31.2	10.5
JDR164	5.7	11.4	6.2	3.2	63.4	27.5	9.9
JDR165	21.9	55	28.9	61.1	170.2	241.2	72.9
JDR166	23.3	51.3	29.5	71.8	188.2	275.5	73.6
JDR167	21.5	55.6	28.6	64.7	163.5	256.5	63.5
JDR168	21	52.1	30.8	39.3	196.2	245.9	65.3
JDR169	23.1	51.4	31.1	48.1	204.7	276.2	61.7
JDR170	20.2	50.5	27.2	15.5	220.6	222	45.6
JDR171	19.6	52.5	27.2	14.5	201.7	207.3	46
JDR172	21.8	52.9	26.7	14.5	190.9	206.6	46.5
JDR173	20.7	50	27.1	13.8	189.7	217.5	45.2
JDR174	22.9	56.8	24.9	12.8	167.6	204.5	51.4
JDR176	22.2	35.5	27.6	15	268.6	175.7	29.6
JDR177	20.9	37.9	27.5	14.5	266.3	167.8	28.9
JDR178	22.5	37.3	27.8	15	284.1	175.2	31.1
JDR179	21.9	38.2	35.5	14.9	255.4	161	29.8
JDR180	25.1	43.5	29.1	13	199.9	183.2	38.3
JDR181	28.2	43.7	29.6	13.8	196.3	178	39.6
JDR182	26.8	43	27.6	11.8	194.7	186.8	41.2
JDR183	25.9	46.3	29.4	13.2	196.5	184.5	40.1
JDR184	25.7	44.5	28.8	13.2	188.2	186.8	39.6

Appendix III: INAA elemental data for ochre from Jiskairumoko, Peru.
Values are presented in ppm except those marked %.

ID	*Block*	*Provenance*	*Context*	*Munsell*	*Color*
305	3	X35a/7/VIIIa	Pithouse fill	2.5 YR 3/4	Dark red-brown
306	3	Y36c/7/VIIIa	Pithouse fill	2.5 YR 5/6	Red
307	3	Y34a/oa/VII	Matrix	10R 3/6	Dark red
308	3	W34b/5/VII	Pithouse Fill	2.5 YR 4/8	Red
309	3	Y35d7/Viiia	Pithouse External Stain	2.5 YR 6/6	Light red
310	3	Y34d/oa/VII	Matrix	2.5 YR 2.5/4	Dark red-brown
311	4	GG24c/oa/IV	Outside Rectangular Structure 1	2.5 YR 3/3	Dark red-brown
312	4	FF21c/F14/VII	Hardpan-Occupation Interface	2.5 YR 2.5/3	Dark red-brown
313	4	KK24b/oa/IV	Outside Ritual Area	2.5 YR 3/3	Dark red-brown
314	4	JJ21c/F1/VII	Hardpan-Occupation Interface	2.5 YR 2.5/4	Dark red-brown
315	4	II21d/F1/VII	Hardpan-Occupation Interface	2.5YR 3/4	Dark red-brown
316	6	KK-25-C/F3/III	Outside Ritual Area	2.5 YR 3/6	Dark red
317	6	LL-31B/F6/III	Rectangular Structure 2 Edge	10 YR 4/8	Dark yellow brown
318	6	MM32A/Oa/III	Outside Rectangular Structure 2	2.5 YR 3/2	Dark red-brown
319	6	LL28d/HF1/III	Rectangular Structure 2 Edge	2.5 YR 2.5/3	Dark red-brown
320	6	LL28c/ob/IV	Rectangular Structure 2 Edge	2.5 YR 3/4	Dark red-brown
321	6	LL27c/ob/IV	Rectangular Structure 2 Edge	2.5 YR 2.5/3	Dark red-brown
322	6	LL25d/ob/IV	Outside Ritual Area	5 R 3/2	Dark brown
323	8	P22a/10/IV	Pithouse floor	10 R 3/3	Dusky red
324	8	Q23c/10/IV	Pithouse Occupation Surface	2.5 YR 3/4	Dark red-brown
325	8	P23a/10/IV	Pithouse Occupation Surface	10 R 3/2	Dusky red
326	9	KK21D/F1/IV	Late Archaic Pithouse Fill	10 R 5/2	Weak red
327	9	x26c/F8/x	Late Archaic Pithouse Fill	2.5 YR 3/3	Dark red-brown
328	9	X26B/F8/X	Late Archaic Pithouse FIll	7.5 YR 3/2	Dark brown
329	9	X28d/F8/X	Late Archaic Pithouse Lower Fill	7.5 YR 3/2	Dark brown
330	9	Y28a/F8/X	Late Archaic Pithouse Fill	10 R 3/2	Dusky red
331	9	Y28a/F6/IX	Late Archaic Pithouse Fill	10 R 3/2	Dusky red
332	9	Y28b/F6/IX	Late Archaic Pithouse Fill	7.5 YR 3/1	Very dark gray
333	9	Y28c/F6/IX	Late Archaic Pithouse Fill	7.5 YR 3/2	Dark brown
334	9	Y28d/F6/IX	Late Archaic Pithouse Fill	7.5 R 3/4	Dark brown
335	9	Y28d/F6/IX	Late Archaic Pithouse Fill	7.5 R 4/1	Dark gray
336	9	Y27a/F1/ii	Plowzone	7.5 R 4/3	Brown

337	9	X26c/F3/X	Late Archaic Pithouse Fill	2.5 YR 3/3	Dark red-brown
338	9	AA/28c/F2/IX	Hearth in Upper Late Archaic Fill	10 R 3/2	Dusky red
339	9	X28c/F12/IX	Late Archaic Pithouse Fill	10 R 3/3	Dusky red
340	9	Y28d/F8/X	Late Archaic Pithouse Fill	10 R 3/2	Dusky red
341	9	Z28b/F3/IX	Late Archaic Pithouse Fill	10 R 3/2	Dusky red
342	9	Y27/F7/vii	Late Archaic Pithouse Fill	10 R 3/2	Dusky red
343	9	X26d/F9/vii	Late Archaic Pithouse Fill	7.5 R 3/6	Dark brown
344	9	Y27b/F7/vii	Late Archaic Pithouse Fill	7.5 R 3/4	Dark brown
345	9	Y27a/F7/vii	Late Archaic Pithouse Fill	7.5 R 3/2	Dark brown
346	9	BB25d/F1/ii	Plowzone	2.5 YR 3/3	Dark red-brown
347	9	A25c/F1/ii	Plowzone	5 R 3/4	Dark brown
348	9	BB25b/F1/ii	Plowzone	10 R 3/4	Dusky red
349	9	Y25b/F1/ii	Plowzone	7.5 R 3/2	Moderate red brown
350	9	AA25b/F1/ii	Plowzone	7.5 R 3/2	Moderate red brown
351	9	BB24d/F1/ii	Plowzone	2.5 YR 3/3	Dark red-brown
352	9	AA28a/F1/ii	Plowzone	7.5 R 3/2	Moderate red brown
353	9	X26c/F8/viii	Late Archaic Pithouse Fill	7.5 R 3/3	Moderate red brown
354	9	Z27b/F7/IX	Late Archaic Pithouse Fill	10 R 3/4	Dusky red
355	9	Y27c/F8/viii	Late Archaic Pithouse Fill Near a Small Hearth	7.5 R 3/4	Dark brown
356	9	BB28a/F7/v	Hearth in Upper Late Archaic Fill	7.5 R 3/6	Dark brown
357	9	Z28c/F4/IX	Hearth in Upper Late Archaic Fill	7.5 R 3/2	Dark brown
358	9	AA26c/F1/ii	Plowzone	7.5 YR 4/4	Dark brown
359	9	AA24c/F2/iii	Plowzone	10 R 4/2	Dusky red
361	9	X24d/oa/v	Late Archaic Pithouse Fill	10 R 3/2	Dusky red
362	9	AA27b/F8/V	Late Archaic Pithouse Fill	10 R 3/2	Dusky red
363	9	Y25d/F9/viii	Outside Stain (Shallow)	7.5 R 2.5/4	Dark brown
364	9	Z27c/F2/IX	Hearth in Upper Late Archaic Fill	10 R 3/4	Dusky red
365	9	BB27d/oa/vii	Matrix	10 R 3/3	Dusky red
366	9	X26B/F9/xiv	Hearth in Base of Late Archaic Pithouse	7.5 R 2.5/4	Dark brown
367	9	Y27bF11/XIII	Hearth in Base of Late Archaic Pithouse	10 R 3/4	Dusky red
368	9	Y27d/F11/XII	Hearth in Base of Late Archaic Pithouse	10 R 3/3	Dusky red
369	9	Y27d/F11/XII	Hearth in Base of Late Archaic Pithouse	10 R 3/4	Dusky red
370	9	AA24c/F2/iii	Plowzone	7.5 YR 4/4	Dark brown

anid	Al (%)	As	Ba (%)	Ca (%)	Ce	Co	Cr
JDR305	2.44	449.2	3.05	0.159	166	57.7	12.5
JDR306	6.63	392.3	0.81	0.210	129	5.7	34.0
JDR307	6.71	191.3	0.03	0.145	274	5.2	9.7
JDR308	10.30	32.8	0.53	0.262	52	1.1	12.8
JDR309	9.87	9.2	0.13	1.402	93	6.7	63.8
JDR310	0.97	734.7	0.06	0.471	34	9.1	31.7
JDR311	0.70	81.3	0.22	0.155	162	1.8	3.0
JDR312	1.28	297.1	0.04	0.282	171	14.3	8.9
JDR313	4.09	62.8	2.64	0.635	54	5.6	9.7
JDR314	0.42	163.6	0.58	0.108	114	5.9	6.4
JDR315	1.09	92.3	0.17	0.224	5	0.6	5.5
JDR316	2.43	292.4	0.03	0.140	173	14.0	7.9
JDR317	2.99	106.1	0.11	0.320	226	1.2	164.6
JDR318	2.00	63.6	1.02	0.000	12	0.2	2.3
JDR319	0.54	126.5	19.65	0.000	524	0.9	7.4
JDR320	0.50	280.8	2.99	0.150	568	14.6	8.2
JDR321	0.59	68.8	0.25	0.347	31	1.5	2.5
JDR322	0.80	69.2	0.45	0.728	173	566.9	5.0
JDR323	6.62	79.4	0.27	0.257	67	20.1	7.0
JDR324	1.81	223.3	0.25	0.181	202	7.8	9.1
JDR325	1.77	200.5	1.19	0.435	202	11.6	8.6
JDR326	1.37	108.8	6.55	0.420	78	1.7	53.2
JDR327	2.92	132.3	0.10	0.252	274	7.5	12.0
JDR328	1.67	94.9	0.18	0.611	190	4.3	11.0
JDR329	4.93	40.3	0.12	0.352	70	14.2	21.4
JDR330	2.80	100.2	0.64	0.000	150	1.4	10.3
JDR331	0.00	192.6	0.09	0.000	327	186.4	3.5
JDR332	3.30	102.2	1.10	0.111	111	4.1	11.3
JDR333	5.55	41.9	0.01	0.000	76	1.1	20.9
JDR334	4.48	93.1	0.10	0.173	210	4.0	7.1
JDR335	1.24	92.7	0.34	0.070	235	1.4	8.4
JDR336	2.95	226.9	0.18	0.172	153	4.8	16.5
JDR337	2.86	171.6	0.91	1.735	402	12.1	16.0
JDR338	2.58	108.0	2.00	0.176	134	2.7	11.7
JDR339	1.23	137.3	0.03	0.000	231	3.2	15.7
JDR340	4.50	69.3	0.08	0.491	93	6.8	10.8
JDR341	0.59	206.7	0.02	0.084	143	2.2	12.4
JDR342	0.00	214.6	0.01	0.064	46	5.1	5.5
JDR343	0.89	131.7	0.01	0.259	525	1.9	11.2
JDR344	1.01	349.5	0.01	0.000	96	2.9	7.8
JDR345	1.69	186.2	0.04	0.131	66	3.8	9.0
JDR346	0.21	147.2	0.03	0.059	240	0.9	3.6
JDR347	1.30	58.5	0.01	0.083	13	4.2	14.3
JDR348	0.40	164.8	0.02	0.000	42	0.5	7.2
JDR349	0.73	133.0	0.00	0.081	12	1.9	6.7
JDR350	1.45	93.3	0.04	0.308	61	5.4	12.2
JDR351	3.79	127.2	0.06	0.204	201	15.8	13.8

JDR352	0.45	69.3	0.01	0.000	6	0.6	7.4
JDR353	6.24	160.3	0.54	0.451	149	7.2	14.9
JDR354	1.43	126.6	0.24	0.248	144	10.1	11.7
JDR355	0.93	516.7	0.05	0.077	58	2.6	12.5
JDR356	2.63	176.6	0.09	0.469	181	2.7	15.2
JDR357	7.57	66.4	0.31	0.406	35	8.0	11.8
JDR358	8.62	11.0	0.15	1.278	74	14.0	49.6
JDR359	1.17	132.8	0.04	0.158	265	3.5	8.6
JDR361	5.24	107.6	0.10	1.198	101	20.5	43.1
JDR362	2.86	181.5	0.04	0.189	167	9.5	28.2
JDR363	1.03	110.6	0.05	0.105	265	101.3	8.9
JDR364	3.77	81.6	0.07	0.738	167	5.3	10.5
JDR365	0.38	402.5	0.01	0.459	1707	3.6	12.1
JDR366	2.11	61.2	0.04	0.288	86	3.0	25.9
JDR367	3.73	138.3	0.50	0.656	159	14.0	23.0
JDR368	0.43	143.5	0.03	0.144	187	3.0	6.2
JDR369	2.59	139.4	0.12	1.010	175	8.7	14.9
JDR370	0.51	172.9	0.04	0.117	47	1.4	6.8
JDR371	0.46	69.2	0.00	5.630	15	1.5	7.6
JDR372	7.02	80.3	1.07	2.982	57	11.7	30.9
JDR373	1.09	72.6	0.04	2.022	0	1441.4	9.4

anid	Cs	Dy	Eu	Fe (%)	Hf	K (%)	La	Lu
JDR305	2.31	1.07	2.17	34.15	0.561	0.000	169.5	0.146
JDR306	15.05	2.25	1.41	25.49	3.231	5.708	130.5	0.291
JDR307	0.97	60.68	11.52	39.12	3.149	0.292	298.9	4.127
JDR308	3.40	1.45	0.76	5.80	3.930	9.926	35.2	0.268
JDR309	8.93	2.69	1.17	4.27	7.576	2.504	53.3	0.223
JDR310	1.98	3.36	2.83	21.87	0.178	0.000	33.0	0.182
JDR311	0.74	1.11	1.98	12.57	0.490	0.084	221.4	0.000
JDR312	1.24	1.56	3.37	47.71	1.176	0.387	127.5	0.000
JDR313	2.49	0.89	1.06	13.43	1.905	0.629	49.5	0.000
JDR314	0.74	0.92	2.24	41.53	0.000	0.000	103.2	0.000
JDR315	0.17	0.19	0.13	17.36	0.182	0.000	5.5	0.000
JDR316	0.65	1.58	2.39	55.46	1.287	0.000	137.8	0.193
JDR317	2.10	1.16	1.40	44.70	1.695	0.000	285.1	0.000
JDR318	0.00	0.00	0.19	12.78	0.933	0.000	19.2	0.000
JDR319	0.72	0.59	2.62	34.53	0.000	0.000	773.8	0.000
JDR320	0.55	2.45	8.89	60.71	0.000	0.000	508.8	0.000
JDR321	0.25	0.00	0.46	12.74	0.142	0.000	35.8	0.000
JDR322	0.43	0.00	2.86	17.08	0.343	0.000	135.3	0.082
JDR323	0.72	0.40	0.88	13.54	1.226	0.000	69.6	0.067
JDR324	5.24	1.30	2.48	42.74	0.867	0.369	215.0	0.000
JDR325	1.21	1.13	3.02	35.68	0.716	0.000	173.6	0.000
JDR326	0.30	0.00	0.89	38.68	1.694	0.464	117.7	0.000
JDR327	1.93	2.94	5.24	47.54	1.329	1.315	232.7	0.222
JDR328	1.75	2.36	3.63	39.90	1.042	0.358	154.9	0.082
JDR329	5.96	0.73	0.89	18.02	3.361	1.767	50.4	0.104
JDR330	0.91	0.57	0.94	49.33	0.735	0.000	168.1	0.000
JDR331	0.00	0.00	6.41	66.75	0.000	0.000	290.4	0.000
JDR332	0.64	0.82	1.21	50.36	2.335	0.000	100.6	0.000
JDR333	0.36	1.16	0.90	24.24	5.122	0.000	68.9	0.119
JDR334	0.86	2.12	3.58	36.00	2.001	0.388	172.6	0.194
JDR335	0.94	3.55	4.07	36.61	0.268	0.751	169.0	0.415
JDR336	0.48	0.73	1.90	55.49	2.494	0.000	157.3	0.000
JDR337	3.29	2.84	5.16	45.75	1.935	1.007	414.5	0.222
JDR338	1.27	0.62	1.27	39.59	1.424	0.399	146.2	0.000
JDR339	0.51	1.10	1.87	36.78	0.908	0.000	235.8	0.000
JDR340	2.58	1.23	0.67	31.43	1.831	0.815	93.2	0.000
JDR341	0.79	0.74	2.13	60.72	0.807	0.202	168.0	0.000
JDR342	1.58	0.73	0.44	66.01	0.439	0.000	22.7	0.000
JDR343	0.72	4.28	9.78	60.05	0.606	0.179	446.2	0.050
JDR344	0.64	1.00	1.92	55.29	0.768	0.066	87.6	0.000
JDR345	0.51	0.52	1.22	46.79	0.742	0.000	60.2	0.000
JDR346	0.00	2.55	3.80	34.20	0.000	0.118	247.0	0.054
JDR347	0.00	0.88	0.20	61.79	0.490	0.105	12.7	0.086
JDR348	0.00	0.43	0.54	55.15	0.297	0.000	58.2	0.000
JDR349	0.00	1.07	0.43	50.33	0.764	0.000	14.4	0.000
JDR350	1.66	2.81	0.69	34.97	0.784	0.000	34.0	0.269
JDR351	11.48	0.99	1.52	43.70	1.650	1.295	247.6	0.146

JDR352	0.25	0.00	0.18	31.43	0.296	0.036	2.9	0.000
JDR353	4.21	2.69	2.59	22.92	2.434	5.621	124.7	0.172
JDR354	1.64	1.49	2.38	39.56	1.197	1.092	124.9	0.000
JDR355	0.94	0.40	0.91	55.74	0.741	0.283	49.8	0.121
JDR356	1.50	1.76	2.72	24.64	5.286	1.332	212.0	0.149
JDR357	1.88	2.28	0.77	16.55	3.111	8.709	22.5	0.274
JDR358	9.90	2.90	1.33	3.84	5.980	2.853	37.5	0.227
JDR359	0.61	2.33	5.34	49.62	1.009	0.240	267.2	0.000
JDR361	5.12	1.90	1.53	18.95	3.372	2.006	72.3	0.094
JDR362	5.70	2.03	1.93	29.55	7.224	0.877	177.7	0.274
JDR363	0.00	1.77	3.68	41.22	0.932	0.000	257.6	0.000
JDR364	1.15	2.67	3.68	35.17	2.466	1.627	142.2	0.077
JDR365	0.83	16.33	35.81	62.47	0.316	0.000	1858.3	2.124
JDR366	1.74	0.81	1.54	37.48	1.803	0.466	88.9	0.046
JDR367	2.95	2.16	2.78	33.34	2.092	0.803	120.4	0.219
JDR368	0.69	1.77	4.28	52.29	0.557	0.000	165.8	0.000
JDR369	3.21	1.28	2.76	40.31	2.020	0.934	136.5	0.043
JDR370	0.42	0.52	0.83	33.24	1.466	0.000	67.8	0.022
JDR371	1.06	0.30	0.36	12.78	0.792	5.698	5.5	0.041
JDR372	9.23	2.41	1.00	9.61	5.575	2.020	37.1	0.219
JDR373	0.00	0.30	0.04	55.92	1.321	0.449	0.7	0.053

anid	Mn (%)	Na (%)	Nd	Ni	Rb	Sb	Sc	Sm
JDR305	0.173	0.121	53.3	0.0	17.1	15.49	9.10	4.04
JDR306	0.018	0.171	40.3	0.0	177.5	27.44	12.93	4.19
JDR307	0.020	0.069	56.1	0.0	0.0	8.04	8.48	14.74
JDR308	0.058	0.206	14.2	0.0	254.2	1.13	18.35	2.11
JDR309	0.023	1.424	35.4	0.0	88.7	0.94	12.60	5.15
JDR310	0.054	0.037	18.9	0.0	0.0	3.80	4.23	3.31
JDR311	0.006	0.068	26.2	0.0	0.0	4.63	0.94	2.61
JDR312	0.139	0.208	34.8	0.0	28.1	8.99	3.35	5.35
JDR313	0.040	0.377	0.0	0.0	25.9	3.19	3.75	2.50
JDR314	0.092	0.038	47.3	0.0	0.0	10.36	1.17	3.87
JDR315	0.004	0.041	0.0	0.0	0.0	3.52	1.16	0.15
JDR316	0.059	0.039	22.1	0.0	0.0	12.63	3.47	3.61
JDR317	0.006	0.061	32.4	0.0	0.0	5.72	6.23	3.82
JDR318	0.002	0.037	10.9	0.0	0.0	5.83	0.31	0.44
JDR319	0.006	0.038	158.0	0.0	6.0	1.23	1.13	2.76
JDR320	0.084	0.042	96.9	0.0	0.0	14.63	1.78	9.37
JDR321	0.006	0.043	0.0	0.0	0.0	4.36	0.84	0.71
JDR322	0.477	0.055	28.3	0.0	0.0	3.96	1.38	4.29
JDR323	0.149	0.073	16.6	0.0	0.0	4.57	4.22	1.55
JDR324	0.037	0.061	21.3	0.0	47.5	8.81	5.05	4.47
JDR325	0.084	0.187	41.6	0.0	16.5	10.56	2.06	4.62
JDR326	0.007	0.091	67.5	0.0	0.0	2.20	3.58	1.31
JDR327	0.025	0.169	53.3	0.0	56.3	5.94	8.18	8.29
JDR328	0.033	0.213	52.5	0.0	20.2	4.41	4.34	6.07
JDR329	0.121	0.524	21.0	0.0	60.5	1.50	8.77	2.55
JDR330	0.017	0.044	25.5	0.0	0.0	3.04	5.24	1.68
JDR331	1.214	0.035	55.5	0.0	0.0	15.41	1.39	8.81
JDR332	0.027	0.044	0.0	0.0	0.0	2.49	8.34	2.34
JDR333	0.015	0.044	14.1	0.0	0.0	2.13	14.93	2.13
JDR334	0.019	0.054	53.6	0.0	0.0	4.86	6.64	6.85
JDR335	0.009	0.053	65.1	0.0	31.2	3.93	4.13	9.74
JDR336	0.082	0.039	35.9	0.0	0.0	13.42	5.46	3.40
JDR337	0.034	0.386	69.2	0.0	34.6	7.97	6.18	7.40
JDR338	0.018	0.133	27.9	0.0	0.0	4.11	5.99	2.38
JDR339	0.020	0.058	39.8	0.0	0.0	4.78	3.51	2.91
JDR340	0.051	0.256	21.4	0.0	31.4	2.66	6.21	2.22
JDR341	0.008	0.056	29.8	0.0	0.0	6.98	2.75	3.25
JDR342	0.206	0.044	0.0	0.0	0.0	11.98	3.35	2.46
JDR343	0.013	0.089	124.7	0.0	0.0	9.35	3.16	14.80
JDR344	0.012	0.055	28.7	0.0	0.0	4.51	4.41	3.11
JDR345	0.015	0.058	21.5	0.0	0.0	7.92	5.26	2.82
JDR346	0.010	0.033	57.0	0.0	0.0	13.91	0.59	6.93
JDR347	0.033	0.033	0.0	0.0	0.0	4.43	4.19	1.48
JDR348	0.004	0.041	0.0	0.0	0.0	1.79	2.20	1.33
JDR349	0.018	0.036	0.0	0.0	0.0	6.59	2.06	1.65
JDR350	0.039	0.044	20.0	0.0	0.0	4.00	3.37	3.61
JDR351	0.078	0.061	40.3	0.0	99.8	6.05	8.93	5.10

JDR352	0.006	0.049	0.0	0.0	0.0	2.80	2.29	0.40
JDR353	0.035	0.143	45.9	0.0	146.9	3.43	12.72	6.41
JDR354	0.132	0.096	39.3	0.0	32.7	5.52	5.97	8.34
JDR355	0.022	0.070	6.3	0.0	0.0	21.05	2.44	1.84
JDR356	0.009	0.198	36.1	0.0	35.3	11.52	3.74	5.20
JDR357	0.034	0.177	15.4	0.0	188.3	3.27	32.65	2.93
JDR358	0.077	1.510	31.2	49.1	107.1	1.12	11.67	5.71
JDR359	0.022	0.062	69.5	0.0	0.0	5.97	5.03	7.76
JDR361	0.192	1.242	18.1	0.0	63.9	4.57	5.20	4.10
JDR362	0.035	0.383	37.3	0.0	37.7	9.32	6.31	4.17
JDR363	0.086	0.052	65.6	0.0	0.0	5.41	3.58	7.08
JDR364	0.031	0.896	50.7	0.0	41.3	3.43	5.15	7.17
JDR365	0.026	0.056	313.6	345.0	0.0	22.49	1.08	50.38
JDR366	0.023	0.286	30.7	0.0	25.7	3.01	4.25	3.22
JDR367	0.053	0.568	27.8	0.0	43.9	6.17	8.95	5.04
JDR368	0.018	0.047	49.1	0.0	0.0	6.48	3.15	6.64
JDR369	0.122	0.300	37.8	0.0	43.3	6.30	6.48	4.93
JDR370	0.010	0.037	7.9	0.0	0.0	7.81	1.70	1.54
JDR371	0.014	1.578	11.3	0.0	0.0	144.34	1.49	1.73
JDR372	0.076	1.559	31.0	0.0	100.7	4.87	11.45	4.14
JDR373	0.029	0.187	0.0	0.0	0.0	1.12	2.40	0.30

anid	Sr	Ta	Tb	Th	Ti	U	V	Yb	Zn	Zr
JDR305	1778	0.000	0.333	2.29	0	5.44	311.9	0.645	193.5	0
JDR306	894	0.618	0.377	5.40	3783	6.62	240.9	1.737	121.3	119
JDR307	3531	0.421	8.452	2.82	4942	18.19	262.2	31.365	60.0	273
JDR308	1022	0.471	0.198	4.04	9210	2.62	321.1	1.670	84.1	142
JDR309	653	0.980	0.437	19.14	5012	5.14	115.9	1.691	116.0	222
JDR310	0	0.000	0.545	0.34	0	2.74	390.9	1.745	313.0	0
JDR311	842	0.000	0.236	0.82	217	5.95	60.8	0.297	11.3	90
JDR312	510	0.000	0.330	2.38	1029	9.73	327.5	0.659	81.0	136
JDR313	705	0.166	0.000	2.51	1593	9.07	69.3	0.412	42.3	98
JDR314	0	0.000	0.176	0.62	0	17.04	126.1	0.000	29.0	170
JDR315	149	0.000	0.000	0.23	449	0.00	74.9	0.000	0.0	0
JDR316	1278	0.000	0.000	1.54	1771	6.47	337.6	0.673	62.6	113
JDR317	3700	0.000	0.000	3.02	1095	1.34	178.4	0.000	17.4	0
JDR318	776	0.105	0.000	0.84	774	1.15	12.8	0.000	0.0	0
JDR319	3642	0.000	0.237	1.50	466	6.04	42.3	0.728	0.0	0
JDR320	633	0.000	0.538	1.65	0	31.78	317.5	0.000	47.2	285
JDR321	453	0.000	0.000	0.27	0	1.29	67.2	0.000	3.9	0
JDR322	894	0.000	0.355	0.76	0	8.98	97.3	0.211	51.7	0
JDR323	1587	0.266	0.136	1.42	748	1.89	94.2	0.268	18.3	49
JDR324	1590	0.000	0.238	2.51	1496	14.31	263.6	0.921	57.9	145
JDR325	994	0.000	0.289	1.69	397	14.91	154.2	0.666	27.1	115
JDR326	1186	0.000	0.000	1.42	3639	3.11	141.5	0.000	17.5	0
JDR327	1245	0.200	0.486	2.62	2171	7.48	166.1	0.896	39.5	119
JDR328	962	0.140	0.293	2.07	1276	5.78	121.0	0.667	26.0	114
JDR329	1010	0.416	0.192	3.92	3542	3.60	148.4	0.758	82.8	85
JDR330	2680	0.000	0.000	2.06	1793	3.69	185.1	0.000	0.0	0
JDR331	0	0.000	0.765	0.77	0	18.15	190.4	0.000	22.6	152
JDR332	1755	0.220	0.000	2.09	4504	4.78	191.8	0.363	0.0	0
JDR333	1516	0.604	0.149	6.03	9696	4.25	162.0	0.745	16.2	128
JDR334	1869	0.346	0.510	1.69	2555	10.61	161.4	0.771	27.6	116
JDR335	348	0.000	0.582	2.15	497	16.59	127.4	1.164	8.9	123
JDR336	152	0.268	0.228	2.26	4942	6.42	279.0	0.600	24.5	0
JDR337	574	0.245	0.487	4.35	2371	9.28	228.2	0.994	132.8	150
JDR338	2417	0.124	0.000	2.53	2363	3.57	124.7	0.272	18.0	64
JDR339	2444	0.193	0.000	1.87	1362	3.90	138.2	0.200	9.0	0
JDR340	1809	0.198	0.000	2.67	2253	4.30	275.0	0.369	60.7	53
JDR341	458	0.000	0.000	1.52	836	11.11	200.6	0.000	0.0	0
JDR342	0	0.000	0.000	0.66	0	13.57	140.2	0.000	27.9	137
JDR343	655	0.100	0.779	2.07	1381	6.56	175.7	1.439	0.0	179
JDR344	366	0.000	0.000	1.07	1454	5.74	99.1	0.463	16.7	0
JDR345	762	0.000	0.000	1.43	1634	10.02	121.6	0.221	21.8	90
JDR346	0	0.000	0.607	1.46	0	3.12	171.2	0.638	0.0	92
JDR347	0	0.000	0.000	1.83	400	6.58	179.0	0.000	15.8	0
JDR348	0	0.000	0.000	0.47	413	6.50	49.1	0.000	0.0	0
JDR349	0	0.000	0.000	0.98	1030	6.75	147.5	0.000	16.1	0
JDR350	0	0.608	0.412	13.37	4797	2.28	441.7	1.809	102.3	78
JDR351	2098	0.207	0.331	4.25	2044	19.43	306.9	0.962	109.1	172

JDR352	0	0.000	0.000	0.99	811	1.65	145.4	0.000	0.0	0
JDR353	1077	0.305	0.435	2.68	3856	4.47	202.2	1.230	337.5	95
JDR354	209	0.000	0.504	1.48	1243	7.95	201.3	0.375	52.9	75
JDR355	527	0.000	0.000	0.79	734	7.57	225.7	0.000	13.7	0
JDR356	1872	0.473	0.449	4.20	2811	3.18	129.8	0.734	31.3	140
JDR357	426	0.353	0.322	3.59	4763	2.20	197.9	1.742	106.6	51
JDR358	520	0.948	0.562	12.53	5291	2.57	96.2	2.249	148.2	175
JDR359	1009	0.000	0.464	1.75	2226	8.57	208.0	0.910	0.0	147
JDR361	526	0.521	0.301	6.84	2819	6.77	143.3	1.007	58.8	123
JDR362	1276	0.546	0.338	4.94	3487	6.67	130.4	1.190	52.3	192
JDR363	2103	0.000	0.393	1.73	1827	6.06	132.7	0.569	11.9	0
JDR364	813	0.311	0.504	4.11	3782	3.62	105.9	1.216	40.5	104
JDR365	340	0.000	3.524	4.28	539	93.55	650.1	8.887	0.0	1042
JDR366	1287	0.262	0.000	2.58	1805	3.40	110.2	0.388	20.8	0
JDR367	338	0.216	0.518	3.04	3365	8.06	158.8	1.088	138.4	137
JDR368	343	0.000	0.544	1.61	539	8.64	123.3	0.498	15.4	157
JDR369	826	0.269	0.432	3.66	2991	6.65	183.4	0.566	85.2	105
JDR370	785	0.134	0.000	1.31	1376	4.04	64.7	0.400	0.0	0
JDR371	757	0.000	0.125	1.05	1582	1.80	0.0	0.409	25.2	28
JDR372	840	0.561	0.539	8.38	3174	3.44	110.8	1.458	80.2	121
JDR373	1112	0.000	0.000	0.00	2503	0.00	159.0	0.433	33.2	0

Appendix IV: INAA elemental data for Arizona ochre sources in this study. Values are presented as ppm except those marked %.

ANID	Location	Munsell
JDR185	Saguaro Knolls	5 YR 7/3
JDR186		5 YR 7/3
JDR187		5 YR 7/3
JDR188		5 YR 7/3
JDR189		5 YR 7/3
JDR190	Saguaro Knolls	5 YR 7/3
JDR191		5 YR 7/3
JDR192		5 YR 7/3
JDR193		5 YR 7/3
JDR194		5 YR 7/3
JDR195	Beehive Hill #1	5 YR 7/3
JDR196		5 YR 7/3
JDR197		5 YR 7/3
JDR198		5 YR 7/3
JDR199		5 YR 7/3
JDR200	Beehive Hill #1	7.5 YR 7/6
JDR201		7.5 YR 7/6
JDR202		7.5 YR 7/6
JDR203		7.5 YR 7/6
JDR204		7.5 YR 7/6
JDR205	Beehive Hill #1	7.5 YR 7/4
JDR206		7.5 YR 7/4
JDR207		7.5 YR 7/4
JDR208		7.5 YR 7/4
JDR209		7.5 YR 7/4
JDR210	Beehive Hill #1	7.5 YR 6/6
JDR211		7.5 YR 6/6
JDR212		7.5 YR 6/6
JDR213		7.5 YR 6/6
JDR214		7.5 YR 6/6
JDR215	Beehive Hill #1	7.5 YR 6/6
JDR216		7.5 YR 6/6
JDR217		7.5 YR 6/6
JDR218		7.5 YR 6/6
JDR219		7.5 YR 6/6
JDR220	Beehive Hill #2	5 YR 4/6
JDR221		5 YR 4/6
JDR222		5 YR 4/6
JDR223		5 YR 4/6
JDR224		5 YR 4/6
JDR225	Beehive Hill #2	5 YR 4/6
JDR226		5 YR 4/6
JDR227		5 YR 4/6
JDR228		5 YR 4/6
JDR229		5 YR 4/6

JDR230	Beehive Hill #2	7.5 YR 6/6
JDR231		7.5 YR 6/6
JDR232		7.5 YR 6/6
JDR233		7.5 YR 6/6
JDR234		7.5 YR 6/6
JDR235	Beehive Hill #2	7.5 YR 6/6
JDR236		7.5 YR 6/6
JDR237		7.5 YR 6/6
JDR238		7.5 YR 6/6
JDR239		7.5 YR 6/6
JDR240	Beehive Hill #2	7.5 YR 6/6
JDR241		7.5 YR 6/6
JDR242		7.5 YR 6/6
JDR243		7.5 YR 6/6
JDR244		7.5 YR 6/6
JDR245	Beehive Hill 2/3	5 YR 4/6
JDR246		5 YR 4/6
JDR247		5 YR 4/6
JDR248		5 YR 4/6
JDR249		5 YR 4/6
JDR250	Rattlesnake Pass	2.5 YR 5/8
JDR251		2.5 YR 5/8
JDR252		2.5 YR 5/8
JDR253		2.5 YR 5/8
JDR254		2.5 YR 5/8
JDR255	Rattlesnake Pass	2.5 YR 4/8
JDR256		2.5 YR 5/8
JDR257		2.5 YR 5/8
JDR258		2.5 YR 5/8
JDR259		2.5 YR 5/8
JDR260	Rattlesnake Pass	7.5 YR 5/6
JDR261		7.5 YR 5/6
JDR262		7.5 YR 5/6
JDR263		7.5 YR 5/6
JDR264		7.5 YR 5/6
JDR265	Rattlesnake Pass	2.5 YR 4/8
JDR266		2.5 YR 4/8
JDR267		2.5 YR 4/8
JDR268		2.5 YR 4/8
JDR269		2.5 YR 4/8
JDR270	Rattlesnake Pass	5 YR 5/8
JDR271		5 YR 5/8
JDR272		5 YR 5/8
JDR273		5 YR 5/8
JDR274		5 YR 5/8
JDR275	Rattlesnake Pass	5 YR 7/6
JDR276		5 YR 7/6
JDR277		5 YR 7/6
JDR278		5 YR 7/6
JDR279		5 YR 7/6
JDR280	Rattlesnake Pass	5 YR 7/6

JDR281		5 YR 7/6
JDR282		5 YR 7/6
JDR283		5 YR 7/6
JDR284		5 YR 7/6
JDR285	Ragged Top	5 YR 4/6
JDR286		5 YR 4/6
JDR287		5 YR 4/6
JDR288		5 YR 4/6
JDR289		5 YR 4/6
JDR290	Ragged Top	2.5 YR 3/6
JDR291		2.5 YR 3/6
JDR292		2.5 YR 3/6
JDR293		2.5 YR 3/6
JDR294		2.5 YR 3/6
JDR295	Ragged Top	2.5 YR 4/4
JDR296		2.5 YR 4/4
JDR297		2.5 YR 4/4
JDR298		2.5 YR 4/4
JDR299		2.5 YR 4/4
JDR300	Ragged Top	2.5 YR 3/4
JDR301		2.5 YR 3/4
JDR302		2.5 YR 3/4
JDR303		2.5 YR 3/4
JDR304		2.5 YR 3/4

anid	Al	As	Ba	Ca	Ce	Co	Cr	Cs
JDR195	7.33	104.5	282.0	1.64	75.17	4.58	7.20	25.09
JDR196	7.41	309.0	372.2	0.13	74.04	0.36	5.43	14.82
JDR197	7.28	114.6	325.5	1.86	75.66	4.06	6.51	26.79
JDR198	7.48	103.9	317.6	1.87	72.63	3.79	7.37	23.32
JDR199	7.22	110.6	323.8	2.07	76.10	3.75	7.56	25.74
JDR200	11.23	45.8	463.9	0.54	79.10	7.17	29.74	45.95
JDR201	10.67	49.4	502.3	0.36	77.80	7.15	30.34	46.62
JDR202	10.21	45.8	377.2	0.51	77.91	7.07	30.48	43.41
JDR203	11.43	44.3	316.3	0.52	80.69	7.81	31.40	48.88
JDR204	10.55	41.7	337.1	0.64	77.24	6.24	28.51	44.87
JDR205	7.87	40.1	378.7	4.18	63.50	5.37	13.66	34.39
JDR206	7.19	43.1	327.5	4.38	62.59	5.05	13.35	29.53
JDR207	7.45	42.5	424.5	3.82	65.23	5.29	13.38	33.50
JDR208	7.96	44.1	384.6	4.45	67.31	5.27	13.64	34.94
JDR209	7.56	42.9	347.4	4.99	63.45	5.68	17.01	38.19
JDR210	11.30	90.4	737.8	1.37	104.08	12.72	28.47	45.04
JDR211	11.56	89.5	491.3	1.13	92.04	11.72	31.17	53.31
JDR212	12.45	89.7	552.5	1.23	88.14	11.08	33.33	58.75
JDR213	12.33	91.3	473.5	1.31	99.00	11.08	34.97	57.54
JDR214	12.37	89.3	513.9	1.51	91.37	11.82	34.22	55.78
JDR215	8.67	94.9	539.0	4.15	70.96	8.09	22.57	53.92
JDR216	9.17	95.2	492.2	4.01	68.57	8.21	24.46	56.66
JDR217	9.06	100.4	257.5	4.59	71.27	7.87	26.04	55.53
JDR218	8.32	88.3	334.6	4.10	69.23	8.20	23.81	51.44
JDR219	8.82	86.1	260.7	4.31	68.34	7.57	20.51	50.32
JDR220	10.17	89.6	341.9	1.09	73.71	7.39	27.93	37.81
JDR221	10.17	91.4	272.6	1.01	73.69	7.52	28.34	38.64
JDR222	10.01	93.8	398.8	0.97	72.94	7.60	30.81	38.65
JDR223	10.21	104.8	322.8	1.02	76.01	8.13	28.78	39.37
JDR224	9.44	100.4	434.6	1.40	73.27	7.74	29.92	38.89
JDR225	9.06	65.7	330.9	0.30	80.88	7.45	25.89	34.82
JDR226	8.85	64.5	343.0	0.49	79.72	7.50	27.83	34.81
JDR227	9.72	68.4	517.8	0.43	76.60	7.69	26.49	36.24
JDR228	9.84	71.7	328.7	0.50	74.45	7.72	26.03	36.30
JDR229	9.33	68.4	364.3	0.46	80.49	7.85	27.63	36.68
JDR230	10.36	44.7	542.6	0.62	76.85	7.15	26.39	38.46
JDR231	10.67	46.3	555.3	0.71	74.40	7.10	26.54	38.31
JDR232	10.79	58.9	590.1	0.73	75.50	7.69	29.36	40.91
JDR233	10.85	44.5	477.1	0.77	76.99	7.47	28.37	40.15
JDR234	10.66	48.3	434.9	0.67	77.60	7.51	26.49	40.96
JDR235	9.61	145.6	574.0	1.73	72.68	9.26	28.94	42.38
JDR236	9.60	170.5	577.6	1.64	69.14	9.06	25.72	40.65
JDR237	10.07	161.5	388.2	1.56	77.04	9.62	28.44	43.23
JDR238	10.02	171.4	421.3	1.81	71.16	9.34	28.12	40.85
JDR239	9.85	146.1	396.3	1.49	69.86	9.23	28.66	43.20
JDR240	10.60	56.0	605.1	1.36	76.09	9.77	34.34	39.65
JDR241	10.16	58.9	619.3	0.94	78.88	10.22	33.05	39.27

JDR242	10.02	60.0	584.3	1.44	76.06	9.22	32.23	36.83
JDR243	10.72	64.4	513.6	1.06	76.24	9.95	33.22	39.35
JDR244	10.17	62.5	666.6	1.13	76.21	10.06	33.83	39.07
JDR245	11.63	61.8	461.9	0.56	74.92	9.66	39.37	33.63
JDR246	11.61	59.4	479.6	0.58	77.08	9.38	39.13	34.27
JDR247	10.37	61.2	453.8	0.49	76.95	9.62	38.11	33.78
JDR248	10.33	62.1	359.2	0.59	75.56	10.08	40.99	34.76
JDR249	10.92	57.9	366.5	0.54	75.44	9.57	40.24	34.09
JDR250	8.80	24.7	916.2	4.18	86.26	6.42	49.90	22.38
JDR251	7.82	23.0	929.3	6.51	78.92	5.99	46.64	20.11
JDR252	5.72	21.2	881.7	13.15	59.05	2.85	31.86	13.38
JDR253	7.76	25.5	1015.6	6.24	76.87	5.91	48.61	19.58
JDR254	7.73	21.7	1340.6	5.59	81.79	5.93	48.35	19.94
JDR255	7.76	17.7	1268.5	4.02	83.34	9.92	56.77	20.14
JDR256	7.69	21.8	1114.9	3.75	88.08	9.79	56.75	19.87
JDR257	8.31	20.4	1133.2	3.90	88.86	9.18	66.35	19.59
JDR258	7.85	22.6	1107.2	3.96	91.74	9.92	60.90	20.29
JDR259	7.67	22.8	1180.9	3.94	88.83	9.56	71.43	20.89
JDR260	7.35	16.3	1296.0	5.77	80.04	7.49	38.25	19.88
JDR261	7.35	17.0	1161.3	5.25	80.80	6.91	34.03	18.96
JDR262	7.10	20.5	1158.0	5.14	85.39	7.08	36.41	19.69
JDR263	6.90	18.5	1190.2	6.03	81.18	7.60	41.64	21.00
JDR264	7.26	21.3	1307.0	5.23	82.05	7.46	39.33	21.28
JDR265	6.70	19.5	971.3	7.05	75.85	7.14	54.22	17.64
JDR266	6.92	18.6	910.1	6.03	79.92	7.44	55.53	19.02
JDR267	6.03	15.5	816.0	10.90	63.56	5.05	39.63	14.72
JDR268	6.73	18.2	1000.4	6.49	72.00	6.65	43.70	18.28
JDR269	7.07	18.2	919.8	7.18	74.80	6.57	44.64	17.97
JDR270	7.74	15.0	740.4	4.75	87.82	10.69	73.94	17.80
JDR271	7.64	14.0	817.1	5.25	84.63	10.83	73.01	15.98
JDR272	7.29	16.6	751.0	5.38	84.27	11.03	75.75	17.07
JDR273	7.58	17.4	667.4	4.84	83.06	10.30	66.87	17.50
JDR274	7.62	16.6	783.4	5.31	82.23	11.01	72.60	16.74
JDR275	5.45	14.0	504.3	14.64	57.14	3.22	32.36	16.29
JDR276	2.30	10.2	549.0	20.76	28.27	1.38	15.44	8.50
JDR277	4.82	14.9	394.8	15.29	54.14	2.84	30.69	17.10
JDR278	1.95	8.6	189.4	24.71	20.90	1.25	12.04	6.80
JDR279	4.91	15.0	491.8	14.41	55.04	3.03	31.07	15.98
JDR289	2.97	27.1	172.6	10.19	26.66	35.55	34.28	26.43
JDR290	7.21	39.9	404.0	0.70	99.65	11.97	38.78	69.33
JDR291	7.79	40.2	493.5	0.74	103.53	12.19	38.48	67.09
JDR292	8.85	43.8	469.3	0.67	101.96	14.15	47.55	80.07
JDR293	7.76	37.1	474.2	0.11	98.72	12.14	39.00	68.62
JDR294	8.06	43.4	448.1	0.73	105.95	14.67	44.72	75.00
JDR295	11.53	39.5	193.8	0.30	72.62	12.91	67.74	94.01
JDR296	10.60	37.6	301.1	0.30	59.09	11.34	58.45	66.43
JDR297	11.07	38.0	163.8	0.00	65.68	11.38	57.29	66.10
JDR298	10.88	44.5	722.6	0.25	68.46	12.44	57.43	70.68
JDR299	7.82	25.6	250.6	0.19	63.24	11.10	39.81	55.45

JDR300	9.58	38.5	546.5	0.74	80.75	15.12	64.67	138.02
JDR301	6.55	22.0	278.7	0.00	68.29	4.03	41.93	23.18
JDR302	8.07	28.9	196.6	0.18	83.48	4.78	29.50	30.05
JDR304	7.10	30.5	170.4	0.18	71.87	5.10	32.12	28.76

anid	Dy	Eu	Fe	Hf	K	La	Lu	Mn
JDR195	4.88	1.51	1.72	5.10	4.42	35.85	0.346	0.086
JDR196	3.77	0.82	4.10	5.51	4.01	34.45	0.328	0.021
JDR197	4.75	1.55	1.92	5.25	4.13	36.72	0.338	0.088
JDR198	4.57	1.37	1.76	5.13	4.34	35.07	0.322	0.100
JDR199	5.36	1.42	1.87	4.90	4.20	37.05	0.371	0.080
JDR200	5.82	1.30	3.14	7.82	3.89	41.21	0.491	0.087
JDR201	4.75	1.25	3.06	7.36	4.16	40.73	0.470	0.092
JDR202	5.19	1.19	2.93	7.09	4.23	40.52	0.436	0.089
JDR203	5.24	1.31	3.16	8.43	3.85	41.76	0.481	0.108
JDR204	4.80	1.19	2.84	6.23	3.95	40.31	0.449	0.088
JDR205	4.26	0.99	2.04	6.23	3.48	32.39	0.392	0.116
JDR206	4.53	0.97	1.95	6.11	3.51	31.00	0.395	0.129
JDR207	4.16	1.02	2.03	5.71	3.01	31.83	0.370	0.143
JDR208	4.14	1.00	2.08	5.88	3.27	33.57	0.399	0.121
JDR209	4.37	1.05	2.21	6.25	3.49	31.88	0.394	0.122
JDR210	5.95	1.90	4.83	8.87	4.60	50.88	0.503	0.143
JDR211	5.73	1.68	4.51	7.76	4.35	46.67	0.479	0.142
JDR212	5.87	1.66	4.56	7.64	4.37	45.20	0.499	0.137
JDR213	5.69	1.70	4.58	8.01	4.52	48.88	0.441	0.121
JDR214	5.61	1.67	4.58	7.98	4.65	45.42	0.516	0.140
JDR215	4.13	1.14	2.83	6.51	3.40	34.24	0.359	0.166
JDR216	4.27	1.16	2.90	6.28	3.46	33.90	0.368	0.140
JDR217	4.71	1.14	2.84	6.80	3.51	35.04	0.362	0.144
JDR218	4.16	1.16	2.79	6.43	3.75	33.12	0.383	0.194
JDR219	4.07	1.17	2.67	7.02	3.71	33.82	0.408	0.130
JDR220	5.18	1.28	3.02	6.69	3.81	38.06	0.458	0.155
JDR221	6.04	1.29	2.99	7.76	3.56	37.67	0.472	0.164
JDR222	5.29	1.28	3.11	7.88	3.45	37.74	0.422	0.167
JDR223	5.22	1.31	3.20	7.59	3.73	38.86	0.446	0.186
JDR224	4.92	1.25	3.15	6.99	3.82	37.48	0.394	0.144
JDR225	4.60	1.28	3.09	7.72	3.69	40.22	0.470	0.142
JDR226	4.50	1.28	3.16	7.87	3.85	39.96	0.523	0.180
JDR227	5.44	1.28	3.16	7.32	3.77	38.32	0.432	0.150
JDR228	5.61	1.34	3.26	7.99	3.84	38.19	0.480	0.153
JDR229	5.38	1.31	3.18	7.41	3.81	40.64	0.464	0.150
JDR230	5.36	1.25	2.98	6.27	4.13	38.43	0.419	0.094
JDR231	4.60	1.18	2.99	6.64	4.36	38.07	0.420	0.095
JDR232	4.63	1.25	3.40	6.19	3.89	38.53	0.443	0.108
JDR233	4.75	1.23	3.11	6.46	3.94	38.63	0.413	0.109
JDR234	5.22	1.25	3.18	6.78	4.07	38.75	0.425	0.104
JDR235	5.77	1.27	3.19	6.78	4.35	37.13	0.430	0.195
JDR236	4.93	1.24	3.11	6.49	4.18	34.26	0.412	0.218
JDR237	4.75	1.30	3.35	7.15	4.07	38.96	0.392	0.203
JDR238	4.85	1.22	3.25	7.07	4.21	35.95	0.411	0.205

JDR239	4.67	1.23	3.20	7.53	3.84	35.18	0.391	0.189
JDR240	4.57	1.34	3.44	7.57	4.40	38.46	0.421	0.114
JDR241	4.44	1.36	3.52	7.87	4.08	39.97	0.436	0.122
JDR242	4.77	1.31	3.26	6.77	4.24	39.09	0.422	0.115
JDR243	5.42	1.26	3.47	9.58	3.95	38.75	0.459	0.120
JDR244	4.73	1.29	3.47	7.83	3.78	38.16	0.448	0.129
JDR245	5.18	1.27	3.87	5.80	3.89	37.88	0.373	0.111
JDR246	5.09	1.27	3.94	5.93	4.05	38.57	0.485	0.113
JDR247	5.57	1.29	3.85	6.50	4.36	38.30	0.402	0.110
JDR248	5.14	1.29	4.01	6.22	3.74	38.44	0.432	0.105
JDR249	4.63	1.24	3.89	6.31	3.89	38.25	0.414	0.107
JDR250	3.66	1.43	4.02	7.32	2.60	41.81	0.250	0.040
JDR251	3.79	1.30	3.59	6.48	2.22	38.27	0.304	0.038
JDR252	2.65	0.97	2.63	4.26	1.39	28.26	0.181	0.014
JDR253	3.83	1.26	3.50	6.33	2.01	37.61	0.276	0.046
JDR254	4.20	1.30	3.64	6.69	2.08	39.07	0.305	0.038
JDR255	3.64	1.40	3.64	7.50	2.75	40.05	0.284	0.101
JDR256	4.13	1.44	3.71	7.46	2.60	43.01	0.298	0.068
JDR257	4.09	1.49	3.65	7.43	2.95	42.52	0.307	0.065
JDR258	4.08	1.49	3.71	7.34	2.51	44.65	0.347	0.084
JDR259	3.49	1.46	3.77	6.96	2.47	42.21	0.254	0.095
JDR260	4.45	1.27	3.32	8.84	2.65	38.22	0.347	0.077
JDR261	4.26	1.36	3.21	10.12	3.08	39.67	0.413	0.077
JDR262	4.12	1.31	3.34	8.94	3.00	42.58	0.371	0.069
JDR263	4.05	1.28	3.39	8.42	2.51	39.70	0.327	0.068
JDR264	3.90	1.36	3.32	8.38	2.61	39.32	0.349	0.074
JDR265	3.47	1.19	3.13	6.28	1.99	36.30	0.219	0.056
JDR266	3.42	1.32	3.36	6.86	1.97	39.19	0.334	0.073
JDR267	2.71	1.08	2.56	5.23	1.83	30.67	0.232	0.032
JDR268	3.33	1.17	3.01	6.00	2.26	35.81	0.288	0.055
JDR269	3.01	1.23	3.08	6.59	2.20	36.17	0.318	0.107
JDR270	4.39	1.46	3.60	8.18	2.39	45.79	0.340	0.085
JDR271	4.25	1.49	3.45	8.18	2.86	42.96	0.373	0.113
JDR272	4.49	1.45	3.65	8.31	2.30	43.26	0.326	0.078
JDR273	4.28	1.42	3.50	7.89	2.01	42.82	0.305	0.104
JDR274	4.40	1.44	3.44	7.61	2.38	41.88	0.323	0.131
JDR275	2.39	0.91	2.57	4.93	1.16	26.46	0.193	0.015
JDR276	0.88	0.45	1.18	2.10	0.54	13.05	0.057	0.005
JDR277	2.08	0.86	2.45	4.34	1.30	24.91	0.148	0.011
JDR278	0.87	0.34	0.88	1.64	0.42	9.49	0.054	0.005
JDR279	1.84	0.91	2.54	3.88	1.31	25.62	0.154	0.012
JDR289	3.15	1.00	4.97	3.55	0.93	11.64	0.302	0.112
JDR290	7.38	1.85	3.92	7.60	2.69	45.90	0.611	0.021
JDR291	7.61	1.93	3.94	6.45	3.06	48.56	0.542	0.023
JDR292	8.31	1.92	4.64	8.55	3.20	48.04	0.644	0.024
JDR293	7.39	1.84	3.97	6.79	3.37	46.21	0.611	0.023

JDR294	7.34	1.97	5.67	8.23	3.05	48.64	0.604	0.025
JDR295	4.81	1.66	6.25	9.22	1.50	33.45	0.390	0.014
JDR296	4.62	1.43	6.98	7.93	1.32	26.72	0.338	0.012
JDR297	4.49	1.53	7.00	8.79	1.62	29.45	0.430	0.012
JDR298	5.00	1.61	6.83	8.21	1.54	31.19	0.413	0.018
JDR299	5.20	1.69	7.14	6.63	1.70	28.62	0.406	0.011
JDR300	7.03	2.33	8.16	8.31	2.63	35.94	0.488	0.017
JDR301	5.22	1.38	3.43	8.34	2.40	29.90	0.499	0.009
JDR302	7.11	1.84	3.49	10.46	2.35	36.73	0.545	0.009
JDR304	5.85	1.70	3.78	9.10	2.49	31.41	0.496	0.010

anid	Na	Nd	Ni	Rb	Sb	Sc	Sm	Sr
JDR195	0.128	36.60	0.0	191.3	8.28	7.12	7.61	422
JDR196	0.090	30.57	0.0	187.4	5.70	5.36	5.80	479
JDR197	0.135	35.02	0.0	193.9	9.32	7.31	7.66	439
JDR198	0.136	35.84	0.0	185.0	8.40	6.90	7.17	363
JDR199	0.138	34.39	0.0	189.0	8.89	7.25	7.51	477
JDR200	0.370	35.99	0.0	239.7	4.49	12.44	7.47	0
JDR201	0.308	34.72	0.0	241.9	4.44	12.49	7.31	114
JDR202	0.318	35.71	0.0	235.1	4.65	11.59	7.16	0
JDR203	0.295	37.03	0.0	251.2	4.60	12.90	7.62	82
JDR204	0.311	32.56	0.0	235.1	4.39	11.74	7.11	84
JDR205	0.332	27.30	0.0	166.4	3.51	7.44	5.79	134
JDR206	0.307	28.51	0.0	156.7	3.61	6.95	5.78	102
JDR207	0.329	25.74	0.0	170.8	3.50	7.48	5.85	103
JDR208	0.318	29.74	0.0	167.5	3.85	7.49	6.02	128
JDR209	0.380	28.58	0.0	171.8	3.73	7.96	5.84	172
JDR210	0.946	49.26	0.0	253.2	3.77	15.02	9.36	168
JDR211	0.698	44.15	0.0	249.4	4.29	15.11	8.38	215
JDR212	0.600	41.15	87.2	255.5	4.54	15.73	8.24	205
JDR213	0.619	46.35	0.0	261.1	4.46	15.58	8.70	116
JDR214	0.671	43.19	0.0	257.2	4.16	15.45	8.20	170
JDR215	0.274	30.38	0.0	209.5	6.21	10.37	6.17	223
JDR216	0.292	32.31	0.0	207.8	5.98	10.74	6.12	169
JDR217	0.281	33.31	0.0	203.5	6.25	10.43	6.17	173
JDR218	0.274	27.84	0.0	201.3	6.11	10.12	5.96	203
JDR219	0.265	31.18	0.0	196.7	6.13	9.81	6.07	188
JDR220	0.309	29.52	0.0	213.0	9.43	11.54	6.36	129
JDR221	0.305	38.44	0.0	220.5	7.81	11.66	6.54	127
JDR222	0.305	38.36	0.0	216.8	8.60	11.65	6.52	125
JDR223	0.303	37.02	0.0	222.5	8.49	11.89	6.73	176
JDR224	0.292	32.99	0.0	223.8	7.75	11.77	6.34	135
JDR225	0.375	38.53	0.0	222.2	4.47	11.24	6.59	121
JDR226	0.345	36.30	0.0	217.0	4.46	11.15	6.59	75
JDR227	0.371	34.34	0.0	218.4	4.53	11.38	6.50	0
JDR228	0.347	33.75	0.0	220.3	4.83	11.40	6.60	0
JDR229	0.360	42.29	479.3	226.1	5.20	11.61	6.72	0
JDR230	0.298	39.09	0.0	233.0	2.37	12.25	6.64	0
JDR231	0.279	35.46	0.0	234.3	2.50	12.29	6.42	0
JDR232	0.254	33.93	0.0	239.2	2.89	12.76	6.45	0
JDR233	0.267	30.13	0.0	236.3	2.42	12.58	6.60	0
JDR234	0.272	34.24	0.0	239.4	2.64	12.70	6.57	77
JDR235	0.178	29.64	0.0	223.0	9.68	11.72	6.13	117
JDR236	0.190	28.98	0.0	220.5	10.62	11.44	5.93	0
JDR237	0.186	31.59	0.0	229.7	10.49	11.98	6.43	91
JDR238	0.173	32.42	0.0	223.7	10.82	11.50	6.29	104

JDR239	0.177	29.58	0.0	229.6	10.63	11.77	6.07	158
JDR240	0.436	38.21	0.0	226.5	5.33	12.63	6.68	116
JDR241	0.439	31.80	0.0	224.0	5.73	12.59	6.71	61
JDR242	0.402	32.12	0.0	212.4	5.72	11.78	6.41	73
JDR243	0.445	37.22	0.0	216.8	6.02	12.51	6.71	85
JDR244	0.430	36.17	0.0	218.6	5.27	12.35	6.63	107
JDR245	0.301	35.24	0.0	226.7	4.93	13.60	6.54	0
JDR246	0.335	40.86	0.0	233.8	5.23	13.78	6.72	0
JDR247	0.320	33.80	0.0	231.2	4.98	13.69	6.69	0
JDR248	0.301	32.09	0.0	239.4	5.17	14.01	6.70	0
JDR249	0.301	29.71	0.0	232.1	4.85	13.69	6.61	82
JDR250	0.378	44.65	0.0	128.3	2.92	11.93	6.68	1838
JDR251	0.371	41.77	0.0	119.1	2.59	10.74	6.05	1746
JDR252	0.147	24.55	0.0	80.9	1.54	8.08	4.41	3046
JDR253	0.392	48.07	0.0	109.5	2.41	10.55	6.05	1752
JDR254	0.348	37.57	0.0	116.4	2.62	11.04	6.26	1839
JDR255	0.624	38.73	0.0	145.4	3.63	11.02	6.45	1191
JDR256	0.633	39.26	0.0	144.1	3.89	11.31	6.87	2732
JDR257	0.637	38.19	0.0	144.7	3.38	11.22	6.71	1211
JDR258	0.629	44.09	0.0	138.2	3.99	11.27	6.94	1318
JDR259	0.586	37.57	36.5	136.7	3.39	11.45	6.80	1373
JDR260	0.750	40.20	0.0	137.2	3.12	9.65	6.17	647
JDR261	0.790	35.96	0.0	157.3	3.36	9.05	6.52	679
JDR262	0.724	41.96	0.0	144.0	3.28	9.52	6.49	716
JDR263	0.743	33.71	0.0	130.1	2.96	9.90	6.38	726
JDR264	0.696	37.56	0.0	137.6	3.20	9.80	6.60	790
JDR265	0.445	32.93	0.0	113.4	3.14	9.86	5.81	1930
JDR266	0.480	36.50	0.0	123.0	2.94	10.46	6.17	1585
JDR267	0.406	30.10	0.0	104.4	2.24	8.22	5.02	1602
JDR268	0.464	32.83	0.0	117.8	2.85	9.39	5.61	1781
JDR269	0.397	36.90	0.0	112.7	4.24	9.73	5.77	1801
JDR270	0.657	37.67	0.0	132.6	4.34	11.84	6.96	908
JDR271	0.764	40.84	84.3	139.5	4.83	11.37	6.84	785
JDR272	0.666	37.83	0.0	126.6	4.42	11.66	6.80	868
JDR273	0.635	36.59	0.0	135.4	5.03	11.43	6.90	799
JDR274	0.667	36.33	0.0	138.7	4.68	11.45	6.68	903
JDR275	0.134	26.59	0.0	75.3	1.48	7.92	4.45	4688
JDR276	0.065	13.43	0.0	36.9	0.67	3.90	2.24	14556
JDR277	0.101	23.71	0.0	69.6	1.30	7.38	4.06	3237
JDR278	0.067	10.40	0.0	26.7	0.50	2.81	1.60	2914
JDR279	0.105	25.03	0.0	76.4	1.41	7.75	4.38	5839
JDR289	0.213	20.97	0.0	35.2	33.01	8.80	3.51	211
JDR290	0.151	45.39	0.0	180.6	17.75	14.84	9.22	132
JDR291	0.159	49.98	0.0	185.9	17.91	14.51	9.64	124
JDR292	0.164	47.34	1784.0	204.3	20.66	17.21	9.62	177
JDR293	0.158	45.96	0.0	184.7	17.52	14.81	9.39	94

JDR294	0.165	45.70	0.0	193.5	21.78	17.48	9.86	0
JDR295	0.045	33.10	0.0	91.5	94.70	16.47	6.87	117
JDR296	0.044	36.42	0.0	85.7	114.53	14.96	5.98	76
JDR297	0.045	28.71	0.0	88.3	107.17	14.98	6.25	0
JDR298	0.044	34.09	0.0	91.1	108.65	16.34	6.78	0
JDR299	0.045	30.88	0.0	106.0	123.70	16.92	7.17	120
JDR300	0.049	46.54	0.0	145.5	129.94	19.46	9.27	130
JDR301	0.054	34.41	0.0	109.2	61.02	8.93	7.21	116
JDR302	0.056	43.22	0.0	113.4	65.86	12.16	9.29	258
JDR304	0.054	34.32	0.0	116.6	85.80	10.88	8.31	161

anid	Ta	Tb	Th	Ti	U	V	Yb	Zn	Zr
JDR195	0.98	0.94	10.65	1520	2.97	30.39	2.54	178.0	143.2
JDR196	1.10	0.57	11.43	1428	4.62	27.90	2.38	106.1	142.5
JDR197	0.95	0.88	10.87	1452	4.11	28.81	2.54	175.1	134.1
JDR198	0.93	0.80	10.56	1235	4.67	24.66	2.57	169.3	168.2
JDR199	0.97	0.90	10.90	2172	4.15	26.32	2.21	167.3	127.9
JDR200	0.98	0.87	14.82	2391	4.11	71.68	3.35	152.3	187.2
JDR201	1.10	0.80	14.68	1881	4.73	75.41	3.43	155.6	172.3
JDR202	1.11	0.91	15.24	2778	3.78	70.87	3.00	146.0	184.6
JDR203	1.08	0.86	15.72	2748	3.42	74.23	3.67	153.2	227.0
JDR204	1.06	0.87	15.67	1517	4.14	80.63	3.14	149.0	119.3
JDR205	0.91	0.74	11.76	3182	3.20	65.02	2.71	119.0	191.0
JDR206	0.90	0.72	10.47	2860	5.01	28.96	2.61	106.4	142.5
JDR207	0.98	0.73	10.99	2870	3.75	63.49	2.60	103.0	156.0
JDR208	0.89	0.79	10.95	1769	4.36	47.16	2.66	120.9	191.0
JDR209	0.93	0.71	11.06	2345	4.04	52.55	2.85	128.0	161.6
JDR210	1.04	0.99	14.24	5220	6.71	149.06	3.68	126.7	268.4
JDR211	0.94	1.04	13.98	4500	4.32	142.19	3.02	145.0	228.7
JDR212	0.91	0.92	13.78	4319	5.70	136.92	3.00	158.4	242.2
JDR213	0.93	0.93	15.00	5499	5.37	124.07	3.10	160.3	167.2
JDR214	0.91	0.88	14.10	4515	4.30	127.80	3.76	158.6	228.3
JDR215	0.89	0.81	11.97	2138	4.48	71.36	2.93	391.0	168.9
JDR216	0.93	0.82	12.27	2519	4.07	86.43	2.53	394.7	117.5
JDR217	0.83	0.77	11.85	3146	4.43	72.00	2.66	376.6	152.4
JDR218	0.84	0.75	11.43	2888	4.62	63.44	2.71	378.4	180.7
JDR219	0.85	0.74	11.47	2210	3.60	75.81	2.43	354.7	177.0
JDR220	0.85	0.83	13.12	2767	4.14	75.76	3.66	161.8	179.0
JDR221	0.96	0.79	12.94	2202	3.69	78.81	3.37	153.8	245.4
JDR222	0.94	0.81	14.12	2909	3.99	92.27	2.88	160.0	191.2
JDR223	0.93	0.92	13.18	2716	4.48	81.45	3.54	206.3	204.1
JDR224	0.95	0.82	12.99	3266	5.63	57.70	3.03	157.1	158.4
JDR225	0.91	0.81	14.11	2408	3.59	68.68	3.46	99.7	191.3
JDR226	0.93	0.77	14.03	2157	4.47	67.22	3.39	105.8	210.0
JDR227	1.00	0.83	13.14	2054	3.76	78.34	2.67	105.9	225.0
JDR228	0.93	1.02	12.60	2986	3.70	64.79	3.28	112.1	237.7
JDR229	1.00	0.83	13.62	1736	4.70	74.14	3.14	98.5	181.6
JDR230	0.90	0.80	13.30	2993	3.24	72.31	3.09	100.6	164.0
JDR231	0.93	0.74	13.18	2645	3.99	75.95	2.89	94.0	149.9
JDR232	0.92	0.74	13.13	2149	4.09	84.25	2.63	113.2	171.9
JDR233	0.94	0.78	13.69	2500	4.32	77.65	3.11	100.1	160.2
JDR234	0.86	0.93	13.16	2571	3.94	85.90	3.23	95.0	177.8
JDR235	0.84	0.76	12.38	3161	3.12	81.75	2.71	334.2	208.3
JDR236	0.87	0.72	11.77	2934	3.36	84.62	3.01	380.0	135.7
JDR237	0.83	0.64	12.94	2626	4.18	95.41	2.69	365.4	164.1
JDR238	0.96	0.77	12.23	2075	3.99	97.24	3.19	407.5	166.7

JDR239	0.82	0.74	12.12	2203	3.10	92.77	2.54	365.8	180.6
JDR240	1.01	0.86	13.70	4052	3.50	89.43	3.36	110.0	199.7
JDR241	0.96	0.78	13.23	2516	4.23	87.41	3.23	115.0	265.4
JDR242	0.94	0.78	13.26	3307	3.32	85.86	3.14	102.0	176.3
JDR243	0.92	0.77	13.40	3799	3.82	93.98	3.32	115.5	229.4
JDR244	0.96	0.75	13.30	3228	3.35	97.16	3.22	110.0	180.1
JDR245	0.92	0.82	14.48	2213	3.67	94.37	2.96	152.9	103.9
JDR246	0.90	0.86	14.38	2665	4.10	103.39	3.10	152.8	124.0
JDR247	0.88	0.82	14.10	2321	3.85	87.34	3.24	150.1	163.6
JDR248	0.89	0.82	14.04	2571	3.68	87.83	3.49	152.7	118.7
JDR249	0.90	0.83	14.00	2566	4.75	101.84	3.09	148.5	138.9
JDR250	0.81	0.64	11.09	4687	2.73	157.86	1.98	56.7	201.6
JDR251	0.75	0.61	9.99	4239	3.05	140.19	1.76	52.8	159.3
JDR252	0.52	0.40	7.08	3230	2.61	116.01	1.11	30.3	124.5
JDR253	0.76	0.57	9.82	4534	4.09	145.34	1.73	50.8	190.1
JDR254	0.74	0.55	10.00	4160	2.76	151.58	1.80	52.9	177.9
JDR255	0.84	0.57	10.40	4260	3.65	140.54	2.41	64.4	186.5
JDR256	0.81	0.59	12.02	4099	3.25	117.00	2.24	66.5	229.5
JDR257	0.83	0.62	10.40	5303	5.09	131.47	2.28	64.3	221.5
JDR258	0.84	0.68	10.70	4144	2.98	130.29	2.74	63.1	172.1
JDR259	0.86	0.68	10.68	4311	3.47	122.87	2.28	65.2	210.0
JDR260	0.87	0.81	10.30	4189	3.69	108.48	2.55	66.7	252.2
JDR261	0.94	0.75	11.09	2922	3.73	86.18	2.86	65.7	283.8
JDR262	0.91	0.70	11.83	5648	5.40	107.19	2.41	63.2	254.8
JDR263	0.91	0.65	11.30	4086	3.85	87.40	2.34	75.1	226.1
JDR264	0.88	0.77	10.93	3807	4.24	94.02	2.98	74.1	265.0
JDR265	0.72	0.58	9.33	5010	3.39	127.06	1.76	64.0	178.4
JDR266	0.77	0.54	9.98	5109	3.63	137.12	2.61	55.8	213.9
JDR267	0.62	0.54	8.44	4154	3.19	101.29	1.61	49.1	173.3
JDR268	0.73	0.59	9.15	4382	3.03	119.03	1.78	64.9	201.9
JDR269	0.72	0.62	9.74	3860	3.23	115.79	1.81	61.9	256.8
JDR270	0.91	0.73	12.03	3382	3.51	95.32	2.61	76.9	258.1
JDR271	0.88	0.71	11.92	4323	2.62	80.26	2.52	79.9	245.0
JDR272	0.97	0.71	10.59	4626	3.02	102.00	2.60	77.0	248.5
JDR273	1.07	0.69	10.76	4321	3.08	93.14	2.37	77.4	231.1
JDR274	0.88	0.70	10.42	4338	2.77	122.29	2.53	72.2	211.5
JDR275	0.48	0.36	6.88	2758	2.66	110.72	1.26	33.9	143.6
JDR276	0.26	0.24	3.42	1431	1.42	51.27	0.66	16.3	86.5
JDR277	0.41	0.34	6.38	2679	1.69	92.89	1.43	32.5	110.9
JDR278	0.18	0.15	2.59	1062	1.09	43.02	0.66	12.0	54.3
JDR279	0.41	0.39	6.62	2618	2.60	114.72	1.08	33.6	103.9
JDR289	0.42	0.52	2.55	5045	3.37	113.22	2.17	106.1	116.7
JDR290	1.03	1.28	16.21	3633	2.57	86.99	5.22	65.7	202.7
JDR291	1.04	1.23	15.42	3387	3.20	93.43	4.59	60.1	155.1
JDR292	1.20	1.34	17.22	4078	2.48	111.39	5.20	65.3	222.5
JDR293	1.07	1.19	15.64	4023	2.60	85.89	5.14	63.7	213.4

JDR294	1.16	1.40	17.13	3378	2.15	103.22	5.12	67.0	242.4
JDR295	0.96	0.74	8.16	10004	2.57	160.66	3.24	132.8	217.7
JDR296	0.85	0.72	6.56	8627	3.03	180.96	2.82	91.9	206.0
JDR297	0.87	0.77	7.63	9004	1.95	184.91	3.07	87.7	270.4
JDR298	1.03	1.03	7.83	9805	2.18	182.26	3.25	90.8	200.1
JDR299	0.84	0.79	7.05	7132	2.81	131.29	3.29	80.6	142.9
JDR300	1.00	1.15	8.07	10585	3.10	179.54	4.04	95.9	276.2
JDR301	0.90	1.01	7.73	5954	2.59	81.45	3.79	45.1	209.1
JDR302	1.22	1.13	10.18	6357	3.41	72.94	4.28	49.9	343.3
JDR304	1.41	1.00	8.64	5919	3.94	76.39	3.87	47.3	208.1

Appendix V: INAA elemental data for North American ochre sources in this study. Values are presented as ppm except hose marked as %. Values for Al, Ca, Dy, K, Mn, Ti and V are not reported for some samples as the short irradiations were not performed.

anid	Sample ID	Sample Location	City/County/State
JDR001		Petaluma, CA #4	Sonoma Co., CA
JDR002		Placedor Gulch	Eastern Oregon
JDR003		Dayville, OR	Grant Co., OR
JDR004		Grimes Canyon #2	Ventura Co., CA
JDR005		Grimes Canyon #1	Ventura Co., CA
JDR006		New Almaden, Santa Clara #1	Santa Clara Co., CA
JDR007		Cape Perpetua #1	Lincoln Co., OR
JDR008		Murderer's Creek	Grant Co., OR
JDR009		New Almaden, Santa Clara #2	Santa Clara Co., CA
JDR010		Catlinite, Pipestone #2	Pipestone Co., MN
JDR011		Redwood Ochre B	Oakland, Alameda Co., CA
JDR012		Redwood Ochre C	Oakland, Alameda Co., CA
JDR013		Redwood Ochre A	Oakland, Alameda Co., CA
JDR014		Catlinite, Pipestone #1	Pipestone Co., MN
JDR015		China Creek	Lane Co, OR
JDR016		Tajiguas	Santa Barbara Co., CA
JDR017		Blue Mountain	NE OR
JDR018		Sunrise Mine	WY
JDR019		Gold Harbor	Dall Island, SE AK
JDR020		Minam Grade	Wallowa Co, OR
JDR021		Sulphur Bank	San Francisco, CA
JDR022		Red Rock Quarry	San Luis Obispo Co, CA
JDR031	94-17-130		Northern CA
JDR032	94-23-607		Northern CA
JDR033	94-23-622		Northern CA
JDR034	94-24-475		Northern CA
JDR035	94-24-479		Northern CA
JDR036	94-24-488		Northern CA
JDR037	94-24-504		Northern CA
JDR038	94-24-512		Northern CA
JDR039	CA-NAP-39 Unit 7-77		Napa Co., CA
JDR040	CA-NAP-39 Unit 9-118		Napa Co., CA
JDR041	CA-NAP-39 Unit 16		Napa Co., CA
JDR042		Big Creek	Lane Co, OR
JDR043		Running Springs	San Miguel Island, CA
JDR044	AN-1997-134.60		Alaska
JDR045	AN-1998-73.180		Alaska
JDR046	AN-1998-73.496		Alaska
JDR047	AN-1998-73.606		Alaska
JDR048	AN-2000-29.269		Alaska
JDR049	AN-2000-29.682		Alaska
JDR050	AN-2000-29.714		Alaska

anid	Al (%)	As	Ba	Ca (%)	Ce	Co	Cr	Cs
JDR001	0.00	4.1	351.6	0.00	60.5	20.6	26.4	10.07
JDR002	0.00	0.0	828.8	0.00	35.9	17.2	27.9	0.27
JDR003	0.00	4.3	0.0	0.00	34.1	23.6	40.0	3.56
JDR004	0.00	16.0	1030.7	0.00	46.8	9.5	185.1	4.08
JDR005	0.00	25.9	636.6	0.00	53.1	5.9	324.8	4.79
JDR006	0.00	120.2	0.0	0.00	3.6	32.1	3349.7	9.61
JDR007	0.00	0.0	382.9	0.00	80.9	17.9	6.2	0.41
JDR008	0.00	0.0	247.3	0.00	42.3	19.9	29.1	2.49
JDR009	0.00	102.9	0.0	0.00	4.8	36.6	3144.6	7.02
JDR010	0.00	3.4	304.1	0.00	107.8	1.1	38.8	0.19
JDR011	0.00	54.3	448.0	0.00	3.0	2.3	52.0	0.37
JDR012	0.00	1041.3	449.2	0.00	1.9	6.1	30.1	1.76
JDR013	0.00	45.3	135.3	0.00	5.1	1.2	51.1	4.07
JDR014	0.00	10.6	166.2	0.00	179.9	5.0	19.5	1.30
JDR015	0.00	9.5	492.6	0.00	92.8	10.3	175.6	3.13
JDR016	0.00	40.6	966.2	0.00	19.1	6.1	138.3	2.32
JDR017	0.00	0.0	392.1	0.00	32.0	5.8	11.2	1.90
JDR018	0.00	161.4	355.8	0.00	11.0	208.7	44.4	55.77
JDR019	0.00	26.1	1716.7	0.00	71.9	26.4	93.6	3.57
JDR020	0.00	0.0	892.3	0.00	94.6	55.2	11.3	3.28
JDR021	0.00	125.8	232.4	0.00	15.7	0.3	255.1	0.00
JDR022	0.00	14.0	298.8	0.00	14.1	34.5	163.2	0.72
JDR023	0.00	3.1	968.4	0.00	63.6	1.4	7.7	5.12
JDR024	0.00	4.0	867.7	0.00	62.0	1.4	5.4	5.13
JDR025	0.00	4.9	989.9	0.00	64.3	1.5	6.9	5.43
JDR026	0.00	6.1	894.2	0.00	63.4	1.5	5.8	5.19
JDR031	12.85	33.6	527.8	0.50	23.5	26.5	81.0	1.78
JDR032	8.01	4.8	851.6	0.35	23.7	46.0	11.3	5.88
JDR033	8.30	19.3	0.0	0.52	44.0	16.9	58.4	1.33
JDR034	7.30	0.0	940.0	1.17	13.0	7.5	31.6	4.56
JDR035	7.24	8.6	758.3	1.43	17.5	6.7	20.9	5.61
JDR036	9.16	0.0	447.9	2.73	30.2	24.3	47.1	2.65
JDR037	8.80	0.0	197.8	0.29	18.3	23.9	100.2	1.72
JDR038	7.85	0.0	358.5	0.46	28.4	12.5	68.4	4.18
JDR039	10.18	0.0	413.7	1.07	42.9	21.3	28.1	1.69
JDR040	9.66	0.0	675.5	1.73	19.0	24.2	33.1	1.64
JDR041	9.10	29.6	659.2	1.79	36.5	43.3	72.8	0.45
JDR042	10.93	0.0	0.0	0.67	48.8	28.1	16.0	0.62
JDR043	9.11	6.6	619.3	1.26	51.2	16.6	93.3	2.48
JDR044	6.01	10.2	388.6	0.27	12.1	6.6	18.3	1.99
JDR045	10.95	19.0	280.6	2.05	188.4	14.1	211.8	4.16
JDR046	10.33	22.0	320.6	1.78	226.9	22.4	141.1	5.66
JDR047	5.10	5.0	318.8	22.15	22.7	7.8	31.9	1.12
JDR048	10.21	7.8	463.4	1.33	31.8	19.5	43.5	1.38
JDR049	8.25	4.9	92.5	0.25	250.0	30.5	167.0	0.54
JDR050	9.93	15.5	262.1	0.56	9.6	20.5	44.6	2.75

anid	Dy	Eu	Fe (%)	Hf	K (%)	La	Lu	Mn (%)	Na (%)
JDR001	0.00	2.617	7.11	6.96	0.000	31.6	1.126	0.000	1.607
JDR002	0.00	1.502	6.10	4.21	0.000	17.8	0.644	0.000	2.132
JDR003	0.00	2.093	8.36	6.41	0.000	23.0	0.509	0.000	0.926
JDR004	0.00	0.783	3.35	2.72	0.000	26.5	0.250	0.000	1.207
JDR005	0.00	0.698	2.51	2.92	0.000	24.3	0.000	0.000	1.273
JDR006	0.00	0.165	53.87	2.68	0.000	2.1	0.240	0.000	0.018
JDR007	0.00	2.659	5.55	9.25	0.000	38.4	0.284	0.000	2.681
JDR008	0.00	1.503	6.69	8.09	0.000	21.1	0.650	0.000	1.270
JDR009	0.00	0.185	55.58	2.27	0.000	2.8	0.187	0.000	0.000
JDR010	0.00	1.121	3.14	26.57	0.000	29.0	2.683	0.000	0.070
JDR011	0.00	0.147	30.01	1.23	0.000	1.8	0.113	0.000	0.130
JDR012	0.00	0.000	53.36	0.96	0.000	1.5	0.165	0.000	0.030
JDR013	0.00	0.088	45.74	1.52	0.000	3.1	0.132	0.000	0.041
JDR014	0.00	2.834	3.09	12.70	0.000	108.1	0.927	0.000	0.031
JDR015	0.00	1.844	5.80	9.57	0.000	44.1	0.355	0.000	0.824
JDR016	0.00	0.418	9.90	2.00	0.000	9.7	0.171	0.000	0.997
JDR017	0.00	0.605	2.15	3.85	0.000	10.6	0.237	0.000	0.932
JDR018	0.00	3.948	65.96	1.66	0.000	6.4	0.246	0.000	0.000
JDR019	0.00	2.586	9.55	6.50	0.000	62.6	0.757	0.000	0.231
JDR020	0.00	2.873	14.32	8.50	0.000	40.2	0.910	0.000	0.183
JDR021	0.00	0.399	25.33	3.10	0.000	8.9	0.000	0.000	0.294
JDR022	0.00	0.378	13.32	0.93	0.000	7.2	0.237	0.000	0.210
JDR023	0.00	0.804	1.46	8.09	0.000	30.7	0.709	0.000	3.462
JDR024	0.00	0.750	1.42	7.88	0.000	29.7	0.716	0.000	3.368
JDR025	0.00	0.788	1.45	8.13	0.000	31.0	0.785	0.000	3.526
JDR026	0.00	0.775	1.43	7.99	0.000	30.4	0.654	0.000	3.382
JDR031	2.29	0.537	4.53	6.29	1.206	12.0	0.194	0.029	0.186
JDR032	6.09	1.375	10.81	7.14	1.451	9.5	0.574	0.065	0.127
JDR033	4.72	1.518	17.82	7.59	0.000	19.5	0.510	0.147	0.150
JDR034	2.55	1.551	14.39	7.04	1.855	9.0	0.201	0.050	1.779
JDR035	2.31	1.566	10.94	7.09	1.568	10.0	0.219	0.064	2.060
JDR036	5.44	1.599	10.18	6.99	1.486	14.4	0.526	0.120	2.158
JDR037	4.99	1.228	24.07	8.01	0.788	31.6	0.444	0.093	0.221
JDR038	6.41	2.055	14.55	12.61	0.681	74.8	0.472	0.068	0.349
JDR039	2.69	0.802	9.19	6.43	1.318	14.3	0.308	0.097	1.120
JDR040	3.23	0.598	8.91	7.09	1.092	9.1	0.277	0.149	1.432
JDR041	6.87	1.704	16.34	7.43	0.854	20.0	0.417	0.330	1.278
JDR042	11.28	4.622	13.96	10.47	0.911	64.3	0.673	0.080	0.262
JDR043	3.84	0.960	5.03	5.45	1.510	22.6	0.388	0.031	1.853
JDR044	1.86	0.363	2.20	2.77	1.636	4.1	0.176	0.014	1.219
JDR045	4.23	2.936	6.15	3.88	2.594	95.2	0.325	0.069	3.133
JDR046	4.81	3.038	5.78	4.42	2.688	102.4	0.313	0.229	2.801
JDR047	2.51	0.643	2.73	1.89	1.079	11.7	0.141	0.049	0.946
JDR048	3.09	0.784	5.96	4.65	0.858	13.0	0.311	0.049	2.428
JDR049	3.60	3.839	7.58	2.61	0.897	126.0	0.269	0.183	4.254
JDR050	2.79	0.627	8.77	5.09	1.543	9.3	0.405	0.058	2.091

anid	Nd	Ni	Rb	Sb	Sc	Sm	Sr	Ta
JDR001	43.62	0.0	27.2	0.40	27.61	9.65	266.8	1.145
JDR002	23.74	0.0	10.1	0.35	22.12	5.19	420.8	0.752
JDR003	21.73	0.0	40.3	0.53	30.12	7.43	184.8	1.326
JDR004	25.86	0.0	68.1	10.46	10.18	4.68	490.2	0.626
JDR005	21.42	0.0	73.2	11.73	8.03	8.32	214.2	0.776
JDR006	0.00	0.0	30.9	8.61	6.96	0.53	0.0	0.000
JDR007	31.28	0.0	31.7	0.44	22.06	8.36	492.5	3.747
JDR008	26.14	0.0	18.8	0.47	22.33	5.64	308.5	1.189
JDR009	0.00	0.0	41.8	6.72	6.58	0.60	0.0	0.257
JDR010	21.81	0.0	100.8	1.81	16.52	7.10	0.0	4.619
JDR011	0.00	0.0	7.2	2.70	6.24	0.53	0.0	0.000
JDR012	0.00	0.0	0.0	11.49	8.81	0.33	0.0	0.000
JDR013	0.00	0.0	33.0	4.28	9.46	0.54	0.0	0.000
JDR014	86.31	0.0	13.8	0.98	11.63	16.23	93.0	2.885
JDR015	34.84	0.0	33.4	0.66	17.30	7.45	133.8	3.066
JDR016	0.00	0.0	35.8	9.37	7.31	2.14	228.8	0.385
JDR017	15.09	0.0	28.1	0.19	8.92	2.66	128.8	0.324
JDR018	41.37	0.0	641.7	2.26	64.27	16.78	2859.4	0.000
JDR019	47.97	0.0	47.1	4.55	34.41	10.27	0.0	1.020
JDR020	45.19	0.0	32.0	0.00	56.01	10.90	0.0	1.234
JDR021	8.73	0.0	39.0	1.34	5.10	1.71	262.0	0.412
JDR022	4.72	0.0	0.0	2.39	9.57	1.49	0.0	0.149
JDR023	24.78	0.0	127.2	1.91	5.06	6.09	67.4	1.337
JDR024	25.34	0.0	124.3	1.35	4.96	5.92	0.0	1.272
JDR025	27.78	0.0	125.3	3.02	5.10	6.24	70.4	1.287
JDR026	27.98	0.0	125.7	1.51	5.04	6.03	0.0	1.335
JDR031	12.13	158.0	45.5	2.48	25.67	2.73	0.0	1.053
JDR032	16.64	0.0	146.4	0.74	56.50	4.60	0.0	1.073
JDR033	23.78	0.0	26.0	1.53	57.46	6.46	0.0	1.064
JDR034	13.36	102.7	86.5	1.09	32.06	2.93	0.0	1.048
JDR035	10.85	0.0	100.5	0.75	32.84	2.63	121.4	1.066
JDR036	20.41	61.1	63.0	0.00	32.32	5.23	114.5	0.922
JDR037	18.55	0.0	37.9	1.36	56.81	4.79	0.0	1.138
JDR038	56.38	0.0	47.6	1.51	48.56	10.34	0.0	1.960
JDR039	12.69	84.9	59.9	1.00	23.46	3.18	97.4	1.029
JDR040	6.47	0.0	70.3	0.91	22.72	2.57	201.1	1.283
JDR041	24.53	0.0	26.6	1.22	29.55	6.89	176.9	1.527
JDR042	59.85	0.0	29.8	0.00	18.82	13.50	0.0	4.415
JDR043	19.75	62.1	59.5	0.94	12.92	4.21	240.9	0.953
JDR044	8.30	0.0	48.6	1.42	7.01	1.56	0.0	0.165
JDR045	88.00	0.0	179.5	0.79	19.89	11.67	490.9	6.470
JDR046	90.88	0.0	165.7	1.28	21.40	11.67	547.9	6.874
JDR047	14.65	0.0	33.3	0.56	8.76	2.67	302.3	0.240
JDR048	15.39	0.0	38.6	0.90	13.62	3.01	439.4	0.466
JDR049	122.52	91.4	47.3	0.84	21.90	16.73	152.0	6.248
JDR050	0.00	0.0	64.3	1.18	17.76	2.33	232.1	0.402

anid	Tb	Th	Ti (%)	U	V	Yb	Zn	Zr
JDR001	1.913	6.14	0.000	2.22	0.0	7.38	168.0	177.2
JDR002	0.883	2.87	0.000	0.00	0.0	4.41	171.4	132.1
JDR003	1.148	4.10	0.000	4.05	0.0	3.36	129.4	221.2
JDR004	0.427	9.02	0.000	16.36	0.0	1.79	231.5	160.6
JDR005	0.511	9.34	0.000	59.43	0.0	1.34	458.9	444.0
JDR006	0.000	2.20	0.000	0.00	0.0	1.83	36.5	0.0
JDR007	1.107	4.86	0.000	0.00	0.0	2.19	124.4	301.1
JDR008	0.953	7.32	0.000	0.00	0.0	3.93	93.8	192.0
JDR009	0.000	1.80	0.000	0.00	0.0	1.43	30.7	0.0
JDR010	2.291	57.04	0.000	11.05	0.0	19.32	0.0	592.4
JDR011	0.234	2.38	0.000	0.00	0.0	0.82	0.0	0.0
JDR012	0.000	2.19	0.000	0.00	0.0	0.82	365.6	0.0
JDR013	0.000	2.87	0.000	0.63	0.0	0.96	104.6	0.0
JDR014	2.075	40.82	0.000	5.96	0.0	6.89	54.2	382.8
JDR015	1.037	11.58	0.000	5.03	0.0	2.60	66.9	325.4
JDR016	0.341	3.51	0.000	3.55	0.0	1.28	136.2	97.7
JDR017	0.419	3.33	0.000	1.25	0.0	1.52	44.4	102.7
JDR018	0.627	1.45	0.000	6.98	0.0	1.89	6938.6	0.0
JDR019	1.409	8.74	0.000	5.54	0.0	5.22	474.5	319.5
JDR020	1.850	7.67	0.000	5.02	0.0	6.03	234.0	225.9
JDR021	0.000	6.16	0.000	1.88	0.0	0.00	0.0	0.0
JDR022	0.000	1.55	0.000	0.00	0.0	1.47	151.8	0.0
JDR023	1.062	12.13	0.000	5.51	0.0	4.54	51.8	251.1
JDR024	1.041	11.75	0.000	6.50	0.0	4.26	48.5	233.3
JDR025	1.058	12.25	0.000	5.38	0.0	5.00	50.2	234.8
JDR026	1.106	11.89	0.000	5.12	0.0	4.75	49.7	234.3
JDR031	0.396	8.05	1.440	2.40	120.9	1.84	62.0	231.3
JDR032	0.779	7.80	1.784	4.72	197.3	3.54	320.4	294.8
JDR033	0.887	8.09	1.798	6.50	266.7	3.18	101.4	219.0
JDR034	0.359	7.20	0.819	3.59	104.0	1.32	115.9	185.5
JDR035	0.443	7.28	0.828	2.28	94.4	1.30	133.0	188.0
JDR036	1.066	5.71	1.427	2.55	271.8	3.47	176.3	208.4
JDR037	0.682	6.94	2.112	2.56	415.4	3.47	83.6	270.3
JDR038	1.187	11.17	1.628	6.69	271.6	3.26	140.3	326.7
JDR039	0.361	7.34	1.431	2.39	146.7	2.22	87.5	207.0
JDR040	0.378	5.95	1.384	1.24	112.9	1.65	105.5	190.1
JDR041	1.034	4.56	1.649	0.00	233.8	3.17	103.8	224.3
JDR042	2.033	5.65	2.463	2.55	172.6	5.02	87.3	329.9
JDR043	0.665	12.73	0.464	1.66	62.4	2.69	92.6	100.6
JDR044	0.182	2.05	0.280	2.18	131.9	1.62	42.8	0.0
JDR045	0.767	14.76	1.317	4.89	346.9	1.71	67.7	289.3
JDR046	0.926	8.50	1.324	8.28	299.3	1.95	54.4	292.9
JDR047	0.409	2.60	0.267	3.18	92.2	1.41	66.6	107.7
JDR048	0.362	3.73	0.638	3.70	203.8	2.48	68.2	233.9
JDR049	0.753	29.93	1.204	0.00	124.7	2.15	87.5	140.7
JDR050	0.349	6.12	0.390	4.29	191.8	2.56	87.1	154.7

Appendix VI: Elemental data for obsidian from Peru by PXRF. Data are presented as ppm.

ID	Sr	Rb	Zr	Zn	Fe	Mn	Source
OBS-14	49	248	126	37	4865	674	Chivay
OBS-33	48	259	128	34	4869	661	Chivay
OBS-83	68	253	78	29	4900	671	Chivay
OBS-104	56	240	80	30	4932	661	Chivay
OBS-107	36	260	121	33	4882	668	Chivay
OBS-137	60	225	98	34	4908	675	Chivay
OBS-167	53	249	98	32	4886	681	Chivay
OBS-171	155	117	161	25	5130	412	Unknown
OBS-176	49	264	125	33	4852	677	Chivay
OBS-199	52	280	132	27	4832	677	Chivay
OBS-237	61	261	121	31	4865	661	Chivay
OBS-246	74	271	118	31	4802	704	Chivay
OBS-248	49	242	91	38	4901	678	Chivay
OBS-276	85	275	101	34	4797	709	Chivay
OBS-277	95	273	106	33	4771	722	Chivay
OBS-300	50	310	119	35	4831	655	Chivay
OBS-309	41	245	108	32	4904	671	Chivay
OBS-343	67	249	121	34	4843	686	Chivay
OBS-347	58	300	172	35	4779	656	Chivay
OBS-363	55	228	116	35	4841	725	Chivay
OBS-367	93	241	131	32	4826	678	Chivay
OBS-394	55	224	109	27	4950	635	Chivay
OBS-396	58	247	119	32	4873	670	Chivay
OBS-399	77	265	147	30	4821	660	Chivay
OBS-436	96	272	131	33	4805	662	Chivay
OBS-462	68	253	79	35	4897	667	Chivay
OBS-465	82	267	121	32	4816	683	Chivay
OBS-485	38	233	131	29	4906	662	Chivay
OBS-487	63	250	139	34	4833	681	Chivay
OBS-494	71	270	129	35	4827	668	Chivay
OBS-499	72	282	70	36	4838	701	Chivay
OBS-526	81	286	85	32	4855	660	Chivay
OBS-544	77	258	83	32	4873	676	Chivay
OBS-591	72	282	70	36	4838	701	Chivay
OBS-607	79	254	98	29	4856	684	Chivay
OBS-622	65	268	88	35	4834	710	Chivay
OBS-625	72	250	101	39	4874	664	Chivay
OBS-630	36	246	94	29	4903	692	Chivay
OBS-634	62	275	95	33	4849	686	Chivay
OBS-645	51	240	85	31	4901	692	Chivay
OBS-646	46	225	94	29	4949	657	Chivay
OBS-662	79	264	112	31	4821	694	Chivay
OBS-664	87	302	122	32	4786	671	Chivay
OBS-665	58	252	122	30	4861	677	Chivay
OBS-671	87	302	122	32	4786	671	Chivay
OBS-676	64	250	91	36	4856	703	Chivay

OBS-681	63	262	124	32	4826	693	Chivay
OBS-686	39	240	150	30	4883	658	Chivay
OBS-687	48	244	100	39	4904	665	Chivay
OBS-694	90	282	181	30	4733	684	Chivay
OBS-695	238	173	130	27	4864	568	Unknown
OBS-723	69	265	106	37	4840	684	Chivay
OBS-725	76	267	107	32	4858	660	Chivay
OBS-745	51	246	77	28	4890	708	Chivay
OBS-751	62	243	99	29	4927	640	Chivay
OBS-752	74	270	126	32	4854	644	Chivay
OBS-766	44	268	126	34	4852	675	Chivay
OBS-767	48	208	98	31	4951	664	Chivay
OBS-773	64	244	118	29	4871	674	Chivay
OBS-783	57	239	169	33	4822	681	Chivay
OBS-786	48	280	131	36	4823	682	Chivay
OBS-793	41	229	108	34	4901	687	Chivay
OBS-841	78	262	126	39	4825	670	Chivay
OBS-846	68	240	104	34	4862	692	Chivay
OBS-853	63	247	82	34	4917	656	Chivay
OBS-858	49	234	115	35	4897	670	Chivay
OBS-860	53	238	135	32	4879	662	Chivay
OBS-899	67	224	64	31	4923	692	Chivay

References

1. Tite, M. S., Archaeological Chemistry. *Accounts of Chemical Research* **2002,** 35, (8), 583-584.
2. McGovern, P. E.; Sever, T. L.; Myers, J. W.; Myers, E. E.; Bevan, B.; Miller, N. F.; Bottema, S.; Hongo, H.; Meadow, R. H.; Kuniholm, P. I.; Bowman, S. G. E.; Leese, M. N.; Hedges, R. E. M.; Matson, F. R.; Freestone, I. C.; Vaughan, S. J.; Henderson, J.; Vandiver, P. B.; Tumosa, C. S.; Beck, C. W.; Smith, P.; Child, A. M.; Pollard, A. M.; Thuesen, I.; Sease, C., Science in Archaeology: A Review. *American Journal of Archaeology* **1995,** 99, (1), 79-142.
3. Ciliberto, E.; Spoto, G., *Modern analytical methods in art and archaeology*. Wiley-Interscience: New York, 2000; p xxiv, 755 p.
4. Brothwell, D. R.; Pollard, A. M., *Handbook of archaeological sciences*. Wiley: New York, 2001; p xx, 762 p.
5. Killick, D.; Young, S. M. M., Archaeology and archaeometry: from casual dating to a meaningful relationship? *Antiquity* **1997,** 71, (273), 518-524.
6. Lambert, J. B., *Traces of the past: unraveling the secrets of archaeology through chemistry*. Addison-Wesley: Reading, Mass., 1997; p 319 p.
7. Gill, R., *Modern analytical geochemistry: an introduction to quantitative chemical analysis for earth, environmental, and materials scientists*. Longman: Harlow, England, 1997; p x, 329 p.
8. Taylor, L.; Papp, R. B.; Pollard, B. D., *Instrumental methods for determining elements*. VCH: New York, 1994; p ix, 322 p.
9. Janssens, K.; Vittiglio, G.; Deraedt, I.; Aerts, A.; Vekemans, B.; Vincze, L.; Wei, F.; Deryck, I.; Schalm, O.; Adams, F.; Rindby, A.; Knochel, A.; Simionovici, A.; Snigirev, A., Use of microscopic XRF for non-destructive analysis in art and archaeometry. *X-Ray Spectrometry* **2000,** 29, (1), 73-91.
10. Bishop, R. L.; Canouts, V.; Crown, P. L.; de Atley, S. P., Sensitivity, Precision, and Accuracy: Their Roles in Ceramic Compositional Data Bases. **1990,** 55, (3).
11. Loveland, W. D.; Morrissey, D. J.; Seaborg, G. T., *Modern nuclear chemistry*. Wiley-Interscience: Hoboken, N.J., 2006; p xvi, 671 p.
12. Munita, C. S.; Paiva, R. P.; Alves, M. A.; de Oliveria, P. M. S.; Momose, E. F., Contribution of neutron activation analysis to archaeological studies. *Journal of Trace and Microprobe Techniques* **2000,** 18, (3), 381-387.
13. Glascock, M., Characterization of Archaeological Ceramics at MURR by Neutron Activation Analysis and Multivariate Statistics. In *Chemical Characterization of Ceramic Pastes in Archaeology*, Neff, H., Ed. Prehistory Press: Madison, 1992; pp 11-26.
14. Harbottle, G., Neutron activation analysis in archaeological chemistry. In *Chemical applications of nuclear probes*, Yoshihara, K., Ed. Springer-Verlag: Berlin, 1990; pp 59-91.
15. Soete, D. d.; Gijbels, R.; Hoste, J., *Neutron activation analysis*. Wiley-Interscience: London, New York,, 1972; p xx, 836 p.
16. Glascock, M. D., *Tables for Neutron Activation Analysis*. Fifth Edition ed.; Research Reactor Center, University of Missouri-Columbia: Columbia, Missouri, 2004; p 150.
17. Johansson, S. A. E.; Campbell, J. L., *PIXE: A Novel Technique for Elemental Analysis*. John Wiley and Sons: Chichester, 1988.

18. Johansson, S. A. E.; Campbell, J. L.; Malmqvist, K. G., *Particle-Induced X-Ray Emission Spectrometry (PIXE)*. John Wiley and Sons Inc.: New York, 1995; Vol. 133.
19. Pappalardo, L., A portable PIXE system for the in situ characterization of black and red pigments in neolithic, copper age and bronze age pottery. *Nuclear Instruments & Methods in Physics Research, Section B: Beam Interactions with Materials and Atoms* **1999,** 150, (1-4), 576-580.
20. Pappalardo, L.; Karydas, A. G.; Kotzamani, N.; Pappalardo, G.; Romano, F. P.; Zarkadas, C., Complementary use of PIXE-alpha and XRF portable systems for the non-destructive and in situ characterization of gemstones in museums. *Nuclear Instruments and Methods in Physics Research, Section B: Beam Interactions with Materials and Atoms* **2005,** 239, (1-2), 114-121.
21. Pappalardo, L.; Romano, F. P.; Garraffo, S.; De Sanoit, J.; Marchetta, C.; Pappalardo, G., The improved LNS PIXE-alpha portable system: Archaeometric applications. *Archaeometry* **2003,** 45, (2), 333-339.
22. Wong, A. S.; Robertson, J. D., Multi-Elemental Analysis of Coal and its By-Products by Simultaneous Proton-Induced Gamma-Ray/X-ray Emission Analysis. *Journal of Coal Quality* **1993,** 12, (4), 146-150.
23. Pappalardo, G.; de Sanoit, J.; Musumarra, A.; Calvi, G.; Marchetta, C., Feasibility study of a portable PIXE system using a 210Po alpha source. *Nuclear Instruments & Methods in Physics Research, Section B: Beam Interactions with Materials and Atoms* **1996,** 109/110, 214-217.
24. Neelmeijer, C.; Brissaud, I.; Calligaro, T.; Demortier, G.; Hautojarvi, A.; Mader, M.; Martinot, L.; Schreiner, M.; Tuurnala, T.; Weber, G., Paintings-a challenge for XRF and PIXE analysis. *X-Ray Spectrometry* **2000,** 29, (1), 101-110.
25. Zucchiati, A.; Prati, P.; Bouquillon, A.; Giuntini, L.; Massi, M.; Migliori, A.; Cagnana, A.; Roascio, S., Characterization of early medieval frescoes by micro-PIXE, SEM and Raman spectroscopy. *Nuclear Instruments & Methods in Physics Research, Section B: Beam Interactions with Materials and Atoms* **2004,** 219-220, 20-25.
26. Menu, M.; Walter, P., Prehistoric Cave Painting PIXE Analysis for the Identification of Paint "Pots". *Nuclear Instruments and Methods in Physics Research B* **1992,** B64, 547-552.
27. Demortier, G.; Ruvalcaba-Sil, J. L., Quantitative ion beam analysis of complex gold-based artefacts. *Nuclear Instruments and Methods in Physics Research, Section B: Beam Interactions with Materials and Atoms* **2005,** 239, (1-2), 1-15.
28. Pages-Camagna, S.; Calligaro, T., Micro-PIXE and micro-Raman spectrometry applied to a polychrome wooden altarpiece from the 16th century. *Journal of Raman Spectroscopy* **2004,** 35, 633-639.
29. Ontalba Salamanca, M. A.; Ruvalcaba-Sil, J. L.; Bucio, L.; Manzanilla, L.; Miranda, J., Ion beam analysis of pottery from Teotihuacan, Mexico. *Nuclear Instruments & Methods in Physics Research, Section B: Beam Interactions with Materials and Atoms* **2000,** 161-163, 762-768.
30. Chen, T.-H.; Calligaro, T.; Pages-Camagna, S.; Menu, M., Investigation of Chinese archaic jade by PIXE and micro-Raman spectrometry. *Applied Physics A* **2004,** 79, 177-180.
31. Malmqvist, K. G., Comparison between PIXE and XRF for applications in art and archaeology. *Nuclear Instruments and Methods in Physics Research, Section B: Beam Interactions with Materials and Atoms* **1985,** 14, (1), 86-92.

32. Chalmin, E.; Vignaud, C.; Menu, M., Palaeolithic painting matter: Natural or heat-treated pigment? *Applied Physics A: Materials Science and Processing* **2004,** 79, (2), 187-191.
33. Chalmin, E.; Menu, M.; Vignaud, C., Analysis of rock art painting and technology of Palaeolithic painters. *Measurement Science and Technology* **2003,** 14, (9), 1590-1597.
34. Pomie?s, M. P.; Menu, M.; Vignaud, C., Red Palaeolithic pigments: Natural hematite or heated goethite? *Archaeometry* **1999,** 41\, (2\), 275\-285\.
35. Amsel, G.; Menu, M.; Moulin, J.; Salomon, J., 2 MV tandem Pelletron accelerator of the Louvre Museum. *Nuclear Instruments and Methods in Physics Research, Section B: Beam Interactions with Materials and Atoms* **1990,** 45, (1-4), 296-301.
36. Maxwell, J. A.; Campbell, J. L.; Teesdale, W. J., The Guelph PIXE software package. *Nuclear Instruments & Methods in Physics Research, Section B: Beam Interactions with Materials and Atoms* **1989,** B43, (2), 218-30.
37. Robertson, J. D.; Neff, H.; Higgins, B., Microanalysis of ceramics with PIXE and LA-ICP-MS. *Nuclear Instruments and Methods in Physics Research, Section B: Beam Interactions with Materials and Atoms* **2002,** 189, (1-4), 378-381.
38. Papp, R. B., X-ray Fluorescence Spectrometry. In *Instrumental methods for determining elements*, Taylor, L.; Papp, R. B.; Pollard, B. D., Eds. VCH: New York, 1994; pp 211-255.
39. Spectro http://www.spectro.com/pages/e/p010504.htm (July 15),
40. Punyadeera, C.; Pillay, A. E.; Jacobson, L.; Whitelaw, G., Application of XRF and correspondence analysis to provenance studies of coastal and inland archaeological pottery from the Mngeni river area, South Africa. *X-Ray Spectrometry* **1997,** 26, (5), 249-256.
41. Padilla, R.; Espen, P. V.; Torres, P. P. G., The suitability of XRF analysis for compositional classification of archaeological ceramic fabric: A comparison with a previous NAA study. *Analytica Chimica Acta* **2006,** 558, (1-2), 283-289.
42. Romano, F. P.; Pappalardo, G.; Pappalardo, L.; Garraffo, S.; Gigli, R.; Pautasso, A., Quantitative non-destructive determination of trace elements in archaeological pottery using a portable beam stability-controlled XRF spectrometer. *X-Ray Spectrometry* **2006,** 35, (1), 1-7.
43. Leung, P. L.; Stokes, M. J.; Li, M. T. W.; Peng, Z.; Wu, S., EDXRF Studies on the Chemical Composition of Ancient Porcelain Bodies from Linjiang, Jiangxi, China. *X-Ray Spectrometry* **1998,** 27, (1), 11-16.
44. Jenkins, R.; Gould, R. W.; Gedcke, D., *Quantitative X-ray spectrometry*. 2nd ed.; M. Dekker: New York, 1995; p xi, 484 p.
45. Rousseau, R. M.; Willis, J. P.; Duncan, A. R., Practical XRF Calibration Procedures for Major and Trace Elements. *X-Ray Spectrometry* **1996,** 25, (4), 179-189.
46. Thomsen, V.; Schatzlein, D., Advances in Field-Portable XRF. *Spectroscopy* **2002,** 17, (7), 14-21.
47. Adams, M. J.; Allen, J. R., Variable selection and multivariate calibration models for X-ray fluorescence spectrometry. *Journal of Analytical Atomic Spectrometry* **1998,** 13, (2), 119-124.
48. Beckhoff, B.; Kanngießer, B.; Langhoff, N.; Wedell, R.; Wolff, H., *Handbook of practical X-ray fluorescence analysis*. 1st ed.; Springer: Berlin, 2006; p xiv, 832 p.
49. Piorek, S., Field-portable X-ray fluorescence spectrometry: Past, present, and future. *Field Analytical Chemistry and Technology* **1997,** 1, (6), 317-329.

50. Bichlmeier, S.; Janssens, K.; Heckel, J.; Gibson, D.; Hoffmann, P.; Ortner, H. M., Component selection for a compact micro-XRF spectrometer. *X-Ray Spectrometry* **2001,** 30, (1), 8-14.
51. Potts, P. J.; Webb, P. C.; Williams-Thorpe, O., Investigation of a correction procedure for surface irregularity effects based on scatter peak intensities in the field analysis of geological and archaeological rock samples by portable X-ray fluorescence spectrometry. *Journal of Analytical Atomic Spectrometry* **1997,** 12, (7), 769-776.
52. Weigand, P. C.; Harbottle, G.; Sayre, E. V., *Turquoise Sources and Source Analysis: Mesoamerica and the Southwestern U.S.A.* Academic Press: New York, 1977.
53. Wilson, L.; Pollard, A. M., The Provenance Hypothesis. In *Handbook of Archaeological Sciences*, Brothwell, D. R.; Pollard, A. M., Eds. John Wiley and Sons, Ltd.: Chichester, 2001; pp 507-517.
54. Neff, H.; Glascock, M. D., The state of nuclear archaeology in North America. *Journal of Radioanalytical and Nuclear Chemistry, Articles* **1995,** 196, (2), 275-286.
55. Glascock, M. D.; Neff, H., Neutron activation analysis and provenance research in archaeology. *Measurement Science and Technology* **2003,** 14, (9), 1516-1526.
56. Harbottle, G., Chemical characterization in archaeology. In *Contexts for Prehistoric Exchange*, Ericson, J. E.; Earle, T. K., Eds. Academic Press: New York, 1982; pp 13-51.
57. Baxter, M. J.; Freestone, I. C., Log-Ratio Compositional Data Analysis in Archaeometry. *Archaeometry* **2006,** 48, (3), 511-531.
58. Bishop, R. L.; Neff, H., Compositional Data Analysis in Archaeology. In *Archaeological chemistry IV : developed from a symposium sponsored by the Division of History of Chemistry at the 193rd meeting of the American Chemical Society, Denver, Colorado, April 5-10, 1987*, Allen, R. O., Ed. American Chemical Society: Washington, DC, 1989; pp xiii, 508 p.
59. Baxter, M. J., *Exploratory multivariate analysis in archaeology*. Edinburgh University Press: Edinburgh, 1994; p xii, 307 p.
60. Glascock, M. D.; Neff, H., GAUSS Software. In 2006.
61. Neff, H., RQ-Mode principal components analysis of ceramic compositional data. *Archaeometry* **1994,** 36, (1), 115-130.
62. Baxter, M. J., Multivariate Analysis in Archaeometry. In *Handbook of Archaeological Sciences*, Brothwell, D. R.; Pollard, A. M., Eds. John Wiley and Sons, Ltd.: Chichester, 2001; pp 685-694.
63. Baxter, M. J., Archaeological uses of the biplot - a neglected technique? In *Computer Applications and Quantitative Methods in Archaeology 1991*, Lock, G.; Moffett, J., Eds. Tempvs Reparatvm: Oxford, 1992; pp 141-148.
64. Glascock, M. D.; Braswell, G. E.; Cobean, R. H., A systematic approach to obsidian source characterization. In *Archaeological Obsidian Studies: Method and Theory*, Shackley, M. S., Ed. Plenum Press: New York and London, 1998; pp 15-65.
65. Bishop, R. L.; Rands, R. L.; Holley, G. R., Ceramic compositional analysis in archaeological perspective. In *Advances in Archaeological Method and Theory, Volume 5*, Schiffer, M. B., Ed. Academic Press: New York, 1982; pp 275-330.
66. Aldenderfer, M. S.; Blashfield, R. K., *Cluster Analysis*. Sage Publications, Inc.: Newbury Park, 1984; Vol. 44.
67. Statsoft http://www.statsoft.com/textbook/stathome.html (August 1),
68. Clustan *Clustan*, 2006.

69. Baxter, M. J., Standardization and transformation in principal components analysis, with applications to archaeometry. *Applied Statistics* **1995,** 44, (4), 513-527.
70. Dunteman, G. H., *Principal Components Analysis*. Sage Publications, Inc.: Thousand Oaks, CA, 1989; Vol. 69.
71. Bieber, A. M., Jr.; Brooks, D. W.; Harbottle, G.; Sayre, E. V., Application of multivariate techniques to analytical data on Aegean ceramics. *Archaeometry* **1976,** 18, (1), 59-74.
72. Klecka, W. R., *Discriminant Analysis*. Sage Publications, Inc.: Thousand Oaks, CA, 1980; Vol. 19.
73. Glascock, M. D., Activation analysis. In *Instrumental Multi-Element Chemical Analysis*, Alfassi, Z. B., Ed. Kluwer Academic: Dordrecht, The Netherlands, 1998; pp 93-150.
74. Poulsen, J.; French, A. Discriminant Function Analysis. http://online.sfsu.edu/~efc/classes/biol710/discrim/discrim.pdf
75. Aitchison, J.; Barcelo-Vidal, C.; Pawlowsky-Glahn, V., Some comments on compositional data analysis in archaeometry, in particular the fallacies in Tangri and Wright's dismissal of logratio analysis. *Archaeometry* **2002,** 44, (2), 295-304.
76. Baxter, M. J.; Beardah, C. C.; Cool, H. E. M.; Jackson, C. M., Compositional Data Analysis of Some Alkaline Glasses. *Mathematical Geology* **2005,** 37, (2), 183-196.
77. Aitchison, J.; Greenacre, M., Biplots of compositional data. *Journal of the Royal Statistical Society. Series C: Applied Statistics* **2002,** 51, (4), 375-392.
78. Aitchison, J. A., Logratios and natural laws in compositional data analysis. *Mathematical Geology* **1999,** 31, (5), 563-589.
79. Green, T. J.; Munson, C. A., Mississippian Settlement Patterns in Southwestern Indiana. In *Mississippian Settlement Patterns*, Smith, B. D., Ed. Academic Press: New York, 1978; pp 292-330.
80. Pollack, D.; Munson, C. A., Caborn-Welborn Ceramics: Intersite Comparisons and Extraregional Interaction. In In *Current Archaeological Research in Kentucky*, Charles D. Hockensmith, K. C. C., Charles Stout, and Sara J. Rivers, Ed. Kentucky Heritage Council: Frankfort, Kentucky, 1998; Vol. 5, pp 163-202.
81. Shergur, J.; Popelka, R. S.; Robertson, J. D.; Pollack, D., Distinct Chemical Patterns In Late Mississippian Caborn-Welborn Ceramics of the Lower Ohio River Valley. *North American Archaeologist* **2003,** 24, (3), 221-243.
82. House, J. H., Dating the Kent Phase. *Southeastern Archaeology* **1993,** 12, 21.
83. Blanchard, L. J.; Robertson, J. D.; Srikantapura, S.; Parekh, B. K., PIXE analysis of the hydrothermal leaching of trace elements in coal. *Journal of Radioanalytical and Nuclear Chemistry* **1997,** 221, (1-2), 23-28.
84. Cogswell, J. W.; Neff, H.; Glascock, M. D., Analysis of shell-tempered pottery replicates: Implications for provenance studies. *American Antiquity* **1998,** 63, (1), 63-72.
85. Steponaitis, V. P.; Blackman, M. J.; Neff, H., Large-scale patterns in the chemical composition of Mississippian pottery. *American Antiquity* **1996,** 61, (3), 555-572.
86. Edwards, H. G. M.; Farwell, D. W.; De Faria, D. L. A.; Monteiro, A. M. F.; Afonso, M. C.; De Blasis, P.; Eggers, S., Raman spectroscopic study of 3000-year-old human skeletal remains from a sambaqui, Santa Catarina, Brazil. *Journal of Raman Spectroscopy* **2001,** 32, (1), 17-22.

87. Diaz-Granados, C.; Duncan, J., *The Petroglyphs and Pictographs of Missouri*. University of Alabama Press: Tuscaloosa, 2000.
88. Mrzlack, H. Ochre at 49-PET-408. Thesis, University of Colorado at Denver, Denver, 2003.
89. Chalmin, E.; Menu, M.; Vignaud, C., Analysis of Rock Art Painting and Technology of Paleolithic Painters. *Measurement Science and Technology* **2003,** 14, 1590-1597.
90. Gorecki, P.; Grant, M.; Salmon, M., Rock Art from the Gregory Range, Gulf of Carpentaria. In 1996.
91. Moffatt, E. A.; Sirois, P. J.; Miller, J., Analysis of the paintings on a selection of Naskapi artifacts in ethnographic collections. *Studies in Conservation* **1997,** 42, 65-73.
92. Clark, R. J. H.; Curri, M. L., The identification by Raman microscopy and x-ray diffraction of iron-oxide pigments and of the red pigments found on Italian pottery fragments. *Journal of Molecular Structure* **1998,** 440, (1-3), 105-111.
93. Dinator, M. I.; Morales, J. R., Characterization of Colour Pigments in Pre-Columbian Chilean Potteries by PIXE Elemental Analysis. *Journal of Radioanalytical and Nuclear Chemistry* **1989,** 140, (1), 133-139.
94. Young, T., The Paviland Ochres: Characterisation and Sourcing. In *Paviland Cave and the 'Red Lady'*, Aldhouse-Green, S., Ed. Western Academic & Specialist Press Limited: Bristol, England, 2000; pp 205-226.
95. Tankersley, K. B.; Tankersley, K. O.; Shaffer, N. R.; Hess, M. D.; Benz, J. S.; Turner, F. R.; Stafford, M. D.; Zeimans, G.; Frison, G. C., They Have a Rock That Bleeds: Sunrise Red Ochre and its Early Paleoindian Occurrence at the Hell Gap Site, Wyoming. *Plains Anthropologist* **1995,** 40, (152), 185-194.
96. Cornell, R. M.; Schewertmann, U., *The iron oxides*. Wiley-VCH Verlag GmbH &Co. : Weinheim, 2003.
97. Craig, N. The Formation of Early Settled Villages and the Emergence of Leadership: A Test of Three Theoretical Models in the Rio Ilave, Lake Titicaca Basin, Southern Peru. Dissertation, University of California at Santa Barbara, Santa Barbara, 2005.
98. Hovers, E.; Ilani, S.; Bar-Yosef, O.; Vandermeersch, B., An Early Case of Color Symbolism. *Current Anthropology* **2003,** 44, (4), 491-522.
99. Ellis, L. W.; Caran, S. C.; Glascock, M. D.; Tweedy, S. W.; Neff, H., Appendix H: Geochemical and Mineralogical Characterization of Ocher from an Archaeological Context. In *Hot Rock Cooking on the Greater Edwards Plateau: Four Burned Rock Midden Sites in West Central Texas.*, Black, S. L.; Linda W. Ellis; Darrell G. Creel; Goode, G. T., Eds. Texas Archeological Research Laboratory, University of Texas at Austin.: Austin, 1997.
100. Singh, A.; Jain, B. K.; Chandra, K., Mossbauer Studies of Naturally Occurring Red Ochre and Yellow Ochre. *Journal of Physics D: Applied Physics* **1978,** 11, 55-62.
101. Casellato, U.; Vigato, P. A.; Russo, U.; Matteini, M., A Mo¨ssbauer approach to the physico-chemical characterization of iron-containing pigments for historical wall paintings. *Journal of Cultural Heritage* **2000,** 1, (3), 217-232.
102. Smith, D. C.; Bouchard, M.; Lorblanchet, M., An Initial Raman Microscopic Investigation of Prehistoric Rock Art in Caves of the Quercy District, S.W. France. *Journal of Raman Spectroscopy* **1999,** 30, 347-354.
103. David, A. R.; Edwards, H. G. M.; Farwell, D. W.; De Faria, D. L. A., Raman Spectroscopic Analysis of Ancient Egyptian Pigments. *Archaeometry* **2001,** 43, (4), 461-473.

104. Zoppi, A.; Signorini, G.; Lucarelli, F.; Bachechi, L., Characterization of painting materials from Eritrea rock art sites with non-destructive spectroscopic techniques. *Journal of Cultural Heritage* **2002**, (3), 299-308.
105. Chalmin, E.; Vignaud, C.; Salomon, H.; Farges, F.; Susini, J.; Menu, M., Minerals discovered in paleolithic black pigments by transmission electron microscopy and micro-X-ray absorption near-edge structure. *Applied Physics A: Materials Science and Processing* **2006,** 83, (2), 213-218.
106. Edwards, H. G. M.; Chalmers, J. M.; Royal Society of Chemistry (Great Britain), *Raman spectroscopy in archaeology and art history*. Royal Society of Chemistry: Cambridge, 2005; p xxi, 476 p.
107. Smith, G. D.; Clark, R. J. H., Raman microscopy in archaeological science. *Journal of Archaeological Science* **2004,** 31, (8), 1137-1160.
108. Scott, D. A.; Scheerer, S.; Reeves, D. J., Technical examination of some rock art pigments and encrustations from the Chumash Indian site of San Emigdio, California. *Studies in Conservation* **2002,** 47, (3), 184-194.
109. Erlandson, J. M.; Robertson, J. D.; Descantes, C., Geochemical Analysis of Eight Red Ochres from Western North America. *American Antiquity* **1999,** 64, (3), 517-526.
110. Popelka-Filcoff, R. S.; Craig, N.; Glascock, M. D.; Robertson, J. D.; Aldenderfer, M.; Speakman, R. J., INAA of Ochre Artifacts from Jiskairumoko, Peru. In *Archaeological Chemistry: Analytical Techniques and Archaeological Interpretation*, Glascock, M. D.; Speakman, R. J.; Popelka-Filcoff, R. S., Eds. American Chemical Society: Washington D.C., in press.
111. Popelka-Filcoff, R. S.; Miksa, E.; Robertson, J. D.; Glascock, M. D.; Wallace, H., Elemental Analysis and Characterization of Ochre Sources from Southern Arizona. **in progress**.
112. Popelka-Filcoff, R. S.; Mrzlack, H.; Erlandson, J. M.; Robertson, J. D.; Glascock, M. D.; Descantes, C.; Wallace, H.; Miksa, E.; Creel, D.; Dixon, E. J., Investigation the Geochemistry of Ochres in North America by Instrumental Multi-Elemental Analysis. **in progress**.
113. Popelka-Filcoff, R. S.; Robertson, J. D.; Glascock, M. D.; Descantes, C., Trace Element Characterization of Ochre from Geological Sources *Journal of Radioanalytical and Nuclear Chemistry* **in progress**.
114. Weinstein-Evron, M.; Ilani, S., Provenance of Ochre in the Natufian Layers of el-Wad Cave, Mount Carmel, Israel. *Journal of Archaeological Science* **1994,** 21, 461-467.
115. Rowe, M. W., Physical and Chemical Analysis. In *Handbook of Rock Art*, Whitley, D. S., Ed. Altamira Press: Walnut Creek, CA, 2001; pp 190-220.
116. Mooney, S. D.; Geiss, C.; Smith, M. A., The use of mineral magnetic parameters to characterize archaeological ochres. *Journal of Archaeological Science* **2003,** 30, (5), 511-523.
117. Smith, M. A.; Pell, S., Oxygen-Isotope Ratios in Quartz as Indicators of the Provenance of Archaeological Ochres. *Journal of Archaeological Science* **1997,** 24, 773-778.
118. Jercher, M.; Pring, A.; Jones, P. G.; Raven, M. D., Rietveld x-ray diffraction and x-ray fluorescence analysis of Australian aboriginal ochres. *Archaeometry* **1998,** 40, (2), 383-401.
119. Goodall, R.; David, B.; Bartley, J., Non-destructive Techniques for the Analysis and Characterization of Pigments from Archaeological Sites: The Case of Fern Cave. In

Australian Archaeology '95: Proceedings of the 1995 Australian Archaeological Association Annual Conference, Ulm, S.; Lilley, I.; Ross, A., Eds. The University of Queensland: St Lucia, Queensland, 1996; Vol. 6, pp 183-187.
120. David, B.; Clayton, E.; Watchman, A. L., Initial Results of PIXE Analysis on Northern Australian Ochres. *Australian Archaeology* **1993,** 36, 56-57.
121. Clarke, J., Two Aboriginal Rock Art Pigments from Western Australia: Their Properties, Use and Durability. *Studies in Conservation* **1976,** 21, 134-142.
122. Clarke, J.; North, N., Chemistry of Deterioration of Post-Estuarine Rock Art in Kakadu National Park. In *Rock Art and Posterity: Conserving, Managing and Recording Rock Art*, Pearson, C.; Swartz Jr., B. K., Eds. Australian Rock Art Research Association: Melbourne, 1991; pp 88-92.
123. Hradil, D.; Grygar, T.; Hradilova, J.; Bezdicka, P., Clay and iron oxide pigments in the history of painting. *Applied Clay Science* **2003,** 22, (5), 223-236.
124. Grygar, T.; Hradilova, J.; Hradil, D.; Bezdicka, P.; Bakardjieva, S., Analysis of earthy pigments in grounds of Baroque paintings. *Analytical and Bioanalytical Chemistry* **2003,** 375, (8), 1154-1160.
125. Stafford, M. D.; Frison, G. C.; Stanford, D.; Zeimans, G., Digging for the Color of Life: Paleoindian Red Ochre Mining at the Powars II Site, Platte Country, Wyoming, U.S.A. *Geoarchaeology: An International Journal* **2003,** 18, (1), 71-90.
126. Erlandson, J. M., In Robertson, J. D., Ed. 1998.
127. Wallace, W. J., An Aboriginal Hematite Quarry in Oakland, California. *American Antiquity* **1947,** 12, (4), 272-273.
128. Stafford, M. D.; Frison, G. C.; Stanford, D.; Zeimans, G., Digging for the Color of Life: Paleoindian Red Ochre Mining at the Powars II Site, Platte County, Wyoming, U.S.A. *Geoarchaeology* **2003,** 18, (1), 71-90.
129. Holmes, W. H., Traces of Aboriginal Operations in an Iron Mine near Leslie, MO. In *Annual Report of the Board of Regents of the Smithsonian Institution*, Government Printing Office: Washington, D.C., 1904; pp 723-726.
130. Silver, J., *Chemistry of Iron*. Blackie Academic and Professional: London, 1993.
131. Chase, H. D. A Study of the Iron Ores at Iron Mountain, Missouri. Bachelors, Massachusetts Institute of Technology, Boston, 1931.
132. Crane, G. W., *The Iron Ores of Missouri*. Jefferson City, Missouri, 1912.
133. Murrie, G. W. The Distribution of Selected Trace Elements in Magnetite in the Pilot Knob Ore Body Iron County, Missouri. Masters, Southern Illinois University, 1973.
134. Seeger, C., Southeast Missouri Iron Metallogenic Province: Characteristics and General Chemistry. In *Hydrothermal Iron Oxide Copper Gold and Related Deposits*, Second ed.; Porter, T. M., Ed. PGC Publishing: Adelaide, 2002; Vol. 1, pp 237-248.
135. James, H. L., Chapter W. Chemistry of the iron-Rich Sedimentary Rocks: Chemical composition an occurrence of iron-bearing minerals of sedimentary rocks, and composition, distribution and geochemistry of ironstones and iron-formations. In *Data of Geochemistry*, Sixth Edition ed.; Fleischer, M., Ed. United States Government Printing Office: Washington D.C., 1966.
136. Jolivet, J.-P.; Chaneac, C.; Tronc, E., Iron oxide chemsitry. From molecular clusters to extended solid networks. *ChemComm* **2004**, 481-487.

137. Elias, M.; Chartier, C.; Pre´vot, G.; Garay, H.; Vignaud, C., The colour of ochres explained by their composition. *Materials Science and Engineering B: Solid-State Materials for Advanced Technology* **2006,** 127, (1), 70-80.
138. Ford, T. D., Iron mining in the Peak district. *Mining History* **2003,** 15, (3), 8-14.
139. Singh, B.; Wilson, M. J.; McHardy, W. J.; Fraser, A. R.; Merrington, G., Mineralogy and chemistry of ochre sediments from an acid mine drainage near a disused mine in Cornwall, UK. *Clay Minerals* **1999,** 34, (2), 301-317.
140. Lintnerova, O.; Sucha, V.; Stresko, V., Mineralogy and geochemistry of acid mine Fe-precipitates from the main Slovak mining regions. *Geologica Carpathica* **1999,** 50, (5), 395-404.
141. Bigham, J. M.; Murad, E., Mineralogy of ochre deposits formed by the oxidation of iron sulfide minerals. *Soils and environment: soil processes from mineral to landscape scale* **1997,** 30, 193-225.
142. Bowell, R. J.; Bruce, I., Geochemistry of iron ochres and mine waters from Levant Mine, Cornwall. *Applied Geochemistry* **1995,** 10, (2), 237-250.
143. Mauney, S. S., Natural iron oxide pigments. Rebirth through innovation. *Mining Engineering* **1994,** 46, (1), 70-73.
144. Pumpelly, R.; T.B.Brooks; Schmidt, A., *Iron Ores of Missouri and Michigan: Topographical and Geological Atlas*. G.P. Putnam's Sons: New York, 1874; p 220.
145. Mortimore, J.; Marshall, L.-J. R.; Almond, M.; Hollins, P.; Matthews, W., Analysis of red and yellow ochre samples from Clearwell Caves and Catalhoyok by vibrational spectroscopy and other techniques. *Spectrochimica Acta Part A* **2003,** 60, 1179-1188.
146. Robertson, A. H. F., Origins of ochres and umbers: evidence from Skouriotissa, Troodos Massif, Cyprus. *Transactions of the Institution of Mining and Metallurgy-Section B- Applied Earth Science* **1976,** 85, 245-51.
147. Deer, W. A.; Howie, R. A.; Zussman, J., *An introduction to the rock-forming minerals*. 2nd ed.; Longman Scientific & Technical;Wiley: Harlow, Essex, England New York, NY, 1992; p xvi, 696 p.
148. Marshall, L. J. R.; Williams, J. R.; Almond, M. J.; Atkinson, S. D. M.; Cook, S. R.; Matthews, W.; Mortimore, J. L., Analysis of ochres from Clearwell Caves: The role of particle size in determining colour. *Spectrochimica Acta - Part A: Molecular and Biomolecular Spectroscopy* **2005,** 61, (1-2), 233-241.
149. Paine, R. R.; Lewis, P. J., An archaic human burial from Yoakum County, Texas: The crossroads of bioarchaeology and forensic anthropology. *Texas Journal of Science* **2000,** 52, (1), 13-24.
150. Kiehn, A. V.; Brook, G. A.; Glascock, M. D.; Dake, J. Z.; Robbins, L. H.; Campbell, A. C.; Murphy, M. L., Fingerprinting Specular Hematite from Mines in Botswana, Southern Africa. In *Archaeological Chemistry: Analytical Techniques and Archaeological Interpretation*, Glascock, M. D.; Speakman, R. J.; Popelka-Filcoff, R. S., Eds. American Chemical Society: Washington D.C., in press.
151. authors, V. *Archaeological Survey of Missouri Reports*.
152. Seeger, C., In 2005.
153. Craig, N.; Moyes, H.; Aldenderfer, M., Multivariate Visualization and Analysis of Photomapped Artifact Scatters. *Journal of Archaeological Science* **in press**.
154. Henderson, P., *Rare earth element geochemistry*. Elsevier: Amsterdam ; New York, 1984; p xii, 510 p.

155. Melquiades, F. L.; Appoloni, C. R., Application of XRF and field portable XRF for environmental analysis. *Journal of Radioanalytical and Nuclear Chemistry* **2004,** 262, (2), 533-541.
156. Zwicky, C. N.; Lienemann, P., Quantitative or semi-quantitative? - laboratory-based WDXRF versus portable EDXRF spectrometer: results obtained from measurements on nickel-base alloys. *X-Ray Spectrometry* **2004,** 33, (4), 294-300.
157. Bjeoumikhov, A.; Langhoff, N.; Rabe, J.; Wedell, R., A modular system for XRF and XRD applications consisting of a microfocus X-ray source and different capillary optics. *X-Ray Spectrometry* **2004,** 33, (4), 312-316.
158. Potts, P. J.; Webb, P. C.; Williams-Thorpe, O.; Kilworth, R., Analysis of Silicate Rocks Using Field-portable X-Ray Fluorescence Instrumentation Incorporating a Mercury (II) Iodide Detector: A Preliminary Assessment of Analytical Performance. *Analyst* **1995,** 120, 1273-1278.
159. Longoni, A.; Fiorini, C.; Leutenegger, P.; Sciuti, S.; Fronterotta, G.; Strüder, L.; Lechner, P., A portable XRF spectrometer for non-destructive analyses in archaeometry. *Nuclear Instruments and Methods in Physics Research, Section A: Accelerators, Spectrometers, Detectors and Associated Equipment* **1998,** 409, (1-3), 407-409.
160. Castoldi, A.; Fiorini, C.; Guazzoni, C.; Longoni, A.; Strüder, L., Semiconductor drift detectors: Applications and new devices. *X-Ray Spectrometry* **1999,** 28, (5), 312-316.
161. Cesareo, R.; Gigante, G. E.; Castellano, A.; Rosales, M. A.; Aliphat, M.; De La Fuente, F.; Meitin, J. J.; Mendoza, A.; Iwanczyk, J. S.; Pantazis, J. A., Portable systems for energy dispersive X-ray fluorescence analysis of works of art. *Journal of Trace and Microprobe Techniques* **1996,** 14, (4), 711-725.
162. Zarkadas, C.; Karydas, A. G., A portable semi-micro-x-ray fluorescence spectrometer for archaeometrical studies. *Spectrochimica Acta - Part B Atomic Spectroscopy* **2004,** 59, (10-11), 1611-1618.
163. Nakai, I.; Yamada, S.; Terada, Y.; Shindo, Y.; Utaka, T., Development of a portable x-ray fluorescence spectrometer equipped with two monochromatic x-ray sources and silicon drift detector and field analysis of Islamic glasses at an excavation site in Egypt. *X-Ray Spectrometry* **2005,** 34, (1), 46-51.
164. Adams, F.; Adriaens, A.; Aerts, A.; De Raedt, K.; Janssens, K.; Schalm, O., Micro and Surface Analysis in Art and Archaeology. *Journal of Analytical and Atomic Spectrometry* **1997,** 12, 257-265.
165. Röhrs, S.; Stege, H., Analysis of Limoges painted enamels from the 16th to 19th centuries by using a portable micro x-ray fluorescence spectrometer. *X-Ray Spectrometry* **2004,** 33, (6), 396-401.
166. Bichlmeier, S.; Janssens, K.; Heckel, J.; Hoffmann, P.; Ortner, H. M., Comparative material characterization of historical and industrial samples by using a compact micro-XRF spectrometer. *X-Ray Spectrometry* **2002,** 31, (1), 87-91.
167. Cesareo, R.; Castellano, A.; Buccolieri, G.; Quarta, S.; Marabelli, M., Giotto in the Chapel of the Scrovegni: EDXRF analysis of the golden haloes with portable equipment. *X-Ray Spectrometry* **2004,** 33, (4), 289-293.
168. Karydas, A. G.; Kotzamani, D.; Bernard, R.; Barrandon, J. N.; Zarkadas, C., A compositional study of a museum jewellery collection (7th-1st BC) by means of a portable XRF spectrometer. *Nuclear Instruments and Methods in Physics Research, Section B: Beam Interactions with Materials and Atoms* **2004,** 226, (1-2), 15-28.

169. Williams-Thorpe, O.; Webb, P. C.; Jones, M. C., Non-destructive geochemical and magnetic characterisation of Group XVIII dolerite stone axes and shaft-hole implements from England. *Journal of Archaeological Science* **2003,** 30, (10), 1237-1267.
170. Leutenegger, P.; Longoni, A.; Fiorini, C.; Strüder, L.; Kemmer, J.; Lechner, P.; Sciuti, S.; Cesareo, R., Works of art investigation with silicon drift detectors. *Nuclear Instruments and Methods in Physics Research, Section A: Accelerators, Spectrometers, Detectors and Associated Equipment* **2000,** 439, (2), 458-470.
171. Ferrero, J. L.; Roldan, C.; Juanes, D.; Rollano, E.; Morera, C., Analysis of pigments from Spanish works of art using a portable EDXRF spectrometer. *X-Ray Spectrometry* **2002,** 31, 441-447.
172. Szökefalvi-Nagy, Z.; Demeter, I.; Kocsonya, A.; Kovács, I., Non-destructive XRF analysis of paintings. *Nuclear Instruments and Methods in Physics Research, Section B: Beam Interactions with Materials and Atoms* **2004,** 226, (1-2), 53-59.
173. Moioli, P.; Seccaroni, C., Analysis of Art Objects Using a Portable X-ray Fluorescence Spectrometer. *X-Ray Spectrometry* **2000,** 29, (1), 48-52.
174. Craig, N.; Speakman, R. J.; Popelka-Filcoff, R. S.; Glascock, M. D.; Robertson, D. J.; Shackley, S. M.; Aldenderfer, M. S., Comparison of XRF and PXRF for analysis of archaeological obsidian from southern Perú. **in progress**.
175. Glascock, M. D., Obsidian provenance research in the Americas. *Accounts of Chemical Research* **2002,** 35, (8), 611-617.
176. Shackley, M. S., Precison versus accuracy in the XRF analysis of archaeological obsidian: some lessons for archaeometry and archaeology. In *Archaeometry 98, Proceedings of the 31st International Symposium on Archaeometry*, Jerem, E.; Biro, K. T., Eds. BAR International Series 1043 (2): Budapest, Hungary, 2002; pp 805-809.
177. Bellot-Gurlet, L.; Poupeau, G.; Salomon, J.; Calligaro, T.; Moignard, B.; Dran, J.-C.; Barrat, J.-A.; Pichon, L., Obsidian provenance studies in archaeology: a comparison between PIXE, ICP-AES and ICP-MS. *Nuclear Instruments and Methods in Physics Research Section B: Beam Interactions with Materials and Atoms* **2005,** 240, (1-2), 583-588.
178. Burger, R. L.; Mohr Chavez, K. L.; Chaves, S. J., Through the glass darkly: Prehispanic obsidian procurement and exchange in southern Peru and northern Bolivia. *Journal of World Prehistory* **2000,** 14, (3), 267-362.
179. Glascock, M. D.; Neff, H.; Stryker, K. S.; Johnson, T. N., Sourcing archaeological obsidian by an abbreviated NAA procedure. *Journal of Radioanalytical and Nuclear Chemistry* **1994,** 180, (1), 29-35.
180. Shackley, S. M.; Eklund, E.; Ogasawara, C. *Source Provenance of Obsidian Artifacts Jiskairumoko (189), Peru*; University of California Berkeley Archaeological XRF Laboratory: Department of Anthropology, May 2004, 2004; p 10.
181. Amptek www.amptek.com
182. NIST, X-Ray Mass Attenuation Coefficients. In 2006.
183. Potts, P. J.; Williams-Thorpe, O.; Webb, P. c., The Bulk Analysis of Silicate Rocks by Portable X-ray Fluorescence: Effect of Sample Mineralogy in Relation to the Size of the Excited Volume. *Geostandards Newsletter* **1997,** 21, (1), 29-41.
184. Currie, L. A., Limits for Qualitative Detection and Quantitative Determination. *Analytical Chemistry* **1968,** 40, (3), 586-593.

VITA

Rachel Sarah Popelka-Filcoff was born on October 23, 1977 in Los Angeles, California. In 1981, her family moved to St. Louis, where she spent her childhood and college years and attended private and public schools in St. Louis. She attended Washington University in St. Louis and graduated in 1999 with a Bachelor of Arts degree in archaeology and classics, which included field excavation seasons in Greece, Jordan and Italy. After spending twoyears working for Community of Science, a company in Baltimore, Maryland, she returned to Missouri in 2001 to complete her Ph.D. in chemistry from the University of Missouri-Columbia. After graduation in December 2006, she will be a National Research Council Post-Doctoral Research Associate at the National Institute of Standards and Technology in Gaithersburg, Maryland and continue research in analytical chemistry and archaeometry. She married David Filcoff in May 2005.